TRANSPORTATION POOLED FUND PROGRAM
QUARTERLY PROGRESS REPORT

Lead Agency (FHWA or State DOT): INDOT - Indiana Department of Transportation

INSTRUCTIONS:
Project Managers and/or research project investigators should complete a quarterly progress report for each calendar quarter during which the projects are active. Please provide a project schedule status of the research activities tied to each task that is defined in the proposal; a percentage completion of each task; a concise discussion (2 or 3 sentences) of the current status, including accomplishments and problems encountered, if any. List all tasks, even if no work was done during this period.

Transportation Pooled Fund Program Project # *(i.e, SPR-2(XXX), SPR-3(XXX) or TPF-5(XXX)* TPF - 5 (179) SPR 3280	**Transportation Pooled Fund Program - Report Period:** ☐Quarter 1 (January 1 – March 31) ☐Quarter 2 (April 1 – June 30) ☐Quarter 3 (July 1 – September 30) ☑Quarter 4 (October 1 – December 31)

Project Title:
Evaluation of Test Methods for Permeability (Transport) and development of Performance Guidlines for Durability

Name of Project Manager(s): Tommy Nantung	**Phone Number:** (765) 463-1521 ext. 248	**E-Mail** tnantung@indot.in.gov
Lead Agency Project ID: INDOT	**Other Project ID (i.e., contract #):**	**Project Start Date:** 07/01/2008
Original Project End Date: 06/30/2012	**Current Project End Date:** 12/31/2013	**Number of Extensions:** 1

Project schedule status:

☐ On schedule ☑ On revised schedule ☐ Ahead of schedule ☐ Behind schedule

Overall Project Statistics:

Total Project Budget	Total Cost to Date for Project	Percentage of Work Completed to Date
$978,000.00	$723,039.32	88%

Quarterly Project Statistics:

Total Project Expenses and Percentage This Quarter	Total Amount of Funds Expended This Quarter	Total Percentage of Time Used to Date
$37,881.05 (3.9%)	$37,881.05	82%

Project Description:

The primary purpose of this project is to develop a test procedure that directly evaluates the permeability (transport properties) of concrete and relates these to anticipated field performance with the use of exposure conditions. This consists of the following distinct objectives:

- Evaluation of existing permeability (transport) test procedures.
- Development of new, or improvement of existing test, procedures to evaluate permeability (transport) properties of concrete.
- Correlation between permeability (transport) properties and measured material response to existing 'durability' tests.
- Develop guidelines to relate permeability, exposure conditions, and field performance for use in specifications and quality control processes

Progress this Quarter (includes meetings, work plan status, contract status, significant progress, etc.):

Please see the report attached. It will be divided in the following sessions:
Session 1: Purdue University
Session 2: Papers from this and previous quarters
Session 3: NRMCA National Ready Mixed Concrete Association

Anticipated work next quarter:

Rapid conditioning study:
A literature review has been conducted on existing conditioning methods for gas and liquid permeability. Many of the existing methods are mainly based on concrete strength or mass change and are time consuming. Alternative methodologies will be investigated in order to develop a flexible and rapid conditioning procedure is needed. Specifically, a vacuum oven has been installed for this study. The vacuum oven will be compared with a standard convection oven using a range of temperatures and relative humidities. The samples for the first cycle (50 C conditioning) have been prepared and the conditioning process will be initiated in the following week. The first results will be presented in the next quarterly progress report.

Ruggedness testing of permeability tests:
The first of a series of large concrete castings was completed. The focus of this study is to evaluate transport properties with several test methods for typical mixtures currently used for concrete bridges. The sensitivity of different testing techniques to changes in mixture proportions will be quantified. Other large castings are planned in the following months.

Gas Transport Measurements:
Additional testing will be performed using oxygen permeameter and oxygen diffusivity to better quantify the influence of moisture distribution and the pressure influence on gas transport measurements of mortar samples. This work is part of the study conducted at Purdue in collaboration with EMPA swiss laboratory. The complete write-up of the study is nearly complete will be presented in next quarter report.

Significant Results:

During the last quarter the following two items were documented in papers.

Transport properties are known to be related to the moisture content and the distribution of moisture in the concrete. Many factors can influence the drying and wetting process in concrete including pore structure, environmental conditions, and liquid properties. A study was conducted to describe the influence of the liquid properties on the drying process by analyzing the non-linear moisture diffusion coefficient in presence of deicing salts. It has been found that the presence of deicing salt causes a shift of the non-linear moisture diffusion coefficient as a function of relative humidity. As a result, samples containing deicing salt solutions are likely to have a higher degree of saturation than samples without deicing salt solutions in practice. The related paper is attached.

A study on the influence of deicing salts on gas transport of cementitious materials has been completed. Specifically, the influence of deicing salts on the gas permeability and gas diffusivity of mortar has been studied. Mortar samples were initially saturated with different deicing salt solutions and then exposed to drying. The deicing salt solutions were found to influence the degree of saturation and as such they influenced the gas transport properties. Mortar containing deicing salts had lower permeability and diffusivity due to higher degree of saturation, compared to samples saturated with pure water. These findings were further confirmed through the evaluation of the desorption spectra of samples saturated in aqueous solution containing salts. This study suggests that care must be taken when performing investigations using concrete that may have been previously exposed to deicing salts either in situ or when this concrete is taken back to the laboratory. The related paper is attached.

Circumstance affecting project or budget. (Please describe any challenges encountered or anticipated that might affect the completion of the project within the time, scope and fiscal constraints set forth in the agreement, along with recommended solutions to those problems).

Potential Implementation:

List of papers attached

The following draft papers will be attached at the end of this report:

[1] Castro, J. Bentz, D., and Weiss, W. J., (2011) “Effect of Sample Conditioning on the Water Absorption of Concrete,” Cement & Concrete Composites 33, p. 805–813 (2011)

[2] Castro, J., Spragg, R., and Weiss, W. J., “Internal Curing for W/C Systems Between 0.30 and 0.45: Impact on Water Absorption and Electrical Conductivity,” ASCE Journal of Civil Engineering Materials

[3] Di Bella, C., C. Villani, E. Hausheer, and J. Weiss. "Chloride Transport Measurements for a Plain and Internally Cured Concrete Mixture." ACI Special Publication 290, (2012)

[4] Li, W., Pour-Ghaz, M., Castro, J., and Weiss, W. J., (accepted) “Water Absorption and the Critical Degree of Saturation as it relates to Freeze-Thaw Damage in Concrete Pavement Joints,” ASCE Journal of Civil Engineering Materials

[5] Poursaee, A., and Weiss, W. J., (2010) “An Automated Electrical Monitoring System (AEMS) to Assess Concrete Property Development’, Journal of Automation in Construction, Volume 19, Issue 4, 2010, p. 485-490 (2010)

[6] M. Pour-Ghaz, R. Spragg, J. Weiss, ‘Moisture profiles and diffusion coefficient in mortars containing shrinkage reducing admixtures’, International RILEM Conference on Use of Superabsorbent Polymers, Denmark (2011)

[7] Sant, G., Rajabipour, F., and Weiss, W.J., (2008) ‘The Influence of Temperature on Electrical Conductivity Measurements and Maturity Predictions in Cementitious Materials during Hydration’, Indian Concrete Journal, p. 10 (2008)

[8] R. Spragg, J. Castro, W. Li, M.Pour-Ghaz, P.Huang, J. Weiss, Wetting and Drying Concrete Using Aqueous Solutions Containing Deicing Salts, Cement and Concrete Composites, Vol. 33, p. 535-542 (2011)

[9] R.P. Spragg, J. Castro, T Nantung, M. Paredes, and J. Weiss, ‘Variability analysis of the bulk resistivity measured using concrete cylinders’, Advances in Civil Engineering Materials, Vol.1

[10] W. J. Weiss, K. A. Snyder, J. W. Bullard and D. P. Bentz, Using a Saturation Function to Interpret the Electrical Properties of Partially Saturated Concrete, Journal of Materials in Civil Engineering (2012), accepted

[11] Villani, C., Spragg, R., Pour-Ghaz, M. & Weiss, J.W., 2012. The role of deicing salts on the non-linear moisture diffusion coefficient of cementitious materials during drying. In Brandt, A.M., Olek, J., Glinicki, M.A. & Leung, C.K.Y., eds. 10th Tenth International Symposium on Brittle Matrix Composites. Warsaw, 2012. Institute of Fundamental Technological Research PAS.

[12] Villani, C., Imbrock, P., Nantung, T. & Weiss, J.W., The influence of deicing salt exposure on gas transport, SMCT 3th International Conference on Sustainable Construction Materials & Technologies, August 18 – 21, 2013, Kyoto, Japan (Submitted)

Cement & Concrete Composites 33 (2011) 805–813

Contents lists available at ScienceDirect

Cement & Concrete Composites

journal homepage: www.elsevier.com/locate/cemconcomp

Effect of sample conditioning on the water absorption of concrete

Javier Castro [a,*], Dale Bentz [b,1], Jason Weiss [c,2]

[a] Pontificia Universidad Catolica de Chile, School of Engineering, Casilla 306, Correo 22, Santiago, Chile
[b] National Institute of Standards and Technology, Materials and Construction Research Division, Engineering Laboratory, 100 Bureau Drive, Stop 7313, Gaithersburg, MD 20899-7313, USA
[c] School of Civil Engineering, Purdue University, 550 Stadium Mall, West Lafayette, IN 47907-2051, USA

ARTICLE INFO

Article history:
Received 23 November 2010
Received in revised form 17 May 2011
Accepted 19 May 2011
Available online 25 May 2011

Keywords:
Water absorption
Sample conditioning
Moisture effect
Relative humidity

ABSTRACT

ASTM C1585 is commonly used to determine the absorption and rate of absorption of water in unsaturated hydraulic cement concretes. Unfortunately, a wide range of relative humidities can exist in the samples after this relatively short conditioning period and such variation may considerably influence the test results. Three main variables were studied in this program: the water to cement ratio, the paste volume fraction, and the effect of sample conditioning. The results confirm that water absorption testing is considerably influenced by sample preparation. Samples conditioned at 50% relative humidity can show up to six times greater total absorption than similar samples conditioned at 80% relative humidity. Samples that were conditioned in the oven at 105 °C do not appear to follow a similar trend when compared with specimens conditioned in chambers at lower temperatures for a longer duration. The absorption is also influenced by the volume of paste in the samples. The experiments show that a lack of control on moisture content or lack of consideration of the material composition may lead to a misunderstanding of the actual absorption behavior.

1. Introduction

The durability of concrete subjected to aggressive environments depends largely on transport properties, which are influenced by the pore system [1–7]. Three main mechanisms govern transport in cementitious systems: permeability, diffusion and absorption. Permeability is the measure of the flow of fluids under a pressure gradient, while diffusion is the movement of ions due to a concentration gradient. Absorption can be described as the ability to take in water by means of capillary suction. All three mechanisms are heavily influenced by the volume of pores as well as the connectivity of the pore network. A large fraction of concrete in service is only partly saturated and the initial ingress of water and dissolved salts is influenced, at least in part, by capillary absorption [7]. As such, water absorption has been used as an important factor for quantifying the durability of cementitious systems [4–11]. Water absorption is the primary focus of this study since it is being increasingly used by specifiers and in forensic studies to provide a parameter that can describe an aspect of concrete durability. It is also important that these properties be adequately described for use in service life models [6,11].

1.1. Water absorption test

ASTM C1585 [1] is commonly used to determine the absorption and rate of absorption (commonly referred to as sorptivity) of water in unsaturated hydraulic cement concretes. This test method, based on work reviewed by Hall [12], consists of preconditioning cylindrical samples (2″ (51 mm) in thickness and 4″ (102 mm) in diameter) to a known moisture content, then exposing the bottom surface of the sample to liquid water and measuring the increase in mass resulting from water absorption. According to the standard conditioning procedure, samples are conditioned for 18 days. This conditioning period begins by first placing the sample in a 50 °C and 80% relative humidity (RH) environment for 3 days. The samples are then removed from this environment and placed in individually sealed containers where they remain for a minimum 15 days at 23 °C, to allow internal moisture to redistribute throughout the specimens before the test begins.

The absorption test involves recording incremental mass change measurements at relatively frequent intervals during the first 6 h after the sample comes in contact with water and subsequently taking one measurement every day for the next 8 days. The amount of absorbed water is normalized by the cross-section area of the specimen exposed to the fluid using Eq. (1):

$$i = \frac{m_t}{(a \cdot \rho)} \tag{1}$$

---

[*] Corresponding author. Tel.: +56 2 354 4245.
E-mail addresses: jecastro@ing.puc.cl (J. Castro), dale.bentz@nist.gov (D. Bentz), wjweiss@purdue.edu (J. Weiss).
[1] Tel.: +1 301 975 5865.
[2] Tel.: +1 765 494 2215.

0958-9465/$ - see front matter © 2011 Elsevier Ltd. All rights reserved.
doi:10.1016/j.cemconcomp.2011.05.007

where i is the normalized absorbed fluid volume, m_t is the change in specimen mass at time t; a is the area of the specimen exposed to the fluid (i.e., that of the bottom face), and ρ is the density of the absorbed fluid (taken to be 1000 kg/m^3 at 23 °C for water).

These absorbed fluid volumes are then plotted as a function of the square root of time. The initial sorptivity is determined as the slope of the curve during the first 6 h, while secondary sorptivity is determined using the slope of the same measurements between 1 and 8 days, as outlined in ASTM C1585 [1]. It should be noted that these times work well for water though they may not work as well for other fluids with different surface tension and/or viscosity [13].

The initial and secondary sorptivities can be used to evaluate the connectivity of the pore network [9]. Additionally, the secondary sorptivity, combined with exposure conditions, has been used for performing service life predictions [11].

1.2. The role of the relative humidity

Water ingress in unsaturated concrete is dominated by capillary suction upon initial contact with water [7,12–18]. Capillary absorption can be related to the volume of the pores and pore size distribution, as well as the size (i.e. radius) of the partially empty capillary pores (Fig. 1a). The relation between the equilibrated relative humidity and the radius of the smallest empty pore is given by the Kelvin-Laplace equation (Eq. (2)).

$$\mathrm{Ln}(RH) = \frac{2\sigma V_m}{r_m RT} \tag{2}$$

where: RH is the relative humidity, σ is the surface tension of water (pore solution), V_m is the molar volume of water, r_m is the average radius of curvature, R is the universal gas constant, and T is the absolute temperature.

It should be noted that this expression is simplified as it does not consider the effect of water that is absorbed on the walls of the pores. Largely the concrete community has considered two sizes of pores as introduced by Powers [19]. The gel pores are considered to be small pores (<10 nm diameter) that are a part of the hydration products. Capillary pores are larger pores that occur due to excess water. Capillary porosity is particularly of concern in transport, as is the interconnectivity of the capillary pores.

Fig. 1b shows a conceptual illustration based on Powers [19] that uses a desorption isotherm to illustrate the volume of water located in the different size pores at different relative humidities.

The relative humidity used to condition the sample prior to the sorption test can have a significant impact on the results [1]. Previous test results by Parrot [20,21] indicated that the water absorption rate was very sensitive to the moisture content of the concrete, particularly at relative humidities above 60% which were common for field exposure. Water leaves the largest accessible pores first. It can be seen from Fig. 1b that capillary pores occupy the range of humidity from approximately 80% to 100% RH. As such, initially upon drying water leaves the capillary pores. The lower the relative humidity, the greater the total volume of pores that are empty and available to be filled with water during the sorption test. Further, the lower humidity will empty smaller pores, creating a higher suction force in the materials and resulting in a greater sorption rate and a larger overall total absorption.

According to ASTM C1585, the standardized test conditioning will generally provide an internal relative humidity similar to relative humidities found near the surface in some field concrete structures [1,22,23]. This range of relative humidities can represent what is found in samples in the field; however, it is wide enough to considerably affect the test results.

Castro et al. [24] shows that the relative humidity of samples that were kept in the field under different exposure conditions was in the range of 80–100% depending on the type of exposure, which is somewhat higher than what is mentioned in ASTM C1585.

1.3. Research objectives

The objectives of this research are threefold. First, this research will examine the influence of conditioning relative humidity (oven dry, 50%, 65% and 80% RH) on the results of sorption tests performed on mortars with different *w*/*c*, containing a fixed volume of aggregate. Second, this research will examine the influence of the volume of aggregate (or equivalently the paste content) on the results of sorption testing. Third, this research will examine the effect of the conditioning method specified in ASTM C1585-04.

2. Materials

An ASTM C150 Type I ordinary portland cement (OPC) was used in this study, with a Blaine fineness of 370 m^2/kg and an estimated Bogue composition of 56% C_3S, 16% C_2S, 12% C_3A, 7% C_4AF and a Na_2O equivalent of 0.68% by mass.

A polycarboxylate-based high-range water-reducing admixture (HRWRA) was added in varying rates as indicated in Table 1, depending on the mixture proportions, to maintain similar consistencies (i.e., workability). The sand used was natural river sand with a fineness modulus of 2.71, an apparent specific gravity of 2.58, and a water absorption of 1.8% by mass.

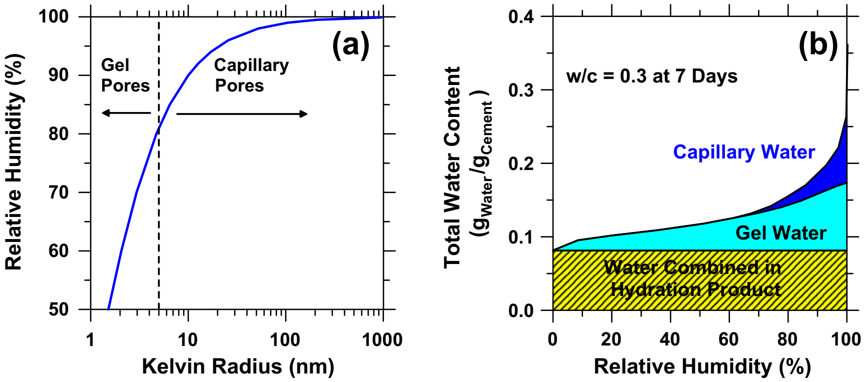

Fig. 1. Relation between relative humidity and partially empty pores in cement paste.

Table 1
Mixture proportions in saturated surface dry (SSD) conditions.

Material	55/0.35	55/0.40	55/0.45	55/0.50	45/0.50	35/0.50
Volume fraction of aggregate	55%	55%	55%	55%	45%	35%
w/c	0.35	0.40	0.45	0.50	0.50	0.50
Cement (kg/m^3)	673	626	585	549	671	793
Water (kg/m^3)	235	250	263	275	336	397
Fine aggregate (kg/m^3), SSD	1442	1442	1442	1442	1180	918
HRWRA (g/100 g cement)	0.60	0.40	0.20	0.00	0.00	0.00

2.1. Mixture proportioning

Six different mixtures were prepared in total. Four of the mixtures were mortars with a single volume fraction of fine aggregate (55% of the total volume) and different *w/c* (0.35, 0.40, 0.45, and 0.50). These mixtures were designated as 55/0.35, 55/0.40, 55/0.45 and 55/0.50, with the number on the left representing the volume fraction of fine aggregate and the number on the right representing *w/c*. Additionally, two other mortars were prepared with *w/c* of 0.50, but with different volume fractions of fine aggregate (35% and 45% of the total volume). They were designated as 35/0.50, 45/0.50. A list of the mixture proportions can be found in Table 1.

2.2. Mixing procedure

The mixing procedure used for the mortar was in accordance with ASTM C192-06 [25]. The aggregate was oven dried and cooled for 24 h before mixing. The volume of water was corrected by the absorption of the aggregate. The water and cement were conditioned for 24 h at room temperature prior to mixing.

3. Experimental method

Six 100 mm × 200 mm cylinders were cast for each mixture. After 1 day of curing, the samples were demolded and then sealed in double plastic bags for sealed curing. Bags were stored in a room at 23 ± 1 °C until samples reached an age of 28 d. After that, cylinders were removed from bags and three 50 mm ± 2 mm thick samples were cut from the central portion of each cylinder with a wet saw using water as the cooling fluid.

After cutting, samples were conditioned by placing them in environmental chambers at 23 ± 0.5 °C. Specimens from mixtures 55/0.35, 55/0.40, 55/0.45 and 55/0.50 were placed in environmental chambers at three different relative humidities (50 ± 1%, 65 ± 1% and 80 ± 1%). Specimens from mixtures 35/0.50 and 45/0.50 were placed in an environmental chamber at 50 ± 1% relative humidity. Samples were kept in the environmental chamber until they reached mass equilibrium, defined as a mass change of less than 0.02% over a 15 day period. Mixture 55/0.35 placed at 50 ± 1% relative humidity required the longest period of time (14 months) to reach mass equilibrium. However, all samples were maintained in the chambers for 14 months to test them all at the same age.

Additional specimens from mixtures 55/0.35, 55/0.40, 55/0.45 and 55/0.50 were placed at 50 ± 1% RH. After the 14 months, these specimens were dried in an oven at 105 ± 2 °C until they reached mass equilibrium.

Once the samples were removed from the chambers or from the oven, the side surface (i.e. outer circumference) was sealed with epoxy. A section of plastic is clamped to the surfaces during the application of epoxy to keep the surfaces clean. This also helped to limit drying during the curing process. After the epoxy was dry, the top surface was covered with plastic to avoid evaporation from the sample during testing. After the samples were prepared, testing occurred in accordance with ASTM C1585-04 [1]. Specimens from mixtures 55/0.35, 55/0.40, 55/0.45 and 55/0.50 were tested over a period of 90 days. Specimens from mixtures 35/0.50 and 45/0.50 were tested over a period of 8 days.

Two additional 100 mm × 200 mm cylinders were cast for each mortar mixture. After 1 day of curing, the samples were demolded and then sealed in double plastic bags for sealed curing. Bags were stored in a room at 23 ± 1 °C until samples reached an age of 28 d. After that, cylinders were removed from bags and 10 mm ± 2 mm thick samples were cut from the central portion of each cylinder with a wet saw. After cutting, mortar samples were vacuum saturated for 24 h. After that, specimens were placed in environmental chambers at six different relative humidities (93 ± 1%, 87 ± 1%, 80 ± 1%, 75 ± 1%, 65 ± 1% and 50 ± 1%) to determine their desorption isotherms.

4. Experimental results and discussion

4.1. Desorption isotherms

Fig. 2 shows the desorption isotherm curves measured using 10 mm thick samples. Mass change was monitored at regular intervals until it reached equilibrium, defined as a mass change of less than 0.02% over a 15 day period. At the end, all samples were oven dried to express water absorption in terms of the dry mass of the sample.

It can be noticed that while the values of the moisture content are similar at 50% and lower RH (lower RH results not shown in Fig. 2), as it refers to the small gel pore system [19], the capillary pores at high RH are strongly influenced by the *w/c*.

4.2. Effect of initial conditioning on water absorption tests

4.2.1. Effects of relative humidity on sorption test

Fig. 3 shows the absorbed water during the 90 days of testing performed on mortars conditioned at different relative humidities

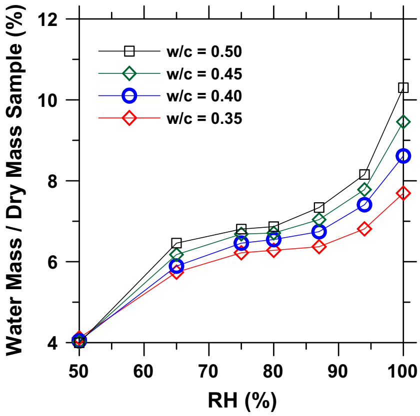

Fig. 2. Desorption curves for 14 months mortar samples (typical standard deviation in the average of three samples is lower than 0.2%).

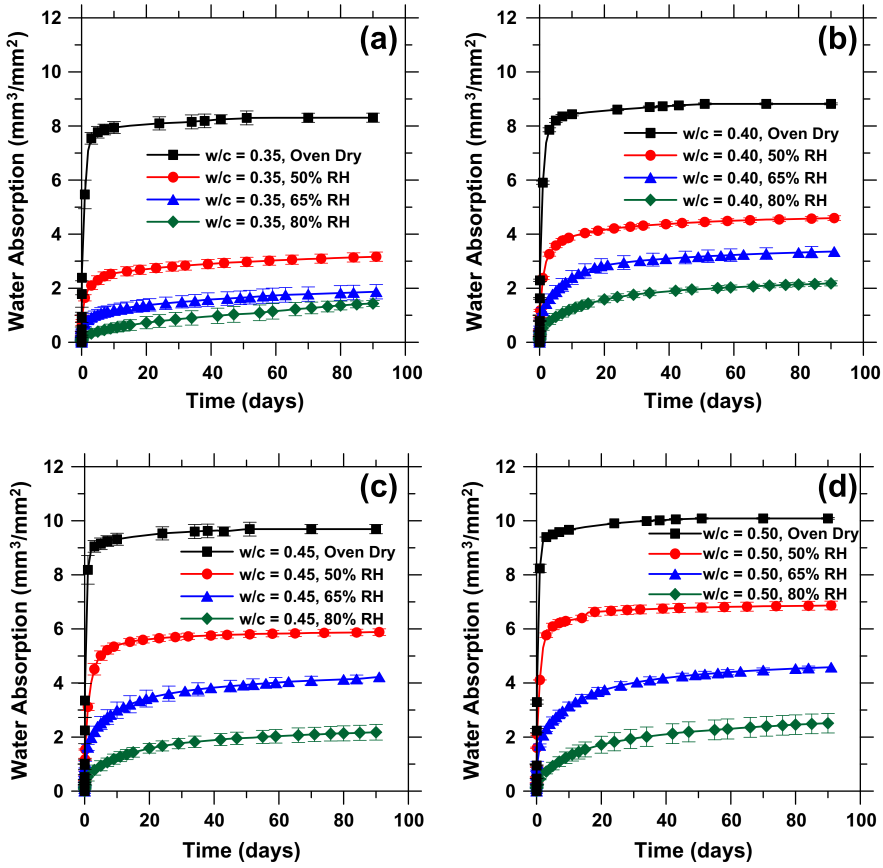

Fig. 3. Absorbed water in mortars as a function of relative humidity (a) mixture 55/0.35, (b) mixture 55/0.40, (c) mixture 55/0.45, (d) mixture 55/0.50. Error bars represent the standard deviation for the average of three samples.

(mixtures 55/0.35, 55/0.40, 55/0.45 and 55/0.50). It can be noticed that the water absorption is very sensitive to the relative humidity at which the specimens were pre-conditioned before testing. In each case, as the conditioning relative humidity increases, more water is retained in the pore system and thus the absorption decreases.

These results can be viewed in a slightly different manner if they include the initial amount of water held in the pores before the test. In order to do this, samples were oven dried at the end of the sorption test to calculate the amount of water they held before starting the test. Additional specimens that were kept at 50 ± 1% RH during the 14 months were oven dried and then saturated by the procedure described in ASTM C642-07 [26] to measure the total amount of interconnected porosity in the systems. Results from Fig. 3 were then normalized by the total amount of pores in the system, which can be viewed as the degree of saturation of the sample as a function of time. This is presented in Fig. 4. Fig. 5 shows the total degree of saturation for the samples after 90 days.

Figs. 4 and 5 show that samples prepared at different relative humidities with a low *w*/*c* (e.g. *w*/*c* = 0.35) do not reach values near to saturation even after 90 days of being in contact with water. It may be attributed to the refined pore network of this low *w*/*c* system which makes it difficult for water to move through the sample to fill all the pores. This is commonly referred to as depercolation, which occurs after different hydration times for different *w*/*c* [27].

In contrast after 90 days, samples prepared with a higher *w*/*c* (e.g. *w*/*c* = 0.50) reach much higher levels of saturation. It can be noted from Fig. 4 that samples conditioned at 50% RH reach values near saturation after about 40 days of testing, similar to what is obtained with oven dry samples. Again this may be attributed to the connectivity of the pore network and the size of these pores. In this case, a more interconnected pore network will facilitate the movement of water to the interior of the specimens and the diffusion of water vapor out of the sample. However, when these samples were conditioned at higher relative humilities (65 and 80% RH), the amount of initially retained water is high enough to reduce the diffusion of vapor out of the sample. As a result, this may explain why the level of saturation of these specimens is lower.

4.2.2. Effects of relative humidity on the amount of absorbed water after 8 days

Fig. 6 shows the cumulative water that was absorbed after 8 days of testing performed on mortars conditioned at different relative humidities, expressed as a function of *w*/*c* (Fig. 6a) and as a function of the relative humidity (Fig. 6b).

Fig. 6a shows that mixture 55/0.50 can exhibit six times higher absorption when the samples are conditioned at 50% RH compared with similar samples conditioned at 80% RH.

Fig. 7 shows a normalization of the data presented in Fig. 6. In Fig. 7a the normalization is made with respect to the absorption of samples with *w*/*c* = 0.35 (mixture 55/0.35). In Fig. 7b the normalization is made with respect to the absorption of samples conditioned at 50% relative humidity. It can be seen that the values follow a consistent trend in each case, except for the oven dry samples. This is in general agreement with the parallel nature of the desorption isotherms for the mortars provided in Fig. 2.

4.2.3. Effects of relative humidity on initial sorptivity

Fig. 8 shows the initial sorptivity calculated as the slope of the absorption vs. the square root of time during the first 6 h of test [1].

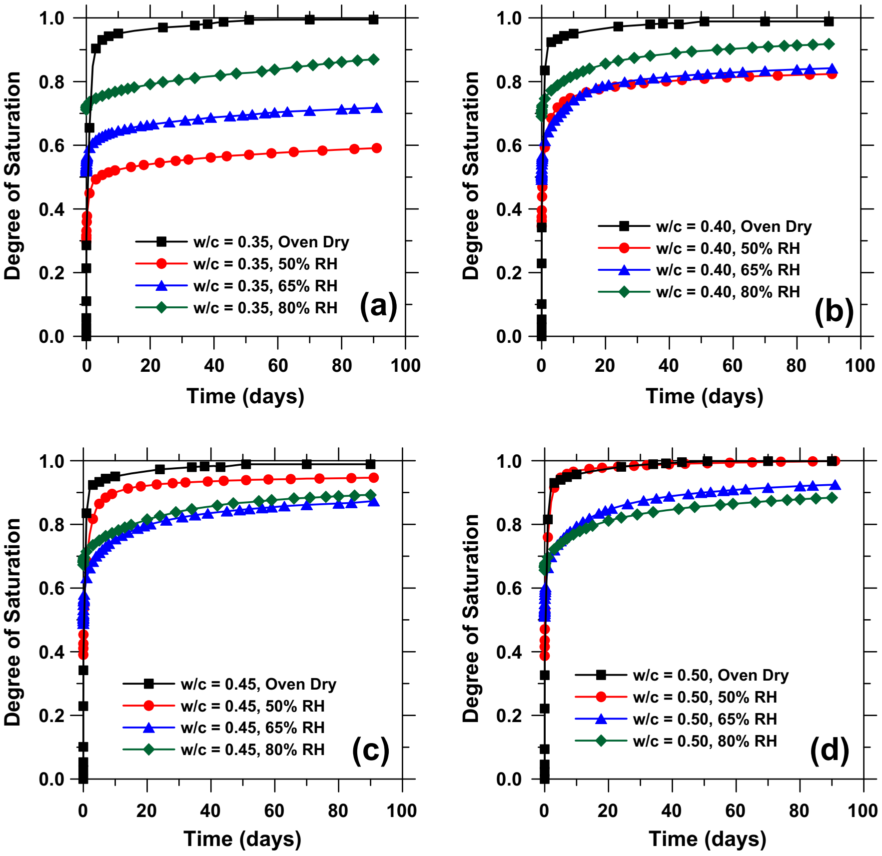

Fig. 4. Degree of saturation as a function of time during the water absorption test: (a) mixture 55/0.35, (b) mixture 55/0.40, (c) mixture 55/0.45, (d) mixture 55/0.50. Typical standard deviation of the average of three samples is lower than 0.02 points in the degree of saturation.

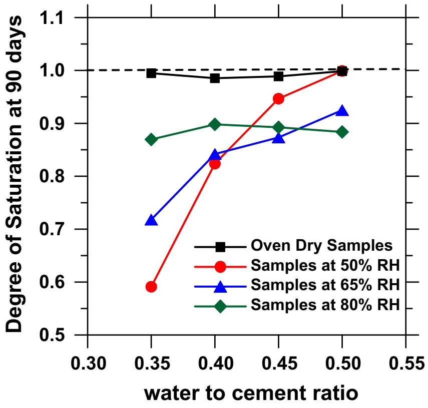

Fig. 5. Degree of saturation after 90 d in contact with water as a function of the *w*/*c*.

Fig. 8a shows that mixture 55/0.50 can exhibit a ten times higher initial sorptivity when the samples are conditioned at 50% RH compared with similar samples conditioned at 80% RH.

It needs to be noted that the oven dry samples show a much higher initial sorptivity, due to the fact that the gel's capillary pores are empty. It is also possible that the samples exhibit microcracking around the aggregates due to differential thermal expansion and contraction which may result in the aggregate restraining paste movement. This would be in addition to any microcracking caused by moisture gradients that may occur in the samples that have dried. During drying, the paste may contract much more than the aggregates that do not really lose moisture or at least not as much moisture loss. Even with some moisture loss from the aggregate, they would likely shrink much less than the surrounding paste due to their higher modulus. While the increase in sorptivity is observed to be linear for the specimens conditioned at 50%, 65% and 80% relative humidity, this trend appears to break down for the oven dry samples which may be attributed to increased micro-cracking generated during the sample preparation [28–32].

4.2.4. Effects of relative humidity on secondary sorptivity

Fig. 9 shows the secondary sorptivity calculated as the slope of the absorption vs. the square root of time between 1 d and 8 d of testing. Trends are similar to those observed for the initial sorptivity. However, it needs to be noted that samples that were oven dry prior to the test present a considerably lower secondary absorption with respect to the samples conditioned in environmental chambers. This may be explained by the high initial absorption of the oven dry samples shown in Fig. 8. During this initial absorption it can be noticed that since a majority of the water was already absorbed in the first hours of the test, the secondary rate of absorption will be much lower. It can also be expected that microcracking enabled a more rapid ingress of water [33].

Fig. 9 shows a similar trend to what was noted in the case of total absorption and initial sorptivity, namely that the secondary sorptivity of samples conditioned in chambers exhibits a consistent trend when the results are plotted against the *w*/*c* or the relative humidity at which samples were conditioned. However, samples that are conditioned by drying them in an oven at 105 °C do not follow the same tendency.

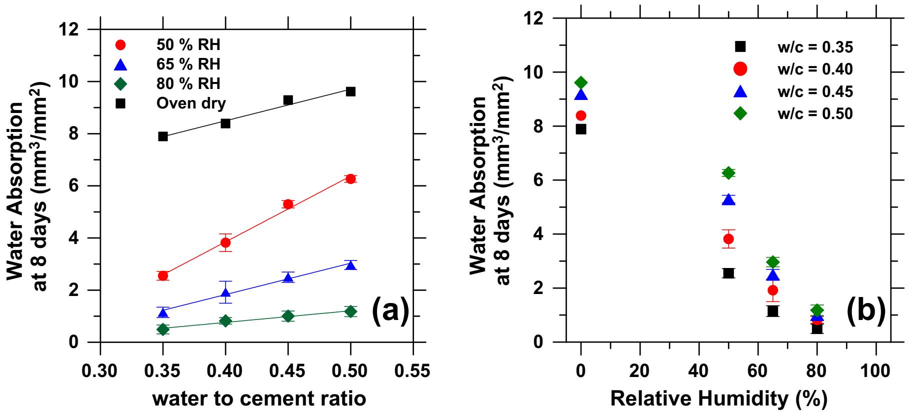

Fig. 6. Cumulative absorption at 8 d for mortars with 55% aggregates versus: (a) *w/c*, (b) relative humidity. Solid lines are provided only to show a general tendency in the data. Error bars represent the standard deviation on the average of three samples.

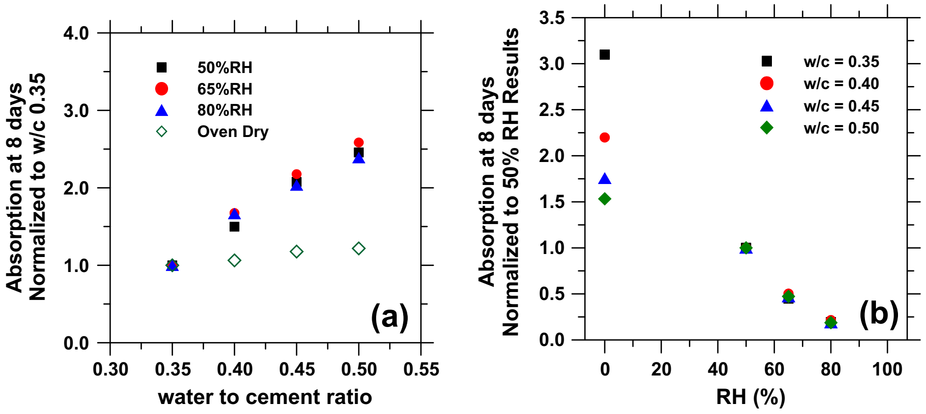

Fig. 7. Cumulative absorption at 8 days versus *w/c* and relative humidity: (a) normalized to absorption of mixture 55/0.35, (b) normalized to absorption at 50%RH.

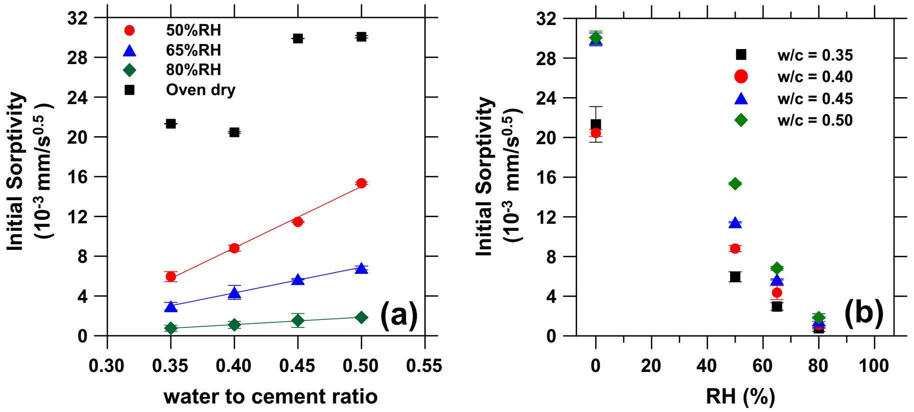

Fig. 8. Initial absorption of the 55% aggregate mortars conditioned at different RH as a function of: (a) *w/c*, (b) relative humidity. Solid lines are provided to show a general tendency in the data. Error bars represent the standard deviation on the average of three samples.

4.3. Effects of initial moisture of samples on ASTM C1585 conditioning method

At the age of 24 months, samples from each mixture conditioned at the three different relative humidities were removed from the chambers. The side surface was sealed with epoxy to be then "re-conditioned" using the 18 day procedure described in ASTM C1585. In addition, three other samples from each mixture were saturated following the procedure described in ASTM C642 [26], to then be "re-conditioned" following the same 18 day procedure. While such a resaturation procedure was employed in the initial sorption testing upon which the ASTM C1585 standard was based [34], it was subsequently omitted from the standard. After samples were fully prepared, testing was performed in accordance with ASTM C1585 over a period of 8 days, with results provided in Fig. 10. In addition, Fig. 11 shows the calculated initial and

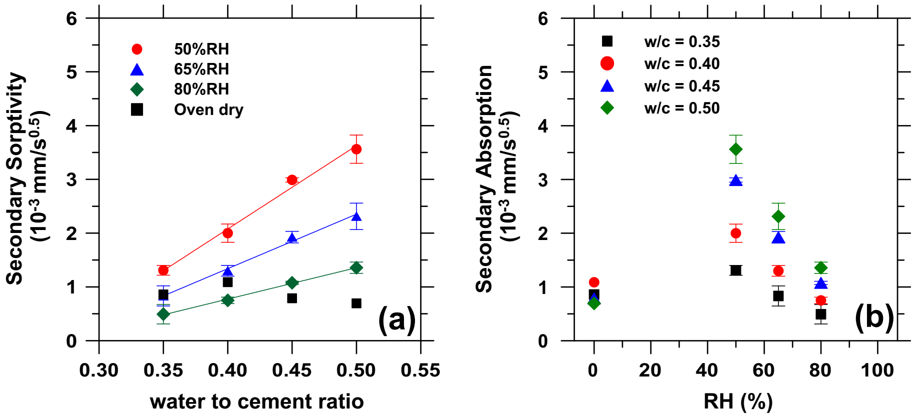

Fig. 9. Secondary absorption on mortars with 55% aggregates conditioned at different RH as a function of: (a) *w/c*, (b) relative humidity. Solid lines are provided to show a general tendency in the data. Error bars represent the standard deviation on the average of three samples.

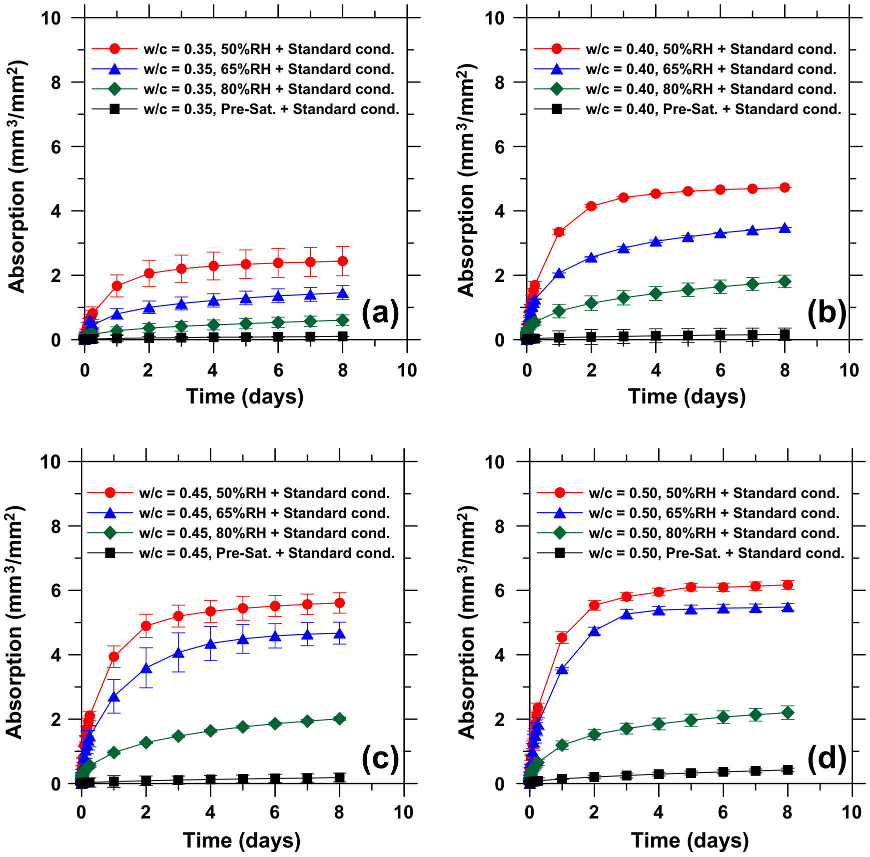

Fig. 10. Effect of initial moisture on the conditioning procedure established in ASTM C1585-04 (a) mixture 55/0.35, (b) mixture 55/0.40, (c) mixture 55/0.45, (d) mixture 55/0.50. Error bars represent the standard deviation for the average of three samples.

secondary sorptivities from these tests. Secondary sorptivity values are not reported when the correlation coefficient is lower than 0.98.

Figs. 10 and 11 show that the 3 days of controlled drying at 50 ± 2 °C and 80% RH followed by the 15 days for internal moisture equilibration is not capable of eliminating the effects of the "moisture history". These results suggest that the ASTM C1585 preparation method does not prepare all the samples to the same water content before a water absorption test. As such this accelerated method can make a substantial difference in how the data is interpreted. This may be due to a moisture hysteresis effect [35]. It should be noted that this can be a concern for field samples evaluated using this method, as their as-received relative humidities may easily vary between the extremes examined in this study.

4.4. Effects of volume of aggregate on sorption test

Fig. 12 shows the absorbed water during 8 days of testing performed on mortars containing different volumes of aggregate (mixtures 55/0.50, 45/0.50 and 35/0.50) conditioned at 50% relative humidity. In Fig. 12a the effect of a higher volume of paste is observed as the mixture containing the lower volume of aggregate

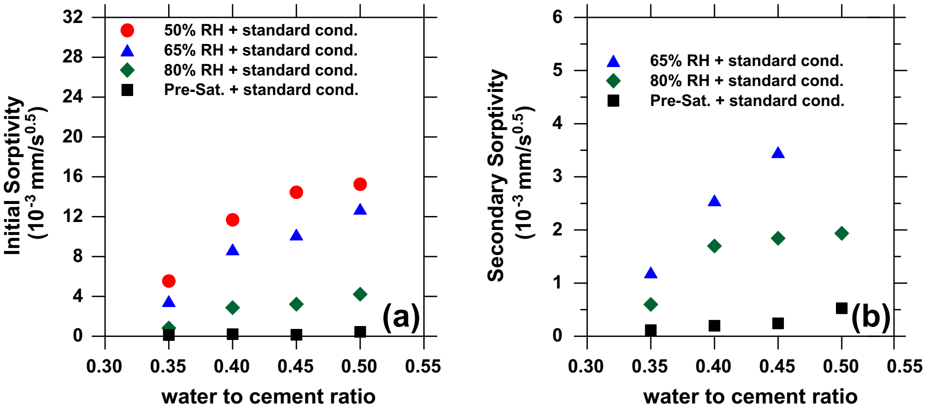

Fig. 11. Initial and secondary sorptivities on mortars with different initial moisture contents, conditioned with the procedure established in ASTM C1585-04.

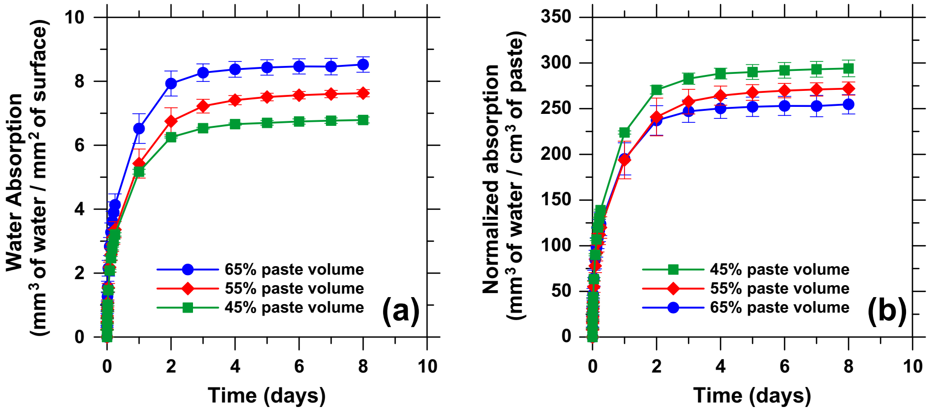

Fig. 12. Water absorption in mortars containing different volume of aggregates: (a) normalized by surface in contact with water, (b) normalized by volume of paste.

has the higher absorption. However, when the results are normalized by the volume of paste (volume of the main absorbent material), a reversal in the order of the samples is observed (Fig. 12b). The samples with the higher volume of aggregates have a higher absorption.

Water absorption is typically reported without considering the effect of the absorption of the aggregate in the samples. To better understand its effect, Fig. 13 was calculated assuming five different sand absorptions (0.0%, 0.6%, 1.2%, 1.8%, and 2.4%) to then subtract these values from the absorption in Fig. 12b. When the sand absorption is assumed to be 0.0%, the resulting absorption at 8 days will be the same as the absorption presented in Fig. 12b. From Fig. 13, it can be noticed that for the assumed 1.8% sand absorption, the normalized water absorbed for the sample is the same after 8 days, independent of the amount of aggregate in the sample.

Fig. 14 shows a desorption isotherm for the sand used in these mixtures. It can be noted that at 50% RH (humidity at which the samples were conditioned), the amount of water on the sand is

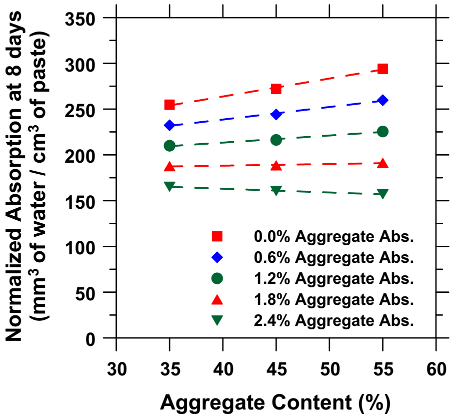

Fig. 13. Water absorption at 8 d normalized by volume of paste, corrected by different values of aggregate absorption.

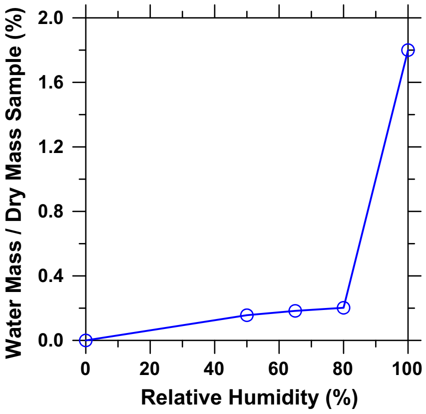

Fig. 14. Desorption isotherm for the sand used in this research.

about 0.2%. Considering that the aggregate used in this study has a 24 h absorption of 1.8%, this would imply that an effective aggregate desorption of 1.6% would have occurred in the samples at 50% relative humidity. This is reasonably consistent with the difference in water absorption of samples containing different amounts of aggregate and their absorption can be explained mainly by the amount of water absorbed by the aggregates.

5. Conclusions

This paper has described the absorption behavior of mortars conditioned at different relative humidities. As was shown in previous works by Hall [12], Hooton et al. [4,7] and Martys and Ferraris [16,34], the water absorption test is considerably affected by the relative humidity of the samples before starting the test, which if not properly accounted for can lead to a misunderstanding of the actual absorption behavior. Samples conditioned at a 50% relative humidity can show a total absorption that is approximately six times greater than similar samples conditioned at 80% relative humidity. This is consistent with expectations based on the mortars' desorption curves.

Initial sorptivity, secondary sorptivity and total absorption at 8 days for samples conditioned in chambers show a linear trend related to the *w/c* and the relative humidity at which samples were conditioned. Samples that are conditioned by drying in an oven at 105 °C do not follow the same trend as samples conditioned in other approaches. This is attributed to two factors: (1) emptying of a wider range of pores, and (2) the potential for microcracking. The conditioning procedure described in ASTM C1585-04 is not able to eliminate the "moisture history" of the samples, and thus can lead to a misunderstanding of the water absorption test results, especially in field samples which have obtained a lower relative humidity. It is recommended that field samples be pre-saturated prior to being exposed to the conditioning regimen of ASTM C1585.

Comparing samples containing different volumes of aggregate can also lead to a misunderstanding of the actual absorption behavior. Samples containing higher volumes of cement paste will absorb more water. When the results are normalized by the volume of cement paste, the sample containing lower volumes of cement paste will absorb more water. However, for the materials examined in this study, this difference can be mainly explained by the amount of water absorbed by the aggregates in the sample.

Acknowledgments

This work was supported in part by the Joint Transportation Research Program administered by the Indiana Department of Transportation and Purdue University (Project SPR 3093). The contents of this paper reflect the views of the authors, who are responsible for the facts and the accuracy of the data presented herein, and do not necessarily reflect the official views or policies of the Federal Highway Administration and the Indiana Department of Transportation, nor do the contents constitute a standard, specification, or regulation. The authors gratefully acknowledge support received from the Center for Advanced Cement Based Materials.

References

[1] ASTM International, ASTM C1585. Standard test method for measurement of rate of absorption of water by hydraulic-cement concretes; 2004.
[2] Sabir B, Wild S, O'Farrell M. A water sorptivity test for mortar and concrete. Mater Struct 1998;31(8):568–74.
[3] Maltais Y, Samson E, Marchand J. Predicting the durability of Portland cement systems in aggressive environments – laboratory validation. Cement Concrete Res 2004;34(9):1579–89.
[4] Hooton RD, Mesisc T, Beal DL. Sorptivity testing of concrete as an indicator of concrete durability and curing efficiency. In: Proceedings of the third Canadian symposium on cement and concrete, Ottawa, Ontario; 1993. p. 264–75.
[5] Parrot LJ. Water absorption in cover concrete. Mater Struct 1992;25(5):284–92.
[6] Fagerlund G. Predicting the service-life of concrete exposed to frost action through a modeling of the water absorption process in the air pore system. In: Jennings H, Kropp J, Scrivener K, editors. The modeling of microstructure and its potential for studying transport properties and durability. The Netherlands; 1996. p. 503–39.
[7] Hearn N, Hooton D, Mills R. Pore structure and permeability. In: Klieger P, Lamond J, editors. Significance of tests and properties of concrete and concrete-making materials. ASTM STP 169C; 1994. p. 240–62.
[8] Henkensiefken R, Castro J, Bentz D, Nantung T, Weiss J. Water absorption in internally cured mortar made with water-filled lightweight aggregate. Cem Concr Res 2009;39(10):883–92.
[9] Neithalath N. Analysis of moisture transport in mortars and concrete using sorption-diffusion approach. ACI Mater J 2006;103(3):209–18.
[10] Yang Z. Assessing cumulative damage in concrete and quantifying its influence on life cycle performance modeling. PhD thesis, Purdue University; 2004.
[11] Bentz DP, Ehlen MA, Ferraris CF, Garboczi EJ. Sorptivity-based service life predictions for concrete pavements. In: Proceedings 7th international conference on concrete pavements, Orlando FL; 2001. p. 181–93.
[12] Hall C. Water sorptivity of mortars and concretes: a review. Mag Concr Res 1989;41(146):51–61.
[13] Spragg R, Castro J, Li W, Pour-Ghaz M, Huang P, Weiss J. Wetting and drying of concrete using aqueous solution containing deicing salt. Cem Concr Compos 2011;33(5):535–42.
[14] Yang Z, Weiss J, Olek J. Water absorption in partially saturated fracture concrete. RILEM workshop: transport mechanism in cracked concrete. Ghent; 2007.
[15] Martys NS. Diffusion in partially saturated porous materials. Mater Struct 1999;32(8):991–1004.
[16] Martys N, Ferraris CF. Capillary transport in mortar and concrete. Cem Concr Res 1997;27(5):747–60.
[17] Lockington D, Parlange JY, Dux P. Sorptivity and the estimation of water penetration into unsaturated concrete. Mater Struct 1999;32(5):342–7.
[18] Hall C. Anomalous diffusion in unsaturated flow: fact or fiction? Cem Concr Res 2007;37(3):378–85.
[19] Powers TC, Brownyard TL. Studies of the physical properties of hardened Portland cement paste. Am Concr Inst Proc 1946;43:469–82.
[20] Parrott LJ. Moisture conditioning and transport properties of concrete test specimens. Mater Struct 1994;27(8):460–8.
[21] Parrott LJ. Factor influencing relative humidity in concrete. Mag Concr Res 1991;43(154):45–52.
[22] DeSouza SJ, Hooton RD, Bickley JA. Evaluation of laboratory drying procedures relevant to field conditions for concrete sorptivity measurements. Cem Concr Agg 1997;19(2):59–63.
[23] DeSouza SJ, Hooton RD, Bickley JA. A field test for evaluating high performance concrete covercrete quality. Can J Civil Eng 1998;25(3):551–6.
[24] Castro J, Kompare P, Poursaee P, Nantung T, Weiss J. JTRP Report SPR-3093, Portland cement concrete pavement performance relative to permeability. Indiana Department of Transportation; 2010.
[25] ASTM International, ASTM C305. Standard practice for mechanical mixing of hydraulic cement pastes and mortars of plastic consistency; 2006.
[26] ASTM International ASTM C642. Standard test method for density, absorption, and voids in hardened concrete; 2006.
[27] Powers TC, Copeland LI, Mann HM. Capillary continuity or discontinuity in cement pastes. J. PCA Res. Dev. Lab 1959;1(2):38–48.
[28] Hwang C, Young J. Drying shrinkage of portland cement pastes. Microcracking during drying. Cem Concr Res 1984;14(4):585–94.
[29] Chatterji S. Drying shrinkage of cement paste and concrete: a reappraisal of the measurement technique and its significance. Cem Concr Res 1976;6(1):145–8.
[30] Van BisschopJ, Mier J. How to study drying shrinkage microcracking in cement-based materials using optical and scanning electron microscopy? Cem Concr Res 2002;32(2):279–87.
[31] Samaha H, Hover K. Influence of microcracking on the mass transport properties of concrete. ACI Mater J 1992;89(4):416–24.
[32] Yang Z, Weiss J, Olek J. Water transport on concrete damaged by tensile loading and freeze–thaw cycling. J Mater Civil Eng 2006;18(3):424–34.
[33] Yang Z. Assessing cumulative damage in concrete and quantifying its influence on life cycle performance modeling. PhD thesis, Purdue University, West Lafayette, Indiana; 2004.
[34] Bentz DP, Ehlen CF, Ferraris CF, Winpigler JA. Service life prediction based on sorptivity for highway concrete exposed to sulfate attack and freeze–thaw conditions, FHWA-RD-01-162, US Department of Transportation; 2002. p. 62.
[35] Nilsson LO. Hygroscopic moisture in concrete – drying, measurements and related material properties. PhD thesis. Lund University; 1980.

Water Absorption and Electrical Conductivity for Internally Cured Mortars with a W/C between 0.30 and 0.45

Javier Castro[1]; Robert Spragg[2]; and Jason Weiss, M.ASCE[3]

Abstract: Internal curing has emerged over the last decade as an approach to counteract the negative effects associated with self-desiccation in low water-to-cement ratio (w/c) mixtures. Specifically, much of the early research on internal curing focused on the reduction of autogenous shrinkage. Recent work has demonstrated, however, that internal curing can also be beneficial in reducing drying-shrinkage cracking, reducing the propensity for thermal cracking, reducing fluid absorption, and reducing ion diffusion in concrete. However, several aspects of internal curing still require closer examination. One of these aspects is the application of internal curing for mixtures with a wider range of water-to-cement ratios. This paper describes results from experiments that investigated the potential use of internal curing in mortar systems with w/c ratios of 0.30, 0.36, 0.42, and 0.45 that were cured under sealed conditions, in terms of water absorption and electrical conductivity. Test results show that internal curing reduces the water absorption in all the systems. Similarly, results obtained on electrical conductivity at late ages (1 year) also show a benefit. Care needs to be taken to analyze electrical conductivity results at early ages because of the increased amount of fluid resulting from the inclusion of the prewetted lightweight aggregate. **DOI: 10.1061/(ASCE)MT.1943-5533.0000377.**

CE Database subject headings: Aggregates; Hydration; Mortars; Mixtures; Absorption; Electrical conductivity.

Author keywords: Internal curing; Lightweight aggregate; Water absorption; Electrical conductivity.

Background on Internal Curing

Internal curing has emerged over the last decade as a method to improve the performance of low water-to-cement ratio (w/c) mixtures [Rilem 2007; American Concrete Institute (ACI) 2008; ACI Committee 231 2010; Schlitter et al. 2010; Bentz and Weiss 2011]. Specifically, internal curing refers to the use of prewetted lightweight aggregate (LWA) or other water filled inclusions, such as super absorbent polymers (SAP) or cellular fibers that can provide curing water throughout the cross section of the concrete. This differs from conventional water curing in which water is provided after placement, and in which the water is applied only at the surface of the concrete. Internal curing was originally promoted to reduce autogenous shrinkage and autogenous shrinkage cracking (Bentz and Snyder 1999; Jensen and Hansen 2001a; Jensen and Hansen 2001b; Jensen 2005; Cusson and Hoogeveen 2008; Lopez et al. 2009). However, its potential benefits include reducing drying-shrinkage cracking (Henkensiefken et al. 2009a), reducing the likelihood of thermal cracking (Schlitter et al. 2010; Byard et al. 2010) and reducing the likelihood of plastic-shrinkage cracking (Henkensiefken et al. 2010). Internal curing can also improve freeze-thaw resistance (INDOT 2010), increase the resistance to fluid absorption (Bentz and Snyder 1999; Henkensiefken et al. 2009b; Peled et al. 2010) and reduce ion diffusion (Bentz 2009) in concrete. Internal curing has great potential for the concrete industry to create a longer lasting, more sustainable product. Several aspects of internal curing still require closer examination. One of these aspects is the use of internal curing for mixtures containing a wider range of water-to-cement ratios (e.g., mixtures with a w/c between 0.30 and 0.45), for which only a few publications are available (Espinoza and Lopez 2011).

To fully understand how internal curing works it must be recognized that the hydration of cement paste causes a volume reduction that is known as chemical shrinkage (Le Chatelier 1900; Powers 1935; L'Hermite 1960). While chemical shrinkage begins when the water comes in contact with the cement, it has different impacts on the system before and after the paste sets. Before setting, chemical shrinkage causes bulk shrinkage of the cement paste that is equal to the total external volume change. After setting, however, the cement paste becomes stiff enough to resist a portion of the volume change caused by chemical shrinkage (Barcelo et al. 1999; Sant et al. 2006). Contact between the cement particles does not permit this volume reduction to occur. As a result, vapor-filled pockets form inside the cement paste in the largest pores (Jensen and Hansen 2001b; Couch et al. 2006; Lura et al. 2009). This is known as self-desiccation.

Chemical shrinkage occurs in all cementitious materials, irrespective of the w/c (Geiker 1983). In low w/c mixtures, these vapor-filled cavities can result in substantial relative humidity reduction and shrinkage because the vapor-filled cavities form in relatively small pores with a small radius of curvature (Bentz and Jensen 2004; Radlinska et al. 2008; Lura et al. 2009). In higher w/c mixtures, these vapor-filled spaces also develop, however they occur in much larger pores with less impact on volume change. As a result, it is thought that many of the higher w/c systems would not derive as much benefit from internal curing.

---

[1] Assistant Professor, Pontificia Universidad Catolica de Chile, School of Engineering, Casilla 306, Correo 22, Santiago, Chile (corresponding author). E-mail: jecastro@ing.puc.cl

[2] Undergraduate Research Assistant, School of Civil Engineering, Purdue Univ., 550 Stadium Mall Dr., West Lafayette, IN 47907. E-mail: rspragg@purdue.edu

[3] Professor, Director of Pankow Materials Laboratory, Purdue Univ., 550 Stadium Mall Dr., West Lafayette, IN 47907. E-mail: wjweiss@ecn.purdue.edu

Note. This manuscript was submitted on February 21, 2011; approved on August 17, 2011; published online on August 19, 2011. Discussion period open until July 1, 2012; separate discussions must be submitted for individual papers. This paper is part of the ***Journal of Materials in Civil Engineering***, Vol. 24, No. 2, February 1, 2012. ©ASCE, ISSN 0899-1561/2012/2-223–231/$25.00.

Lightweight aggregates are used as a water reservoir that can provide water to replenish the empty pore volume that is created by chemical shrinkage during hydration. Since water is removed from large pores to small pores, the ideal lightweight aggregate would have pore sizes larger than the pore size that develops in the cement paste (Bentz 2009; Castro et al. 2011a). This is the case for many commercially available expanded clays, slates, and shales (Castro et al. 2011a).

Approaches for Mixture Proportioning of Internally Cured Concrete

The design of concrete for internal curing requires that a sufficient amount of water is placed in the concrete to aid in hydration and to overcome the effects of self-desiccation. Different approaches have been used during recent years to determine and quantify the amount of water needed for internal curing. Two of the most widely used approaches are discussed here.

Bentz and Snyder Approach

Bentz and Snyder (1999) developed an approach to determine the volume of prewetted LWA that should be used to "ensure adequate water for complete curing of concrete, which means that the cement reaches the maximum degree of hydration that is possible, given the space limitation for forming hydration products in low w/c systems." It is derived from the concept of filling the volume of pores created by chemical shrinkage with water from the LWA (Bentz et al. 2005). This approach was first published by Bentz and Snyder (1999), shown as

$$M_{\mathrm{LWA}} = \frac{C_f \times CS \times \alpha_{\max}}{S \times \phi_{\mathrm{LWA}}} \tag{1}$$

where M_{LWA} ($\mathrm{kg/m^3}$) = mass of LWA (in a dry state) that needs to be water-filled to provide water to fill in the voids created by chemical shrinkage; C_f ($\mathrm{kg/m^3}$) = cement content of the mixture; CS (g of water per g of cement) = chemical shrinkage of the cement; $\alpha_{\max}$ (unitless) = expected maximum degree of hydration: [(w/c)/0.36] for w/c below 0.36, or 1 for w/c higher than 0.36; Φ_{LWA} (kg of water/kg of dry LWA) = absorption capacity of LWA (24 h absorption value); and S (unitless) = expected degree of saturation of the LWA, expressed as a function of absorption value (Φ_{LWA}). Water absorption and S values from the most used LWA in America were previously reported by Castro et al. (2011a).

In theory, this approach may overestimate the amount of water required for internal curing because it considers the volume change that occurs before setting (Henkensiefken et al. 2009a), however this approach is preferred because of its simplicity.

Jensen and Hansen Approach

Jensen and Hansen (2001a) developed an approach to proportion internally cured mixtures with the intention of limiting the negative effects of self-desiccation in cementitious systems by maximizing the volume of cement that can react. The equations were developed on the basis of the Powers' model to calculate the minimum amount of water that needs to be stored (entrained) to enable the maximum degree of hydration. It was published by Jensen and Hansen (2001a) and is expressed as

$$(\mathrm{w/c})_e = \begin{cases} 0.18(\mathrm{w/c}); & \text{for w/c} < 0.36 \\ 0.42 - (\mathrm{w/c}); & \text{for } 0.36 \le \text{w/c} \le 0.42 \\ 0 & \text{for w/c} > 0.42 \end{cases} \tag{2}$$

where $(\mathrm{w/c})_e$ = amount of additional water for internal curing, expressed as g of water per g of cement; and w/c = original water-to-cement ratio of the system.

Extension of Internal Curing to High W/C Systems

Fig. 1 (after Bentz et al. 2005) illustrates both approaches as a function of w/c. Below a w/c of 0.36, both approaches are identical. The Bentz approach adds water to fill all of the chemical shrinkage volume, which causes it to stay constant above a w/c of 0.36, while the Jensen approach considers adding only the water needed for full hydration—resulting in the recommend quantity of water decreasing above a w/c of 0.36.

Both approaches assume that all of the mixing water will be accessible to react with the unhydrated cement. Issues associated with the distance that the water needs to travel, a lack of adequate mixing, or excessive evaporation from the specimens, are not considered. These issues may decrease the amount of hydration that occurs and may increase the porosity of the system and its connectivity.

Research Objectives

The objective of this research is to examine the potential benefits of internal curing in mortar systems with a w/c of 0.30–0.45. In particular, this research will evaluate the benefits (in terms of water absorption and electrical conductivity) of systems with w/c of 0.30, 0.36, 0.42, or 0.45.

Materials

ASTM C150 Type I ordinary portland cement (OPC) was used in this study, with a Blaine fineness of 370 $\mathrm{m^2/kg}$ and an estimated Bogue composition of 56% C_3S, 16% C_2S, 12% C_3A, 7% C_4AF, and a Na_2O equivalent of 0.68% by mass.

The sand used was natural river sand with a fineness modulus of 2.71, an apparent specific gravity of 2.58, and water absorption of 1.0% by mass. Portions of the normal weight sand were replaced with expanded shale with a fineness modulus of 3.10 and a specific gravity of 1.45. The 24 h absorption of the fine lightweight aggregate was determined to be 17.5% by the paper towel method (NYDOT 2008, Castro et al. 2011a). This test involves immersing

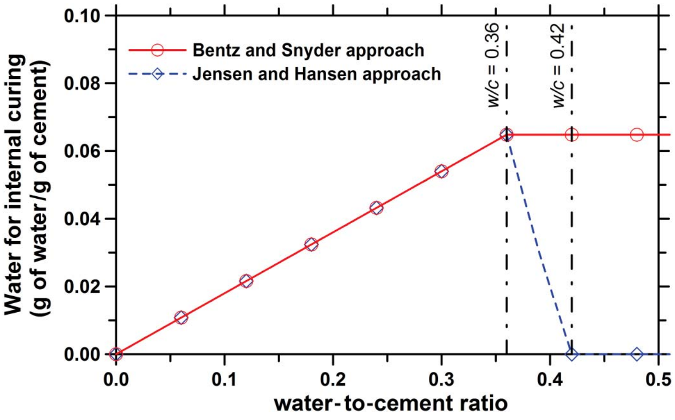

Fig. 1. Water for internal curing required to maintain saturated condition in cement paste (data from Bentz et al. 2005)

the aggregate in water for 24 h, after which time the water is decanted and the surface of the aggregate is patted dry. The paper towel method spreads the aggregate out, and the paper towel is placed across the surface of the aggregate. This process is repeated at different moisture contents [preferably near the surface dry (SD) condition]. Once it appears that the paper towel is no longer picking up moisture (as determined by visual inspection for a change in color of the paper towel) from the aggregate, it is assumed that an SD condition has been reached and the aggregate moisture can be determined.

Mixture Proportioning

Twenty different mixtures were prepared. The mortars had a single volume fraction of fine aggregate (55% of the total volume) and different w/c (0.30, 0.36, 0.42, or 0.45). For each system, fine LWA (FLWA) was used as a replacement for NWA sand at five different levels: 0, 25, 50, 75, and 100% of the values calculated using Eq. (1). The replacement is performed on a total volume basis; the volume of aggregate (FLWA and sand) remained constant at 55% because only the sand was replaced with FLWA. A list of the mixture proportions can be found in Table 1.

Mixing Procedure

The mixing procedure used for the mortar was in accordance with ASTM C305 (ASTM 2006). The FLWA was oven dried, air cooled, and then submerged in water for 24 ± 1 h prior to mixing. The volume of water used to submerge the FLWA included both mixing water and the water the FLWA would absorb in 24 h. The excess water (water not absorbed in 24 h) was then decanted and used as the mixing water. The normal weight sand was oven dried and cooled for 24 h before mixing.

Experimental Procedures

Water Absorption

Six 100 mm × 200 mm cylinders were cast for water absorption testing for each mixture. After one day of curing, the samples were demolded and then sealed in a double layer of plastic bags for sealed curing. Bags were stored at 23 ± 1°C until samples reached an age of 90 d. At that point, the cylinders were removed from the bags and three 50 ± 2 mm thick samples were cut from the central portion of each cylinder using a wet saw. Obtaining samples from the central portion of the cylinders allows for testing of the core of the material, instead of testing the finishing of the surface.

After cutting, samples were conditioned by placing them in environmental chambers at 23 ± 0.5°C and at two different relative humidities (65 ± 1% and 80 ± 1%). Samples were kept in the environmental chamber until they reached mass equilibrium, defined as a mass change of less than 0.02% over a 15-day period. Mixtures conditioned at 65 ± 1% RH required the longest period of time (9 months) to reach mass equilibrium. However, all samples were maintained in the chambers for 9 months to test them all at the same age.

This conditioning procedure was preferred to the procedure described in ASTM C1585 (ASTM 2004) because it has been shown (Castro et al. 2011b) that the standard procedure is unable to eliminate the "moisture history" of the samples. As the mortars used in this research have different amounts of LWA (i.e., different initial amounts of water), the samples will have different initial moisture content, and the ASTM C1585 (ASTM 2004) procedure will be not able to correctly condition the samples.

Once the samples were removed from the chambers, the side surface (i.e., outer circumference) was sealed with aluminum tape, and the top surface was covered with plastic, to avoid evaporation from the sample during testing. After the samples were prepared, absorption testing was conducted in accordance with ASTM C1585

Table 1. Mixture Proportions for the Internally Cured Mixtures

	% LWA	Cement	Mixing water	NWA, SSD	LWA, dry	IC water	Aggregate volume (%)		
w/c	from Eq. (1)	(kg/m^3)	(kg/m^3)	(kg/m^3)	(kg/m^3)	(kg/m^3)	NWA	LWA	Total
0.30	0%	727.0	218.1	1,429.7	0.0	0.0	55.0	0.0	55.0
	25%	727.0	218.1	1,330.2	55.4	9.7	51.2	3.8	55.0
	50%	727.0	218.1	1,230.6	110.8	19.4	47.3	7.7	55.0
	75%	727.0	218.1	1,131.1	166.2	29.1	43.5	11.5	55.0
	100%	727.0	218.1	1,031.5	221.6	38.8	39.7	15.3	55.0
0.36	0%	662.6	238.6	1,419.7	0.0	0.0	55.0	0.0	55.0
	25%	662.6	238.6	1,320.9	60.6	10.6	50.8	4.2	55.0
	50%	662.6	238.6	1,212.0	121.2	21.2	46.6	8.4	55.0
	75%	662.6	238.6	1,103.1	181.8	31.8	42.4	12.6	55.0
	100%	662.6	238.6	994.2	242.4	42.4	38.2	16.8	55.0
0.42	0%	608.7	255.7	1,429.7	0.0	0.0	55.0	0.0	55.0
	25%	608.7	255.7	1,329.7	55.7	9.7	51.2	3.8	55.0
	50%	608.7	255.7	1,229.7	111.4	19.4	47.3	7.7	55.0
	75%	608.7	255.7	1,129.7	167.1	29.1	43.5	11.5	55.0
	100%	608.7	255.7	1,029.7	222.8	38.8	39.6	15.4	55.0
0.45	0%	584.9	263.2	1,429.7	0.0	0.0	55.0	0.0	55.0
	25%	584.9	263.2	1,333.6	53.5	9.4	51.3	3.7	55.0
	50%	584.9	263.2	1,237.5	107.0	18.8	47.6	7.4	55.0
	75%	584.9	263.2	1,141.4	160.5	28.2	43.9	11.1	55.0
	100%	584.9	263.2	1,045.3	214.0	37.6	40.2	14.8	55.0

(ASTM 2004), with the exception of the conditioning method described above.

The effect of internal curing can be increased under the sealed conditions employed in this study as compared with other curing conditions (unsealed curing or curing under lime water). Using sealed curing, the internally cured specimens will have a greater amount of water available for hydration, and will likely hydrate further, producing a denser microstructure with lower transport coefficients. The authors consider that the sealed curing condition can isolate the effect of internal curing on the specimens. However, the authors also consider that differences in the curing conditions for both internally and not internally cured specimens can affect the performance of the specimens.

Electrical Impedance

The electrical conductivity of mortar samples was measured using cylindrical specimens (70-mm height and 35-mm diameter). Two 2.5-mm diameter rods, spaced 20 mm apart, were embedded longitudinally inside each mold (Fig. 2).

A Solartron 1260 Impedance Gain-Phase analyzer measured the impedance response of each specimen. The measurements were made over a frequency range from 1 MHz to 1 Hz, using a 100 mV AC signal. Measurements were performed at 3 d, 7 d, 90 d, and 365 d.

The electrical conductivity was obtained from the measured bulk resistance as follows:

$$\sigma = \frac{k}{R} \tag{3}$$

where σ = conductivity (S/m); k = geometry factor (1/m); and R = bulk resistance (ohm). A geometry factor of $k = 22.15/\mathrm{m}^{-1}$ was determined for the molds used in this study, through the use of a solution with a known electrical conductivity.

A modified parallel model is normally used to describe the electrical conductivity of the concrete (McCarter and Brousseau 1990; Rajabipour 2006). Because the conductivity of the liquid phase is several orders of magnitude higher than the conductivity of the solid and vapor phases, concrete is normally considered a composite material with a single conductive component, and the modified parallel model can be simplified to Eq. (4). This typically assumes that only the fluid phase is conductive. For internally cured concrete mixtures, however, the water in the LWA may also be conductive and the implications of this will be discussed later in the paper.

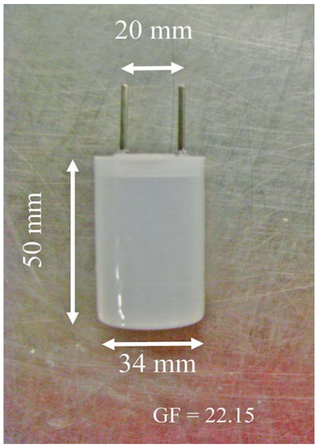

Fig. 2. Mold used for continuous electrical conductivity measurements

$$\sigma = \sigma_o \phi_o \beta_o \tag{4}$$

where σ_o = conductivity of the pore solution, sigma notch (S/m); ϕ_o = volume fraction of pore solution (unitless); and β_o = connectivity of pore structure (unitless).

Experimental Results and Discussion

Water Absorption

Fig. 3 shows the cumulative absorbed water in the samples that were 1 year old (3 months of sealed curing and 9 months of conditioning) after 8 d of testing, for samples conditioned at 65 and 80% relative humidity. Fig. 4 shows the initial sorptivity (i.e., related to the rate of water absorption) for samples conditioned at 65 and 80% relative humidity, calculated as the slope of the absorption versus the square root of time during the first six hours of testing. Fig. 5 shows the secondary sorptivity for samples conditioned at 65 and 80% relative humidity, calculated as the slope of the absorption versus the square root of time from the second to the eighth day of testing.

In Figs. 3–5, the water absorption is very sensitive to both the relative humidity at which the specimens were preconditioned before testing (Castro et al. 2011b) and the w/c of the systems. Samples conditioned at 65% relative humidity show higher values than similar samples conditioned at 80% relative humidity. Samples from mixtures with a higher w/c show higher absorption values

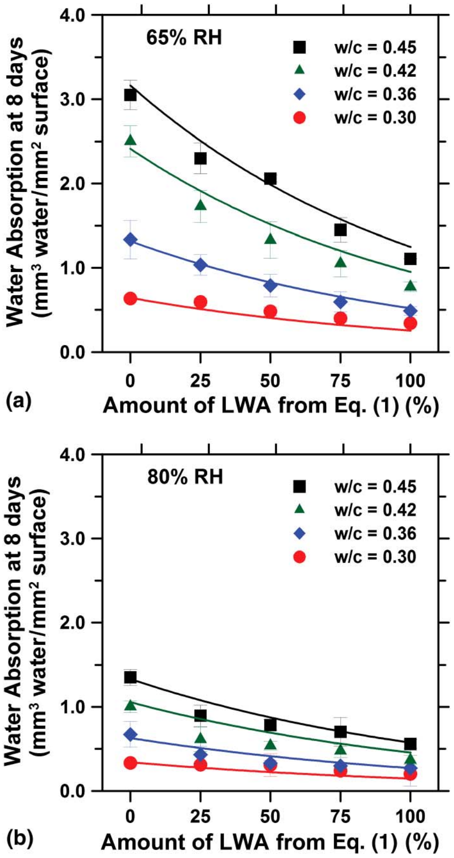

Fig. 3. Cumulative amount of water absorbed after 8 days of testing for samples conditioned at (a) 65% RH, (b) 80% RH; error bars represent standard deviation of 3 samples; continuous lines represent empirical equations described subsequently

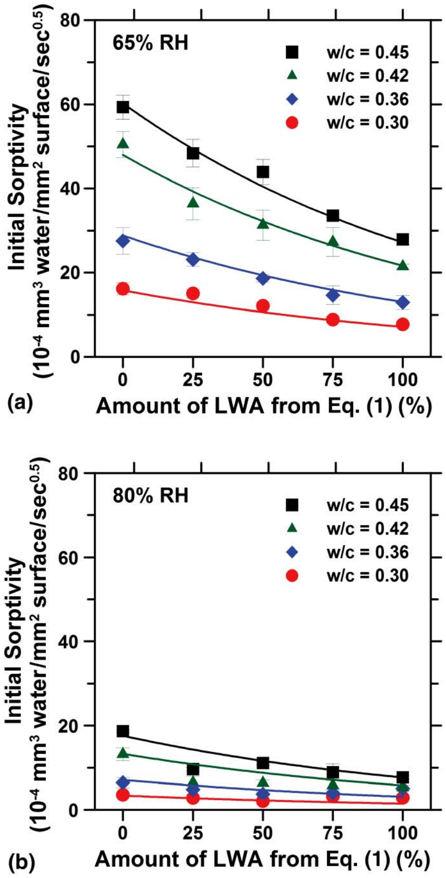

Fig. 4. Initial sorptivity as a function of w/c and the amount of LWA for samples conditioned at (a) 65% RH, (b) 80% RH; error bars represent standard deviation of 3 samples; continuous lines represent empirical equations described subsequently

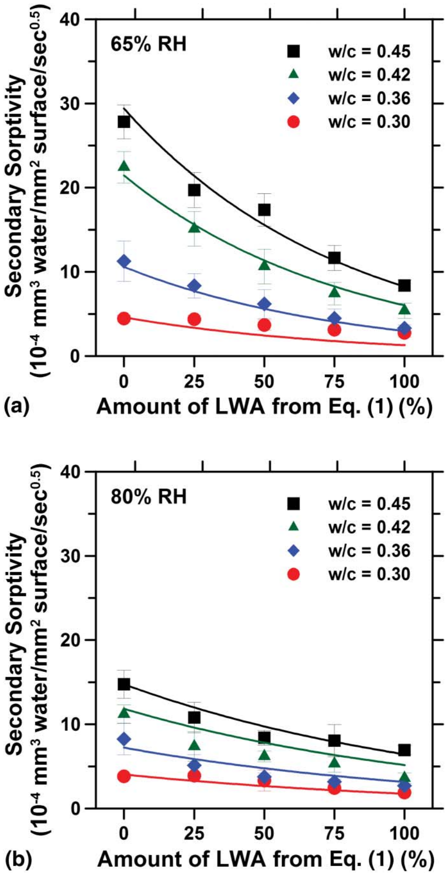

Fig. 5. Secondary sorptivity as a function of the w/c and the amount of LWA for samples conditioned at (a) 65% RH, (b) 80% RH; error bars represent standard deviation of 3 samples; continuous lines represent empirical equations described subsequently

compared with samples with lower w/c, both conditioned at the same relative humidity.

These trends can be explained by the fact that water ingress in unsaturated concrete is dominated by capillary suction upon initial contact with water (Hall 1989). Capillary absorption is related to the volume of the pores, as well as the size of empty capillary pores. Systems with higher w/c will have a greater proportion of capillary pores. The relationship between the equilibrated relative humidity and the radius of the smallest empty pore is given by the Kelvin-Laplace equation. Using this equation, it is possible to calculate that these capillary pores are filled with water vapor at relative humidities above 80%.

As such, the relative humidity used to condition the sample prior to the sorption test and the w/c of the system can have a significant impact on the results. The higher the w/c of the system, the greater the total volume of the capillary pores. The lower the relative humidity, the greater the total volume of pores that are empty and available to be filled with water during the sorption test. Further, the lower humidity will empty smaller pores, creating a higher suction force in the materials and resulting in a greater sorption rate and a larger overall total absorption.

In Figs. 3–5, the total volume of water and the rate of absorbed water decrease when a higher amount of FLWA is used. This observation is independent of both the relative humidity used for conditioning and the w/c of the system. Even more, it seems that a greater benefit is obtained in those mixtures containing the highest w/c.

When water leaves the pores of the LWA, it is available in the cement paste to enable additional hydration. This additional hydration results in a paste microstructure that is more dense, which has a large impact on the cement paste matrix (Henkensiefken et al. 2009b). Internal curing can also increase the hydration of the areas surrounding the LWA (Henkensiefken et al. 2009b), producing a more dense interfacial transition zone (ITZ; Zhang and Gjørv 1990; Elsharief et al. 2005). Considering that the ITZ of the normal weight aggregate (NWA) can be percolated across the 3D microstructure, the inclusion of the LWA could depercolate these ITZ pathways (Winslow et al. 1994; Bentz 2009; Peled et al. 2010). If LWA, with the more dense ITZ it creates, was added to the system, the NWA ITZ may not be as percolated, resulting in a lower absorption. As more LWA is used, the potential for percolation of the normal weight aggregate ITZ also decreases. If enough LWA is used, the ITZ of the NWA would depercolate (Bentz 2009). For this reason, it could be expected that the absorption of mortars with LWA could be lower, even in systems with a high w/c.

The benefits of internal curing are most dramatic for specimens cured under sealed conditions like those used in the study (as compared with curing under lime water). Under sealed conditions, the internally cured specimens have a greater amount of water available for hydration than the plain samples. This increased hydration produces a more dense microstructure with lower transport coefficients (Bentz and Weiss 2011).

Electrical Impedance

Fig. 6 shows the electrical conductivity of sealed samples at of 3, 7, 90, and 365 days after casting. The systems with higher w/c have a higher conductivity mainly because of the higher volume of pore fluid described by Eq. (4). The conductivity decreases with time as a result of continued hydration, which reduces the volume of conductive pore fluid and also makes the conduction path more tortuous.

The mixture with a w/c of 0.30 shows that internal curing results in a reduction of the measured conductivity that can be explained by the effect of the water provided for internal curing helping to increase the hydration of areas surrounding the FLWA (Henkensiefken et al. 2009b). However, in the systems with higher w/c, an increase in the FLWA content increases the electrical conductivity at early ages. This may be explained by the fact that these systems have water contained in the FLWA particles that remains for a longer time in the FLWA pores without reacting with unhydrated cement. As a result, the total amount of fluid in the system will increase with additional FLWA, thereby increasing the measured electrical conductivity of the samples.

As the samples hydrate (e.g., for 90 days), the system with $w/c = 0.36$ starts to show the benefits of internal curing, decreasing the conductivity. At this time, systems with higher w/c still show higher conductivity with the use of FLWA (again because of additional water in the system). Finally, at 365 days, all the systems show the benefits of the use of internal curing. At this age, a considerable reduction of the measured electrical conductivity can be observed.

The water for internal curing requires longer times to leave the FLWA pores in higher w/c systems because of the lack of a driving force (which is the under-pressure build-up resulting from self-desiccation in the case of a low w/c system). However, at some point, the smaller pores of the cement paste will develop a meniscus that will make the water move from the FLWA pores to the cement paste. Eventually, this water will react with the unhydrated cement to increase the amount of hydration product, reducing both the total porosity and the fluid filling the pores of the system. This will produce a reduction in the measured electrical conductivity. If the cement in high w/c systems is able to hydrate further than low w/c systems, high w/c systems will require more cement hydration to depercolate (Powers 1948), which can also explain the benefit of internal curing in these mixtures.

A direct comparison of the electrical conductivity of the systems containing different w/c presents some difficulties, mainly because of complications associated with determining the volume fraction of the pore solution at different ages. For this reason, after the electrical conductivity of the samples was measured in a sealed condition at 365 d, samples were soaked with tap water under vacuum for 3 h at 29 mm Hg and then kept under water until 24 h without release of the vacuum. After saturation, electrical conductivity was measured again and results are shown in Fig. 7.

The conductivities presented in Fig. 7 are proportional to the total volume of accessible pores and their connectivity through the samples. These are parameters that can be used to describe the transport of fluid in concrete (Rajabipour and Weiss 2007). Fig. 7 shows that using internal curing on systems with high w/c helps to reduce the connectivity of the porosity, which helps to reduce the fluid transport in concrete.

Comparing Figs. 6(d) and 7, it can be observed that the electrical conductivity increases when samples were resaturated. This can be

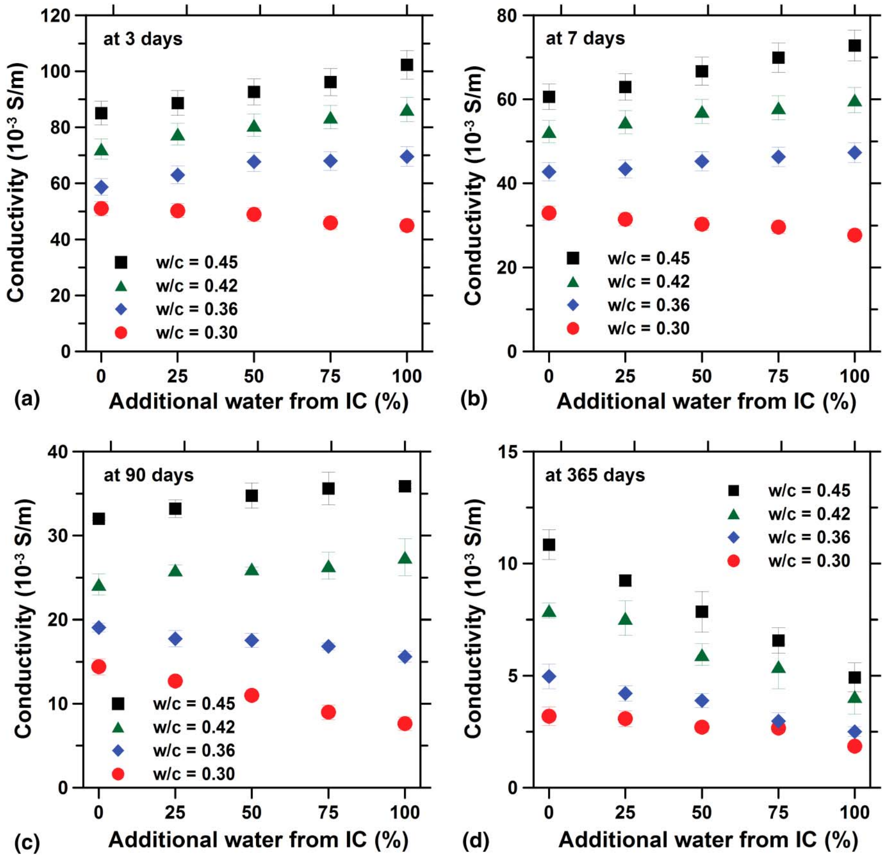

Fig. 6. Electrical conductivity of sealed samples as a function of the amount of LWA at (a) 3 days, (b) 7 days, (c) 90 days, and (d) 365 days; error bars represent the standard deviation of 3 samples

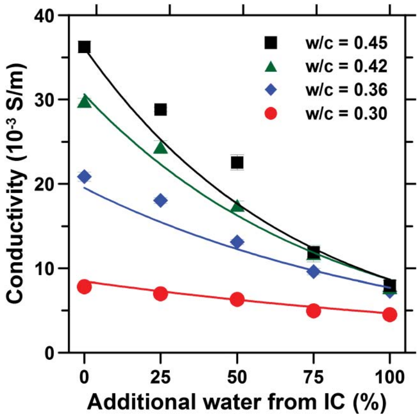

Fig. 7. Electrical conductivity of vacuum-saturated samples at 365 days; error bars represent the standard deviation of 3 samples; continuous lines represent empirical relations described subsequently

explained by the fact that resaturation results in a higher volume of pore fluid, as described by Eq. (4). However, sample resaturation does not seem to fill the FLWA pores, because an increase of conductivity with the percentage of FLWA is not observed.

Empirical Relationship for Water Absorption and Electrical Conductivity

From Figs. 3–5, it is possible to obtain an empirical relationship for the cumulative absorption (for samples conditioned at 65 and 80% RH), which is presented in Eq. (5). A similar form of equation can be used to characterize initial and secondary sorptivities. From Fig. 7, it is possible to obtain an empirical relationship for the saturated electrical conductivity, which is presented in Eq. (6).

$$\text{Absorption} = C_1 \cdot (\text{w/c})^{C_2} \cdot \exp(-C_3 \cdot \text{IC}) \tag{5}$$

$$\text{Conductivity} = [C_4 \cdot (\text{w/c}) - C_5] \cdot \exp[(-C_6 \cdot (\text{w/c}) + C_7) \cdot \text{IC}] \tag{6}$$

where w/c = water-to-cement ratio (e.g., 0.36); IC = internal curing percentage from Eq. (1) (e.g., IC = 50 means 50% of the IC water predicted from Eq. (1)); and C_1, C_2, C_3, C_4, C_5, C_6 and C_7 = regression constants (values in Table 2).

Fig. 8 illustrates the proportional reduction of water absorption, initial sorptivity, and secondary sorptivity for internally cured samples. Fig. 9 illustrates the proportional reduction of electrical conductivity of 1 year old saturated, internally cured samples.

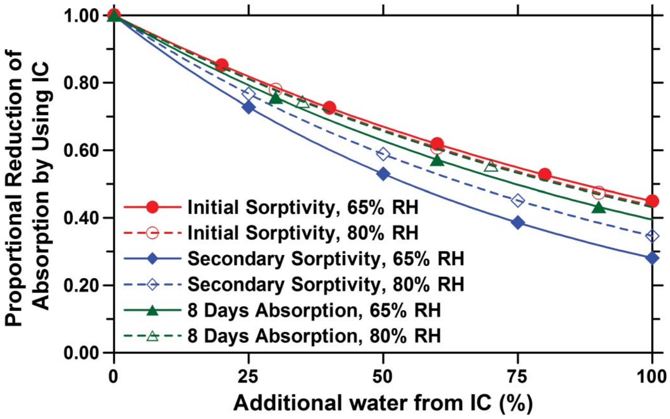

Fig. 8. Proportional reduction of absorption, initial sorptivity, and secondary sorptivity of internally cured samples

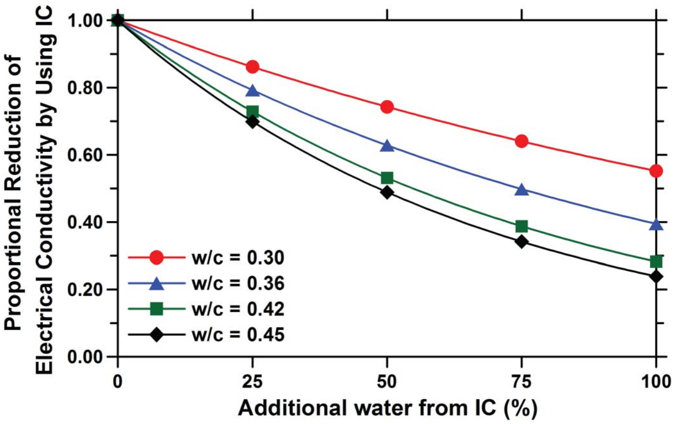

Fig. 9. Proportional reduction of electrical conductivity of 1-year-old saturated, internally cured samples

In Fig. 8, when FLWA is added according to the Bentz and Snyder approach [Eq. (1)], the internally cured system shows an average reduction of 55% in the initial sorptivity and the 8-d cumulative absorption, and 70% in the secondary sorptivity, independent of the relative humidity at which the samples were conditioned prior to testing and the w/c of the mixtures.

In Fig. 9, internal curing is more efficient for reducing the electrical conductivity in high w/c systems than low w/c systems. A 40% reduction in conductivity is observed in the system with a w/c of 0.30, but a reduction of 75% is observed in the system with a w/c of 0.45.

Conclusions

A series of 20 mortars were prepared to evaluate the effect of internal curing on the fluid transport properties of mortars over

Table 2. Parameters for Eqs. (5) and (6)

	Water absorption at 8 d		Initial sorptivity		Secondary sorptivity		(1 year) Electrical conductivity
Parameters	65% RH	80% RH	65% RH	80% RH	65% RH	80% RH	Saturated
C_1	72.776	19.391	0.084	0.045	0.113	0.019	—
C_2	3.93	3.35	3.30	4.06	4.57	3.20	—
C_3	0.0093	0.0084	0.0080	0.0083	0.0127	0.0106	—
C_4	—	—	—	—	—	—	184.59
C_5	—	—	—	—	—	—	46.915
C_6	—	—	—	—	—	—	0.0558
C_7	—	—	—	—	—	—	0.0108

a range of water-to-cement ratios. The effect of internal curing was evaluated using water absorption and electrical conductivity measurements.

The total absorbed water was reduced when the level of internal curing was increased. This reduction in water absorption was known for systems with low w/c, but the results show that the benefits extend to systems with higher w/c. These benefits were also observed in reducing the rate of water absorption, showing a lower initial and secondary sorptivity. An average maximum reduction of 55% was observed in both the initial sorptivity and cumulative absorption, and a maximum reduction of 70% was observed in the secondary sorptivity.

Electrical conductivity tests, performed on sealed samples a year after casting, show a benefit in the use of internal curing in mortar systems containing low w/c as expected, but also in systems with higher w/c. The effect of internal curing is proportionally larger in samples prepared with the highest w/c. A reduction of 40% is observed in the system with a w/c of 0.30; this reduction was observed to increase to 75% in the system with a w/c of 0.45.

The benefits of internal curing are most dramatic for specimens cured in this sealed condition used in this study as compared with curing under lime water. Under sealed conditions, the internally cured specimens have a greater amount of water available for hydration than in plain samples. This increased hydration produces a more dense microstructure with lower transport coefficients.

Precaution is needed to interpret the electrical properties of IC concrete at an early age because of the higher amount of fluid present in the system when prewetted LWA is added.

Acknowledgments

This work was supported in part by the Expanded Shale, Clay, and Slate Institute (ESCSI) and by the Joint Transportation Research Program administered by the Indiana Department. of Transportation and Purdue University (Project SPR 3211), and the authors gratefully acknowledge that support. The contents of this paper reflect the views of the authors, who are responsible for the facts and the accuracy of the data presented herein, and do not necessarily reflect the official views or policies of the Indiana Dept. of Transportation or ESCSI, nor do the contents constitute a standard, specification, or regulation. The experiments reported in this paper were conducted in the Pankow Materials Laboratories at Purdue University. The authors acknowledge the support that has made this laboratory and its operation possible.

References

American Concrete Institute (ACI). (2008). “Internal curing of high performance concrete: laboratory and field experiences.” *ACI SP-256*, Farmington Hills, MI.

American Concrete Institute (ACI) Committee 231. (2010). “Report on early-age cracking: Causes, measurement and mitigation.” Farmington Hills, MI.

ASTM. (2004). “Standard test method for measurement of rate of absorption of water by hydraulic-cement concretes.” *C1585*, West Conshohocken, PA.

ASTM. (2006). “Standard practice for mechanical mixing of hydraulic cement pastes and mortars of plastic consistency.” *C305*, West Conshohocken, PA.

Barcelo, L., Boivin, S., Rigaud, S., Acker, P., and Clauvaud, B. (1999). “Linear vs volumetric autogenous shrinkage measurements: Material behavior or experimental artefact.” *Proc. of the second int. sem. on self-desiccation and its importance in concrete technology*, B. Persson and G. Fagerlund, Lund University, Sweden, 109–125.

Bentz, D. P. (2009). “Influence of internal curing using lightweight aggregates on interfacial transition zone percolation and chloride ingress in mortars.” *Cem. Concr. Compos.*, 31(5), 285–289.

Bentz, D. P., and Jensen, O. M. (2004). “Mitigation strategies for autogenous shrinkage cracking.” *Cem. Concr. Compos.*, 26(6), 677–685.

Bentz, D. P., Lura, P., and Roberts, J. W. (2005). “Mixture proportioning for internal curing.” *Concr. Inter.*, 27(2), 35–40.

Bentz, D. P., and Snyder, K. A. (1999). “Protected paste volume in concrete: Extension to internal curing using saturated lightweight fine aggregate.” *Cem. Concr. Res.*, 29(11), 1863–1867.

Bentz, D. P., and Weiss, J. (2011). “Internal curing: A 2010 state of the art review.” *National NISTIR 7765*, Institute of Standards and Technology, U.S. Dept. of Commerce, Gaithersburg, MD.

Byard, B. E., Schindler, A. K., Barnes, R. W., and Rao, A. (2010). “Cracking tendency of bridge deck concrete.” *Transportation Research Record 2164*, Transportation Research Board, Washington, DC.

Castro, J., Bentz, D., and Weiss, J. (2011a). “Effect of sample conditioning on the water absorption of concrete.” *Cem. Concr. Compos.*, 33(8), 805–813.

Castro, J., Keiser, L., Golias, M., and Weiss, J. (2011b). “Absorption and desorption properties of fine lightweight aggregate for application to internally cured concrete mixtures.” *Cem. Concr. Compos.*, 33(10), 1001–1008.

Couch, J., Lura, P., Jensen, O., and Weiss, J. (2006). “Use of acoustic emission to detect cavitation and solidification (time zero) in cement pastes.” *Int. RILEM Conf. on Volume Changes of Hardening Concrete: Testing and Mitigation*, O. Jensen, P. Lura and K. Kovler, eds., RILEM Publications S.A.R.L., Bagneux, France, 393–400.

Cusson, D., and Hoogeveen, T. (2008). “Internal curing of high-performance concrete with pre-soaked lightweight aggregate sand for prevention of autogenous shrinkage cracking.” *Cem. Concr. Res.*, 38(6), 757–765.

Elsharief, A., Cohen, M., and Olek, J. (2005). “Influence of lightweight aggregate on the microstructure and durability of mortar.” *Cem. Concr. Res.*, 35(7), 1368–1376.

Espinoza-Hijazin, G., and Lopez, M. (2011). “Extending internal curing to concrete mixtures with W/C higher than 0.42.” *Constr. Build. Mat.*, 25(3), 1236–1242.

Geiker, M. (1983). “Studies of portland cement hydration by measurements of chemical shrinkage and a systematic evaluation of hydration curves by means of the dispersion model.” Ph.D. dissertation, Technical Univ. of Denmark, Lyngby, Denmark.

Hall, C. (1989). “Water sorptivity of mortars and concretes: A review.” *Mag. Concr. Res.*, 41(147), 51–61.

Henkensiefken, R., Bentz, D., Nantung, T., and Weiss, J. (2009a). “Volume change and cracking in internally cured mixtures made with saturated lightweight aggregate under sealed and unsealed conditions.” *Cem. Concr. Compos.*, 31(7), 427–437.

Henkensiefken, R., Briatka, P., Bentz, D., Nantung, T., and Weiss, J. (2010). “Plastic shrinkage cracking in internally cured mixtures: Prewetted lightweight aggregate can reduce cracking.” *Concr. Inter.*, 32(2), 49–54.

Henkensiefken, R., Castro, J., Bentz, D., Nantung, T., and Weiss, J. (2009b). “Water absorption in internally cured mortar made with water-filled lightweight aggregate.” *Cem. Concr. Res.*, 39(10), 883–892.

Jensen, O. M. (2005). “Autogenous phenomena in cement-based materials.” Ph.D. thesis, Aalborg Univ., Aalborg, Denmark.

Jensen, O. M., and Hansen, P. F. (2001a). “Water-entrained cement-based materials: I. Principles and theoretical background.” *Cem Concr Res*, 31(4), 647–654.

Jensen, O. M., and Hansen, P. F. (2001b). “Autogenous deformation and RH-change in perspective.” *Cem. Concr. Res.*, 31(12), 1859–1865.

Le Chatelier, H. (1900). “Sur les changements de volume qui accompagnent le durcissement des ciments.” *Bulletin Societe de l’encouragement pour l’industrie nationale*, 5eme serie, tome 5, Paris, France, 54–57.

L’Hermite, R. G. (1960). “Volume changes of concrete.” *4th Int. Symp. on the Chemistry of Cement*, U.S. Dept. of Commerce, National Bureau of Standards, Washington, DC, 659–694.

Lopez, M., Kahn, L. F., and Kurtis, K. E. (2009). “Characterization of elastic and time-dependent deformations in high performance lightweight concrete by image analysis.” *Cem. Concr. Res.*, 39(7), 610–619.

Lura, P., Couch, J., Jensen, O. M., and Weiss, J. (2009). "Early age acoustic emission measurement in hydrating cement paste: Evidence for cavitation during solidification due to self-desiccation." *Cem. Concr. Res.*, 39(10), 861–867.

McCarter, W., and Brousseau, R. (1990). "The A.C. response of hardened cement paste." *Cem. Concr. Res.*, 20(6), 891–900.

New York State Dept. of Transportation (NYDOT). (2008). "Test Method No.: NY 703-19 E: Moisture content of lightweight fine aggregate." Materials Bureau, Albany, NY.

Peled, A., Castro, J., and Weiss, J. (2010). "Atomic force microscopy examinations of mortar made by using water-filled lightweight aggregates." *Transportation Research Record 2141*, Transportation Research Board, Washington, DC.

Powers, T. (1935). "Absorption of water by portland cement paste during the hardening process." *Ind. Eng Chem.*, 27(7), 790–794.

Powers, T. C. (1948). "A discussion of cement hydration in relation to the curing of concrete." *Bulletin 25*, Portland Cement Association, Chicago.

Radlinska, A., Rajabipour, F., Bucher, B., Henkensiefken, R., Sant, G., and Weiss, J. (2008). "Shrinkage mitigation strategies in cementitious systems: A closer look at sealed and unsealed material behavior." *Transportation Research Record 2070*, Transportation Research Board, Washington, DC.

Rajabipour, F. (2006)., "In situ electrical sensing and material health monitoring in concrete structures." Ph.D. dissertation, Purdue Univ., West Lafayette, IN.

Rajabipour, F., and Weiss, J. (2007). "Electrical conductivity of drying cement paste." *Mater. Struct.*, 40(10), 1143–1160.

RILEM. (2007). "Internal curing of concrete—State of the art." *Rep. 41*, K. Kovler, and O. M. Jensen, eds., RILEM Publications S.A.R.L, Bagneux, France.

Sant, G., Lura, P., and Weiss, J. (2006). "Measurement of volume change in cementitious materials at early ages: Review of testing protocols and interpretation of results." *Transportation Research Record 1979*, Transportation Research Board, Washington, DC.

Schlitter, J., Henkensiefken, R., Castro, J., Raoufi, K., Weiss, J., and Nantung, T. (2010). "Development of internally cured concrete for increased service life." *Rep. SPR-3211*, Joint Transportation Research Program, Indiana Dept. of Transportation and Purdue Univ., West Lafayette, IN.

Winslow, D. N., Cohen, M., Bentz, D., Snyder, K., and Garboczi, E. (1994). "Percolation and pore structure in mortars and concrete." *Cem. Concr. Res.*, 24(1), 25–37.

Zhang, M.-H., and Gjørv, O. E. (1990). "Microstructure of the interfacial zone between lightweight aggregate and cement paste." *Cem. Concr. Res.*, 20(4), 610–618.

Chloride Transport Measurements for a Plain and Internally Cured Concrete Mixture

Carmelo Di Bella, Chiara Villani, Elizabeth Hausheer and Jason Weiss

Synopsis: Over the last fifteen years there has been growing interest in using internally cured concrete. While the original intention of using internal curing was to reduce autogenous shrinkage, it has been observed that the internally cured concretes have additional benefits. For example, previous research has shown that internally cured concrete has lower water absorption than comparable conventional (plain) concrete mixtures. This paper presents results of chloride transport experiments performed using a conventional (plain) concrete mixture and an internally cured concrete mixture. Chloride transport performance was evaluated using a series of experimental techniques including: 1) resistivity, 2) rapid chloride penetration (RCP), 3) rapid chloride migration (the Nord Test), 4) migration cell testing (STADIUM cells) and 5) chloride ponding and profiling. Tests were performed 28, 56, and 91 days after casting. The results indicate that internally cured concretes have similar or superior performance to plain concrete. Several testing artifacts are noted associated with the pre-wetted lightweight aggregate that overestimate the transport measures for the internally cured concrete. The experimental results suggest that by reducing the chloride transport rate the use of internally cured concrete can result in structures with improved durability (due to the time it takes chloride ions to cause corrosion at the reinforcing steel).

Keywords: chloride transport, internal curing, lightweight aggregate, rapid-chloride penetrability, resistivity, service life, titration

Carmelo Di Bella is a graduate student at Purdue University. He received his BS in Materials Science from Milano-Bicocca University. His research interests include internal curing and chloride transport.

Chiara Villani is a graduate student at Purdue University. She received her BS and MS in Civil Engineering from the Polytechnic of Turin. Her research interests include transport testing methodologies for concrete.

Elizabeth Hausheer is an undergraduate research assistant at Purdue University. Her research interest includes chloride ingress in concrete.

FACI **Jason Weiss** is a Professor of Civil Engineering at Purdue University, West Lafayette, IN. He earned his BAE from Penn State University, and his MS and PhD from Northwestern University. Over the last fifteen years he has been active in developing and implementing new technologies to reduce unwanted cracking and to increase the service life of concrete structures.

1.0 INTRODUCTION

Transportation agencies strive to construct durable reinforced concrete structures. The durability of the concrete structures is largely governed by the fluid transport properties of the concrete which include: 1) absorption, 2) permeation and 3) diffusion of ionic species [1]. For example, the ingress of chloride ions is of particular interest in bridge decks due to the application of deicing salt and in marine structures due to the salinity of the water. If the chloride ions reach the reinforcing steel they can reduce the passivity of the reinforcing steel and promote the formation of corrosion products. The time that it takes the reinforcing steel to begin to corrode in a structure is strongly related to the rate of chloride ions penetration [2, 3]. Corrosion is a concern since it can shorten the service life of reinforced concrete structures.

It is generally known that the transport ionic species in concrete (absorption, diffusion and permeability) can be reduced by using mixtures with a lower porosity (i.e., a low water to cement ratio, w/c) and with the use of supplementary cementitious materials [1, 4]. While these low w/c mixtures reduce transport, they have in many cases exacerbated the problem of early-age cracking [5, 6].

The use of prewetted lightweight aggregate as an internal curing agent has been shown to mitigate early age cracking [7, 8, 9]. In addition, it has been shown that internal curing can reduce the fluid transport properties of concrete such as water absorption and chloride transport [10, 14]. The fluid transport properties in an internally cured concrete are reduced for three reasons. First, internal curing supplies additional water that enables increased hydration thereby reducing the porosity of the concrete [8]. Second, internal curing densifies the interfacial transition zone around the LWA. The more dense ITZ zone can disconnect the preferential transport paths resulting in higher resistance to ionic and fluid transport [11]. Third, internal curing reduces unwanted early-age cracking thereby reducing paths for fluid to reach the reinforcing steel [7, 12].

2.0 RESEARCH SIGNIFICANCE

While internal curing has been shown to be beneficial in reducing shrinkage and early-age cracking, relatively little research has documented the effects of internal curing on reducing ionic ingress and transport [8]. This paper describes the transport properties of a conventional (plain) and internally cured concrete bridge deck mixture. These concrete mixtures are identical to those used in a comparative field evaluation in Monroe County Indiana in September 2010. Chloride transport performance was evaluated using a series of tests including: 1) resistivity, 2) rapid chloride penetration (RCP), 3) rapid chloride migration (the Nord Test), 4) migration cell testing (Stadium Cells), and 5) chloride ponding and profiling. Tests were performed 28, 56, and 91 days after casting. These results of this study can be useful in determining the chloride transport performance of internally cured concrete which has implications on the time to corrosion and service life of reinforced concrete elements.

3.0 CONSTITUENT MATERIALS AND MIXTURE PROPORTIONS

Two different concrete mixtures are compared in this study. The first mixture is a conventional (plain) mixture that is commonly used by a local ready mixed concrete provider to meet the INDOT Bridge deck specifications. The second mixture is similar; however a portion of the volume of the fine aggregate has been replaced with an equivalent volume of prewetted lightweight aggregate. The second mixture will be referred to as the internally cured concrete mixture. The samples were prepared in laboratory with identical proportions to the mixtures that were eventually used in the Monroe County bridge deck trials [13]. Table 1 shows the mixture proportions.

Table 1 – Mixture proportions for plain and internally cured concretes.

	Cement Content (kg/m^3)	W/C	Fine Aggregate (kg/m^3)	Fine LWA (kg/m^3)	Coarse Aggregate (kg/m^3)	Mixture Water (kg/m^3)	Water in LWA (kg/m^3)	WRA (%)^A	AE (%)^A
Plain Concrete	390	0.39	726	-	1046	152	-	0.22	0.22
Internally Cured Concrete	390	0.39	313	270	1046	152	25	0.08	0.08

^{A} Percentage referred to the cement weight.

These proportions are based on the saturated surface dry condition of the materials with the exception of the LWA which is given in oven dry condition. An additional column is used to represent the water to maintain the 24 hour prewetted surface dry conditions.

The volume of the sum of the fine aggregate and fine lightweight aggregate was the same for both mixtures.

The lightweight aggregate used for the internally cured mixture was a fine lightweight aggregate (Haydite AX, Brooklyn IN). The 24 hours absorption of the LWA, based on the paper towel testing procedure outlined by the NYDOT, was 10.4%. The specific gravity of the lightweight aggregate was 1.56. The absorption of the coarse and fine aggregate was 1.1 % and 1.6 % respectively. The specific gravity of the coarse and fine aggregate was 2.672 and 2.647 respectively.

The cement used for the plain and internally cured mixture is an ordinary portland cement (OPC) conforming to ASTM C150 type I specification. The characteristics of the cement used are given in Table 2.

Table 2 – Characteristics of ordinary portland cement used in this study.

	SiO_2	Al_2O_3	Fe_2O_3	CaO	MgO	SO_3	Na_2O Equiv.	Blaine (m^2/kg)
OPC Type I	20.4%	4.8%	3.2%	63.2%	2.1%	3.4%	0.67%	398

4.0 MIXING, CURING AND SAMPLE PREPARATION

Prior to mixing, the aggregate (including lightweight aggregate) was dried in an oven at 105 ± 5 °C for 24 hours. The aggregate was then allowed to cool down to room temperature. The lightweight aggregate was soaked in the mixture water for 24 +/- 1 hours being careful that the water remained above the top surface of the lightweight aggregate. In order to avoid loss of water to evaporation the lightweight aggregate was covered with plastic sheets. After 24 hours the excess water was decanted and used in mixing.

The coarse and fine aggregate were placed in the pan mixer. Water was then added to the mixture (along with lightweight aggregate in the case of the internally cured mixture). Cement and admixtures were then added. After all the materials were placed in the mixer they were mixed for 3 minutes, followed by a 3 minutes rest and a 2 minutes final mixing in accordance with ASTM C 192.

Cylindrical sample were prepared. The cylinders had a diameter of 102 mm (4 in.) and length of 203 mm (8 in.). External vibration was used to consolidate the specimens. Immediately after casting the cylinders were covered. These specimens were demolded after one day and sealed in double plastic bags until the test age were reached: 28, 56, 91 days (with the exception of the surface resistivity samples). At the time of testing the samples were prepared using the procedures described in the following section.

5.0 EXPERIMENTAL METHODS

In this study the transport properties of the concrete were evaluated using five experimental techniques. These techniques include: 1) surface resistivity, 2) rapid chloride penetration (RCP),

3) rapid chloride migration (the Nord Test), 4) migration cell testing (Stadium Cells), and 5) chloride ponding and profiling. The experimental procedures are described in the following section.

5.1 Surface resistivity

The electrical resistivity at the surface of water-stored concrete samples was measured using the four-point Wenner probe surface (Figure 1). Measurements of electrical resistivity were conducted as described in AASHTO TP 95-11 using cylindrical samples that were 102 mm (4 in.) in diameter and 203 mm (8 in.) long. The samples were demolded at 24 h after casting and kept under lime water until the time of testing at a temperature of 23 ± 1 ºC. It should be noted that by storing the samples under water it is believed that the samples will absorb water during the test which may increase the degree of hydration of the specimen [14].

In the surface resistivity test a current is applied at the outer probes and the potential difference is measured between the two inner probes. Assuming that the concrete has homogeneous semi-infinite geometry the concrete resistivity is described by equation 1:

$$\rho = (2 \cdot \pi \cdot a) \cdot \frac{V}{I} \qquad \text{eq. 1}$$

where a is the electrode spacing, V is the voltage, and I is the current.

Morris et al. [15] showed that for concrete cylinders the surface resistivity (ρ_{surface}) requires a correction to attain the true resistivity (ρ) of the material that depends on probe spacing and sample geometry. A geometry correction (K) of approximately 1.9 can be used for probe spacing (a = 38 mm, 1.5 in) and specimen size used in this study (Equation 2). This has been recently confirmed through experiments by Spragg et al. [21].

$$\rho_{bulk} = \rho_{surface}/K \qquad \text{eq. 2}$$

Relationships have been developed between RCP test and surface resistivity test results [16, 17] (assuming saturation) since both tests are based on measures of the electrical resistance of the concrete. It should however be noted that the RCP test test may contain artifacts related to sample heating caused by the joule effect.

Figure 1 – Surface resistivity measurements using a Wenner probe.

5.2 Rapid Chloride Penetration (RCP)

The rapid chloride penetration (RCP) test was performed in accordance with ASTM C 1202. A cylindrical specimen was prepared that was 102 mm (4 in.) diameter and 51 ± 3 mm (2 in.) long. Prior to testing the sample was vacuum saturated as described in ASTM C 1202. During the test one surface of the sample was exposed to a sodium chloride solution (3% NaCl) and the other surface was exposed to a sodium hydroxide solution (0.3 M NaOH). A 60 V externally applied potential and the current at 15 minute intervals was recorded for a 6 hour period. Figure 2 shows the experimental set up with four samples being tested simultaneously.

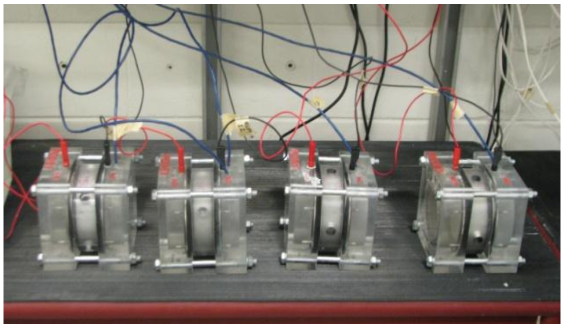

Figure 2 – Rapid Chloride Penetration (RCP) test cells.

5.3 Rapid Chloride Migration (RCM)

The rapid chloride migration test was conducted to determine the non – steady state chloride migration coefficients following the NT Build 492 procedure [18]. The RCM test is a non-steady state migration test to accelerate the chloride transport by means of the application of a potential across a 50 mm thick specimen for a specified period of time.

The test was performed using specimens cut from a concrete cylinder to produce a disk that is 51 ± 3 mm (2 in.) thick and 102 mm (4 in.) diameter. The samples are vacuum saturated after cutting. The sample is then placed in a rubber sleeve. The top portion of the sleeve is used to create a reservoir where 0.3 M NaOH is placed in contact with the upper surface of the sample. The bottom of the sample is placed in a solution of 10% NaCl. The test is illustrated in Figure 3. An initial potential of 30 V is applied to the specimen. This potential is adjusted according to the current response (as outlined in the NT Build standard) and the applied potential is maintained for a 24 hour period.

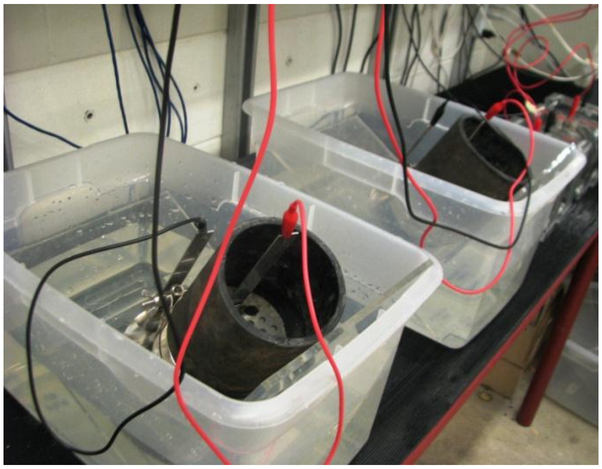

Figure 3 – Rapid Chloride Migration (RCM) experimental set up.

At the end of the 24 hour period where voltage is applied the sample is rinsed with distilled water and the surface is wiped with a cloth. The sample is then split into two pieces as shown in Figure 4. A 0.1 M silver nitrate solution is sprayed on the sample. Where sufficient chloride is present, the silver nitrate causes white silver chloride to precipitate as shown in Figure 4. The chloride penetration depth is measured at 10 locations across the section and used to determine an average depth of penetration.

Figure 4 – A Sample from the Rapid Chloride Migration (RCM) test that was split after and sprayed with Silver Nitrate (AgNO3). The white portion of the sample at the top represents the chloride penetration while the brown area represents the portion of the concrete that has not received substantial chloride penetration. The sample is 101 mm (4 in wide) and 50 mm (2 in tall).

The chloride non steady state migration coefficient (D_{nssm}) is calculated using equation 3, assuming the migration process as dominant and that the chloride binding capacity during the test to be constant [2, 19].

$$D_{nssm} = \frac{0.0239(273+T)L}{(U-2)t}\left(x_d - 0.0238\sqrt{\frac{(273+T)Lx_d}{U-2}}\right) \qquad \text{eq. 3}$$

where D_{nssm} is the non steady state migration coefficient (x10^{-12} m^2/s), U is the absolute value of the applied voltage (V), T is the average value of the initial and final temperatures in the solution

(C), L is the thickness of the specimen (mm), x_d is average value of the average chloride penetration depth (mm) and t is the test duration (hour).

5.4 Migration cell

The diffusion coefficients for specific ionic species were measured using a migration cell (Stadium Cell) as shown in Figure 5. The test method consists of monitoring the intensity of electrical current passed through a cylindrical test specimen (50 ± 2 mm (2 in.) thick and 100 ± 2 mm (4 in.) in diameter over 14-days testing period). Before testing the samples are vacuum saturated with 0.3M NaOH for approximately 18 hours. After vacuum saturation the sample was mounted in between the downstream cell filled with 0.3M NaOH solution and the upstream cell filled with 0.5 NaCl + 0.3M NaOH solution. A constant DC potential of 20 V is maintained across the specimen. The data (voltage, current, and temperature) are automatically recorded at 15 minute intervals. These data, along with the porosity (volume of permeable voids) value determined in accordance with ASTM C642, are entered into STADIUM Lab software to evaluate the ion diffusion coefficients [20].

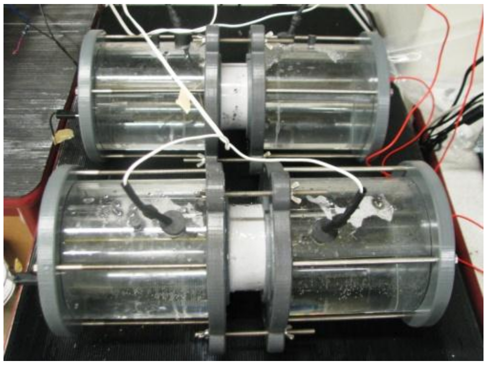

Figure 5 – Migration cell experimental set up.

5.5 Chloride Ponding and Profiling

The penetration of chloride ions into concrete was assessed from a chloride ponding test in which a 3% NaCl solution was ponded on the surface of the specimen following the approach described in ASTM C1543-10. A cylindrical specimen was prepared that was 102 mm (4 in.) diameter and 203 mm (8 in.) long and allowed to cure for 28 days sealed in plastic bags stored at 23 ± 1 °C. After 28 days, the sample was cut obtaining two half cylinders that were 102 mm (4 in.) diameter and 102 mm (4 in.) long. The sides of each concrete specimen were coated with epoxy. After the epoxy hardened and dried, a plastic cylinder was affixed to around the top of each sample, in order to form a dam to contain the salt solutions to be used for ponding. A sketch of the sample is shown in Figure 6.

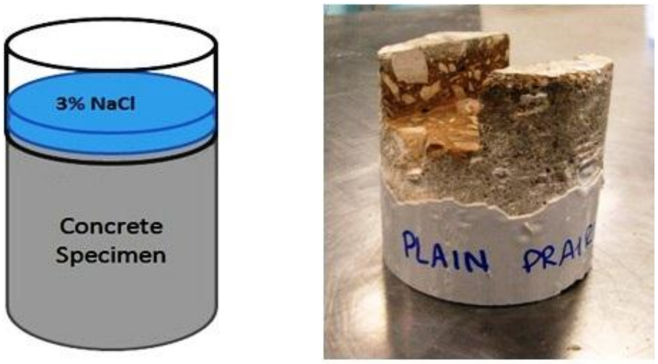

Figure 6 – A sketch of the sample used for chloride ponding and the sample after profile grinding.

After the dam was affixed to the surface water was placed on the specimen to insure that the dam was water-tight. The water was then removed and the sample was filled with a 3% NaCl solution. It should be noted that water could be reabsorbed by the sample, however the samples were not vacuum saturated. The samples were stored in a chamber at 23 ± 1 °C and 50 ± 2% RH. Periodically (approximately every 10 days), the salt solution was replaced with fresh solution. Once the testing ages were reached (28, 56 and 91 days) the plastic dam was removed and the epoxy sealed sides were removed. The concrete was placed on a milling machine and ground with successively 2 mm steps using a 50 mm diamond tipped drill bit. The powder that was collected at different depths was analyzed to determine the chloride content as described in the following section.

An automated system was used to titrate up to 14 samples (a sample here refers to the powder obtained at each grinding depth) simultaneously. The acid-soluble chloride content was determined using a procedure similar to AASHTO T 260; however some modifications to the specification were adopted as highlighted below. First, 3 grams of ground powder from the concrete were placed in contact with 10 ml of hot distilled water. This was mixed for several mixtures. Then, 3 ml of nitric acid was added to the suspension, stirring the solution continuously. Next, the solution was diluted with an additional 40 ml of hot distilled water, yielding approximately 50 ml of sample. Each sample was covered and boiled for 1 minute. It should be noted that some layers may have a very low chloride concentration that was difficult for the titrator to detect and as such a full analysis would be done that was both time consuming and consumed silver nitrate. In order to alleviate this problem, 1 ml of 0.01M sodium chloride solution was added to each sample prior to titration.

The titration probe used in this study did not require the sample to be filtered. The solution was placed in the titration unit shown in (Figure 7). While stirring the solution, the titrator adds 0.01M silver nitrate to the solution in 0.2 ml increments (this addition rate however decreases while approaching the saturation point), while simultaneously monitoring the electric potential of the solution with a silver reference electrode. A plot of the electrical potential versus volume-of-titrant (i.e., volume of silver nitrate) is then prepared. The principle of the test is that as the chloride (Cl- ions) are paired with the silver (Ag+) ions causing the solution to neutralize and change the electric potential. A typical example of this change is shown in Figure 8. The chloride content of the sample is determined using the maxima of the first derivative curve of the potential. Once the inflection point is reached, the dosing unit stops adding silver nitrate to the sample and begins to process the next sample. This entire process takes approximately 5 minutes for each sample, as compared to approximately 1 hour when the test was performed manually. The chloride concentration is computed using equation 4 accounting for the silver nitrate that was added to each sample during sample preparation.

$$\% \boldsymbol{Cl} = \frac{\boldsymbol{M_{Cl}} \times [(\boldsymbol{V_{AgNO3}}) - (\boldsymbol{V_{NaCl}})] \times \boldsymbol{C_{AgNO3}}}{\boldsymbol{M_{powder}}} \times \mathbf{100} \qquad \text{eq. 4}$$

where M_{Cl} is the atomic weight of chlorine (35.453 g/mol), V_{AgNO_3} is the total volume of $AgNO_3$ added, V_{NaCl} is the volume of sodium chloride added, C_{AgNO_3} is the concentration of silver nitrate used for the titration (0.0102 mol/l) and M_{powder} is the mass of concrete powder.

The results of the automated method were compared with those obtained by hand as shown in Figure 9. The results shown that the chloride content values obtained from both methods are similar.

Figure 7 – Automated titration unit.

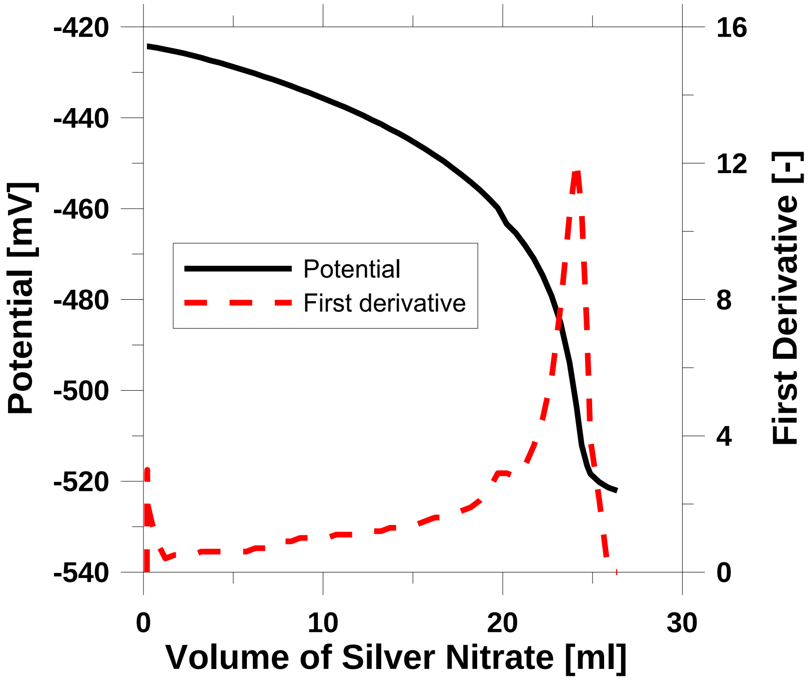

Figure 8 – An example of a titration response illustrating the change in electrical potential and how the inflection point was used to determine the initial chloride content.

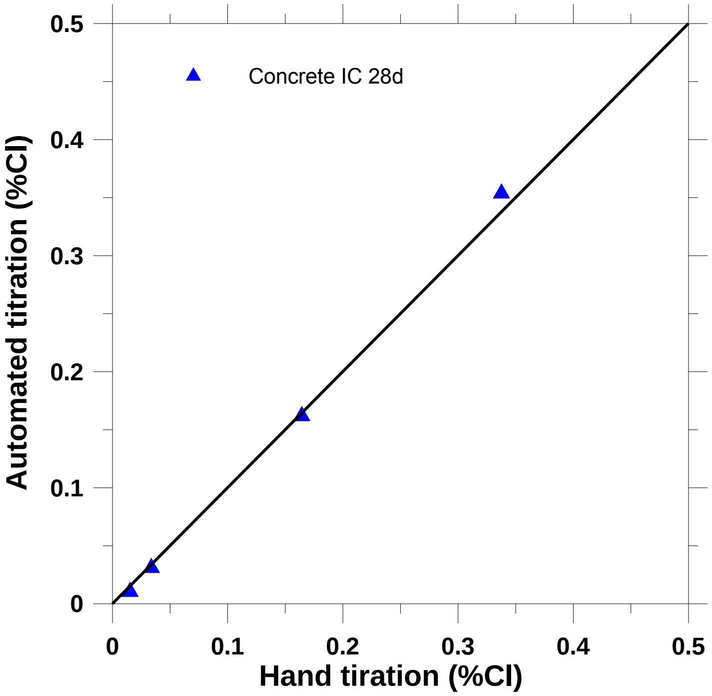

Figure 9 - Comparison of the chloride concentration obtained from a sample of internally cured concrete at 28d using the conventional titration method and using the automated titration system.

6.0 EXPERIMENTAL RESULTS AND DISCUSSION

6.1 Surface resistivity

The electrical resistance of the concrete is known to be related to the pore volume, the ionic concentration of pore solution [16, 17] the degree of saturation in the concrete, and the tortuosity of the pore network. The resistivity of the concrete can be used as a surrogate measurement of the transport properties since the Nernst-Einstein relationship [21] allows the electrical properties to be related to ionic diffusion.

Figure 10 shows the surface resistivity measurements for plain and internally cured samples. Initially the internally cured concrete has a lower resistivity (likely due to the conductive nature of the aggregate [14]); however by 56 days the resistivity of the internally cured concrete has a similar resistivity and at later ages it is more resistive thanks to the enhanced hydration and denser ITZ [8,11] .

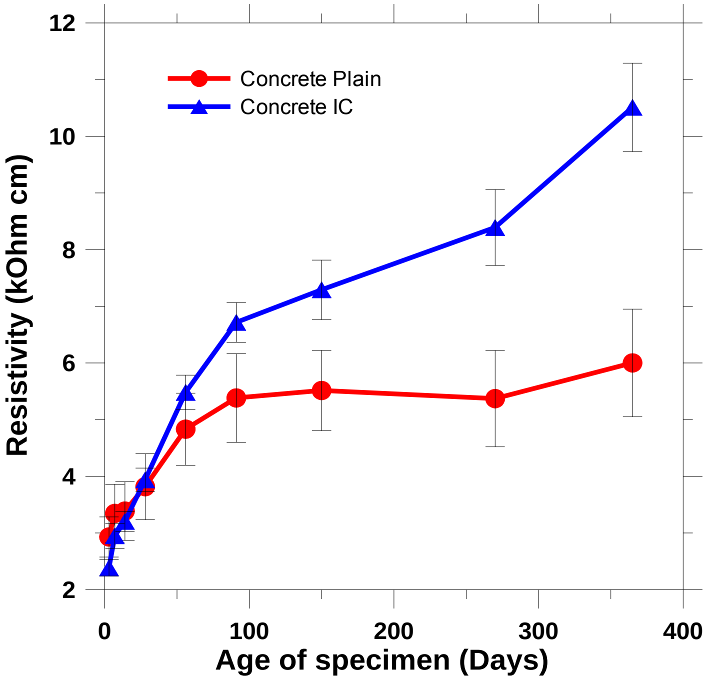

Figure 10 – Electrical resistivity if the plain and an internally cured concrete samples kept in lime water during the testing period.

It should be noted that by storing the samples in lime water they will hydrate more than a sealed sample. While the surface resistivity test is easy to perform, the samples are stored in water through the test which may not represent the way these specimens are cured in the field.

6.2 Rapid Chloride Penetration (RCP)

The most widely used method by transportation agencies to assess a concrete's ability to resist to chlorides ion penetration is ASTM 1202 (or AASHTO T277). Similar to the resistivity test described in section 6.1, the RCP test is influenced by the pore volume, the ionic concentration of pore solution [22, 23] the degree of saturation in the concrete, and the tortuosity of the pore network. However, unlike the resistivity tests, the RCP test samples used in this paper were sealed until the time of testing and then vacuum saturated. The results from the rapid chloride penetrability test are shown in Table 3 for the plain and internally cured concrete. The internally cured mixture shows consistently lower charge passed. For example, at an age of 91 days the internally cured concrete has an RCP value that is approximately 35% lower than the plain concrete.

Table 3 – Rapid Chloride Penetration Test Results for the Plain and Internally Cured Concrete Samples.

	Monroe County Bridge Deck Concrete			
Time [days]	Charge Passed [Coulombs]			
	Plain Concrete	Standard Deviation	Internally Cured Concrete	Standard Deviation
28	4252	116	3822	159
56	2863	560	2458	55
91	3174	450	2065	113

At the age of 56 days the plain concrete shows a lower value than expected. In fact, at 91 days the charge passed increases. This can be addressable to a misleading measurement at the age of 56 days.

The use of the rapid chloride penetration test method can be thought of essentially as a measure of concrete resistivity. However, it should be noted that RCPT was performed with high voltage and the sample heated during testing which increase due to Joule effect. As such there is no need to continue the test for six hours, and changes in the current during this time are most likely due to increases in temperature, not chloride penetration [24, 25]. Therefore alternative ways have been developed to measure concrete resistivity and assess the concrete chloride penetration resistance [23] [22].

6.3 Rapid Chloride Migration (RCM)

Table 4 shows the non steady migration coefficients obtained at 28, 56 and 91 days for the concrete samples with and without internal curing. The internally cured concrete shows benefits of internal curing for each test compared to the plain concrete. For example, at an age of 91 days the internally cured concrete has an RCM value that is approximately 15% lower than the plain concrete.

Table 4 – Chloride diffusion coefficients obtained from the Rapid Chloride Migration Test.

	Monroe County Bridge Deck Concrete			
Time [day]	Diffusion coefficients (m^2/s)			
	Plain Concrete	Standard deviation	IC Concrete	Standard deviation
28	1.42E-11	9.89E-13	1.15E-11	5.65E-13
56	1.26E-11	4.24E-13	8.98E-12	2.83E-13
91	3.99E-12	4.24E-13	3.42E-12	1.91E-13

Although the internally cured concrete shows lower diffusion coefficients than the plain concrete from the test when it is performed following the standard, it should be noticed that the diffusion coefficients may be actually lower for the internally cured concrete. First, the internally cured concrete is cut to perform the test. As such, the cutting of the concrete exposes the porous lightweight aggregate. When these cut aggregates are exposed to the solution the chloride can easily diffuse into the concrete which may not represent what happens in field concrete. As such this may skew the results of test with more resistant matrices [26]. In addition, since the sample is saturated the conductivity of the aggregate may alter the electrical response of the concrete [27]. Despite these testing anomalies the internally cured concrete performed as well, or better than the plain concrete.

6.4 Migration cell

A multi-ionic model considers the electrical coupling between ions, chloride binding, and chemical reactions was used to interpret the results from the migration cell [20]. This analysis was performed using a program called STADIUM Lab which used results from the migration cell along with the porosity results obtained from ASTM C 642 (Table 5). It should be noted that at the current time it is believed that this code does not consider the porosity of the aggregate explicitly. The modeled diffusion coefficients in Table 6 have a similar trend when compared with the rapid chloride migration test; however the diffusion coefficients obtained with this method are not directly comparable with one another.

Table 5 - Tortuosity modeled by Stadium Lab software and porosity determined in accordance with ASTM 642.

	Monroe County Bridge Deck Concrete					
Time [days]	Porosity %				Tortuosity	
	Plain Concrete	STD	IC Concrete	STD	Plain Concrete	IC Concrete
28	12.6	0.49	13.0	0.49	0.0421	0.0284
91	13.3	0.35	14.5	0.83	0.0377	0.0146

Table 6 - Chloride diffusion coefficients obtained using the Migration Cell.

	Monroe County Bridge Deck Concrete	
Time [day]	Diffusion coefficients (m^2/s)	
	Plain Concrete	IC Concrete
28	8.56E-11	5.78E-11
91	7.67E-11	2.97E-11

The differences in the diffusion coefficients between the plain and internally cured concrete obtained by Stadium Lab are greater than that observed from the NT Built test method. For example, at an age of 91 days the internally cured concrete has a chloride diffusion coefficient value that is approximately half that of the plain concrete.

The porosity and the pore characteristics of the concrete play a fundamental role in the permeability and in general on the durability of the concrete. The effects of porosity and pore characteristics can be captured through a single parameter called tortuosity [28]. Tortuosity, in fact, depends on the connectivity of the pore system and represents an important physical quantity for understanding and modeling the transport phenomena that influences the durability performance [29]. STADIUM Lab also provides a measure of the tortuosity of the pore structure in concrete as shown in table 5. While the porosity for internally cured concrete is higher due to the presence of the lightweight aggregates, the tortuosity of the internally cured concrete is lower than that of the plain concrete presumably due to the increased hydration and densified interfacial transition zone in internally cured concrete.

6.5 Chloride Ponding and Profiling

Figures 11 through 13 show the acid-soluble chloride content of samples ponded with a 3% NaCl for a period test of 28 and 91 days, respectively. Figure 11 shows the chloride content for the plain concrete and the internally cured concrete ponded for 28 days.

Within the first 8-10 mm the chloride concentration is greater in the internally cured mixture. This could be explained by the fact that the samples are cut, thereby exposing the pores of the lightweight aggregates at the surface of the sample. The exposed LWA pores are much larger than the paste pores. As a consequence LWA pores can work as reservoirs for the chloride solution which can be easily absorbed and rapidly diffuse into the LWA pores. In addition, the sample preparation for the chloride ponding may allow a partial drying of the larger pores on the surface making them easily accessible by the chloride solution. As a consequence higher chloride concentration may be detected on the surface of the specimen.

To confirm the artifact of the test method two samples were prepared, a plain concrete and internally cured concrete at an age of 91 days. The samples were not exposed to water as the other samples were however they were ponded for 15 minutes with a sodium chloride solution. The solution was then removed and the samples were ground. Figure 12 shows that both concretes absorb fluid. The internally cured concrete however absorbs more solution near the surface due to pores of the LWA being connected to the surface. Field concrete however does not have exposed aggregate and it appears that the increased concentration of the chloride at the surface is in part an experimental artifact of the test method. Additional testing is being done to better quantify this effect. Consequently, due to the higher concentration at the surface in the internally cured concrete it could be expected that the chloride concentration would have been for the entire profile higher compared to the plain concrete. However, as it can be seen from Figure 11 at depths greater than 8-10 mm the concentration of chloride is already similar for both mixtures. This confirms the results above where the diffusion coefficient for the internally cured concrete was found to be lower.

Figure 13 shows the experimental data after 91 days of ponding. The results show a similar trend observed for the mixtures ponded for 28 days with the internally cured concrete again showing a higher chloride concentration within the first 8 mm.

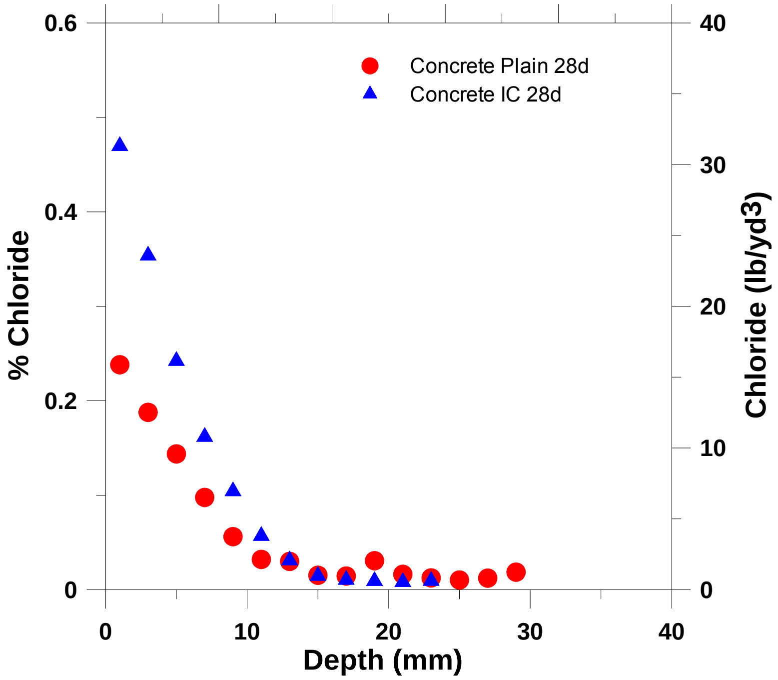

Figure 11 - Chloride content in a plain and internally cured concrete after 28 days of ponding.

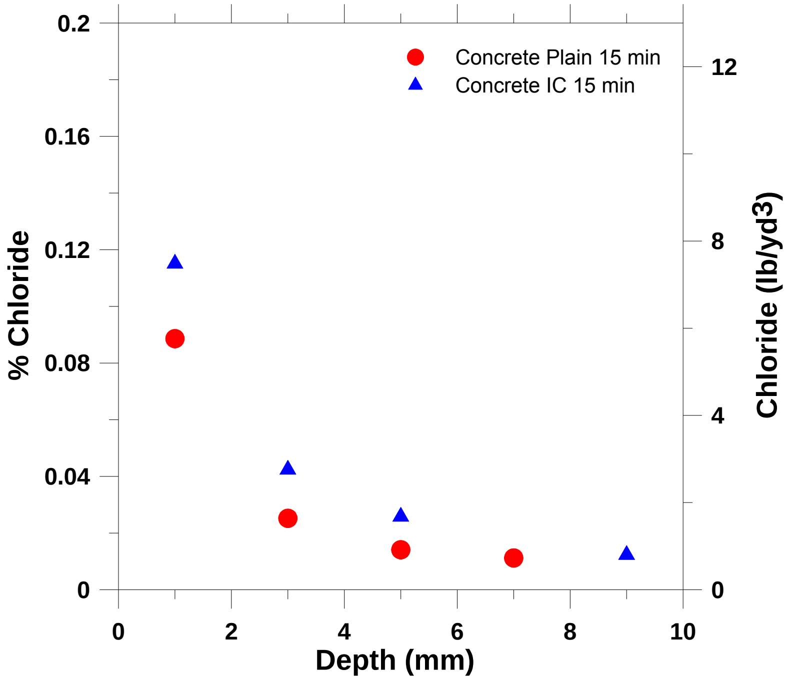

Figure 12 - Chloride content in a plain and internally cured concrete at 91 days after only 15 minutes of ponding.

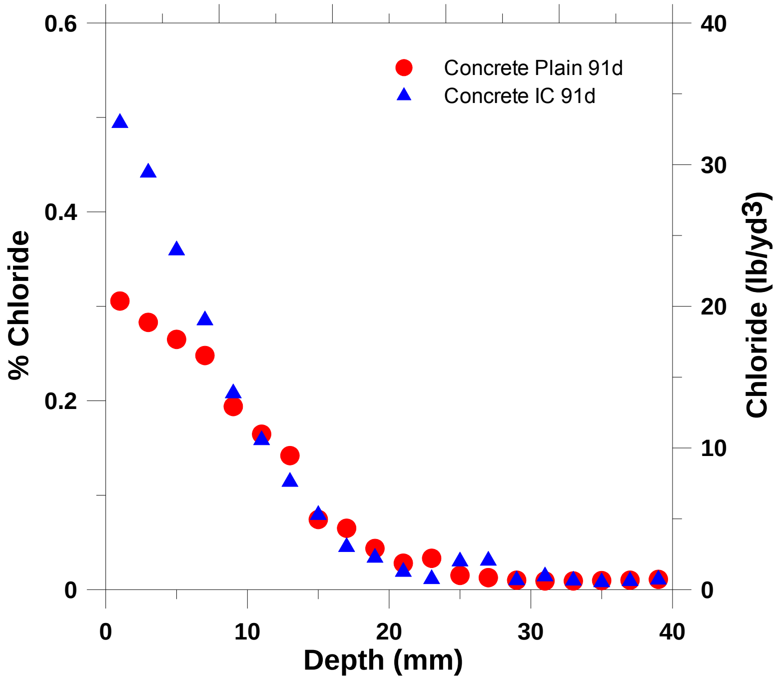

Figure 13 – Chloride content in a plain and internally cured concrete after 91 days of ponding.

7.0 SUMMARY AND CONCLUSIONS

This paper reports results from two concrete mixtures consistent with those used in field trials of concrete placed in bridge decks in Monroe County Indiana. The bridges were in close proximity to one another placed by the same contractor using similar materials and construction methods on consecutive days to obtain a direct comparison of the two mixtures. The first bridge deck was made using conventional concrete (i.e., plain concrete) that satisfied typical INDOT specifications while the second bridge deck was made using a similar mixture however the concrete had a portion of the fine aggregate replaced with an equivalent volume of prewetted lightweight aggregate to make an internally cured concrete. Samples from these mixtures were used to evaluate the chloride transport performance using a series of tests including: 1) resistivity, 2) rapid chloride penetration (RCP), 3) rapid chloride migration (the Nord Test), 4) migration cell testing and 5) chloride ponding and profiling. Tests were performed 28, 56, and 91 days after casting.

The diffusion coefficients measured the rapid chloride migration and the migration cell (STADIUM cell) showed that the internally cured concrete had a lower diffusion coefficient than the plain concrete (15% and 50%, respectively). The rapid chloride penetrability of the internally cured concrete is lower than the plain concrete at all the ages (approximately 35% at 91 days). The electrical surface resistivity of the internally cured concrete is higher than the plain concrete. Finally, the internal curing is able to reduce the diffusion coefficients of the conventional concrete. This demonstrates that the internally cured concrete has the ability to reduce transport properties. It is believed that this is due to increased cement hydration [30] and reduced porosity at the interfacial zone based on earlier studies.

While the all the electrical based tests showed benefits of using internal curing, it should be noted that some artifacts are believed to exist in the test that are caused by the presence of the prewetted lightweight aggregates. The use of the cut surface in samples prepared for the rapid chloride penetration (RCP), rapid chloride migration, migration cell testing and chloride ponding and profiling enable chloride to enter the lightweight aggregate at the surface which appears to influence the testing results. This result much more evident in the chloride ponding where higher chloride concentration on the top of the samples was observed. For example, the chloride penetration was observed to be higher in the internally cured concrete in the 6 to 8 mm near the surface. The diffusion coefficient is however lower in the IC mixtures. In addition, tests that use vacuum saturation enable water to fill the lightweight aggregate which allows them to behave as electrical conductors which reduces the resistivity of the concrete. Procedures are currently being developed to quantify these effects and to develop methodologies to account for these artifacts.

8.0 ACKNOWLEDGMENTS

The authors gratefully acknowledge the financial support from the Indiana Local Technical Assistance Program (IN LTAP) and the Expanded Shale, Clay and Slate Institute (ESCSI).

9.0 REFERENCES

[1] Hooton, R.D., Pun, P., Konjundic, T., Fidjestol, P. (1997) "Influence of silica fume on chloride resistance of concrete" in: Proc. of the PCI/FHWA International Symposium on High Performance Concrete, pp. 245-256.

[2] Tang, L. (1997) "Chloride diffusion coefficient of concrete and relevant test methods - The state of the art and suggestions for future work" SP Report 1997:23, SP Swedish.

[3] Sandberg,P., (1995) " Critical evaluation of factors affecting chloride initiated reinforcement corrosion in concrete" Report TVBM-3068, Division of Building Materials, Lund Institute of Technology, Lund.

[4] Bentz, D.P., Jensen, O.M., Coats, A.M., Glasser F.P. (2000) "Influence of silica fume on diffusivity in cement-based materials I. Experimental and computer modeling studies on cement pastes; Cement and Concrete research" 30 953-962.

[5] Weiss, J. (1999). "Prediction of early-age shrinkage cracking in concrete." Ph.D. thesis. Evanston, IL Northwestern University.

[6] Cusson, D., Lounis, Z., Daigle, L. (2010) "Benefits of internal curing on service life and life-cycle cost of high-performance concrete bridge decks – A case study" Cement &concrete composites 32 339-350.

[7] Jensen, O.M., Hansen, P.F. (2001) "Water-entrained cement based materials: I. Principles and theoretical background" Cement and concrete research 31 647-654.

[8] RILEM TC-196 (2007) "Internal curing of concrete, State of the art report" Rilem publications S.A.R.L., 139p.

[9] Schlitter, J.L., Bentz, D.P. and Weiss, J. (2010b). "Quantifying the residual stress development and reserve strength in restrained internally cured concrete." Submitted to ACI Materials Journal.

[10] Castro, J., Spragg, R., Weiss, J. (2011) "Water absorption and electrical conductivity for internally cured mortars with w/c between 0.30 and 0.45" Journal of Materials in Civil Engineering.

[11] Bentz, D.P. (2009) "Influence of internal curing using lightweight aggregates on interfacial transition zone percolation and chloride ingress in mortars" Cement and concrete composites 31 285-289.

[12] Raoufi, K., Schlitter, J., Bentz, D., Weiss, J. (2011) "Parametric Assessment of Stress Development and Cracking in Internally Cured Restrained Mortars Experiencing Autogenous Deformations and Thermal Loading," Advances in Civil Engineering, Article ID 870128, 16 pages, 2011. doi:10.1155/2011/870128.

[13] Di Bella, C., Schlitter, J., Carbouneau, N., Weiss, J. (2012) "Documenting the Construction of a Plain Concrete Bridge Deck and an Internally Cured Bridge Deck" Joint Transportation Research Program, Indiana Department of Transportation and Purdue University.

[14] Di Bella, C., Villani, C., Phares, N., Hausheer, E., Weiss, J. (2012) "Chloride transport and service life in internally cured concrete" American Society of Civil Engineers Structures Congress, March 29-31 2012, Chicago, Illinois.

[15] Morris, W., Moreno, E.I., Sagues, A.A. (1996) "Practical evaluation of resistivity of concrete in test cylinders using a wenner array probe" Cement and concrete research, Vol. 26, No. 22, pp 1779-1787.

[16] Kessler, R.J., Powers, R.G., Parades M.A. (2005) "Resistivity of water saturated concrete as an indicator of permeability" FDOT, published by NACE International

[17] Spragg, R.P., Castro, J., Nantung, T., Parades, M., Weiss, J. (2011) "Variability Analysis of the Bulk Resistivity Measured Using Concrete Cylinders" Publication FHWA/IN/JTRP-2011/xx. Joint Transportation Research Program, Indiana Department of Transportation and Purdue University, West Lafayette, Indiana, 2011.

[18] NT Build 492, Concrete, mortar and cement based repair materials: chloride migration coefficient from non-steady state migration experiments, Approved 1999-11.

[19] Nanukuttan, S., Basheer, L., Basheer, M., Holmes, N., McCarter, J., Chrisp, M., Starrs, G. (2009) "Testing and Monitoring Concrete Using Novel Methods for Predicting Their Long Term Behaviour" Concrete Technology Forum, American Ready Mix Association.

[20] Samson, E., Marchand, J., Snyder, K.A. (2003) "Calculation of ionic diffusion coefficients on the basis of migration test results" Materials and structures, Vol. 36, April, pp 156-165.

[21] Garboczi, E.J., (1990) "Permeability, Diffusivity, and Microstructural Parameters: a Critical Review", Cement and Concrete Research, Vol. 20 pp591-601.

[22] Joshi, P., Chan, C. (2002) "Rapid chloride permeability testing" Concrete Construction-World of Concrete 47 (12), pp. 37-43.

[23] Kessler, R.J., Powers, R.G., Vivas E., Parades, M.A., Virmani, Y.P. (2008) "Surface resistivity as indicator of concrete chloride penetration resistance" Concrete Bridge Conference, St. Louis, May 4-7, 2008, Missouri.

[24] Julio-Bentancourt, G.A., Hooton, R.D. (2004) "Study of the effect on rapid chloride permeability values and evaluation of related electrical properties of concretes" Cement and concrete research 34 1007-1015.

[25] Snyder, K.A., Ferraris, C., Martys N.S., Garboczi (2000) "Using impedance spectroscopy to assess the viability of the rapid chloride test for determining concrete conductivity" Journal of research of the natl. inst. of stand. technol. vol. 105, No. 4, July-August.

[26] Bentz, D.P., Snyder, K.A., Peltz, M.A., Obla, K., Kim, H. (2011) "Viscosity Modifiers to Enhance Concrete Performance", submitted to ACI Materials Journal.

[27] Weiss, J., Bullard, J., Snyder, K., Bentz, D., Casto, J. (2012) "Electrical Properties of Concrete with Conductive Aggregate: Implications for Internal Curing" work in preparation

[28] Ahmad, S., Azad, A., Loughlin, K. (2005) "A study of permeability and tortuosity of concrete" 30th conference on our world in concrete and structures 23-24 August, Singapore.

[29] Promentilla, M.A., Sugiyama, T. (2007) "Studies on 3D micro-geometry and diffusion tortuosity of cement-based materials using x-ray microtomography" 32nd conference on our world in concrete &structures 28-29 August, Singapore.

[30] Castro, J. (2011). *Moisture Transport in Cement-Based Materials: Appliacations to Transport Tests and Internal Curing.* Ph.D. Thesis. West Lafayette: Purdue University.

Water Absorption and Critical Degree of Saturation Relating to Freeze-Thaw Damage in Concrete Pavement Joints

Wenting Li[1]; Mohammad Pour-Ghaz, M.ASCE[2]; Javier Castro[3]; and Jason Weiss, M.ASCE[4]

Abstract: Fluid ingress is a primary factor that influences freeze-thaw damage in concrete. This paper discusses the influence of fluid ingress on freeze-thaw damage development. Specifically, this paper examines the influence of entrained air content on the rate of water absorption, the degree of saturation, and the relationship between the saturation level and freeze-thaw damage. The results indicate that whereas air content delays the time it takes for concrete to reach a critical degree of saturation it will not prevent the freeze-thaw damage from occurring. The results of the experiments show that when the degree of saturation exceeds 86–88%, freeze-thaw damage is inevitable with or without entrained air even with very few freeze-thaw cycles. **DOI:** **10.1061/(ASCE)MT.1943-5533.0000383.** © *2012 American Society of Civil Engineers.*

CE Database subject headings: Absorption; Emissions; Concrete pavements; Deterioration; Freeze and thaw; Joints.

Author keywords: Absorption; Acoustic emission; Air content; Concrete; Concrete pavement; Degree of saturation; Deterioration; Freeze-thaw; Pavement joint; Water absorption.

Background on the Problem of Joint Deterioration in Concrete Pavements

Concrete pavements represent a large portion of the transportation infrastructure. Whereas many of these pavements provide excellent long-term performance, a portion of these pavements have recently shown premature joint deterioration throughout the Midwestern states (Weiss et al. 2007; Sutter et al. 2006; Leech et al. 2008; Rangaraju et al. 2006). This joint deterioration is problematic because it compromises the performance and potential service life of an otherwise healthy pavement. Fig. 1 is photographs of a typical damaged pavement joint. This type of damage is frequently seen as either the development of cracking parallel to the joint or spalling and cracking at the joint from the bottom of the saw cut to the surface of pavement approximately 4–6 in. from the joint. Unfortunately, damage is not frequently observed at the surface of the pavement until a significant amount of damage has occurred inside the joint. During field inspections it has been observed that where the joints are damaged the sealant is damaged and the joint contained standing water. Research is needed to better understand how this standing water may lead to freeze-thaw damage. Further, this damage occurs in both poorly air entrained and properly air entrained concrete. As a result, the role of air content needed to be quantified which is the reason for this study.

Background on Water Absorption and the Critical Degree of Saturation

Concrete is susceptible to freeze-thaw damage when it is saturated (Sutter et al. 2006; Leech et al. 2008; Fagerlund 1972, 1975, 1977, 1979, 1981, 2004; Bentz et al. 2001; Litvan 1988; Litvan and Sereda 1980; Shimada et al. 1991; Beaudoin and Cameron 1972; Feldman 1987; Scherer 1993; Scherer and Valenza 2005; Sun et al. 2007). Whereas the water content in concrete can be quantified in several different ways, this paper defines the degree of saturation (S) as the ratio of the absolute volume of absorbed water to the total volume of pores (i.e., the total volume of water that can be absorbed by concrete).

It has been suggested that there is a critical degree of saturation (S_{cr}) beyond which freeze-thaw damage can begin to initiate (Fagerlund 1972, 1975, 1977, 1979, 1981, 2004; Bentz et al. 2001; Litvan 1988; Litvan and Sereda 1980; Shimada et al. 1991; Beaudoin and Cameron 1972). For degrees of saturation below the critical degree of saturation freeze-thaw damage is not observed to occur even after a large number of freeze-thaw cycles (Fagerlund 1972, 1975, 1977, 1979, 1981, 2004; Bentz et al. 2001; Litvan 1988; Litvan and Sereda 1980; Shimada et al. 1991; Beaudoin and Cameron 1972).

Fig. 2 schematically illustrates the concept of water absorption and the critical degree of saturation (Fagerlund 2004; Barde et al. 2009). We can begin by assuming that the representative volume element shown in Fig. 2 is filled with pores with different sizes at a given spacing. It is assumed that there are two critical values

---

[1] Graduate Research Assistant, School of Materials Science, Southeast Univ., Nanjing 211189, China, and Graduate Research Assistant, School of Civil Engineering, Purdue Univ., West Lafayette, IN. E-mail: li448@purdue.edu

[2] Assistant Professor, Dept. of Civil, Construction, and Environmental Engineering, North Carolina State Univ., Campus Box 7908, 431C Mann Hall, Raleigh, NC 27695; formerly, Graduate Research Assistant, School of Civil Engineering, Purdue Univ., West Lafayette, IN. E-mail: mpourghaz@ncsu.edu

[3] Assistant Professor, School of Engineering, Pontificia Universidad Catolica de Chile, Casilla 306, Correo 22, Santiago, Chile. E-mail: jecastro@ing.puc.cl

[4] Professor, Director of Pankow Materials Laboratory, Purdue Univ., West Lafayette, IN (corresponding author). E-mail: wjweiss@ecn.purdue.edu

Note. This manuscript was submitted on February 17, 2011; approved on August 29, 2011; published online on August 29, 2011. Discussion period open until August 1, 2012; separate discussions must be submitted for individual papers. This paper is part of the ***Journal of Materials in Civil Engineering***, Vol. 24, No. 3, March 1, 2012. ©ASCE, ISSN 0899-1561/2012/3-299–307/$25.00.

Fig. 1. Field observation showing damage in pavement joints

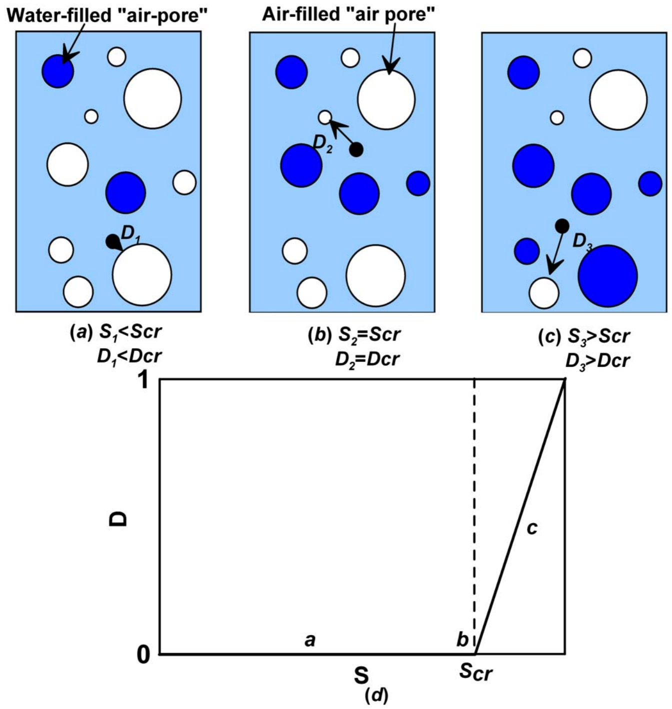

Fig. 2. Schematic of relation between degree of saturation with freeze-thaw damage (10, 19)

that describe the freeze-thaw performance. The first parameter is related to the degree of saturation as described previously. The second parameter is related to a "critical flow distance" (i.e., D_{cr}), which is the maximum distance that water can flow from freezing site to the surrounding nearest air-filled space. Damage doesn't occur when the flow distance (D) is below the critical distance (D_{cr}) and the degree of saturation (S) is less than the critical degree of saturation (S_{cr}), as shown in Fig. 2(a). However, the flow distance increases with the amount of absorbed water (or poor quality air void system) as does the degree of saturation. If either the critical flow distance or the critical degree of saturation is exceeded, frost damage initiates upon the next freezing cycle [Fig. 2(c)]. The degree of damage can be quantified by the reduction in the dynamic elastic modulus of concrete, as shown schematically in Fig. 2(d).

In Fig. 2(d) for all the values of degree of saturation below the critical degree of saturation the amount of damage (reduction is the elastic modulus) is very small. As soon as the degree of saturation exceeds the critical degree of saturation, damage initiates in the material (Fagerlund 1972, 1975, 1977, 2004; Bentz et al. 2001).

The quality of air distribution and the volume of the air are two important parameters affecting the freeze-thaw resistance of the system. The quality of the air system is related to the critical flow distance whereas the quantity of the air voids (volume of air) is related to the critical degree of saturation. A fully saturated system, however, regardless of the quantity and quality of the air cannot even sustain a single freezing cycle without accumulating a significant amount of damage (Litvan 1988).

Background on Use of Acoustic Emission to Quantify Freeze-Thaw Damage

Acoustic emission (AE) is a nondestructive test method that is on the basis of measuring the release of energy in concrete (e.g., the release of energy that occurs at the time of cracking). However, AE can be performed in either a passive (i.e., capturing the acoustic wave generated because of the formation of permanent defect such as crack) or active (i.e., using one transducer to generate a pulse and another transducer to capture the same pulse (in the simplest arrangement). Classically, AE is typically performed in passive mode in cement/concrete studies (Ohtsu 1999, Ohtsu and Shigeishi 1993; Bentz et al. 2008; Hossain et al. 2003; Shah and Weiss 2006; Kim and Weiss 2003; Moon and Weiss 2006; Ouyang et al. 1991a, 1991b; Suaris and Van Mier 1995, 1993; Pour-Ghaz et al. 2010; Puri and Weiss 2006; Yang et al. 2006; Yoon et al. 1999). The AE has been used in concrete to assess damage attributable to restrained shrinkage (Bentz et al. 2008; Hossain et al. 2003; Shah and Weiss 2006; Kim and Weiss 2003; Moon and Weiss 2006) and mechanical loading (Ouyang et al. 1991a, 1991b; Suaris and Van Mier 1995, 1993; Pour-Ghaz et al. 2010; Puri and Weiss 2006; Yang et al. 2006; Yoon et al. 1999). The AE has also been used to monitor freezing and thawing of mortar and it was observed that activity during both freezing and thawing (Shimada et al. 1991; Krishnan 2002).

In the present work the evolution of damage in concrete during freeze-thaw cycles was monitored using both active and passive AE. The reduced relative dynamic elastic modulus was calculated for each cycle according to the transmitting time of waves using active AE. Passive AE was recorded to better understand the damage that develops during the freeze-thaw cycle.

Hypothesis and Outline for Experimental Investigation

There has been a great deal of debate on possible causes of joint deterioration in concrete pavements. It is the hypothesis of this

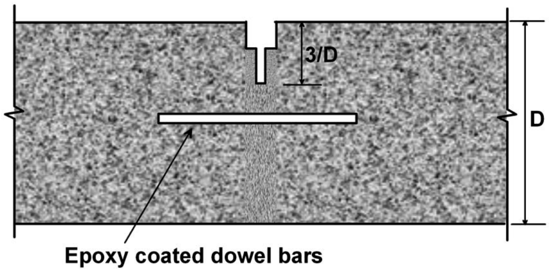

Fig. 3. Cross section of the joints in pavement

work that the presence of water (or solution containing deicing salt solutions) in the joints plays a significant role in the deterioration of concrete pavement joints. First, it is hypothesized that joints can hold water or deicing fluids substantially longer than other parts of the pavement because of the specific geometry of the joint as shown in Fig. 3 (especially if the joint does not crack). This would enable the concrete at the joint to become preferentially saturated. The potential for a joint to hold water increases when the joint sealant is damaged or missing, at low spots in the pavement, and when the joint does not crack and open as designed (as has been noticed in the field). It is hypothesized that this propensity for saturation could make the concrete more susceptible to local freeze-thaw damage. Second, it is hypothesized that the use of air entrainment can increase the resistance to joint deterioration, however, it is also believed that the use of air entrainment will not eliminate the potential for damage to occur. The addition of air entrainment is believed to extend the time required for the concrete to reach to the critical degree of saturation.

Whereas other factors can contribute to joint deterioration (e.g., the use of specific deicers, curing conditions, mixture proportions, construction details), they are not specifically considered in this paper. The scope of this paper is to examine the role of air entrainment on the rate of water ingress and degree of saturation increase in concrete. Second, this paper provides data to relate the degree of saturation to freeze-thaw damage in air entrained and nonair entrained concrete.

Experimental Plan

This section describes mixture proportioning, specimen conditioning, and the procedures of the testing in detail.

Mixture Proportions

Three mortar mixtures were prepared with different air contents (6, 10, 14% air by volume as measured in mortar). The air volume was calculated for an equivalent paste and concrete system, respectively, with the assumptions shown in Table 1. All specimens were made with ordinary Portland cement (Type I) and had a water to cement ratio (w/c) of 0.42 which is typical of concrete pavements in the state of Indiana. Table 1 presents the proportions of the materials that were used.

Table 1. Mixture Proportions and Constituent Materials

Air content of paste (% by volume of mortar[a]/concrete[b])	Cement (Type I) (kg/m^3)	Water (kg/m^3)	Sand (kg/m^3)
13 (6/4)	573.3	240.8	1,333.3
22 (10/7)	548.9	230.6	1,276.5
31 (14/9)	524.5	220.3	1,219.8

[a] In calculating the equivalent air content in mortar it was assumed 45% paste by volume of the mortar.

[b] In calculating the equivalent air content in concrete it was assumed 30% paste by volume of the concrete.

Mixing was performed in accordance with ASTM C192-06 (ASTM 2006). Two specimen geometries were used in this study: cylinders (25 mm height × 100 mm diameter) and prisms (25 mm × 25 mm × 125 mm). Cylindrical specimens were used for the water absorption test. The prisms specimens were used to evaluate the freeze-thaw damage development using AE. These specimens were cut from larger specimens.

Specimen Conditioning

The method of the specimen conditioning prior to water absorption testing can substantially influence the results of the test (Castro et al. 2011, 2010; Spragg et al. 2011). If the specimen is not properly conditioned, it can lead to a misunderstanding of the actual absorption behavior (Castro et al. 2011, 2010; Spragg et al. 2011). Because of the significance of conditioning and necessity for the specimens to reach equilibrium, the standard curing procedures were not used (Scherer and Valenza 2005). The procedure that was used in this study allowed the specimens to equilibrate for a longer period.

The cylindrical specimens were cut 24 h after casting from a larger cylindrical sample and sealed in two layers of plastic. The specimens were stored at 23 ± 1°C for 28 days. After 28 days the specimens were removed from the plastic bag and placed in 50 ± −1, 65 ± 1, and 80 ± 1% relative humidity (RH) environments in which they were kept for more than a year to equilibrate. Table 2 lists the air content and RH of each specimen.

Water Absorption

A procedure similar to ASTM C1585-04 (ASTM 2004) was used, however, the specimens were not conditioned following the accelerated ASTM testing procedure (described previously). After conditioning, the outer circumference of the specimen was sealed with two layers of epoxy resin. After the epoxy hardened, the specimens were placed under water. Two small spacers were placed under the sample to provide a small gap between the bottom of the container and the lower surface of the sample. This allowed water absorption from both circular surfaces (Fig. 4).

Freeze-Thaw Testing

This section describes specimen preparation and procedures used in freeze-thaw testing.

Table 2. Initial Condition, Air Content, and Namely Scheme for Specimens Used in the Present Study

Specimen name	Air content of the paste (%)	RH (%)
50-13[a]	13	50
65-13	13	65
80-13	13	80
50-22	22	50
65-22	22	65
80-22	22	80
50-31	31	50
65-31	31	65
80-31	31	80

[a] The first number shows the initial humidity of the specimen (e.g., 50-13 is 50% RH); the second number shows the air content of mortar of the specimen (e.g., 50-13 is 13% air by volume of paste).

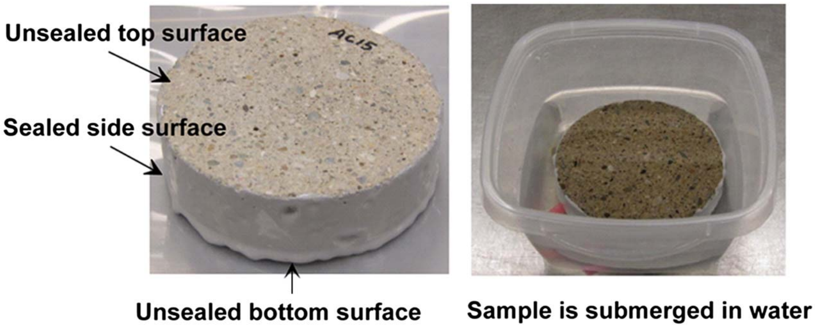

Fig. 4. Double-sided sorption test of specimen with 1-in. thickness

Specimen Saturation

The prismatic specimens were prepared to have different degrees of saturation before freeze-thaw testing was performed. The specimens were oven dried in steps to 105°C where they were maintained for 2 days. The specimens were then placed in a desiccator and evacuated to a residual pressure of 30 mm Hg (4,000 Pa) for 3 h. After evacuation and while still under vacuum, water was introduced into the desiccators to cover the specimens. The specimens were left in the desiccators for 24 h. This condition was considered as saturated (i.e., 100% degree of saturation). The degree of saturation was reduced for some specimens (i.e., 0.96, 0.92, 0.90, 0.86, 0.82, and 0.78) by short periods of drying at 23°C and 50% RH During the drying period, the mass of the specimens was closely monitored. After drying, all the specimens were sealed in plastic bags for a minimum of 3 days to allow moisture to redistribute before freezing and thawing testing.

Preparation of the Specimen for Freezing and Thawing

Fig. 5 shows the procedure used for preparing the specimens for AE testing during freeze-thaw cycles. The specimens were first preconditioned to different degrees of saturation as described previously. After preconditioning, the specimens were wrapped with a thin plastic sheet as shown in Fig. 5(a). The thin plastic sheet was used to protect the sample from further drying during the handling. The specimens were then sealed with a "heat shrink wrap" to further protect the specimens against moisture exchange with surroundings (prevent them from absorbing or releasing water during the freeze-thaw process) as shown in Fig. 5(b). It is important to note that the "heat shrink wrap" was in loose contact with sample (with the exception of the specimen ends) so that the specimen can expand freely during the test whereas minimizing any restraint.

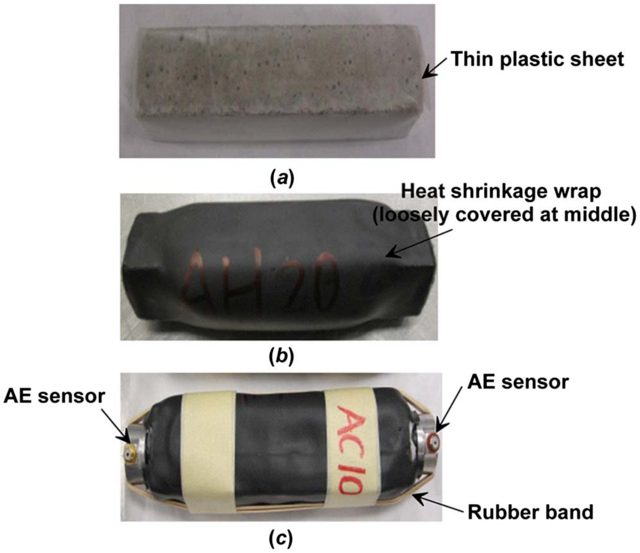

Fig. 5. Specimens prepared for AE testing during freeze-thaw cycle: (a) thin plastic sheet to avoid evaporation during specimen preparation and handling; (b) specimen covered by heat shrinkable wrap to avoid evaporation during specimen preparation and handling; (c) acoustic emission sensors installed at the both ends of the specimens

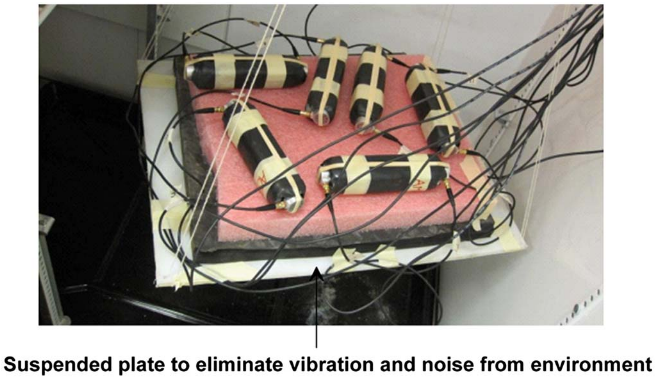

Fig. 6. Specimens placed on a suspended base to eliminate vibration and noise from surrounding environment (inside of freeze-thaw chamber)

The AE sensors (transducers) were attached on the two ends with a thin layer of vacuum grease as shown in Fig. 5(c). Fig. 6 shows that all the specimens were placed on a suspended base in testing to minimize noise/vibration transmission from surrounding environment. The threshold was set at 60 dB and 34 dB for active and passive AE, respectively. Testing was also performed on dry specimens to ensure that sounds were not being recorded from the environment, freezing unit, or coupling agent (Pour-Ghaz and Weiss 2010).

Temperature Cycle used for Freeze-Thaw Testing

Fig. 7 shows the temperature cycle (in air) which allows one cycle per day. Temperature was controlled to vary from 10 ± 1°C to −18 ± 1°C. The rate of the temperature change was 14°C/h resulting in a 2-h transition period and two 10-h periods at 10 ± 1°C and −18 ± 1°C, respectively.

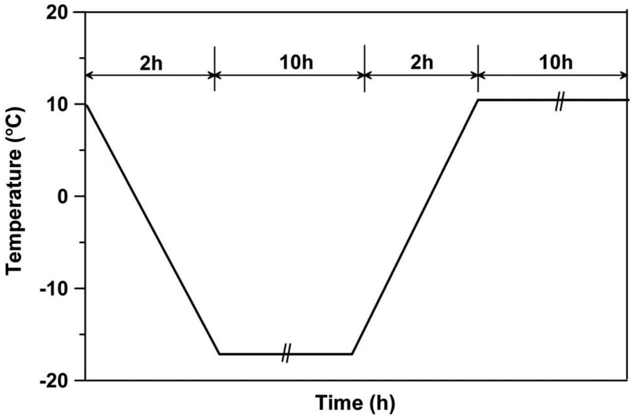

Fig. 7. Temperature cycle used in freeze-thaw experiment (air temperature)

Experimental Results and Discussion

Water Absorption

Sorptivity

The amount of absorbed water (I) is normalized by the cross-sectional area exposed to water as outlined in ASTM C1585 (ASTM 2004)

$$I = m_t/(a.d) \qquad (1)$$

where m_t = change in specimen mass at time t in grams; a = area of the both sides exposed to water in mm^2; and d = density of water in g/mm^3.

Sorptivity is defined as the slope of the water absorption versus square root of time curve (ASTM 2004). The initial sorptivity is the slope of this curve within the first 6 h, whereas the secondary sorptivity is the slope of the curve between 1 and 8 days.

Fig. 8(a) illustrates the sorption results for the specimens conditioned at 50% RH with 13 and 31% air contents by volume of paste. The specimens show a similar sorptivity (slope of the curves) and amount of absorbed water initially; however, over time the specimens with higher volumes of air absorb more water. This occurs because the air voids provide space for water (Helmuth 1961; Warris 1964), however, the diffusion of air and the overpressure in the air bubbles delays water absorption which corresponds for the long time to saturation (Fagerlund 1993, 1995, 2004). Although the secondary sorptivity for sample with higher air content is higher, this sample requires to absorb more water to reach to the critical degree of saturation.

Fig. 8(b) shows the water absorption results for specimens conditioned at 65% RH. Comparing this result with Fig. 8(a) suggests that the amount of absorbed water for the specimens conditioned at 65% RH is lower than that of specimens conditioned at 50% RH with the same air content. Fig. 8(c) shows the absorption for specimens conditioned at 80% RH. The specimens at 65% RH and 50% RH show a nick point at the end of the 6 h on a water absorption square root of time curve, however, the nick point can not be seen on the results of 80% RH and a more graduate rate of absorption can be seen.

The RH in which the specimens were conditioned in has a significant impact on the results (Castro et al. 2011, 2010; Spragg et al. 2011). The driving force of unsaturated fluid transport is the capillary suction (Hall and Hoff 2002; Martys and Ferraris 1997; Hanžič et al. 2010). When samples are in equilibrium with a lower RH, a larger volume of pores are empty and available to be filled with water during the water sorption. Furthermore, at lower humidity, the maximum size of the pores that is filled with water is smaller, creating a higher suction force. The overall effect will be higher rate of water absorption and high volume of absorbed water.

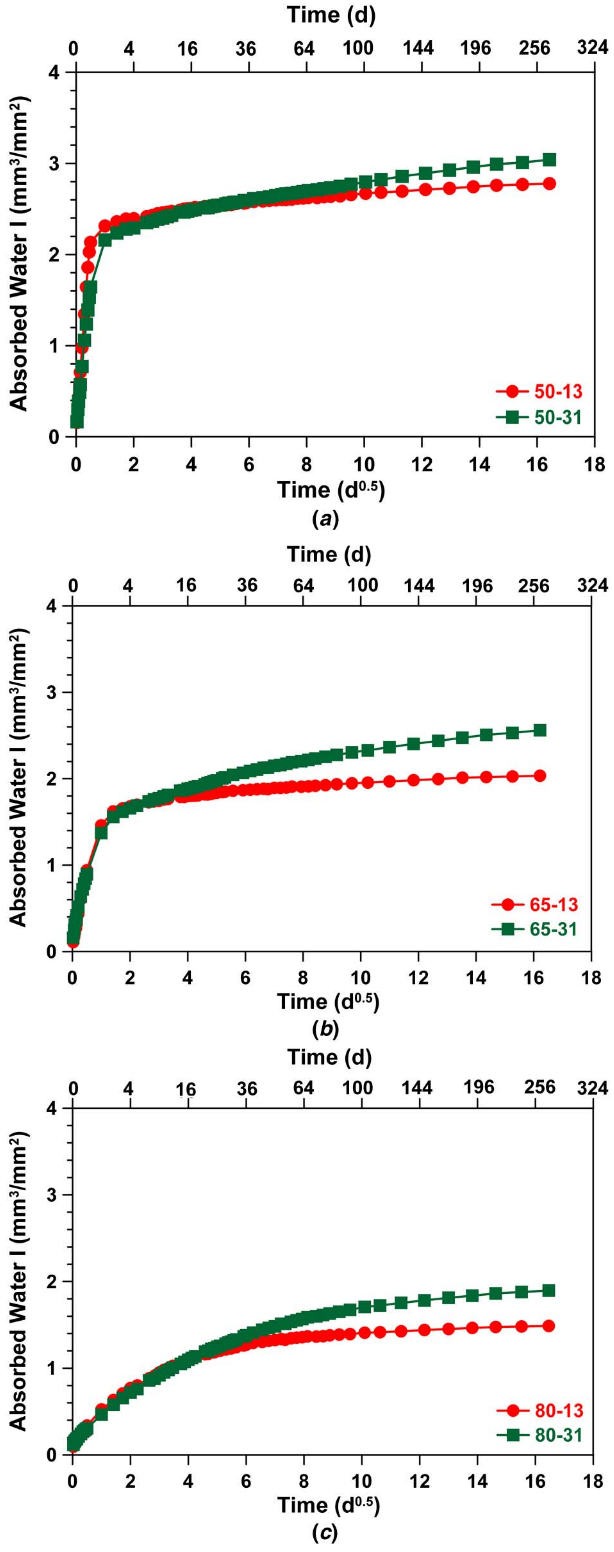

Fig. 8. Effect of air content and initial moisture on water absorbed: (a) 50% RH; (b) 65% RH; (c) 80% RH

Degree of Saturation

Fig. 9 shows the degree of saturation (S) of the specimens conditioned at 50, 65, and 80% RH with two air contents (13 and 31% by volume of paste). The degree of saturation is plotted as a function of

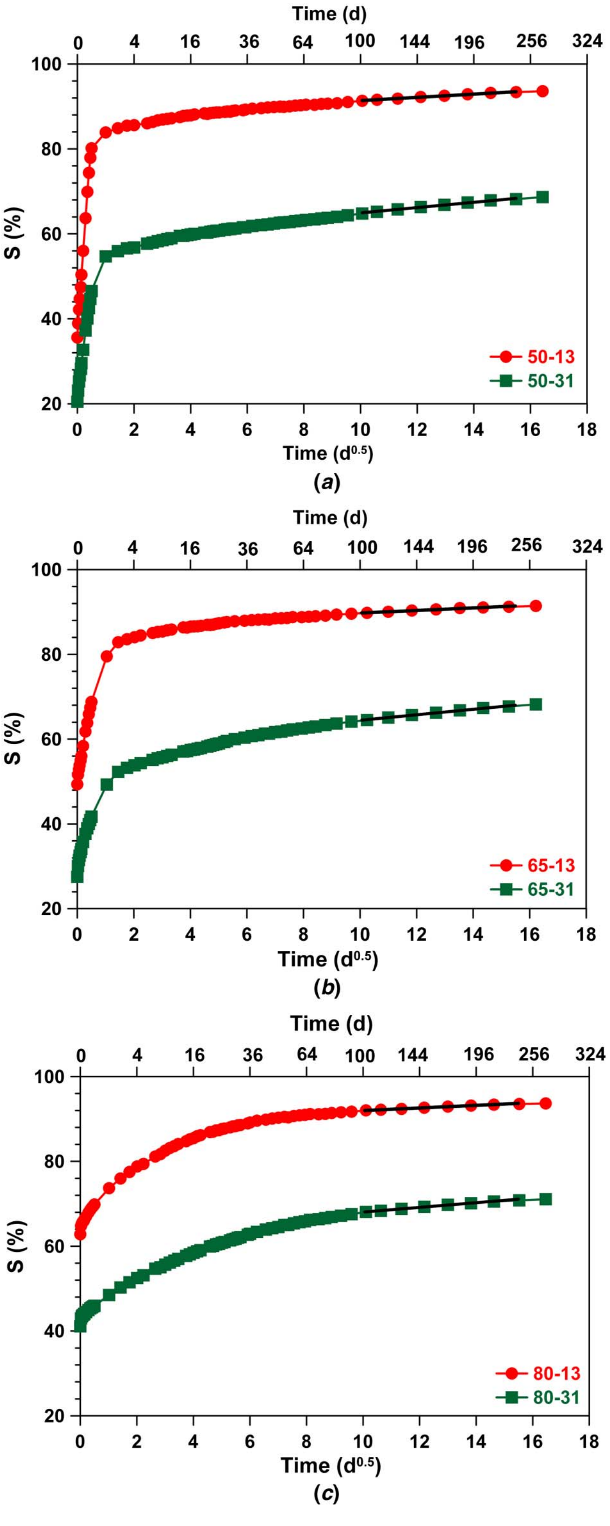

(*a*)

(*b*)

(*c*)

Fig. 9. Results of sorption test provided as increase in the degree of saturation: (a) 50% RH; (b) 65% RH; (c) 80% RH

squareroot of time on the lower x-axis whereas actual time is shown on the upper *x*-axis.

The most striking feature of the graphs in Fig. 9 is the fact that the degree of saturation decreases with air content. At the end of the initial 6-h sorption period, samples with lower air content show higher degree of saturation. For samples equilibrated at 50% RH, the degree of saturation is 39% less when the air content increases 10%, the decrease in degree of saturation for samples equilibrated at 65% and 80% RH is 23% and 26%, respectively.

Table 3. Time to Reach to the Critical Level of Saturation (88%) for the Specimens with Different Air Content

Initial RH (%)	Air content by volume of paste (%)	Secondary sorptivity ($\mathrm{mm^3/mm^2.d^{0.5}}$)	Time to reach the critical degree of saturation (88%) (S_{cr}) in years (±1.7%)
50	13	0.485	0.011 (4*d*)
	22	0.691	5.08
	31	0.750	6.10
65	13	0.368	0.016 (6*d*)
	22	0.513	5.63
	31	0.785	5.90
80	13	0.563	0.015 (5*d*)
	22	0.606	4.00
	31	1.009	5.82

The secondary rate of absorption (Fig. 8) is different for samples with different air content; however, in Fig. 9 the secondary rate of increase in degree of saturation is approximately the same for materials with different air content. This suggests that for an equal time of exposure to water, the specimen with the higher air content has a lower degree of saturation (Fagerlund 1993, 1995, 2004).

The secondary rate of increase in degree of saturation can be fitted with a linear function to estimate the amount of absorbed water over a long period of time. The linear fit used in Fig. 9 is shown with a solid line. Because the objective here is to estimate the degree of saturation over a long period of time, only the date between 100 and 240 days is used in fitting this straight line. Using this linear function, the time to reach to critical degree of saturation is calculated for each specimen with different air content and initial equilibrium condition and reported in Table 3.

Freeze-Thaw Testing

Monitoring the Damage Development Using Active Acoustic Emission

The relative dynamic elastic modulus is frequently used as an index to evaluate the extent of damage (Fagerlund 1972, 1975, 1977, 1979, 1981, 2004; Bentz et al. 2001; Litvan 1988; Litvan and Sereda 1980; Shimada et al. 1991). Using active AE, the transmission time of a single pulse was measured along the sample. The transmission time along the length of the sample was measured in both directions (i.e., from Sensor 1 to 2 and from Sensor 2 to 1). The transmission time was measured three times in each direction and the average transmission time is reported here (average of 6 values). The transmitting time was measured after each cycle when the temperature was stable at 10°C for a minimum of 2 h.

The relative elastic modulus, i.e., E_t/E_o, is square proportional to the velocity of wave transmitting through materials, which is inversely square proportional to the ratio of the wave transmission times (ASTM 2008), as shown in Eq. (2). Damage parameter (D) can also be estimated using Eq. (2).

$$D = 1 - E_t/E_o = 1 - (T_o/T_t)^2 \tag{2}$$

where E_o, T_o = dynamic elastic modulus before freeze-thaw testing began and corresponding transmitting time; and E_t, T_t = dynamic elastic modulus during testing at any time t and corresponding transmitting time.

The main cracks were along the direction of wave propagation and as such the wave is least sensitive to these cracks, however, the damage was still easily recorded.

Fig. 10 illustrates the damage index [Eq. (2)] with increasing cycles of freezing and thawing. The damage initiates during the first cycle when the degree of saturation is above 86 ~ 88%. The specimens with lower degree of saturation do not show damage whereas specimens with a higher degree of saturation show a rapid deterioration. The saturated specimens ($S = 100\%$) can not sustain more than three cycles before complete failure occurs.

Fig. 11 shows the rate of damage (dD) development per freeze-thaw cycle (dN) (as determined by the slope of Fig. 10) for specimens with different degrees of saturation. A critical degree of saturation appears to occur at approximately 86–88%. The critical degree of saturation appears to be independent of the air content.

Acoustic Energy Measured Using Passive Acoustic Emission
Fig. 12 shows the amplitude of the acoustic events as a function time for a specimen with 96% degree of saturation and 13% air content during freezing cycle. The temperature is the temperature measured in the center of the mortar specimen. Fig. 12(a) illustrates the amplitude distribution for the first freeze-thaw cycle and Fig. 12(b) illustrates the amplitude distribution during the second freeze-thaw cycle for the same specimen.

In Fig. 12(a) the acoustic events begin to occur as the temperature of the specimen decreases. A cluster of acoustic event is shown in Fig. 12(a) as highlighted by the ellipsoid. This cluster of data is not seen in Fig. 12(b). These events can be attributed to microcracking of the specimen because of the thermal loading, which may be a result of temperature gradient or a result of thermal expansion coefficient mismatch between the paste and aggregate. Because the thermal loading is not changed during the second cycle, the damage attributed to thermal loading does not exceed the previous level of damage in materials and additional cracking would not be expected (Kaiser 1950; Kline and Egle 1987).

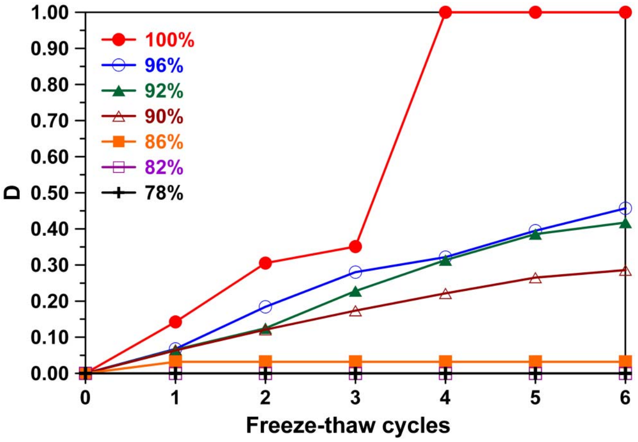

Fig. 10. Decrease of the relative dynamic elastic modulus with freeze-thaw cycles of the specimen with 13% air content by volume of the paste

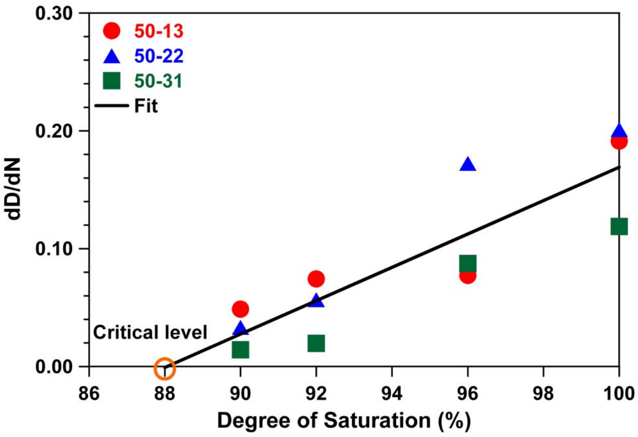

Fig. 11. Rate of decrease of relative dynamic elastic modulus with degree of saturation

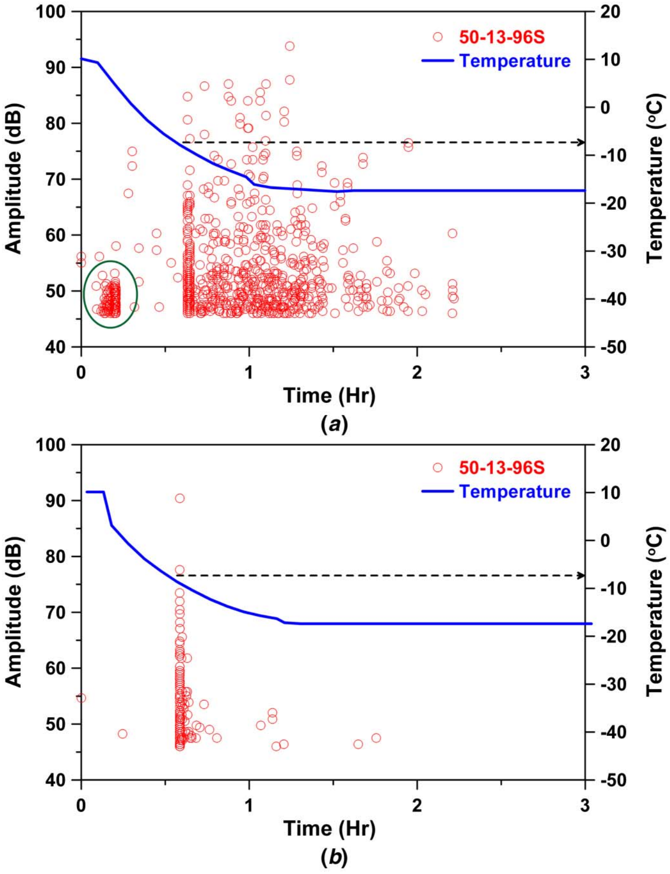

Fig. 12. Amplitude in the transition time of freezing (96S): (a) first cycle; (b) second cycle

In Fig. 12 the acoustic events begin to increase dramatically after the temperature drops below −8°C in both cycles. The number of events is higher in the first cycle compared to the second cycle as more cracking would be expected in the first freeze-thaw cycle whereas these cracks would be expected to extend in the following cycles. The damage at the point (below −8°C) is likely attributed to formation of ice and cracking inside the specimen. This is consistent with the observation that pore solution freezes below 0°C because of pore confinement and dissolved ions in pore solution (Fagerlund 1973; Helmuth 1960).

Desorption Isotherm

Fig. 13 shows the desorption isotherm for the specimens with 13 and 31% air content by volume of paste. The desorption curve demonstrates the mass of water lost from the specimen at each RH step (i.e., different pore sizes begin to empty out at different RHs starting with large pores at high RHs and smaller pores at lower humidities). The profile of the desorption curve is similar for both specimens until high RHs, i.e., 97.5% RH. At RHs higher than 97.5%, a larger difference of the porosity can be seen. This difference corresponds to the air entrained porosity.

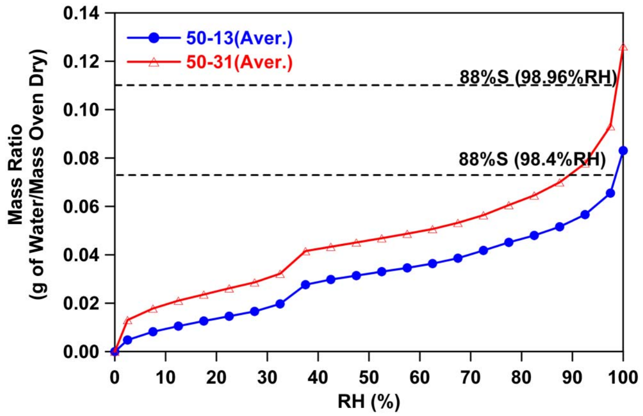

Fig. 13. Mass change at decreasing RH containing deionized water

The critical degree of saturation (88%) corresponds to RH of 98.4% for specimen with 13% air content and 98.96% RH for specimen with 31% air content, respectively. This implies that some of the air entrained pores are water filled when the specimen is at or above critical degree of saturation. The difference in mass loss between the 13 and 31% air content at 2.5% RH is currently unknown, however, this is repeatable between specimens.

Calculated Time to Reach the Critical Degree of Saturation

The rate of absorption of water and its relation to the degree of saturation was discussed previously and the influence of the degree of saturation on freeze-thaw damage was discussed after that. To better understand how these findings can be related to one another to predict the time to freeze-thaw damage, a linear function was fit to the plot of degree of saturation verses squareroot of time data (using the secondary absorption).

Table 3 shows the time required for each specimen equilibrated at different initial conditions to reach the critical degree of saturation (i.e., 88% in this study). Specimens without air entrainment can reach to the critical degree of saturation within days (4 ∼ 6 days). The use of air entrainment raised the air content and decreases the degree of saturation. This increases the time to reach a critical degree of saturation to 3 ∼ 6 years. The rate of water absorption is substantially different in the systems with entrained air compared to nonair entrained systems.

Conclusions

The water absorption of mortar containing different volumes of entrained air was examined in this study. whereas tests like ASTM C 1585-04 (ASTM 2004) can be used to provide an index of water absorption, the differences between nonair entrained and air entrained systems were small when only mass gain was investigated. Whereas the absorption rates in plain and air entrained systems were similar, initially the air entrained system showed a higher rate of ingress at later ages. By normalizing the results of water absorption in terms of the degree of saturation, a clear distinction between the nonair entrained and air entrained mixtures can be made. Whereas the nonair entrained system took 4–6 days to reach 88% saturation, the air entrained system is estimated to require approximately 3–6 years. This shows that entrained air will substantially increase the time to failure.

The damage attributable to freeze-thaw was monitored using both passive and active AE. A critical degree of saturation was observed with specimens that have a degree of saturation greater than the 86–88% exhibiting damage during the few freeze-thaw cycles.

The critical degree of saturation appears to be independent of the air content as materials with a degree of saturation above the critical degree undergoing damage after a few of freeze-thaw cycles irrespective of the air content. The volume of air and quality of the air void system however likely has a strong relation to the critical flow distance.

Increasing the air content resulted in a longer time for the mortar to reach to the critical degree of saturation. Whereas increasing the air content can delay the time freeze-thaw damage initiates in practice, it appears that increasing of the air content can not eliminate the potential for freeze-thaw damage. To solve this problem, the benefits of sealers as well as improving the understanding of the correlation between the critical spacing and the degree of saturation and the freezing rate are being investigated.

Acknowledgments

The experiments reported in this paper were conducted in the Pankow Materials Laboratories at Purdue University. This work was supported in part by Compass Minerals and the Joint Transportation Research Program administered by the Indiana Department of Transportation and Purdue University. The contents of this paper reflect the views of the authors, who are responsible for the facts and the accuracy of the data presented in this paper, and do not necessarily reflect the official views or policies of the Indiana Department of Transportation, nor do the contents constitute a standard, specification, or regulation. The authors appreciate the assistance of Gaurav Sant for his work in casting/cutting the specimens while he was a graduate assistant funded on this project. The authors also acknowledge many useful discussions with Dick Newell, John Poncher, Mike Byers, Tommy Nantung, Dave Andrewski, and Jan Olek.

References

ASTM. (2004). "Standard test method for measurement of rate of absorption of water by hydraulic-cement concretes." *Standard C1585-04*, ASTM International, West Conshohocken, PA.

ASTM. (2006). "Standard practice for making and curing concrete test specimens in the laboratory." *Standard C192*, ASTM International, West Conshohocken, PA.

ASTM. (2008). "Test method for resistance of concrete to rapid freezing and thawing." *Standard C666*, ASTM International, West Conshohocken, PA.

Barde, V., Radlinska, A., Cohen, M., and Weiss, W. J. (2009). "Relating material properties to exposure conditions for predicting service life in concrete bridge decks in Indiana." *The Joint Transportation Research Program of the Indiana Department of Transportation*, Purdue Univ., West Lafayette, IN.

Beaudoin, J. J., and Cameron, M. (1972). "Dimentional changes of hydrated Portland cement paste during slow cooling and warming." *Cement and Concrete Research*, 2(2), 225–240.

Bentz, D. P., Ehlen, M. A., Ferraris, C. F., and Garboczi, E. J. (2001). "Sorptivity-based service life predictions for concrete pavements." *7th Int. Conf. on Concrete Pavements*, NIST, Orlando, FL, 181–193.

Bentz, D. P., Sant, G., and Weiss, J. (2008). "Early-age properties of cement-based materials I: Influence of cement fineness." *J. Mater. Civ. Eng.*, 20(7), 502–508.

Castro, J., Bentz, D., and Weiss, J. (2011). "Effect of sample conditioning on the water absorption of concrete." *Cement and Concrete Compos.*, 33(8), 805–813.

Castro, J., Kompare, P., Poursaee, P., Nantung, T., and Weiss, J. (2010). "Portland cement concrete pavement performance relative to permeability." *JTRP Rep. SPR-3093*, Indiana Department of Transportation, West Lafayette, IN.

Fagerlund, G. (1972). "Critical degrees of saturation at freezing of porous and brittle materials." *Rep. 34*, Div. of Building Technology, Lund Institute of Technology, Lund, Sweden, 408.

Fagerlund, G. (1973). "Determination of pore-size distribution from freezing-point depression." *Mater. Struct.*, 6(3), 215–225.

Fagerlund, G. (1975). "The significance of critical degrees of saturation at freezing of porous and brittle materials." *Conf. on Durability of Concrete, ACI STP, Atlantic*, Vol. 47, New Jersey and Ottawa, Ontario, 13–65.

Fagerlund, G. (1977). "The international cooperative test of the critical degree of saturation method of assessing the freeze/thaw resistance of concrete." *Mater. Struct.*, 10(4), 231–253.

Fagerlund, G. (1979). "Prediction of the service life of concrete exposed to frost action, studies on concrete technology." *Studies on Concrete Technology*, Swedish Cement and Concrete Research Institute, Stockholm, 249–276.

Fagerlund, G. (1981). "The principles of frost resistance of concrete." *Nordisk Betong*, (2), 5–13 (in Swedish).

Fagerlund, G. (1993). "The long-time water absorption in the air-pore structure of concrete." *Rep. TVBM-3051*, Div. of Building Technology, Lund Institute of Technology, Lund, Sweden.

Fagerlund, G. (1995). "The required air content of concrete." *Proc., Int. Workshop on Mass-Energy Transfer and Determination of Building Components*, BRI-Japan and CSTB-France, Paris, 591–609.

Fagerlund, G. (2004). "A service life model for international frost damage in concrete." *Rep. TVBM-3119*, Div. of Building Technology, Lund Institute of Technology, Lund, Sweden.

Feldman, R. F. (1987). "Diffusion measurements in cement paste by water replacement using propan-2-OL." *Cement and Concrete Research*, 17(4), 602–612.

Hall, C., and Hoff, W. D. (2002). "Water in porous materials." *Water-Transport in Brick, Stone and Concrete*, Taylor & Francis, Abingdon, Oxon, 29–41.

Hanžič, L., Kosec, L., and Anžel, I. (2010). "Capillary absorption in concrete and the lucas—washburn equation." *Cement and Concrete Compos.*, 32(1), 84–91.

Helmuth, R. A. (1960). "Capillary size restrictions on ice formation in hardened Portland cement pastes." *Proc., 4th Int. Symp. on Chemistry of Cement*, Paper VI-S2, Portland Cement Association, Research and Development Laboratories, Skokie, IL, 855–869.

Helmuth, R. A. (1961). "Dimensional changes of hardened Portland cement pastes caused by temperature changes." *Proc., Highway Research Board*, Vol. 40, Portland Cement Association, Research and Development Laboratories, Skokie, IL, 315–336.

Hossain, A. B., Pease, B., and Weiss, J. (2003). "Quantifying early-age stress development and cracking in low water-to-cement concrete—restrained-ring test with acoustic emission." *Transportation Research Record*, 1834(1), 24–32.

Kaiser, J. (1950). "A study of acoustic phenomena in tensile tests." Ph.D. dissertation, Technical University of Munich, Bayern, Germany.

Kim, B., and Weiss, J. (2003). "Using acoustic emission to quantify damage in restrained fiber-reinforced cement mortars." *Cement and Concrete Compos.*, 33(2), 207–214.

Kline, R. A., and Egle, D. M. (1987). "A brief note on the Kaiser and Felicity effects." *J. Acoustic Emission*, 6(3), 205–206.

Krishnan, A. (2002). "Durability of concrete containing fly ash or slag exposed to low temperatures at early ages." M.S. thesis, Purdue Univ., West Lafayette, IN.

Leech, C., Lockington, D., Hooton, R. D., Galloway, G., Cowin, G., and Dux, P. (2008). "Validation of Mualem's conductivity model and prediction of saturated permeability from sorptivity." *ACI Mater. J.*, 105(1), 44–51.

Litvan, G. G. (1988). "The mechanism of frost action in concrete-theory and practical implications." *Proc. of Workshop on Low Temperature Effects on Concrete*, National Research Council of Canada, Montreal, Canada, 115–134.

Litvan, G. G., and Sereda, P. J. (1980). "Freeze-thaw durability of porous building materials." *Durability of Building Materials and Components, ASTM STP 691*, P. J. Sereda and G. G. Litvan, eds., ASTM International, West Conshohocken, PA, 455–463.

Martys, N. S., and Ferraris, C. E. (1997). "Capillary transport in mortars and concrete." *Cement and Concrete Research*, 27(5), 747–760.

Moon, J. H., and Weiss, J. (2006). "Estimating residual stress in the restrained ring test under circumferential drying." *Cement and Concrete Compos.*, 28(5), 486–496.

Ohtsu, M. (1999). "Estimation of crack and damage progression in concrete by quantitative acoustic emission analysis." *Mater. Evaluation*, 57(5), 521–525.

Ohtsu, M., and Shigeishi, M. (1993). "Experimental crack identification of mixed mode by acoustic emission." *Int. Conf. on Fracture and Damage of Concrete and Rock (FDCR-2)*, H. P. Rossmanith, ed., E&FN Spon, London, 186–195.

Ouyang, C., Landis, E., and Shah, S. P. (1991a). "Damage assessment in concrete using quantitative acoustic emission." *J. Eng. Mech.*, 117(11), 2681–2698.

Ouyang, C., Landis, E., and Shah, S. P. (1991b). "Detection of microcracking in concrete by acoustic emission." *Experimental Techniques*, 15(3), 24–28.

Pour-Ghaz, M., et al. (2010). "Using electrical, magnetic and acoustic sensors to detect damage in segmental concrete pipes subjected to permanent ground deformation." School of Civil Engineering, Purdue Univ., West Lafayette, IN.

Pour-Ghaz, M., and Weiss, J. (2010). "Quantifying damage due to aggregate expansion in cement matrix." *Advances in the Material Science of Concrete, ACI SP-270-9*, 101–113.

Puri, S., and Weiss, J. (2006). "Assessment of localized damage in concrete under compression using acoustic emission." *ASCE J. Mater. Civ. Eng.*, 18(3), 325–333.

Rangaraju, P. R., Sompura, K. R., and Olek, J. (2006). "Investigation into potential of alkali-acetate-based deicers to cause alkali-silica reaction in concrete." *Transportation Research Record*, 1979, 69–78.

Scherer, G. W. (1993). "Freezing gels." *J. Non-Crystalline Solids*, 155(1), 1–25.

Scherer, G. W., and Valenza, J. J. (2005). "Mechanisms of frost damage." *Mater. Science of Concrete*, 7, 209–246.

Shah, H. R., and Weiss, J. (2006). "Quantifying shrinkage cracking in fiber reinforced concrete using the ring test." *Mater. Struct.*, 39(9), 887–899.

Shimada, H., Sakai, K., and Litvan, G. G. (1991). "Acoustic emissions of mortar subjected to freezing and thawing." *Durability of Concrete: Second Int. Conf.*, V. M. Malhotra, ed., American Concrete Institute, Detroit, 263–278.

Spragg, R., Castro, J., Li, W., Pour-Ghaz, M., Huang, P., and Weiss, J. (2011). "Wetting and drying of concrete in the presence of deicing salt solutions." *Cement and Concrete Compos.*, 33(5), 535–542.

Suaris, W., and Van Mier, J. G. M. (1993). "Acoustic emission and source location in concrete subjected to mixed mode loading." *Int. Conf. on Fracture and Damage of Concrete and Rock (FDCR-2)*, H. P. Rossmanith, ed., E&FN Spon, London, 157–165.

Suaris, W., and Van Mier, J. G. M. (1995). "Acoustic emission source characterization in concrete under biaxial loading." *Mater. Struct.*, 28(8), 444–449.

Sun, Z., Kumpf, D., and Scherer, G. W. (2007). "Kinetics of ice growth in concrete." *Proc., 12th Int. Congress Cement Chemistry*, J. J. Beaudoin, J. M. Makar, and L. Raki, eds., National Research Council of Canada, Montreal, W4–07.1.

Sutter, L., Van Dam, T., Peterson, K. R., and Johnston, D. P. (2006). "Long-term effects of magnesium chloride and other concentrated salt solutions on pavement and structural Portland cement concrete phase I results." *Transp. Res. Rec.*, 1979, 60–68.

Warris, B. (1964). "The influence of air-entrainment on the frost-resistance of concrete, part B, hypothesis and freezing experiments." *Proc., No. 36 Swedish Cement and Concrete Research Institute*, Svenska Forskningsinstitutet för Cement och Betong, Stockholm, 130.

Weiss, W. J., Abraham, D., and Nantung, T. (2007). "SPR3200—A proposal for a research study on saw-cutting and curing of concrete pavements." *The Joint Transportation Research Program of the Indiana Department of Transportation*, Purdue Univ., West Lafayette, IN.

Yang, Z. F., Weiss, W. J., and Olek, J. (2006). "Water transport in concrete damaged by tensile loading and freeze-thaw cycling." *J. Mater. Civ. Eng.*, 18(3), 424–434.

Yoon, D. J., Weiss, W. J., Prine, D. W., and Shah, S. P. (1999). "Assessing corrosion damage in reinforced concrete beams using acoustic emission." *Non-Destr. Eval. Bridg. Highw.*, 3587, 254–263.

Automation in Construction 19 (2010) 485–490

Contents lists available at ScienceDirect

Automation in Construction

journal homepage: www.elsevier.com/locate/autcon

An automated electrical monitoring system (AEMS) to assess property development in concrete

A. Poursaee *, W.J. Weiss

School of Civil Engineering, Purdue University, West Lafayette, IN, 47907, United States

ARTICLE INFO

Article history:
Accepted 29 December 2009

Keywords:
Electrical impedance
Automation
Concrete
Electrical properties
Imaging
LabVIEW

ABSTRACT

Electrical impedance measurement techniques are being increasingly used to measure material property development and permeability of concrete and other cement based materials. This paper describes the development of an automated electrical measurement system (AEMS) for measuring the properties of cementitious materials. The components of this system are an electrical impedance spectrometer, a digital multi-meter, a switching unit, and a customized software (AEMS) which communicates between different components of the system to control the testing and to collect data. This system enables electrical properties of multiple specimens to be measured in an automated fashion thereby making this approach very amenable for use in quality control applications. Further, an extension of this system is proposed which would enable its use to detect flaws in concrete using electrical imaging.

1. Introduction

Electrical impedance measurement techniques have been shown to provide useful information that can be used to characterize cementitious systems [1–3]. This technique studies the system response to the application of a small amplitude alternating potential signal at different frequencies. AC electrical impedance measurements have the advantages of being non-invasive and non-destructive, require little in term of preparation of the sample, and offer the possibility of continual measurements to describe the effect of hydration [4,5] drying [6], or permeability [7].

Electrical impedance techniques have been used in different research projects in concrete to study a wide range of concrete properties specifically this included studies on the microstructural development of cementitious materials [8,9], precipitation of calcium hydroxide on the surface of steel after the setting of the mortar [10], long-term effectiveness of concrete inhibitors for steel in concrete [11–15], the chloride diffusivity in concrete [16], chloride permeability of high performance concrete [17], detection of damage during tensile loading of cement composites [18], freezing of water in Portland cement paste [19], water penetration in concrete [20–22], setting time of concrete [23,24], measuring the concrete internal moisture content [25], and assessing the change in microstructure due to rapid chloride permeability test [26,27].

While numerous applications exit, they are frequently limited to the measurement of one sample at a time. It is regularly necessary to conduct experimental measurements at multiple locations in a sample or on multiple specimens. For example, Schmit [28] described the use of multiple sensors and quantified the influence of sensor position and number in uncertainty of the results. The ability to perform multiple measurements is very valuable for monitoring the hydration process, monitoring multiple specimens, or imaging the crack by electrical impedance measurements [29]. In addition, a single measurement cannot properly represent the behavior of a material. To improve measurements accuracy multiple measurements are needed. This paper describes the development of a user friendly Automatic Electrical Monitoring System (AEMS). By using this system, multiple electrical measurements can be performed on specimens and different properties of concrete materials can be monitored. The developed system is discussed and some applications of the AEMS were shown in this paper.

2. Objective

This paper describes the development of an Automated Electrical Monitoring System (AEMS). The data acquisition system consists of a computer, a Keithley digital multi-meter and switching unit [30], and Solartron 1260 impedance spectrometer[1] [31]. The role of the software is to communicate between all components of the system and to control data collection. This paper shows that the system is reliable for both short and long-term monitoring. Further, this paper points out that while in the past the use of electrical impedance

---

* Corresponding author.
E-mail address: poursaee@purdue.edu (A. Poursaee).

[1] Certain commercial products are identified in this paper to specify the materials used and procedures employed. In no case does such identification imply endorsement by the authors, nor does it indicate that the products are necessarily the best available for the purpose.

0926-5805/$ – see front matter © 2010 Elsevier B.V. All rights reserved.
doi:10.1016/j.autcon.2009.12.016

measurement techniques has been time consuming, automation enables these measurements to be performed efficiently. This enables new applications, like electrical imaging, to be performed effectively and enables EIS to be extended for use in daily quality control processes such as permeability measurements. Since electrical impedance requires less preparation and time, it can be a good replacement for the tests like rapid chloride permeability which is time consuming and can alter the microstructure of the concrete.

3. Component of the measurement system

The system developed for this investigation can be used to measure the AC electrical impedance response of the material. The components in the system consist of an impedance spectrometer, digital multi-meter, and a switching unit.

The electrical impedance spectrometer used in this study is capable of performing only one measurement at a time. There are multi-channel spectrometer units on the commercial market. However, in addition to their high cost most of the units are limited to only a few measurements (up to 16) at a time which also may be a limiting factor.

The digital multi-meter and switching unit chosen for this project included a Keithley model 2750 mainframe which has five slots and a model 2700 which has two slots for inserting the plug-in switch/control modules. Each slot can support a series of multiplexer, matrix, or control modules. For example the Module 7708 which was used in this project has 40 channels. The general features of this module are described in [32]. The role of the mainframe is to communicate between channels. Temperature can also be measured using this system as this is needed for temperature corrections [33].

For each impedance measurement (each sample), 2 channels are required, (i.e., the Keithley model 2750 mainframe with five 7708 modules can be used for 100 impedance measurements). If more than 100 measurements are necessary, several mainframes can be joined together to provide the appropriate number of channels.

To combine the mentioned components, the software (named AEMS) was developed, using LabVIEW. This software selects the sample that will be tested and then runs the impedance spectrometer on that sample. After the measurements are completed, the AEMS, stops the spectrometer, switches the sample and runs the test again. The measurements are performed one by one not simultaneously. In all the graphs shown in the paper, this time is considered. This time for AC measurements is a function of selected frequency and in all examples in this paper it was about 40 s. However, when the concrete is hardened, this time difference is not considerable. If some interval time is necessary between measurements, the AEMS can be programmed to place the necessary time interval between measurements. In addition, the AEMS can communicate with the mainframe to measure voltage, DC resistance and temperature independent from the spectrometer. Fig. 1 schematically shows the component of the system and the actual parts are shown in Fig. 2.

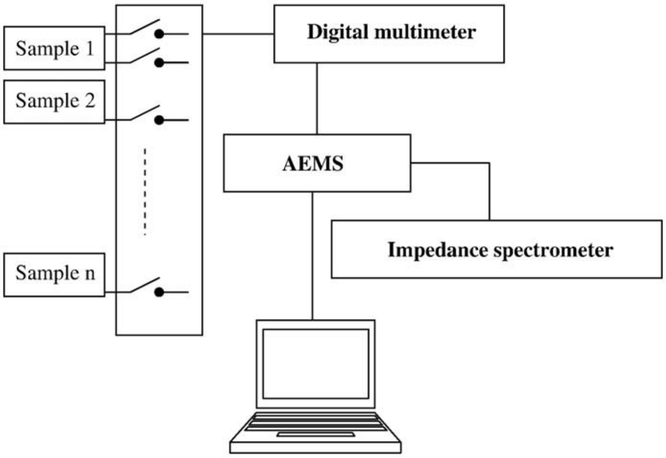

Fig. 1. Schematic relationship between the components of the system.

Fig. 2. Components of the system.

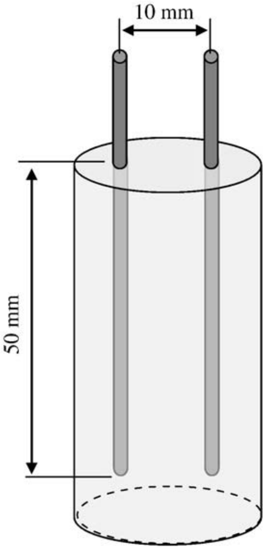

Fig. 3. Schematic view of the cylindrical paste specimens, used to measure variability in cement paste.

While an RS-232 serial port was used to control the multi-meter and switching system in this study, faster data transfer can be performed using a GPIB[2] [34] card. The role of the AEMS software is to control and switch the channels for each measurement, to control and run the spectrometer and save data to the computer for later analysis.

---

[2] The General Purpose Interface Bus (GPIB) is an industry standard published by the Institute of Electrical and Electronic Engineers (IEEE) as ANSI/IEEE Standard 488. GPIB defines the electrical, mechanical, functional, and software specifications of an interfacing system to connect PCs to programmable instrument.

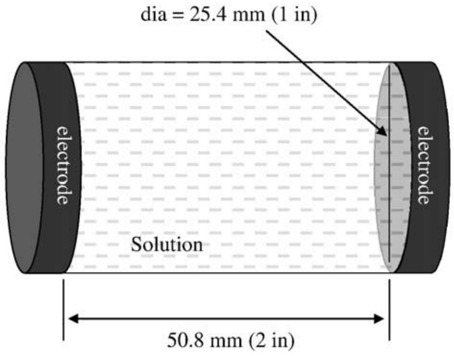

Fig. 4. Schematic view of the container with known geometry, to measure the conductivity of the solutions.

The software contains options which enable the user to set the number of samples, measurement frequency, and the time between each set of measurements. The saved data can be opened and analyzed in Excel®. Based on the number of measurements, one may end up with thousands of data files. Therefore, a macro was developed to automatically analyze individual data and place the summarized results in a worksheet.

4. Experimental results

To verify the performance of the switching units, two simple experiments were conducted. In the first test, a known resistor (10 Ω) was connected to all available channels and the resistance was measured. In the second test, a known potential was measured, using all channels. Results show that there is no significant difference between measured values with each channels and the relative standard deviation was less than 0.005%.

4.1. Electrical conductivity of cement paste sample during hydration

Electrical measurements can provide information about the change in pore structure due to hydration process [23,35]. It is important to use multiple specimens for these measurements due to the inhomogeneity and corresponding variability of cementitious materials. To determine the variation between different samples the electrical conductivity of cement paste samples was measured using cylindrical paste specimens as described in Fig. 3. Type I ordinary Portland cement was used with a Blaine fineness of 360 m^2/kg and a Bogue phase composition of 60% C_3S, 12% C_2S, 12% C_3A, 7% C_4AF and Na_2O equivalent of 0.72%. Fifteen samples were prepared with a *w*/*c* of 0.45 and 5 samples were prepared with a *w*/*c* of 0.50. The measurement frequency range that was used for the tests ranged from 1 MHz to 10 Hz with ten measurements per decade using the 500 mV AC stimulus. To determine the conductivity of the material, the bulk resistance (R_b) obtained from the impedance response normalized for the effects of specimen and electrode geometries, using the following equation:

$$\sigma_t = k / R_b \tag{1}$$

where, σ_t is the conductivity (S/m) of the paste, R_b is the measured bulk resistance (Ω) and k is a geometry factor. The geometry factor

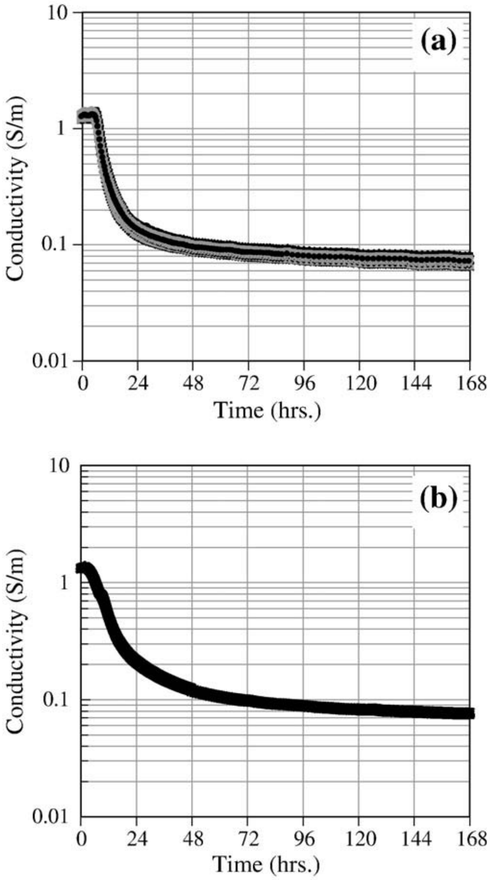

Fig. 5. Development of the conductivity of (a) 15 cement paste samples with *w*/*c* = 0.45 and, (b) 5 cement paste samples with *w*/*c* = 0.5.

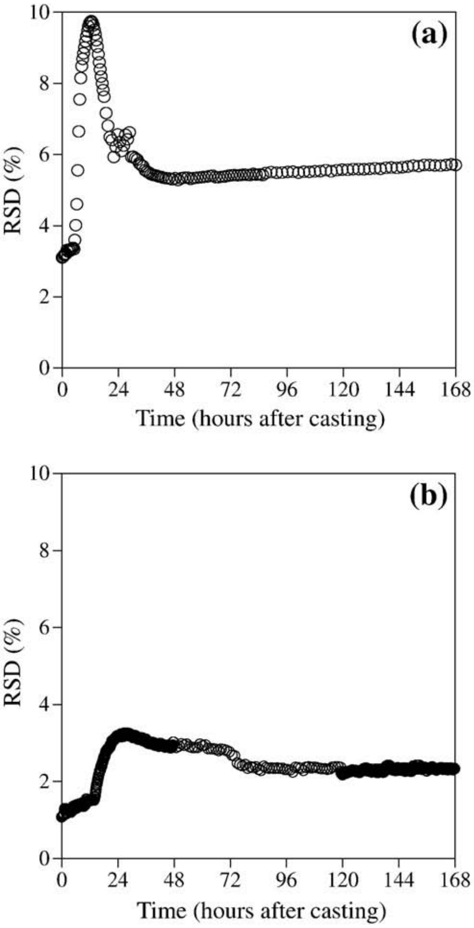

Fig. 6. Relative standard deviation between (a) 15 cement paste samples, with *w*/*c* = 0.45, at different ages and, (b) between 5 cement paste samples, with *w*/*c* = 0.50, at different ages.

was determined by filling the molds with solutions of known conductivity and measuring the bulk resistance between the electrodes. In this experiment two sodium chloride solutions were prepared with two different concentrations (0.1 M and 1 M). The conductivity of the two solutions was measured (7.72 and 1.01 S/m for 1 M and 0.1 M solutions, respectively), using a container with known geometry as shown in Fig. 4. By using this information, the value of the geometry factor, *k*, was calculated to be 15.5/m for the geometry shown in Fig. 3.

The electrical impedance of the samples was measured for 7 days, starting 30 min after casting. Fig. 5 shows the conductivity of the samples with *w*/*c* of 0.45 and 0.50, respectively. At the end of the test, all samples were inspected to ascertain the uniformity of specimen.

It can be seen that the conductivity of all samples follows the same pattern. As expected, the conductivity decreases as the system hydrates [36–38].

To better assess the variation, the relative standard deviation (RSD) can be used. The RSD is useful for comparing the uncertainty between different measurements of varying absolute magnitude. The RSD is the absolute value of the coefficient of variation calculated using Eq. (2):

$$\mathrm{RSD} = \frac{(\text{Standard devation of conductivity})}{\text{Average of conductivity}} \times 100 \qquad (2)$$

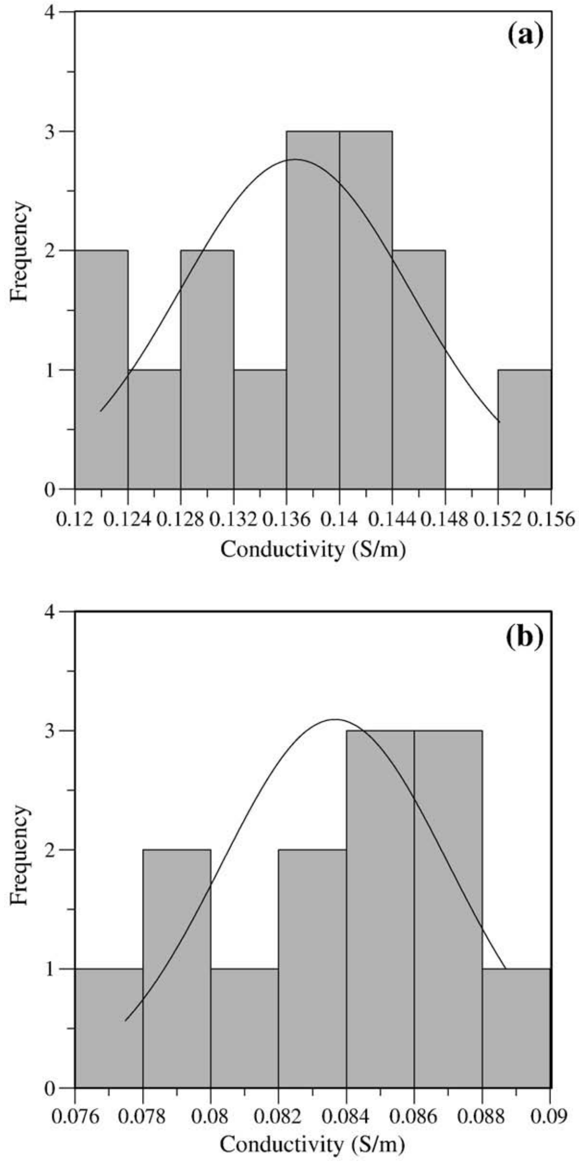

Fig. 7. Histogram of conductivity of paste samples with *w*/*c* = 0.45 (a) 24 h after casting, (b) 72 h after casting.

Table 1
Mixture proportions of concrete samples.

Materials	Batch proportion for 100 kg (kg)		
	w/*c* = 0.48, no WR	*w*/*c* = 0.53, no WR	*w*/*c* = 0.48 with WR
Cement (Type I)	8.0	8.0	8.0
Water	3.9	4.3	3.9
Coarse aggregate	68.9	68.6	68.7
Fine aggregate	19.1	19.0	19.0
Water reducer (WR)	0.0	0.0	0.3

Fig. 6 shows the RSD of the samples at different ages. Results show that, even when the samples are made from one mixture there is variability in the conductivity of the samples, especially at early ages when the properties change most dramatically. However, the RSD decreases over time as the measurements stabilize. This is shown in Fig. 7, which gives the histograms of conductivities for *w*/*c* = 0.45 (15 samples) at two different ages. The maximum difference is less than 10% for *w*/*c* = 0.45 and 3.5% for *w*/*c* = 0.50 at all ages.

4.2. Electrical conductivity of concrete sample

To show the capability of the AEMS, the conductivity of concrete cylinders was measured with different mixture proportions (shown in Table 1). For this purpose, 200 mm (diameter) × 400 mm (length) concrete cylinders were prepared with two (1.9 mm diameter) stainless steel rods as the electrodes. The electrodes were spaced 100 mm apart from each other and fixed in the mold. For each mixture, five cylinders were cast and impedance tests were performed every 15 min. The impedance measurements began 30 min after casting and continued for 7 days. Results show that the conductivities of all five samples of each mixture have very similar results with the RSD between 1 and 2.5% as can be seen in Fig. 9. As can be seen in Fig. 8, at about 10 h, the conductivity of concrete samples is similar. It is obvious from the results that impedance spectroscopy technique is capable to evaluate and compare different samples with different mixture proportions.

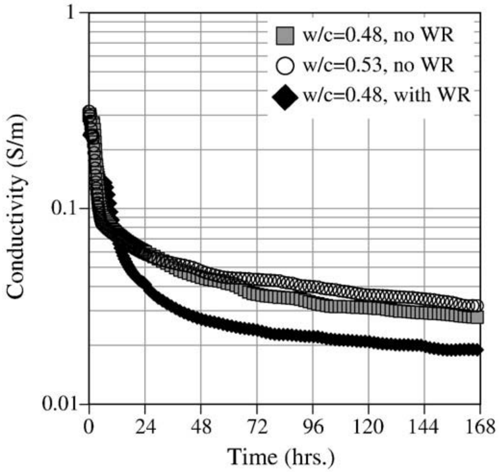

Fig. 8. Conductivity of concrete with three different mixture proportions, shown in Table 1.

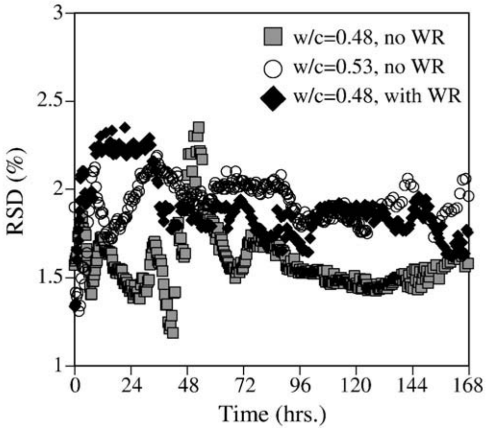

Fig. 9. Relative standard deviation between concrete samples with three different mixture proportions, shown in Table 1, at different ages.

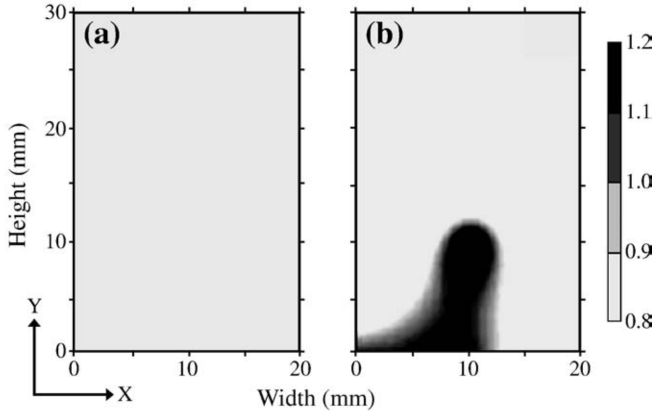

Fig. 11. Image of the concrete sample (a) without and (b) with saw cut, created by electrical impedance measurements.

4.3. Crack imaging in cement paste and concrete, using impedance spectroscopy

Electrical impedance imaging has been used by many researchers in the medical field to monitor various physiological variables [39–41]. Previous studies indicated that this technique can also be used in imaging the defects in cementitious materials [29,42]; however, studies in cement are somewhat limited. The approach consists of measuring the impedance at different locations on the surface of the concrete and constructing electrical conductivity (or resistivity) contour plot from the measured impedances. Since the presence of damage (e.g., a crack) changes the path of electrical flow in the concrete, any damage will appear on the plot. Electrical contour plots can be used to locate visible and invisible damage. In order to investigate this technique a small test unit developed consisting of twenty electrodes, as shown in Fig. 10. The impedance was measured between each pin, in *X* and *Y* directions. Then the measured values were used to construct electrical resistance contour plots. For this experiment, two concrete samples were prepared with water: cement:coarse aggregates:fine aggregates ratio of 0.4:1:3:2.85:2.37. The measurement frequency range was 1 MHz to 10 Hz, with the 500 mV AC stimulus. After performing the measurements, the resistances measured between each pin were normalized based on the maximum measured value in each case and then the normalized values were mapped. Fig. 11 shows the constructed image. The location of the saw cut is clearly visible in this image. A similar setup (with different size and spacing between electrodes) can be used to determine the location of the damaged area beneath the sealed saw cut or joints which is currently under investigation.

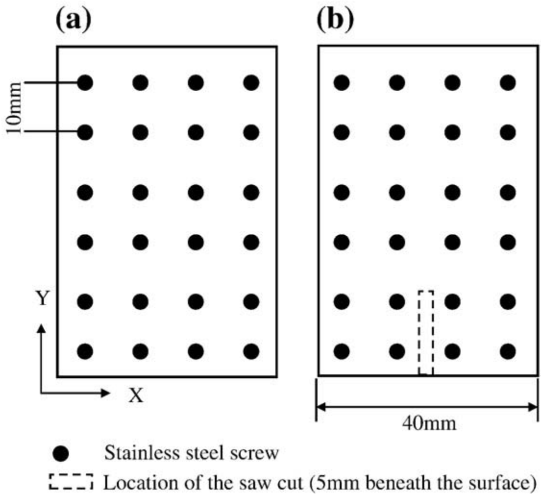

Fig. 10. The dimensions of the concrete samples and the measurement setup, used for imaging: (a) concrete sample with no cut, and (b) concrete sample with the saw cut.

5. Conclusion

This paper described an approach to automate electrical impedance measurements with an automated electrical monitoring system (AEMS) that enable multiple measurements to be made.

This switching system enables measurements to be performed on multiple specimens or where multiple locations are needed. This enables the aging processes be better quantified, allows variability to be qualified for quality control, and enables electrical imaging to be performed.

The system described in this paper was successfully used to investigate the behavior of concrete sample with different mixture proportions by continuously monitoring their conductivity. In addition, variability among different samples was studied and the results show that there is variability between samples even cast from one batch which needs to be considered, specifically in statistical analysis. Constructed electrical image maps can be used to locate the cracked and damaged area, even if it is beneath the surface.

Acknowledgements

This work was supported in part by the Joint Transportation Research Program administered by the Indiana Department of Transportation and Purdue University (study no. TPF-5(179)). The contents of this paper reflect the views of the authors, who are responsible for the facts and the accuracy of the data presented herein, and do not necessarily reflect the official views or policies of the Indiana Department of Transportation, nor do the contents constitute a standard, specification, or regulation.

References

[1] W.J. McCarter, et al., Characterization and monitoring of cement-based systems using intrinsic electrical property measurements, Cement and Concrete Research 33 (2003) 197–206.
[2] B.J. Christensen, et al., Impedance spectroscopy of hydrating cement-based materials: measurement, interpretation, and application, Journal of the American Ceramic Society 77 (1) (1994) 2789–2801.
[3] P. Gu, P. Xie, J.J. Beaudoin, Some applications of AC impedance spectroscopy in cement research, Cement, Concrete and Aggregates 17 (2) (1995) 113–118.
[4] F. Rajabipour, W.J. Weiss, Electrical conductivity of drying cement paste, Materials and Structures 40 (2007) 1143–1160.
[5] W.J. Weiss, J.D. Shane, A. Mieses, T.O. Mason, S.P. Shah. Aspects of monitoring moisture changes using electrical impedance spectroscopy. In 2nd Symposium on Self-Desiccation and Its Importance in Concrete Technology. 1999. Lund, Sweden: Lund Institute of Technology, Division of Building Materials.

[6] A. Schiessl, et al., Assessing the moisture profile of drying concrete using impedance spectroscopy, Concrete Science and Engineering 2 (2) (2000) 106–116.

[7] Z. Liu, J.J. Beaudoin, An assessment of the relative permeability of cement systems using A.C. impedance techniques, Cement and Concrete Research 29 (7) (1999) 1085–1090.

[8] P. Gu, P. Xie, J.J. Beaudoin, Microstructural characterization of the transition zone in cement systems by means of A. C. impedance spectroscopy, Cement and Concrete Research 23 (1993) 581–591.

[9] R.A. Olson, et al., 1995. Microstructure-electrical property relationships in cement-based materials. in Materials Research Society Symposium. Boston, MA, USA: Materials Research Society, Pittsburgh, PA, United States.

[10] L. Lemoine, F. Wenger, J. Galland, Study of the corrosion of concrete reinforcement by electrochemical impedance measurement, Corrosion Rates of Steel in Concrete ASTM STP 1065, American Society for Testing and Materials, 1990.

[11] L. Dhouibi, E. Triki, A. Raharinaivo, The application of electrochemical impedance spectroscopy to determine the long-term effectiveness of corrosion inhibitors for steel in concrete, Cement & Concrete Composites 24 (2002) 35–43.

[12] C. Monticelli, A. Frignani, G. Trabanelli, A study on corrosion inhibitors for concrete application, Cement and Concrete Research 30 (2000) 635–642.

[13] G. Trabanelli, et al., Electrochemical study on inhibitors of rebar corrosion in carbonated concrete, Cement and Concrete Research 35 (2005) 1804–1813.

[14] P. Gu, et al., A study of corrosion inhibitor performance in chloride contaminated concrete by electrochemical impedance spectroscopy, ACI Materials Journal 94 (5) (1997) 385–395.

[15] B.B. Hope, A.K.C. Ip, Corrosion inhibitors for use in concrete, ACI Materials Journal 86 (6) (1989) 602–608.

[16] M. Shi, Z. Chen, J. Sun, Determination of chloride diffusivity in concrete by AC impedance spectroscopy, Cement and Concrete Research 29 (7) (1999) 1111–1115.

[17] M.R. Hansen, et al., 1993. Chloride permeability and AC impedance of high performance concrete. ACI–SP140-06. 140: p. 121–146.

[18] A. Peled, et al., Electrical impedance spectra to monitor damage during tensile loading of cement composites, ACI Materials Journal 98 (4) (2001) 313–322.

[19] S. Perron, J.J. Beaudoin, Freezing of water in Portland cement paste—an AC impedance spectroscopy study, Cement & Concrete Composites 24 (5) (2002).

[20] W.J. McCarter, H. Ezirim, M. Emerson, Properties of concrete in the cover zone: water penetration, sorptivity, and ionic ingress, Magazine of Concrete Research 48 (1996) 149–156.

[21] A. Schieβl, et al., Assessing the moisture profile of drying concrete using impedance spectroscopy, Concrete Science and Engineering 2 (2) (2000) 106–116.

[22] F. Rajabipour, et al., Procedure to interpret electrical conductivity measurements in cover concrete during rewetting, ASCE Journal of Materials in Civil Engineering 17 (5) (2005) 586–594.

[23] Z. Li, L. Xiao, X. Wei, Determination of concrete setting time using electrical resistivity measurement, Journal of Materials Science in Civil Engineering 19 (5) (2007) 423–427.

[24] G. Sant, F. Rajabipour, P. Fishman, P. Lura, W.J. Weiss. Electrical conductivity measurements in cement paste at early ages. in International RILEM Workshop on Advanced Testing of Fresh Cementitious Materials, 2006, Stuttgart, Germany: RILEM.

[25] G.D. Davis, M.J. Rich, L.T. Drzal, Monitoring moisture uptake and delamination in CFRP-reinforced concrete structures with electrochemical impedance sensors, Journal of Nondestructive Evaluation 23 (1) (2004) 1–9.

[26] J.D. Shane, et al., Microstructural and pore solution changes induced by rapid chloride permeability test measured by impedance spectroscopy, Concrete Science and Engineering 1 (2) (1999) 110–119.

[27] C. Shi, Effect of mixing proportions of concrete on its electrical conductivity and the rapid chloride permeability test (ASTM C1202 or ASSHTO T277) results, Cement and Concrete Research 34 (2004) 537–545.

[28] T.J. Schmit, A fundamental investigation on utilizing error propagation, Monte Carlo simulation, and measurement interpretation technique to design efficient in situ covercrete sensing systems MS thesis in Civil Engineering, Purdue University, 2005.

[29] M. Niemuth, Using Impedance Spectroscopy to Detect Flaws in Concrete, Purdue University, MS thesis in Civil Engineering, 2004.

[30] Keithley Instruments Inc., 2700, 2701 and 2750 Multimeter/Data Acquisition/Switch Systems, Keithley Instruments Inc., 2009 http://www.keithley.com/products/dmm/integrasystems/?path=2700/Documents#4.

[31] Solartron Group, 2009. *www.solartronanalytical.com/downloads/datasheets/1260.pdf*.

[32] Keithley Instruments Inc., Integra Series Technical Data Sheet, 2003.

[33] G. Sant, F. Rajabipour, W.J. Weiss, The influence of temperature on electrical conductivity measurements and maturity predictions in cementitious materials during hydration, The Indian Concrete Journal (April 2008) 1–10.

[34] National Instruments, What is NI GPIB?, 2009.

[35] P. Gu, et al., Study of the hydration and setting behavior of OPC-HAC pastes, Cement and Concrete Research 24 (4) (1994) 682–694.

[36] C.A. Scuderi, T.O. Mason, H.M. Jennings, Impedance spectra of hydrating cement pastes, Journal of Materials Science 26 (1991) 349–353.

[37] J.M. Torrents, R. Pallas-Areny, 1997. Measurement of cement setting by impedance monitoring. in IEEE Instrumentation and Measurement, Technology Conference. May 19–21. Ottawa, Canada.

[38] A. Poursaee, C.M. Hansson, Reinforcing steel passivation in mortar and pore solution, Cement and Concrete Research 37 (2007) 1127–1133.

[39] D. Murphy, et al., Impedance imaging in the newborn, Clinical Physics and Physiological Measurement 8 (Suppl. A) (1987) 131–140.

[40] M. Weindling, et al., Electrical impedance to study cerebral haemodynamics in the newborn: which index is best? Biology of the Neonate 45 (1984) 300.

[41] L. Tarassenko, P. Rolfe, Imaging spatial distribution of resistivity—an alternative approach, Electronics letters 20 (1984) 574–576.

[42] T. Hou, J.P. Lynch, Electrical impedance tomographic methods for sensing strain fields and crack damage in cementitious structures, Journal of Intelligent Material Systems and Structures, , 2008, pp. 1–18.

MOISTURE PROFILES AND DIFFUSION COEFFICIENTS IN MORTARS CONTAINING SHRINKAGE REDUCING ADMIXTURES

Mohammad Pour-Ghaz(1), Robert Spragg (1) and Jason Weiss (1)

(1) Purdue University, School of Civil Engineering, West Lafayette, Indiana, USA

Abstract

Shrinkage reducing admixtures (SRAs) have been used over the last three decades to reduce the volume change (i.e., shrinkage) that occurs in cement paste, mortar, and concrete during drying. The goal of reducing shrinkage is to reduce the risk of shrinkage cracking in concrete elements. SRAs alter the properties of the pore solution, such as surface tension and viscosity, which result in a reduction in the magnitude of drying shrinkage, especially at humidities below 80-85%. In addition to altering the magnitude of shrinkage, SRAs appear to alter the rate of drying and diffusivity coefficient. This paper examines the role of SRAs in two ways. First, desorption spectra are measured to obtain the moisture diffusivity of plain mortar and mortar containing SRA. Second, the paper measures relative humidity in slabs to obtain moisture profiles. The relative humidity profile predicted from the non-linear diffusion coefficient is compared with the measured humidity profile.

1. Background

Shrinkage Reducing Admixtures (SRAs) were introduced to the concrete industry in the 1980's [1, 2]. Recent reviews have summarized three decades of research on SRA on concrete properties [3-6]. SRA's are generally observed to reduce shrinkage which can substantially reduce the propensity for restrained shrinkage cracking.

The majority of shrinkage measurements on concrete containing SRA are performed on concrete samples with a relatively large cross section, like those that one may use in standard shrinkage tests like ASTM C-157 [7]. While this type of test can provide information on the benefits of SRA, it has two primary limitations. First, it generally only describes the shrinkage of the concrete at one relative humidity (50% for example for ASTM C-157 [7]). Second, it measures the average length change of the prism and does not explicitly account for moisture gradients.

To overcome the limitation of measuring shrinkage at one relative humidity, a series of tests were performed measuring small paste and mortar samples with and without SRA at different relative humidities [8]. This response can be used to describe the shrinkage that may be expected over a wide range of relative humidities [9-11]. This does however indicate, not surprisingly, that shrinkage is not linearly related to relative humidity [8]. The shrinkage of the paste can be extended to mortar or concrete using the Pickett [12] or Hobbs [13] approaches.

Previous work has been performed to measure relative humidity profiles in concrete. This includes the work of Monfore [14] and Grasley et al. [15] who used resistance based gages to measure humidity in vapor filled cavities in concrete, the work of Molina [16] who measured relative humidity using chilled mirror technology, and work of Schieβl et al. [17] using electrical resistance measurements of concrete to assess the moisture distribution.

Relative humidity measurements in slabs can be complicated by the size of the probe that is used to measure the humidity. Measurements in small cavities with limited vapor volume can make it difficult to use techniques that require a substantial air flow rate like chilled mirrors. Previous measures of electrical resistance of concrete require two assumptions. First, that there are no hysteretic effects [18, 19] and second, that the resistance is measured at the depth of the electrodes. It can be noted that the first assumption is required since electrical measurements measure water content and not relative humidity directly and hysteretic effects due to drying and wetting can complicate the interpretation [19]. The second assumption is more nebulous as the shape of the electrical field that develops between the two electrodes is not symmetric at the plane of the electrodes since more charge will pass through the side containing more liquid [19]. As such it may be beneficial to measure the moisture diffusion coefficient directly rather than measuring relative humidity profiles and back calculating the diffusion coefficient.

One advantage of using desorption measurements to obtain a non-linear diffusion coefficient is the fact that the testing can be performed over a much shorter duration than drying of thick concrete slabs. For example, the non-linear diffusion coefficient measured in this paper took approximately 5 days to measure after casting and curing which is substantially shorter than allowing a concrete slab to dry and back-fitting the diffusion coefficient (which can take many many months). Second, this approach is not subjected so some of the issues that arise in attempting to ascertain the correct depth of the relative humidity measurement or the influence of a relatively large size cavity on the measured value.

2. Research Objective

This paper describes research that is attempting to measure a non-linear moisture diffusion coefficient in a mortar. Mortar was preferred to cement paste to minimize the potential impact of different pore size distributions that may occur between pastes and mortars. In addition the mortar was preferred to minimize potential issues that may occur with inconsistent mixing action that can be encountered in paste samples. This paper has three main objectives:

- First, the paper describes tests on mortar that is dried in a controlled fashion to evaluate the non-linear diffusion coefficient following the approach used by Anderberg and Wadso [20] and Garbalinska [21],
- Second, the paper provides data that illustrates the influence of shrinkage reducing admixture on the non-linear diffusion coefficient, and
- Third, the paper will provide a comparison of the relative humidity profile predicted using the non-linear diffusion coefficient with a measured relative humidity profile in a slab.

3. Relative Humidity Gradient and Cracking Potential

Previous work [9, 10, 22-24] has suggested that the humidity gradient in a slab can be used to predict the free shrinkage, stress development, slab cracking, and curling in a thick concrete element. The background for this type of approach can be found in [10, 25]. Figure 1 schematically illustrates the approach can be taken to utilize the relative humidity profile to compute the stress distribution and gradient. Strong dependence of diffusion coefficient on the shape and magnitude of the relative humidity profile can result in higher stress gradient and increase in cracking potential.

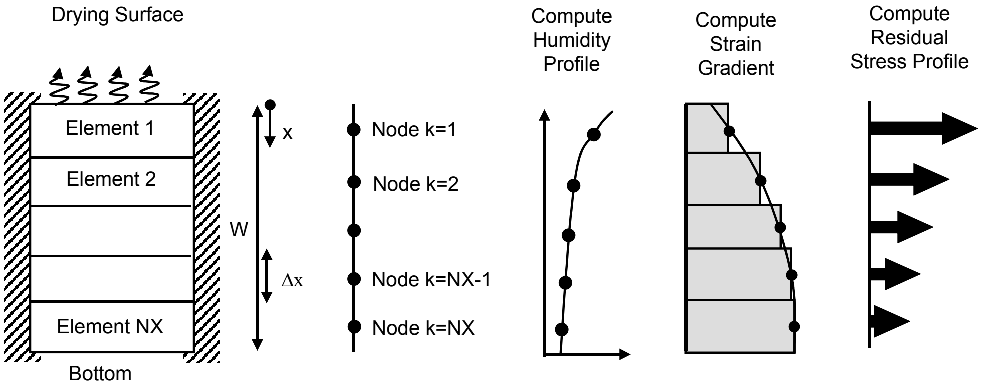

Figure 1: Schematically illustrates the approach can be taken to utilize the relative humidity and moisture content (W) profile to compute the stress distribution [10].

4. Materials and Methods

Three mortar mixtures were prepared for this study. The plain mortar had a water to cement ratio (w/c) of 0.50 and consisted of 55% aggregate by volume. The mortars containing shrinkage reducing admixture (SRA) had 1% and 5% of the mix water replaced with a SRA (denoted as 1% SRA and 5% SRA respectively). ASTM C150 [7] Type I ordinary portland cement (OPC) was used with a Blaine fineness of 370 m^2/kg and an estimated Bogue phase composition of 56 % C_3S, 16 % C_2S, 12 % C_3A, 7 % C_4AF and a Na_2O equivalent of 0.68 % by mass. The normal weight aggregate (NWA) was natural river sand with a fineness modulus of 2.71, an apparent specific gravity of 2.58, and an absorption of 1.8 % by mass.

The SRA was commercially available Tetragaurd AS20. All of the NWA was oven-dried and air-cooled for 24 hr before mixing. The mixing procedure used for the mortar was in accordance with ASTM C192-06 [7]. The samples were all tested in a sealed condition unless otherwise noted.

The experiments that were performed consist primarily of two specimen geometries. The first sample geometry was used for the diffusivity tests. This sample consisted of a 0.8 mm thick by 6 mm diameter mortar disk that was taken from a larger cylinder that was sealed from the time of casting before being exposed to progressive drying at an age of 7 days for determination of the moisture diffusivity. The second sample geometry consisted of slab specimens (177.8 mm x 254.0 mm x 508.0 mm) with relative humidity sensors embedded at four depths (12.7, 25.4, 38.1 and 92 mm) measured from the drying surface. The slabs were exposed to drying at 50 ± 1% at an age of 7 days. The slab geometry is shown in Figure 2.

Figure 2: Slab geometry with one-sided drying

5. Measurements of a Non-Linear Diffusion Coefficient

The samples used for determining the diffusion coefficient were cut from a small cylinder of mortar using a high precision wet saw. The test started approximately 5 minutes after cutting the sample. The samples were kept in water. At the start of the test the sample was removed from the water and was placed in a clean towel for a few seconds to remove the surface water. The sample was then placed in the desorption analyzer. The diffusivity test was performed in an automated absorption/desorption analyzer [26, 27] at $23^{o}C$ in which samples were subjected to isothermal desorption at different relative humidities. The first step in the isothermal desorption was isothermal conditioning at 97.5 % relative humidity. The samples were allowed to equilibrate to 97.5%. After isothermal conditioning at 97.5% the relative humidity was decreased in 5% relative humidity increments. Samples at each step of the desorption were considered to be at equilibrium when the mass change was smaller than 0.001 mg for 15 minutes [26].

For a slab geometry with double-sided drying (where the contribution of mass transfer from the edges of the sample is negligible compared to mass transfer from the surface of the slab [20, 21, 28]) the mass change due to drying (M_t), at any time (t), can be related to the moisture diffusivity, (D), using Equation 1 [20, 21, 28]

$$\frac{M_t}{M_\infty} = \frac{4}{\pi}\left(\frac{Dt}{L^2}\right)^{1/2} \tag{1}$$

where M_∞ is the mass change at equilibrium and L is the thickness of the sample.

The diffusivity over each relative humidity step can be obtained from the linear portion of a plot of $\left(M_t / M_\infty\right)^2$ against $\left(16t / \pi^2 L^2\right)$. Generally the mortar samples tested exhibited the linear portion of their curve between 20 and 80% of the equilibrium mass. For materials for which the diffusivity is a function of relative humidity, Equation 1 can be used provided that the diffusivity can be assumed constant during each isothermal desorption step. In the present work since the samples were subjected to 5% change of relative humidity, the diffusivity can be assumed constant during each step of desorption. Better results can be obtained by decreasing the size of the steps, however the duration of the testing would increase but a sensitivity analysis would need to be determined.

Figure 3 illustrates the calculated diffusivity of the 0.8 mm thick specimens (exposed to 2 sided drying) of plain mortar, and mortar samples with 1 and 5% SRA. Note that the diffusivity at each step is expressed as diffusivity at average relative humidity of that step (e.g., the diffusivity of the samples that is equilibrated at 97.5% relative humidity and exposed to 92.5% relative humidity is reported as diffusivity at 95%). The samples with SRA demonstrate a lower diffusivity than the plain system at higher relative humidity. This lower relative humidity in the SRA system corresponds with a reduced rate of drying (at high relative humidity). This would suggest that plain mortar has a more non-linear moisture diffusivity while samples with SRA are more linear with respect to the diffusivity over a large range of moisture contents. This can have substantial implications on the moisture profile, shrinkage profile, reduction in curling, drying rate, and microcracking at the surface of the slab [29].

6. Relative Humidity Measurements in Slabs

The internal relative humidity and temperature of the slab was measured at four depths (12.7, 25.4, 38.1 and 92 mm) in a series of 250 mm hollow shafts (parallel to the surface) that contain I-button sensors [30] that measure temperature and relative humidity. The depth of the hollow shaft reported is measured from the exposed surface of the slab to the center of the shaft. Slabs were exposed to drying from the top surface.

The I-button data loggers measure the relative humidity with ±1.0% and temperature ±0.1°C accuracy respectively. The advantage of this type of relative humidity sensor is the fact that it measures the relative humidity of the air inside the hollow shaft directly which is in equilibrium with surrounding materials. To ensure accuracy of the measurements all the sensors were compared to two salt solutions with 87 and 78% relative humidities. The sensors were within ±1.0% of the expected relative humidity. In addition to calibration, data were corrected for saturation drift [30].

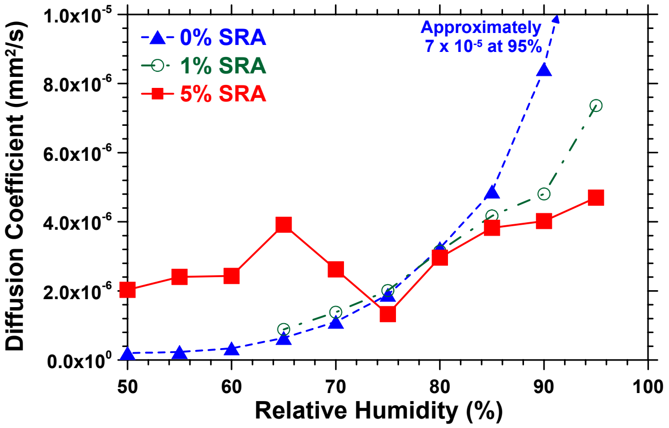

Figure 3: Moisture diffusivity of mortar samples with different loadings of shrinkage reducing admixture (SRA)

At the time of casting the slabs, cylindrical samples (with 2.54 cm diameter and 5.1 cm height) were cast from the same materials used to make the slabs and was kept sealed. These samples were used to measure the internal relative humidity at 7, 28 and 63 days (two samples at each age). The measurements were performed by crushing the samples and placing them in an air-tight container against a temperature and relative humidity sensor [26]. These measurements were performed to account for the self-desiccation effect which is needed in Equation 2.

Figure 4 illustrates the relative humidity of the slabs that have been exposed to drying at an age of 7 days (results are based on the average independent measurement in two slabs). It can be noticed that the relative humidity appears to remain higher in the samples containing SRA. The depth of the sensors is the distance to the center of the hollow shaft (in which sensor in placed in) from the surface of the slab. It is expected that the measured relative humidity with sensor may be more representative of the top of the hollow shaft.

7. Comparing Slab Measurements with Predictions Using the Diffusion Coefficient

Equation 2 describes the relative humidity as a function of time and position [31-35]

$$\frac{\partial H}{\partial t} = div\left(D_H \; grad \; H\right) - \frac{\partial H_s}{\partial t} \qquad (2)$$

where H is the relative humidity, D_H is the moisture diffusivity as a function of relative humidity and H_s is the variation of relative humidity due to self-desiccation.

Equation 2 assumes that the contribution of thermal gradients and aging are negligible [33]. The second term on the right-hand-side of Equation 2 is the contribution of self-desiccation [33]. The self-desiccation term in the present work is measured independently from crushed samples as described above. The boundary conditions at the sealed (bottom) surface of the slab and top (exposed to drying) surface of the slab can be expressed by $\partial H / \partial x = 0$ and $H = 0.50$ respectively. The initial condition of the slab at drying (i.e., humidity at 7 days) is obtained by measuring the internal relative humidity of the crushed samples.

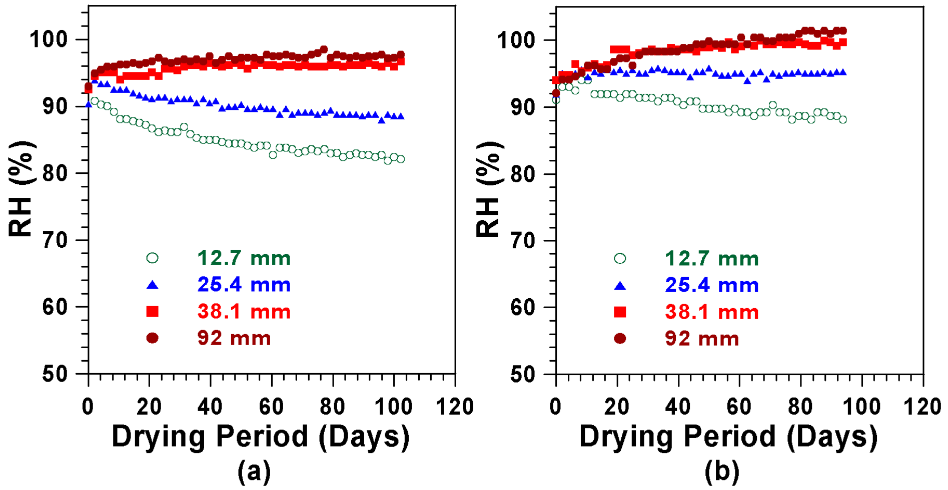

Figure 4: Change of internal relative humidity of slabs at different depth measured from exposed surface of the slab, (a) plain mortar, (b) mortar containing 5% shrinkage reducing admixture (SRA)

A non-linear finite difference scheme [33, 36, 37] was used. To effectively capture the non-linearity caused by the diffusivity, Crank-Nicolson (central difference) scheme was used. Crank-Nicolson scheme is stable [33, 36, 37] and effective in capturing non-linearities caused by strong dependence of diffusivity on relative humidity. In using this scheme any oscillations around the exact solution can be avoided by decreasing the time increments. In each time step the first solution was obtained by time lagging the diffusivity one time step and then improving the solution by subsequent iterations. In subsequent iterations, a weighted average diffusivity of the last two iterations was used. This method of averaging is known as modified Picard iterations [38] and requires less number of iterations in each time step.

Figure 5 illustrates the comparison of the experimentally obtained relative humidity at different locations and the numerically obtained profiles using the non-linear diffusivity coefficients.

8. Implications of Differences in Relative Humidity Profiles

Results of the non-linear diffusion coefficient can be used to describe moisture distribution at early ages and its potential impact on microcracking, curling and through cracking. The SRA's, especially at 5% show a reduced rate of drying. This is confirmed with less mass loss. This work may also provide insight on microcracking and damage localization that ultimately leads to through cracking in restrained elements. Acoustic emission has shown that the inclusion of SRA substantially reduces the acoustic activity due to microcracking in the specimens that contain 5% SRA as compared with the plain mixture.

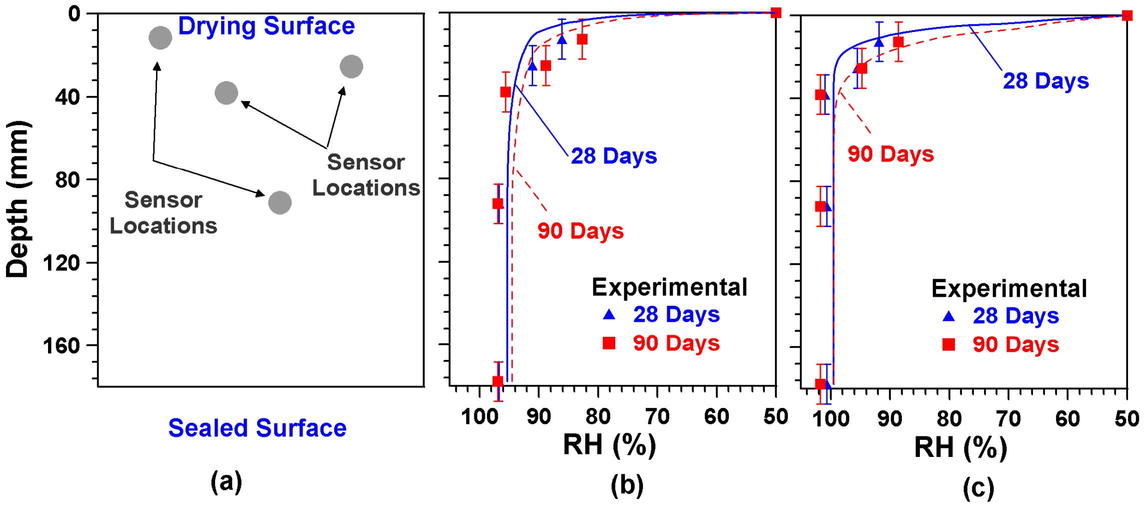

Figure 5: Comparison of the experimentally measured relative humidity and numerically obtained relative humidity profile, (a) illustration of location of the sensors and boundary conditions of the slab, (b) plain mortar, (c) mortar with 5% shrinkage reducing admixture (SRA)

9. Conclusions

This paper examined the role of SRAs on the relative humidity profile that develops in a drying mortar. The paper begins by describing the measurement of desorption spectra to obtain the moisture diffusivity of plain mortar and mortar containing SRA. The paper uses these non-linear diffusion coefficients to predict the moisture profiles that would be expected to occur in drying slabs. The results indicate that SRA dries more slowly at high relative humidities (liquid diffusion) however this trend may be reduced for lower relative humidities when the vapor diffusion prevails. The relative humidity profiles computed using the non-linear diffusion coefficient were directly compared with independently measured relative humidity in slabs. A reasonable comparison was observed given the issues associated with errors in relative humidity depth location and the shortcomings of using a non-aging coefficient. The implications of this approach could be more rapid indications of relative humidity profiles in concrete as well as explanations of shrinkage, stress and cracking distributions throughout the sample cross section.

10. Acknowledgements

The authors gratefully acknowledge the support of BASF, the Construction Chemical Company. This work was conducted in the Charles Pankow Concrete Materials Laboratory at Purdue University. As such, the authors gratefully acknowledge the support which has made this laboratory and its operation possible.

8. References

[1] Sato, T., Goto, T., and Sakai, K., 'Mechanism for Reducing Drying Shrinkage of Hardened Cement by Organic Additives,' *CAJ Review,* (1983) 52-54.

[2] Tomita, R., Simoyama, Y., and Inoue, K., 'Properties of hardened concrete impregnated with cement shrinkage reducing agent,' *CAJ Review,* (1986) 314-317.

[3] ACI.Committee.231, 'Report on Early-Age Cracking: Causes, Measurement, and Mitigation,' American Concrete Institute ACI 231R-10, 2010.

[4] Nmai, C., Tomita, R., Hondo, F., and Buffenbarger, J., 'Shrinkage reducing admixtures,' *Concr. Int.,* **20** (4)(1998) 31-37.

[5] Shah, S.P., Weiss, W.J., and Yang, W., 'Shrinkage cracking – can it be prevented?,' *Concr. Int.,* **20** (4)(1998) 51-55.

[6] Weiss, J. and Berke, N.S., 'Shrinkage reducing admixtures,' in *Early age cracking in cementitious systems, RILEM state-of-the-art report—Report 25*, A. Bentur, Ed., ed Bagneux, France: RILEM, 2002.

[7] *Annual Book of ASTM Standards*. West Conshohocken, PA: American Society for Testing and Materials, ASTM International, 2009.

[8] Weiss, J., Lura, P., Rajabipour, F., and Sant, G., 'Performance of shrinkage-reducing admixtures at different humidities and at early ages,' *ACI Mater. J.,* **105** (5) Sep-Oct (2008) 478-486.

[9] Bazant, Z.P., Ed., *Fourth RILEM International symposium on Creep and Shrinkage of Concrete: Mathematical Modeling* Northwestern University, 1986.

[10] Weiss, W.J., 'Prediction of early-age shrinkage cracking in concrete,' Ph.D., Civil Engineering, Northwestern University, Evanston, IL, 1999.

[11] Moon, J.H., 'Shrinkage, Residual Stress, and Cracking in Heterogeneous Materials,' Ph.D., Civil Engineering, Purdue University, West Lafayette, IN, 2006.

[12] Pickett, G., 'Shrinkage stresses in concrete,' *Mater. Struct.,* **42** (8)(1946) 165-204.

[13] Hobbs, D.W., 'Influence of aggregate restraint on the shrinkage of conrete,' *ACI Journal,* **71-30** (1974) 445-450.

[14] Monfore, G.E., 'A small probe-type gauge for measuring relative humidity,' *Journal of the PCA Research and Development Laboratories,* **5** (2)(1962).

[15] Grasley, Z.C., Lange, D.A., and D'Ambrosia, M.D., 'Internal relative humidity and drying stress gradients in concrete,' *Mater. Struct.,* **39** (9) Nov (2006) 901-909.

[16] Molina, L., 'Measurement of high humidity in cementitious material at an early age,' Swedish Cement and Concrete Research Institute, Stockholm, Sweden1990.

[17] Schielβl, A., Weiss, W.J., Shane, J.D., Berke, N.S., Mason, T.O., and Shah, S.P., 'Assessing the moisture profile of drying concrete using impedance spectroscopy,' *Concr. Sci. Eng.,* **2** (2000) 106-116.

[18] Elkey, W. and Sellevold, E.J., 'Electrical resistivity of concrete,' Norwegian Road Research Laboratory1995.

[19] Rajabipour, F., 'Insitu electrical sensing and materials health monitoring in conrete structures,' Ph.D., Civil Engineering, Purdue University, West Lafayette, IN, 2006.

[20] Anderberg, A. and Wadso, L., 'Method for simultaneous determination of sorption isotherms and diffusivity of cement-based materials,' *Cem. Concr. Res.,* **38** (1) Jan (2008) 89-94.

[21] Garbalinska, H., 'Application of root t-type, logarithmic and half-time methods in desorptive measurements of diffusivity in narrow humidity ranges,' *Cem. Concr. Res.,* **36** (7) Jul (2006) 1294-1303.

[22] Moon, J.H. and Weiss, J., 'Estimating residual stress in the restrained ring test under circumferential drying,' *Cem. Concr. Compos.,* **28** (5) May (2006) 486-496.

[23] Weiss, W.J., Yang, W., and Shah, S.P., 'Shrinkage cracking of restrained concrete slabs,' *J. Eng. Mech.,* **124** (7) Jul (1998) 765-774.

[24] Weiss, W.J., Yang, W., and Shah, S.P., 'Influence of specimen size/geometry on shrinkage cracking of rings,' *J. Eng. Mech.,* **126** (1) Jan (2000) 93-101.

[25] Bazant, Z.P., 'Material Models for Structural Creep Analysis,' in *Mathematical Modeling of Creep and Shrinkage of Concrete*, Z. P. Bazant, Ed., ed New York: John Wiley and Son Ltd, 1988.

[26] Castro, J., Lura, P., Rajabipour, F., and Weiss, J., 'Internal curing: discussion on the role of pore solution on relative humidity measurements and desorption of lightweight aggregate (LWA) ' in *Advances in the Material Science of Concrete*. vol. SP-270, J. H. Ideker and A. Radlinska, Eds., ed Chicago, IL: American Concrete Institute, 2010.

[27] Instruments, T., 'Dynamic Vapor Sorption Analysis: Q5000 SA,' http://www.tainstruments.com2010.

[28] Crank, J., *The Mathematics of Diffusion*, 2nd ed. New York: Oxford University Press, 1980.

[29] Neithalath, N., Pease, B.J., Moon, J.H., Rajabipour, F., Weiss, J., and Attiogbe, E., 'Considering moisture gradients and time-dependent crack growth in restrained concrete elements subjected to drying,' in *High Performance Cement Based Concrete Composites*, J. J. Bernacki*, et al.*, Eds., ed Chennnai, India: American Ceramics Society, 2005, pp. 279-290.

[30] Maxim, 'Data Logger, Temperature/Humidity Loggers, and Sensors,' Sunnyvale, CA, 2010.

[31] Bazant, Z.P. and Kim, J.K., 'Consequences of Diffusion-Theory for Shrinkage of Concrete,' *Mater. Struct.,* **24** (143) Sep (1991) 323-326.

[32] Bazant, Z.P., Kim, J.K., and Panula, L., 'Improved Prediction Model for Time-Dependent Deformations of Concrete .1. Shrinkage,' *Mater. Struct.,* **24** (143) Sep (1991) 327-345.

[33] Bazant, Z.P. and Najjar, L.J., 'Nonlinear water diffusion in nonsaturated concrete,' *Mater. Struct.,* **5** (25)(1972) 3-20.

[34] Xi, Y.P., Bazant, Z.P., and Jennings, H.M., 'Moisture Diffusion in Cementitious Materials - Adsorption-Isotherms,' *Adv. Cem. Based Mater,* **1** (6) Nov (1994) 248-257.

[35] Xi, Y.P., Bazant, Z.P., Molina, L., and Jennings, H.M., 'Moisture Diffusion in Cementitious Materials - Moisture Capacity and Diffusivity,' *Adv. Cem. Based Mater,* **1** (6) Nov (1994) 258-266.

[36] Crank, J. and Nicolson, P., 'A Practical Method for Numerical Evaluation of Solutions of Partial Differential Equations of the Heat-Conduction Type,' *Proceedings of the Cambridge Philosophical Society,* **43** (1)(1947) 50-67.

[37] Ozisik, M.N., *Finite Difference in Heat Transfer*. London: CRC Press, 1994.

[38] Pour-Ghaz, M., 'A novel approach for practical modelling of steel corrosion in concrete,' M.A.Sc, Civil Engineering, Carleton University, Ottawa, Canada, 2007.

The influence of temperature on electrical conductivity measurements and maturity predictions in cementitious materials during hydration

Gaurav Sant, Farshad Rajabipour and Jason Weiss

Electrical property measurements are being increasingly used to assess the transport properties of building materials. While conductivity measurements have been extensively used, the combined dependence of electrical conductivity on measurement temperature and microstructural development (cement hydration) is often overlooked. In this paper the influence of temperature and microstructural development (i.e. hydration) are separated. Two cement paste mixtures are assessed at 283K, 296K, and 309K, and the conductivity response is analysed to differentiate the contribution of maturity (pore structure refinement due to hydration) and temperature (due to changing ionic mobility). The conductivity measurements are used to determine the activation energy of electrical conduction (i.e. temperature dependence of ion mobility) and hydration (i.e. temperature dependence of reaction rates). This work provides an improved understanding of how temperature influences electrical measurements in cementitious systems at early ages, and can provide for an accurate interpretation of the electrical properties of the system. This information will enable improvements in the use of electrical measurements for quality control and quality assurance (QC/QA) testing.

Keywords: *Electrical conductivity, hydration, maturity, temperature, quality control.*

Electrical measurements are powerful non-destructive testing techniques that are capable of providing information about hydration reactions, microstructural features and the transport properties of cement based materials. However, electrical measurements (e.g., conductivity or resistivity) exhibit temperature dependence due to changing ionic mobility with temperature. In an electrolyte, electrical conduction occurs due to the migration of ions through the solution under an applied potential gradient[1]. Consequently, conduction in aqueous electrolytes is dependent on ionic mobility and the solution's concentration. In cementitious materials, temperature change influences ionic mobility and salt solubility resulting in a change in the electrical conduction response as a function of temperature[2]. These considerations highlight the need to account for the temperature dependent conductivity response of cementitious materials. Further, chemical reactions (such as cement hydration) are influenced by temperature[3]. This topic has received significant treatment in the literature with the objective of determining how temperature influences the rate of material property development[4,5,6,7]. Maturity transformations have been extensively used to correlate material properties to the extent of reaction that occurs in the system[8,9].

Due to the influence of temperature on the rate of hydration and ionic mobility it would be reasonable to consider that the electrical properties (conductivity or resistivity) of cement systems are a function of maturity and temperature effects as shown in Equation 1.

$$\sigma(t,T) = f(M) \bullet f(T) \qquad ......(1)$$

where, $\sigma(t,T)$ is the time and temperature dependent electrical property (in this case the conductivity (S/m)) of the sample, $f(M)$ is a function which defines the influence of time and temperature on the sample maturity (microstructure development), and $f(T)$ is a function that defines the influence of sample temperature and accounts for effects such as the ionic mobility and solution concentration.

The temperature dependence of electrical properties in cement based systems was studied several decades ago by Hammond and Robson who used the Hinrichson-Rasch law to describe the conductivity of concrete over a range of temperatures (Equation 2).[10,11]

$$ln\left(\frac{\sigma(T)}{\sigma(T_{REF})}\right) = A\left(\frac{1}{T} - \frac{1}{T_{REF}}\right) \qquad ......(2)$$

where, $\sigma(T)$ is the concrete conductivity (S/m) at temperature T (K), $\sigma(T_{REF})$ is the conductivity (S/m) at a reference temperature T_{REF} (296K for this work) and 'A' is an empirical constant (K). Hammond and Robson indicated 'A' to be equal to 5500K based on work by Spencer[10,12]. Later, Elkey and Sellevold extended the scope of this investigation and determined 'A' to vary between 2000 and 5000K depending on the mixture composition[13].

Whittington et al. used a similar approach to investigate concrete using electrical resistivity[14]. Using a slightly different form of relationship (Equation 3) described by Hammond and Robson they determined concrete to have a negative temperature coefficient of resistivity, equal to 0.022/°C.

$$\frac{\rho(T)}{\rho(T_{REF})} = \frac{1}{1+\alpha(T - T_{REF})} \qquad ......(3)$$

where, $\rho(T) = 1/\sigma(T)$ is the resistivity (ohms.m) at temperature T (K), $\rho(T_{REF})$ is the resistivity (ohms.m) at a reference temperature T_{REF} (K) and α is temperature coefficient of resistivity of the material. The work of Whittington et al translates to an empirical constant 'A' of 2130 K for the concretes tested.

In the 1990s, McCarter determined the temperature coefficient of resistivity of concrete as 0.026/°C.[15] More recently, McCarter proposed a formulation to determine the activation energy of electrical conduction based on the Arrhenius Law (Equation 4)[16,17].

$$\sigma_{Bulk} = A \bullet exp\left[\frac{-E_{aC}}{R \bullet T}\right] \qquad ......(4)$$

where, σ_{Bulk} is the bulk sample conductivity (S/m) at an absolute temperature T (K), R is the universal gas constant (8.314 J/K mol), E_{aC} is the activation energy for the conduction process (J/mol) and A (S/m) is a material constant (theoretically equivalent to the conductivity at infinite temperature; $\sigma(T = \infty)$). The activation energies of electrical conduction were determined to be in the range of 16-30 KJ/mole for the mixtures evaluated in this project.

Research objective

This paper proposes an approach to simultaneously assess the influence of temperature and microstructural changes (i.e. maturity) on the measured electrical conductivity in cementitious systems. The results of this work are aimed at understanding the influence of temperature on early-age conductivity measurements. This understanding would permit the reliable use of electrical measurements in early-age quality control and quality assurance (QC/QA) testing and for specification compliance of cement-based materials.

Materials and mixing procedures

Two different cement paste mixtures were prepared according to the mixture proportions shown in Table 1. Type I ordinary portland cement was used with a Blaine fineness of 360 m^2/kg and a Bogue phase composition of 60% C_3S, 12% C_2S, 12% C_3A, 7% C_4AF and a Na_2O equivalent of 0.72%. To enhance the workability of the mixtures, a high range water reducing admixture was added. A commercially available shrinkage reducing admixture (SRA) was added at a 5% concentration of the initial water content by replacement (by mass) of the initial mixing water. For the measurement of electrical conductivity de-aired, neat cement pastes were prepared using de-ionised water. The water was de-aired by boiling then cooled to room temperature before mixing. The dry constituent materials were placed inside a special mixing chamber[18]. The chamber was then sealed, air was evacuated from the chamber using a vacuum pump, and the solution of water and the chemical admixtures was introduced into the chamber under the same evacuated condition. The chamber was then placed in a commercial paint shaker and shaken for five minutes to uniformly mix the constituents and obtain a consistent cement paste mixture. After mixing, the chamber was opened and the cement paste slurry was placed in the moulds using external vibration.

Table 1. Mixture proportions (mass)

	W/C = 0.30	W/C = 0.30 + 5% SRA
Water	0.300	0.285
Cement	1.000	1.000
HRWRA	0.005	0.005
SRA	~	0.015

Experimental procedures

Electrical conductivity of fresh and mature cement pastes

The electrical conductivity of cement paste samples was measured using cylindrical paste specimens (22 mm diameter, 50 mm height). The specimens were cast and stored in an airtight plastic vial. Two stainless steel electrodes (2.5 mm diameter rods spaced 10 mm centre to centre) were embedded longitudinally inside each vial (Figure 1b). A impedance gain-phase analyser measured the impedance response of each specimen. The measurements were made over a wide frequency range; i.e. 10 MHz to 1 Hz (10 steps/frequency decade) using a 100 mV AC stimulus. The bulk resistance (R_b) obtained from the impedance response was used to determine the material's conductivity after normalising for the effects of specimen and electrode geometry (Equation 5).

$$\sigma_t = \frac{k}{R_b} \qquad ......(5)$$

where, σt is the paste conductivity (S/m), R_b is the bulk resistance (ohms; Ω) and k is a geometry factor (15.76/m) that was determined experimentally for this specific geometry[19]. During measurements, the specimens remained sealed inside plastic vials. Electrical impedance measurements were performed for a duration of 7 days (at a reference temperature of 296K) after casting on

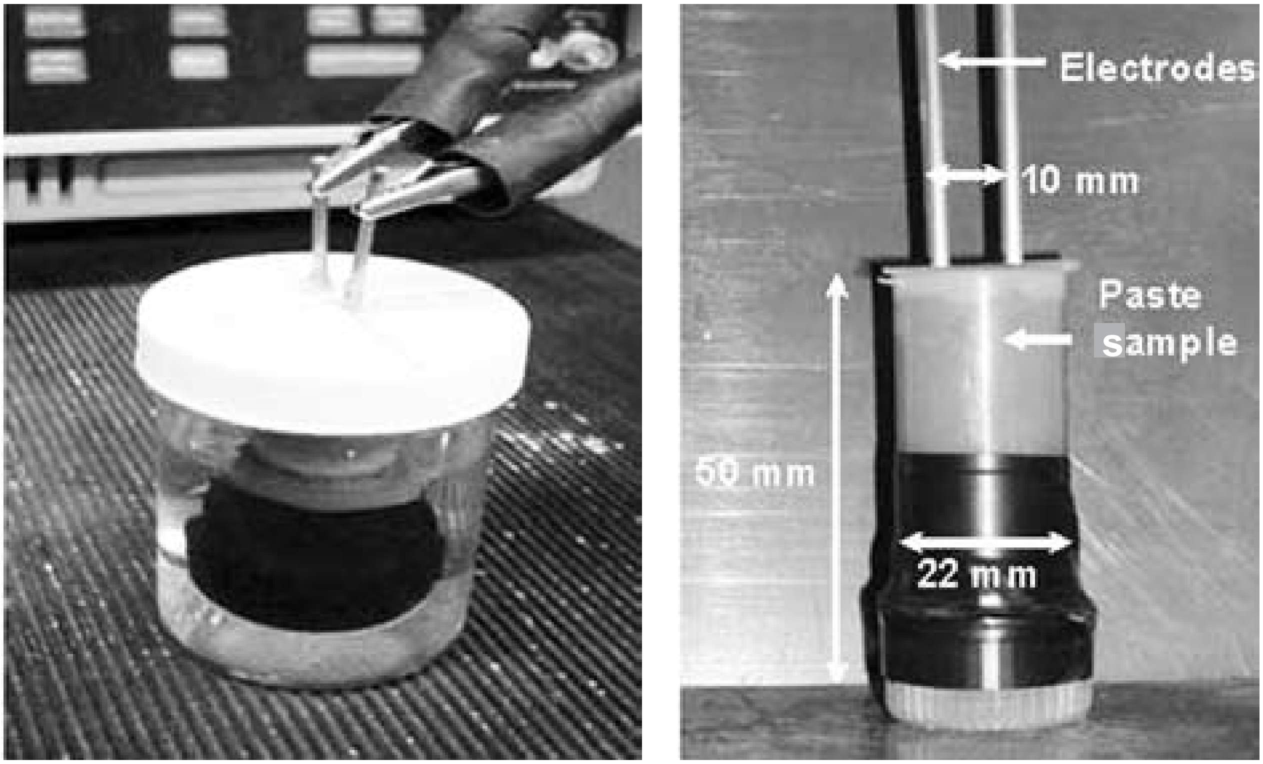

(a) (b)

Figure 1. An illustration of the apparatus used for the measurement of electrical conductivity of cement pastes (a) The conductivity cell for cement pastes immersed in a water bath (b) The vial with embedded electrodes for paste and pore solution conductivity assessment

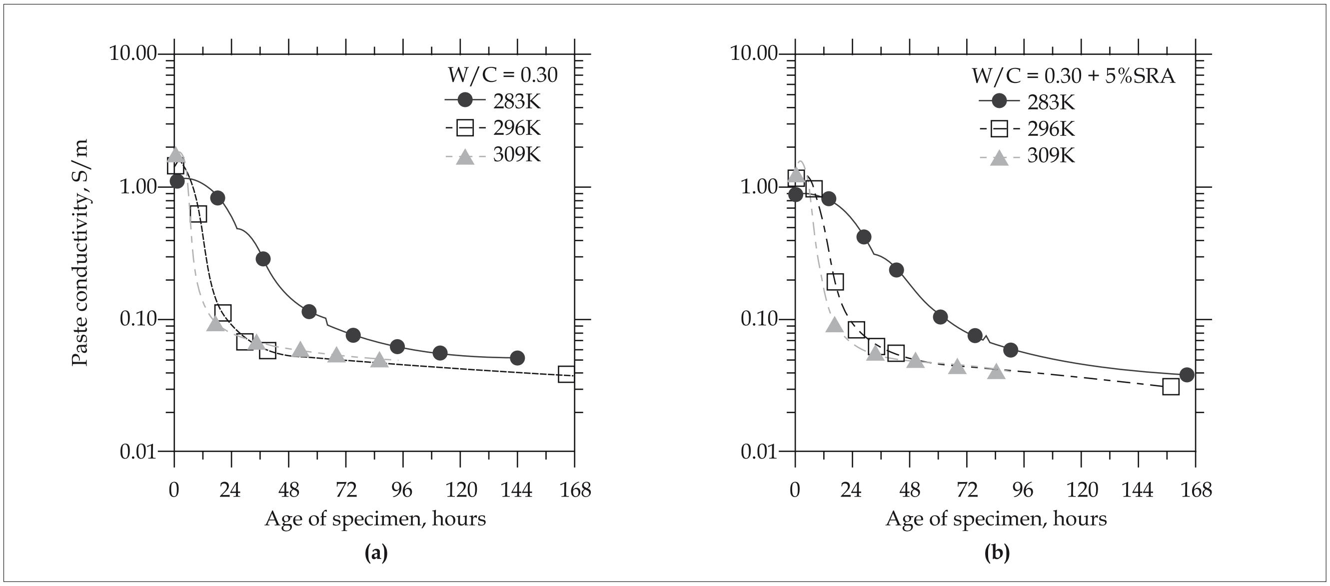

(a) (b)

Figure 2. The electrical conductivity of the cement pastes as function of specimen age (a) W/C = 0.30 and (b) W/C = 0.30 + 5% SRA

specimens which were kept in a water bath to minimise temperature variations (Figure 1a). Measurements were performed on samples cured at 283K (14 days), 296K (7 days) and 309K (4 days). Prior to mixing, the raw materials were temperature conditioned to ensure an appropriate mixture temperature (equivalent to the measuring temperature) at the end of the mixing cycle. For consistency, conductivity measurements until an age of 168 hours (real and equivalent age) are presented in this paper. The measurements were used to determine the activation energy of cement hydration, after a correction to account for the influence of temperature (ionic mobility) on electrical conductivity.

To determine the influence of temperature on the conductivity of the pore solution (i.e. activation energy of electrical conduction; E_{aC} (J/mol)) in cement pastes, conductivity measurements were performed on cement paste samples (cured for 7 days at 296K; ~70% hydration – which corresponds to the maximum degree of hydration for the mixture as computed using Powers model[20] that were conditioned to 283K, 296K and 309K (± 0.5K) in an environmental chamber. Further, companion specimens were cast with thermocouples embedded to monitor the temperature profile of the cement paste mixtures.

Electrical conductivity of synthetic pore solutions

To determine the activation energy of electrical conduction in an electrolyte, synthetic pore solutions of varying concentrations were prepared (0.35 KOH + 0.05 NaOH, 0.70 KOH + 0.10 NaOH, 1.40 KOH + 0.20 NaOH). The solutions were then conditioned to 283K, 296K and 309K (± 0.5K) in an environmental chamber. When the solutions had achieved an equilibrium temperature (measured using thermocouples immersed in the solution), the conductivity of the solutions was measured using a conductivity cell (Figure 1b) connected to a impedance gain-phase analyser[20].

Experimental results

Influence of the rate of reaction on the electrical conductivity

Figure 2 shows the electrical conductivity of cement paste mixtures cured at temperatures of 283K, 296K and 309K. An initial increase in the conductivity is noted for ~1.5 hours for all the cement paste mixtures. This may be explained by the rapid initial dissolution of alkalis and sulphates into the mixing water. After this time (1.5 hours), a reduction in conductivity is noted for all mixtures. A significantly different trend is observed in the rate of measured conductivity (Figure 2) for specimens cured at different temperatures. The samples cured at low temperatures show a gradual decrease in the conductivity, while mixtures cured at higher temperatures exhibit a more rapid decrease. This observation may be explained by the temperature dependence of the rate of hydration in these cement paste mixtures (i.e. the rate of pore structure refinement as a function of the reaction temperature).

Influence of temperature on the electrical conductivity of cement pastes

Figure 3 shows the measured electrical conductivity of two cement paste specimens (cured for 7 days), which have been subjected to thermal cycles. After being cured for 7 days at 296K, the samples were placed at temperatures of 283K and 309K (alternate heating and cooling was performed for 12 hours to ensure equivalent maturity). The results are shown in Figure 3(b). As expected, the measured conductivity is lower at lower temperatures. The lower conductivity of the SRA mixture as compared to the plain mixture is attributed to the non-conductive nature of the SRA in cement paste and pore solution[20,21]. The measured value of conductivity was then used to determine the activation energy of the conduction process in cement pastes. This is further discussed later.

Influence of temperature on the electrical conductivity of pore solution

Figure 4 shows the measured electrical conductivity of synthetic pore solutions (0.35 KOH + 0.05 NaOH, 0.70 KOH + 0.10 NaOH, 1.40 KOH + 0.20 NaOH) conditioned to temperatures of 283K, 296K and 309K. The electrical conductivity is observed to increase linearly over the temperature range from 283K to 309K. This is consistent with the increase in ionic mobility and the extent of dissociation of the dissolved ionic species as a function of temperature. The measured value of conductivity was then used to determine the activation energy of the conduction process in the electrolytes. This is further discussed later.

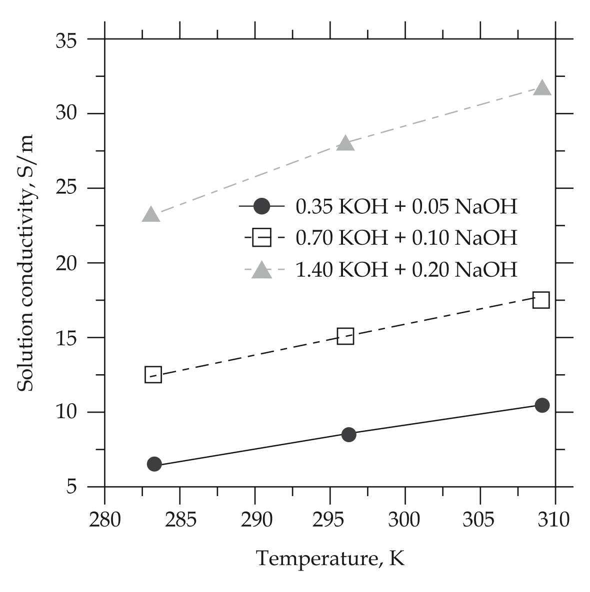

Figure 4. The temperature dependent response of electrical conductivity of synthetic pore solutions investigated in this project

Discussion of experimental results

The electrical conductivity of cementitious materials has been described extensively using a modified parallel

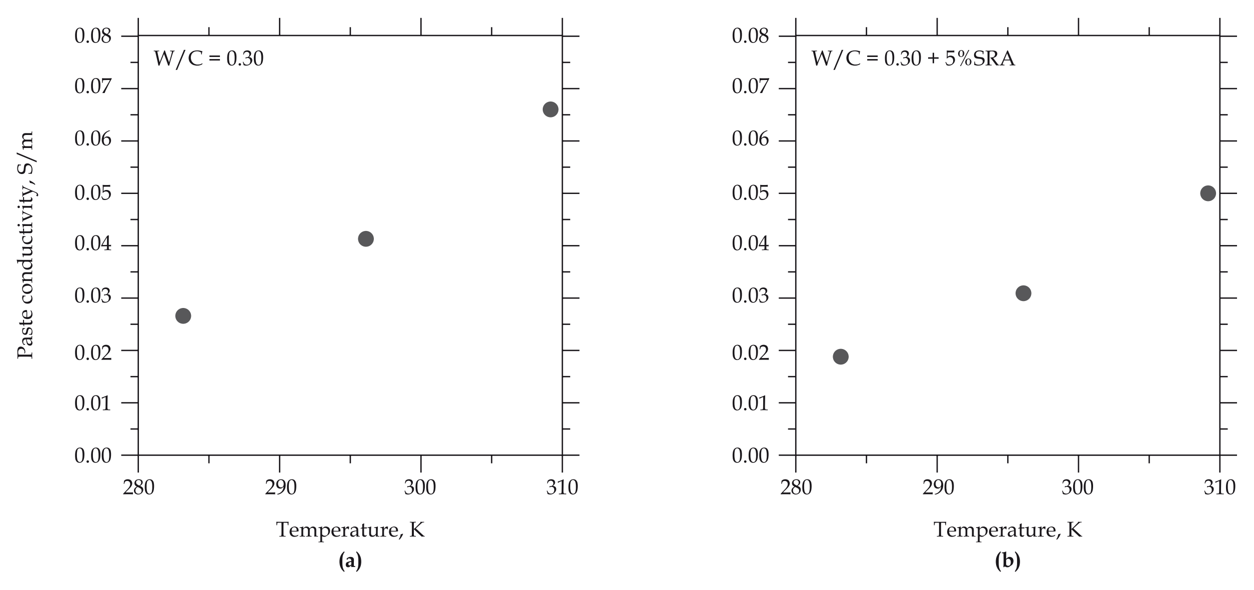

(a)

(b)

Figure 3. The temperature dependent electrical conductivity of the cement pastes (a) W/C = 0.30 and (b) W/C = 0.30 + 5% SRA

law[22,23,24]. This relationship can be described using Equation 6.

$$\sigma_t = \sigma_0 \, \phi \, \beta \qquad ......(6)$$

where, σ_t is the bulk cement paste conductivity (S/m), σ_0 is the pore solution conductivity (S/m), φ is the volume fraction of the solution contained in the pores and β is the pore connectivity. The modified parallel law can be used to determine which parameters are impacted by a change in temperature. The first component which would contribute to the bulk conductivity would be the pore solution conductivity. Considering hydrated products and cement particles to be non-conductive (their conductivity is several orders of magnitude lower than the ionic pore solution), electrical conduction in cementitious materials can be modelled to occur primararily through the ionic pore fluid (in the gel and capillary porosity)[20,23]. This is significant, as temperature influences chemical equilibrium states; impacting ionic mobility (primary effect) and solubility (secondary effect)[25,26]. Ionic mobility (or equivalent conductivity) is noted to increase with increasing temperature due to the decreasing viscosity of the fluid (water), and an increase in the extent of dissociation of the dissolved ionic species, which increases the conductivity of the system[1]. An inverse effect (decreasing conductivity) would be noted with decreasing temperature.

The second component which contributes to the overall conductivity would be the pore fluid volume. For a sealed system, at a given degree of hydration ignoring changes in fluid volume due to changes in density with temperature, the pore fluid volume would be fixed; as solution is not removed from or added to the system. This should however be distinguished from a change in the pore fluid volume due to the consumption of water during hydration.

The third component is the pore fluid connectivity (equivalent to the inverse tortuosity), which decreases due to pore structure refinement with increasing maturity; a function of time and the reaction temperature.

Activation energy of electrical conduction in cement paste and pore solution

Cement paste specimens subjected to thermal cycling were used to determine the influence of temperature on the cement paste conductivity, Figure 3. The results were used to determine the activation energy of electrical conduction (E_{aC}) in cement pastes, Figure 5. The activation energy of conduction was determined to be 25.6 kJ/mol for the plain mixture and 27.6 kJ/mol for the SRA mixture. A higher activation energy of conduction

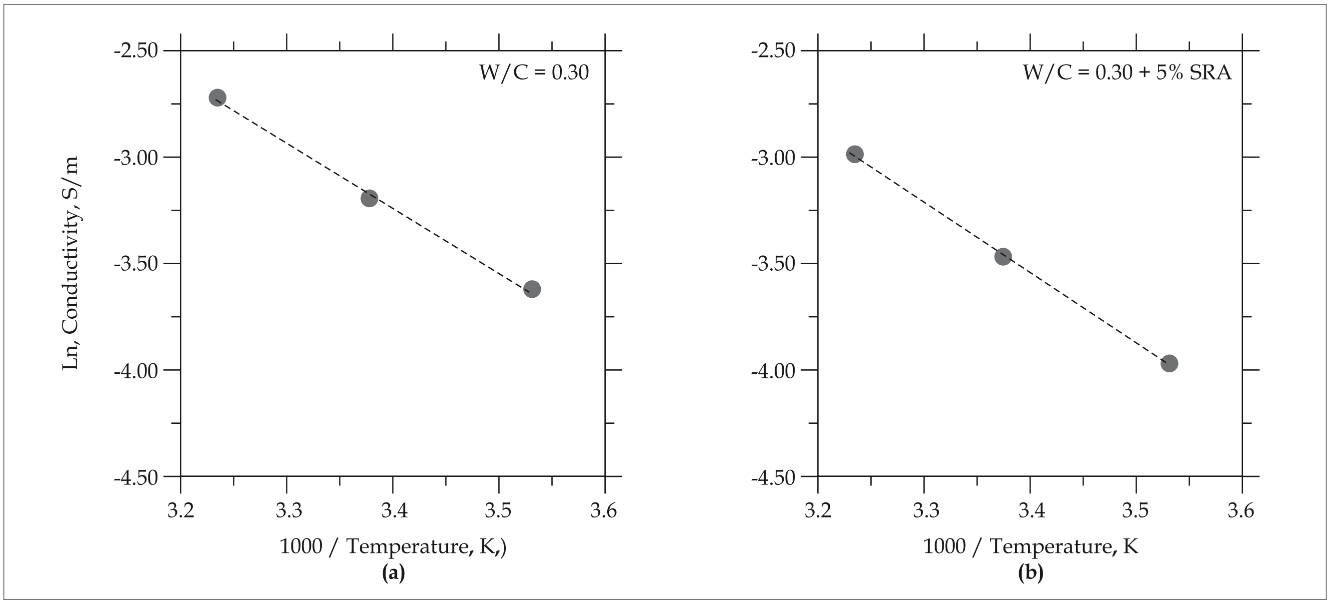

(a) (b)

Figure 5. The activation energy of electrical conduction for cement pastes investigate (a) W/C = 0.30 and (b) W/C = 0.30 + 5% SRA

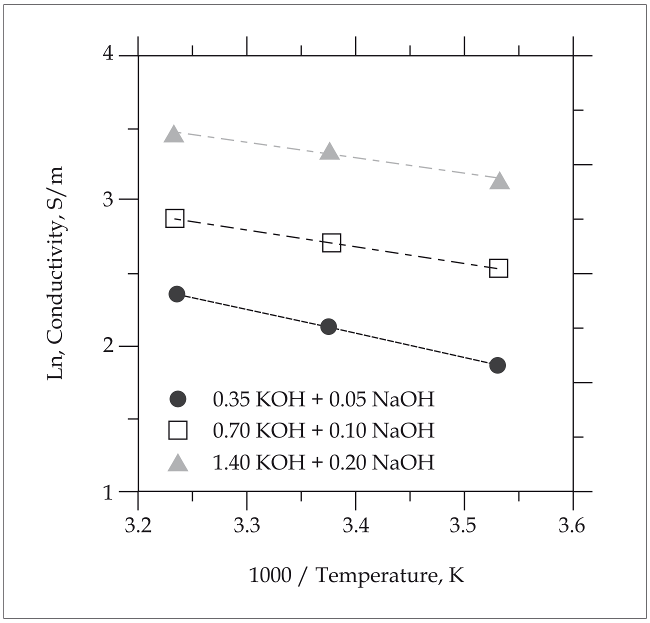

Figure 6. The activation energy of the conduction process for synthetic pore solutions

in mixtures containing a SRA may be explained by the non-conductive nature of the SRA which impedes ion migration in the system. Further, the SRA may bind ions reducing electrical conduction in the system[21].

To fully understand the influence of temperature on the conductivity of an aqueous electrolyte a brief background on electrolytic conductivity is needed. The conductivity of an aqueous electrolyte can be expressed using Equation 7 where, *z* is the species valence (unitless), *c* is the molar concentration of the electrolyte (mol/L) and λ is the equivalent conductivity (cm^2 S/mole) of each species at infinite dilution (which is a function of temperature) and is proportional to the ionic mobility[26]. At low concentrations (< 0.01 mol/l), that is, in dilute solutions the equivalent conductivity is a constant for a specific species. However, at high concentrations the equivalent conductivity is observed to decrease inversely (but non-linearly), due to ion-ion interactions in the solution[19,27].

$$\sigma_{Solution} = \sum z_i c_i \lambda_i \qquad \text{......(7)}$$

Conductivity measurements were performed on synthetic pore solutions subjected to thermal cycling. The solutions were selected to correspond to the concentration of the pore fluid of an early-age cement paste (~ 2 hours), a later age cement paste (48 hours), and a pore fluid with a very high molar (ionic) strength. The results of these tests were used to determine the activation energy of the conduction process (E_{aC}) (Figure 6; 13.55 kJ/mole, 9.65 kJ/mole and 8.98 kJ/mole, respectively, in order of increasing solution concentration) in the ionic solutions. It is noticed that the activation energy decreases with increasing concentration, indicating concentrated solutions are less sensitive to temperature change as compared to dilute solutions. This observation can be explained by the large degree of inter-ionic interactions in concentrated solutions, which significantly alter the conductivity behaviour[27].

Temperature correction for electrical conductivity

The activation energy of conduction in an electrolyte can be used to correct the influence of temperature, by transforming the conductivity at any temperature (in this case 283K or 309K) to a reference temperature (in this case 296K) using the expression shown in Equation 8.

$$\sigma(T_{REF}) = \frac{\sigma(T)}{exp\left(-\frac{E_{ac}}{R}\left(\frac{1}{T} - \frac{1}{T_{REF}}\right)\right)} \qquad \text{......(8)}$$

where, $\sigma(T)$ is the sample conductivity (S/m) at any temperature T (K), $\sigma(T_{REF})$ is the conductivity (S/m) at a reference temperature, T_{REF} (296K), E_{aC} is the activation energy of electrical conduction in an electrolyte (or cement paste) (J/mole) and R is the universal gas constant (J/K.mole). The temperature correction is performed using the activation energy of conduction of the pore solution, having the lowest concentration (conductivity). This solution was selected as it is noted to correspond to the pore solution chemistry (conductivity) of a 2 hour old cement paste (0.35 KOH + 0.05 NaOH), which contains a large fluid volume; whose electrical conductivity behaviour is most sensitive to changes in temperature (Figure 6 – highest E_{aC}).

Determination of the activation energy of the hydration reaction

Electrical conductivity can be corrected to account for the influence of temperature on the rate of hydration and, consequently microstructural development (pore structure refinement). This component may be accounted for using a temperature transformation such as an equivalent age (i.e. maturity) function proposed by Hansen and Pedersen[28]; Equation 9. In this paper, the equivalent age function (Equation 9) is used to determine the activation energy of cement hydration (E_{aR}), after normalising conductivity at any temperature to a reference temperature T(K); using Equation 8.

$$M(t,T) = \int_0^t exp\left(-\frac{E_{aR}}{R}\left(\frac{1}{T}-\frac{1}{T_{REF}}\right)\right) \bullet dt \qquad ......(9)$$

where, M (hours) is the maturity (or equivalent age) of the specimen at a reference temperature T_{REF} (K), E_{aR} (KJ/mol) is the apparent activation energy of the hydration reaction, R (J/(mol · K)) is the gas constant (8.314 J/mol-K), T (K) is the average temperature of the concrete, and dt (hours) is the time interval[28]. The apparent activation energy determined from 10% to 35% hydration; (39.50 kJ/mol) is similar to values determined by other methods (e.g. chemical shrinkage) for the cement systems investigated[20].

Correction for the influence of temperature on hydration and electrical conductivity

As illustrated in Equation 1, the conductivity behaviour of a cementitious material can be expressed as a function of maturity and the measurement temperature. This section will describe a procedure which can be used to simultaneously account for the influence of temperature on cement hydration and electrical conductivity. Due to space considerations, this paper will describe the procedure only for the plain cement mixture (W/C = 0.30).

A function can be fit to describe the experimental conductivity measurement (W/C = 0.30) at the reference temperature (in this case 296K). This function is shown in Equation 10 (R2 = 0.9996).

$$\sigma(t, 296K) = \frac{1.38 - 0.82t + 0.19t^2 - 0.01t^3 + 0.0002t^4}{1.00 - 0.66t + 0.19t^2 - 0.02t^3 + 0.001t^4 + 0.00002t^5} \qquad ......(10)$$

where, $\sigma(t,296K)$ is the measured conductivity at time t (hours) at a measurement temperature of 296K (the reference temperature). The type of fit used to describe the conductivity response is not important. To extend the applicability of this function to describe the electrical conductivity behaviour at any temperature requires the incorporation of a reaction rate constant k_R (unitless) which accounts for the influence of temperature on the rate of cement hydration and an electrical conduction constant k_T (unitless) which accounts for the influence of temperature on electrical conductivity. This approach is described in Equations 11, 12 and 13.

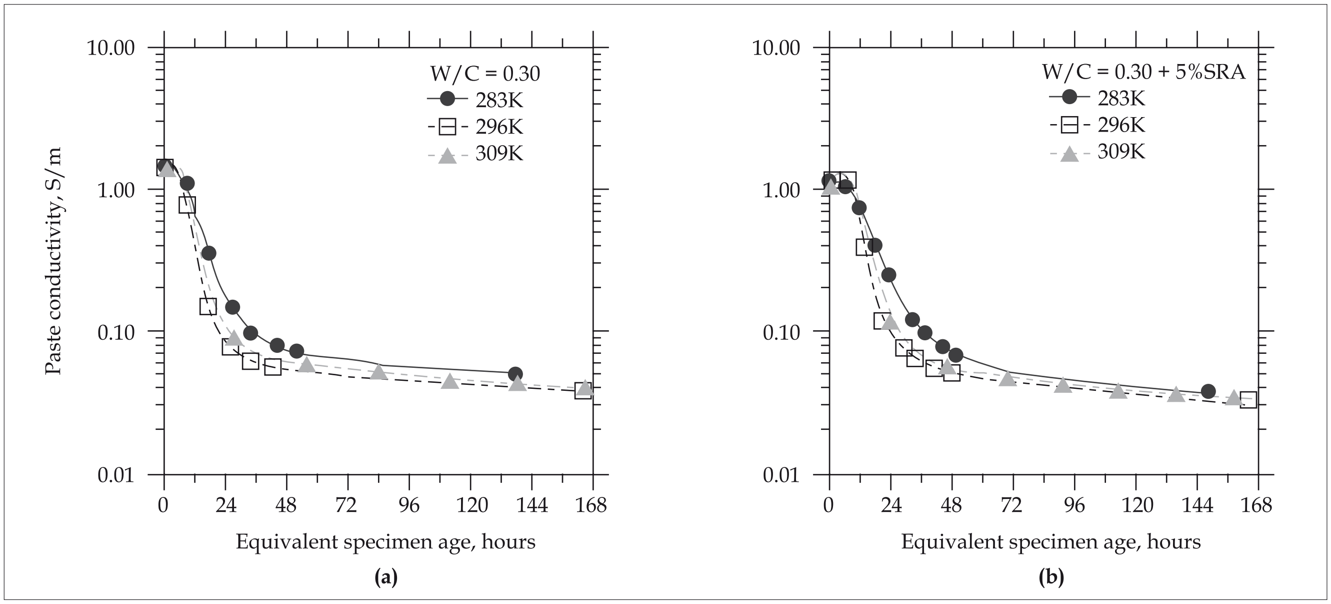

Figure 7. The reaction and solution temperature corrected electrical conductivity of the cement pastes as a function of equivalent specimen age (a) W/C = 0.30 and (b) W/C = 0.30 + 5% SRA

$$\sigma(t,T) = \left(\frac{\begin{array}{c} 1.38 - 0.82(t \bullet k_R) + 0.19(t \bullet k_R)^2 \\ - 0.01(t \bullet k_R)^3 + 0.0002(t \bullet k_R)^4 \end{array}}{\begin{array}{c} 1.00 - 0.66(t \bullet k_R) + 0.19(t \bullet k_R)^2 - 0.02(t \bullet k_R)^3 \\ + 0.001(t \bullet k_R)^4 + 0.00002(t \bullet k_R)^5 \end{array}} \right) \bullet (k_T) \qquad \text{......(11)}$$

where,

$$k_R = exp\left[-\frac{E_{aR}}{R}\left(\frac{1}{T} - \frac{1}{T_{REF}} \right) \right] \qquad \text{......(12)}$$

$$k_T = exp\left[-\frac{E_{aC}}{R}\left(\frac{1}{T} - \frac{1}{T_{REF}} \right) \right] \qquad \text{......(13)}$$

where, k_R (unitless) is the reaction rate constant which accounts for the influence of temperature on the rate of cement hydration, k_T (unitless) is the electrical conduction constant which accounts for the influence of temperature on electrical conductivity and T (K) is the average temperature of the concrete.

Figure 7 shows the electrical conductivity response of the two cement paste mixtures evaluated using the approach described above, to account for the influence of temperature on cement hydration and electrical conductivity; using the activation energy of cement hydration (E_{aR} = 39.50 kJ/mole) and electrical conduction for the electrical conductivity response of an early pore fluid (0.35 KOH + 0.05 NaOH; EaC = 13.55 kJ/mole). It can be seen that (Figure 7), using the approach described in Equation 11, the influence of temperature on hydration and electrical conductivity can be comprehensively described for mixtures cured at any temperature.

An improved approach is proposed to perform the temperature correction for electrical conductivity if the pore solution chemistry (conductivity) at early-ages is well known. This would involve determining the activation energy of electrical conduction in electrolytes (pore fluids) having an age-dependent concentration (and conductivity). This information can be used to perform a comprehensive temperature correction for electrical conductivity. An example of such an approach is illustrated in Figure 8 which shows the activation energy of electrical conduction as a function of the solution's conductivity at the reference temperature (296K)[20,29].

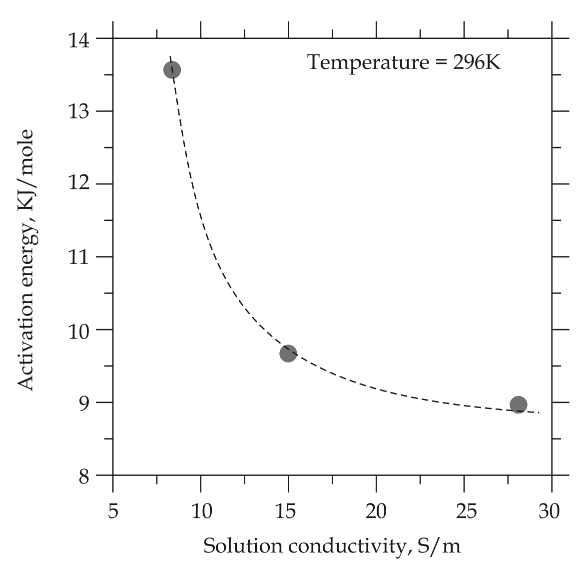

Figure 8. The non-linear relationship between the activation energy of electrical conduction(E_{aC}) and the solution conductivity at 296K

Conclusions

Measurements of electrical conductivity performed on paste, mortar and concrete require a two-part correction to accurately describe early-age behaviour. The first part of this approach accounts for the influence of temperature on cement hydration (pore refinement), and the second part accounts for the influence of temperature on electrical conductivity. This paper demonstrates the successful application of this correction for electrical conductivity measurements using the activation energy of electrical conduction and cement hydration. In this context, the activation energy of electrical conduction has been determined for electrolytes of varying concentrations and for cement pastes. In addition, the activation energy of cement hydration has been determined to be 39.50 kJ/mol (independent of w/c) and is noted to be similar to values determined using other techniques (e.g. chemical shrinkage or heat of hydration). The approach demonstrated in this paper would be crucial for forecasting the long-term durability performance of field concretes, based on the early-age electrical properties of the material using an approach similar to that presented by Lane[30]. An approach of this nature would provide fundamental information needed for quality control and quality assurance (QC/QA) applications and for ensuring the specification compliance of field concretes. This information would have an immense impact in determining how field concrete is specified, evaluated or purchased.

Acknowledgement

The authors gratefully acknowledge the support from the Center for Advanced Cement Based Materials (ACBM) and the National Science Foundation (NSF). This material is based in part on work supported by NSF Grant No. 0134272: a 'CAREER AWARD' granted to the last author. This work was conducted in the Material Characterisation and Sensing Laboratory at Purdue University and as such, the authors gratefully acknowledge the support that has made this laboratory and its operation possible. The contents of this paper reflect the views of the authors, who are responsible for the accuracy of the data presented herein.

References

1. Adamson, A.W., *A Text-book of Physical Chemistry*, Academic Press, USA, 1973.
2. Binder, R.C., *Fluid Mechanics*, Prentice-Hall Inc., Englewood Cliffs, NJ, 1973.
3. Activation Energy, *Encyclopedia Britannica*, 2007.
4. Carino, N.J., The maturity method, *CRC handbook on nondestructive testing of concrete* , Edited by V.M. Malhotra and N.J. Carino, CRC Press, Boca Rotan, Florida, 1991, pp. 101-146.
5. Weiss, W.J., Experimental determination of the 'Time-Zero', *Early age cracking in cementitious systems* – RILEM report TC-EAS, Edited by Arnon Bentur, 2002.
6. Pinto, R.C.A. and Hover, K.C., Application of maturity approach to setting time,' *ACI Materials Journal*, 1999, Vol. 96, No. 6, pp. 686-691.
7. Roy, D.M., Scheetz, B.E., Sabol, S., Brown, P.W., Shi, D., Licastro, P.H., Idorn, G.M., Andersen, P.J., and Johanson, V., Maturity model and curing technology, Strategic Highway Research Program, SHRP-C-625, (1993)
8. Nurse, R.W., Steam curing of concrete, *Magazine of Concrete Research*, 1949, Vol. l, No. 2, pp. 79-88.
9. Saul, A.G.A., Principles underlying the steam curing of concrete at atmospheric pressure, *Magazine of Concrete Research*, 1951, pp. 127-140.
10. Hammond, E., and Robson, T.D., Comparison of Electrical Properties of Various Cements and Concretes, *The Engineer*, 1955, Vol. 199, pp. 78-80.
11. Rasch, E. and Hinrichsen, F.W., Uber eine beziehung zwischen elektrischer leitfahigkeit und Temperatur, *Zeitschrift fur electrochemie*, 1908, Vol. 14, No. 41, pp. 41- 48.
12. Spencer, R.W., Measurement of the Moisture content of concrete, *Journal of the American Concrete Institute*, 1937, Vol. 9, No. 1, pp. 45-61.
13. Elkey, W. and Sellevold, E.J., *Electrical resistivity of concrete, Norwegian Road Research Laboratory*, Publication No. 80, 1995, Oslo.
14. Whittington, H.W., McCarter, W.J. and Forde, M.C., The conduction of electricity through concrete, *Magazine of Concrete Research*, 1981, Vol. 33, No. 114, pp. 48-60.
15. McCarter, W.J., Effects of temperature on conduction and polarization in portland cement mortar, *Journal of the American Ceramic Society*, 1995, Vol. 78, No. 2, pp. 411-415.
16. McCarter, W.J., Starrs, G. and Chrisp, T.M., Electrical conductivity, diffusion, and permeability of portland cement-based mortars, *Cement and Concrete Research*, 2000, Vol. 30, No. 9, pp. 1395-1400.
17. Arrhenius, S., On the reaction velocity of the inversion of cane sugar by acids, Zeitschrift für physikalische Chemie, 4, 226, (1889).
18. Sant, G., Lura, P. and Weiss, W.J., Measurement of volume change in cementitious materials at early ages: Review of testing protocols and interpretation of results, *The Transportation Research Record*, 2006, 1979.
19. Rajabipour, F., Weiss, W.J. and Abraham, D., Insitu electrical conductivity measurements to assess moisture and ionic transport in concrete, Advances in concrete through science and engineering, *Proceedings of the International RILEM Symposium*, Evanston, Illinois, 2004.
20. Sant, G., *Examining volume changes, stress development and cracking in cement-based systems*, MSCE Thesis, Purdue University, West Lafayette, Indiana, USA, 2007.
21. Rajabipour, F., Sant, G. and Weiss, W.J., Interactions between shrinkage reducing admixtures and cement paste's pore solution, *Cement and Concrete Research*, 2008, Vol. 38, pp. 606-615.
22. Garboczi, E.J., Permeability, diffusivity, and microstructural parameters : A critical review, *Cement and Concrete Research*, Vol. 20, No. 4, pp. 591-601.
23. Rajabipour, F., *Insitu electrical sensing and material health monitoring in concrete structures*, PhD Dissertation, Purdue University, West Lafayette, Indiana, USA, 2006.
24. Christensen, B.J., Coverdale, R.T., Olson, R.A., Ford, S.J., Garboczi, E.J., Jennings, H.M. and Mason, T.O., Impedance spectroscopy of hydrating cement-based materials: Measurement, interpretation, and application, The American Ceramic Society, 1994, Vol. 77, No. 11, pp. 2789-2802.
25. Taylor, H.F.W., *Cement Chemistry*, Academic Press, London, (1990)
26. Bockris, J.O.M., and Reddy, A.K.N., *Modern electrochemistry*, Vol. 1, Section 4.4, 1970, Plenum, New York City, NY, USA.
27. Snyder, K.A., Feng, X., Keen, B.D. and Mason, T.O., Estimating the electrical conductivity of cement paste pore solutions from OH-, K+ and Na+ concentrations, *Cement and Concrete Research*, 2003, Vol. 33, No. 6, pp. 793-798.
28. Hansen, F., and Pedersen, E. J., Maturity computer for controlled curing and hardening of concrete, *Nordisk Betong*, 1977, No. 1, pp. 21-25 (in Danish).
29. ______*Standard practice for estimating concrete strength by the maturity method*, ASTM C1074-04, ASTM International, West Conshohocken, Pennsylvania, USA, 2004.
30. Lane, D.S., Supplanting the rapid chloride permeability test with a quick measurement of concrete conductivity, Virginia Transportation Research Council, Charlottesville, Virginia, USA, 2005.

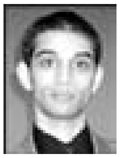

Mr. Gaurav Sant received his bachelor's (BSCE) and master's degrees (MSCE) in civil engineering from Purdue University with an emphasis in construction materials. Currently, he is pursuing his PhD at the School of Civil Engineering at Purdue University. His research interests include early-age shrinkage and cracking, non-destructive testing and moisture transport in cementitious materials.

Dr. Farshad Rajabipour received his BSc from Sharif University of Technology (Tehran) and his MS and PhD from Purdue University. Currently, he is an assistant professor of civil and environmental engineering at the University of Hawaii, Mānoa. His research interests include materials science of concrete, construction sustainability and use of recycled materials, and non-destructive testing and health monitoring.

Prof. Jason Weiss is associate head in the School of Civil Engineering at Purdue University and the associate director of the National Science Foundation, Center for Advanced Cement Based Materials at Northwestern University. His research interests include early-age shrinkage, cracking and its influence on durability, durability of environmentally friendly binders, moisture transport and service-life predictions of civil infrastructure.

Wetting and Drying of Concrete Using Aqueous Solutions Containing Deicing Salts

Robert P. Spragg
Undergraduate Research Assistant
School of Civil Engineering
Purdue University
West Lafayette, IN 47907-2051
E-mail: rspragg@purdue.edu
Phone: 765.494.0358

Javier Castro
Graduate Research Assistant and Ph.D. Candidate
School of Civil Engineering
Purdue University
West Lafayette, IN 47907-2051
E-mail: jcastro@purdue.edu
Phone: 765.494.0358

Wenting Li
Graduate Research Assistant
School of Civil Engineering
Purdue University and Southeast University
West Lafayette, IN 47907-2051
Nanjing, China 211189
E-mail: li448@purdue.edu
Phone: 765.494.0358

Mohammad Pour-Ghaz
Graduate Research Assistant
School of Civil Engineering
Purdue University
West Lafayette, IN 47907-2051
E-mail: mpourghaz@purdue.edu
Phone: 765.494.0358

Pao-Tsung Huang
Graduate Research Assistant
School of Civil Engineering
Purdue University
West Lafayette, IN 47907-2051
E-mail: huang69@purdue.edu
Phone: 765.494.6242

Jason Weiss (Corresponding Author)
Professor and Director of Pankow Materials Laboratory
Associate Director of the Center for Advanced Cement Based Materials
School of Civil Engineering
Purdue University
West Lafayette, IN 47907-2051
E-mail: wjweiss@purdue.edu
Phone: 765.494.2215

Abstract

A series of wetting and drying tests were performed on concrete using different aqueous solutions containing deicing salts. The rate of fluid absorption was generally lower for aqueous solutions containing deicing salts than it was for water. In addition, less fluid was absorbed for samples exposed to aqueous solutions containing deicing salts than for samples exposed to water. The change in the rate of aqueous fluid absorption was proportional to the square root of the ratio of surface tension and viscosity of the absorbed fluid. Concrete that has been exposed to solutions containing deicing salts showed less mass loss during drying. Measures of equilibrium relative humidity over the salt solutions are used to interpret drying behavior. Experimental data indicates that concretes that had previously been exposed to deicing solutions can also exhibit reduced rate of absorption, even if water is the fluid being absorbed.

1. Research Need and Significance

Some jointed plain portland cement concrete pavements in freezing prone climates have shown premature deterioration at the longitudinal and transverse joints. While some have attributed this damage to a chemical attack, inadequate air entrainment, poor mixture design, inadequate constituent materials, or poor construction practices; it is the hypothesis of the authors of this paper that this joint deterioration may be attributed, at least in part, to preferential absorption of fluid at joints. This hypothesis was developed based on observations from the field that show these deteriorated locations frequently occurred at low spots in the pavement, where joint sealers were damaged, where water has collected, or where the joint does not appear to have opened thereby trapping water [1]. Preferential fluid ingress at joints could increase a variety of damage mechanisms including deleterious chemical reactions, crystallization pressure, or freeze thaw damage that may degrade the concrete. To fully evaluate fluid ingress at the joints it is essential that the wetting and drying behavior of concrete is evaluated using aqueous solutions containing deicing salts.

This work is limited in scope as it considers only the ingress of aqueous solutions over short time periods and does not explicitly consider any chemical reaction that occurs between the aqueous solution and the concrete. This information is intended to provide reference for those developing tests to evaluate potential deicer-concrete interactions [2], for developing tests on fluid absorption, for evaluating fluid absorption in concrete [3], for input parameters in computer simulation of fluid ingress at joints [4], and for potential approaches to limit joint deterioration like penetrating sealers for possible use in concrete pavements [5].

2. Fluid Absorption in Porous Materials

Fluid absorption is a frequently used test to provide an indication of the durability of concrete systems since it is simple to perform. Several standard tests exist for measuring water absorption including ASTM C 1585-04 [6], BS 1881-99 [7], and ASTM D6489-99 [8]. While the concept behind these tests is very similar, there are differences in how the samples are conditioned, treated, and tested. In each of these tests water is typically used as the fluid that is being absorbed. Hall [9] discusses that water can interact with the cement matrix adding complexity to the interpretation of results. To overcome some of these limitations or to indicate how absorption can be reduced by fluid composition other solutions have been tested [9-13].

MacInnis and Nathawad [14] assessed the absorption of an aqueous solution consisting of a NaCl deicing salt and reported a decrease in absorption. Sutter et al. [15] reported that sorptivity decreased from highest to lowest in the order of water, NaCl, $CaCl_2$ and $MgCl_2$. Similar data has recently been observed by Janusz [16]. As a result, it can be observed that concrete exposed to deicing salt solutions absorb fluid at a slower rate than they would absorb water; however the previous work has not related this behavior to the fluid properties or described the influence of salt concentration or properties of the aqueous solution.

The results of one-dimensional fluid absorption tests (assuming negligible gravitational effects) are typically reported as the cumulative water absorbed per surface area (surface from which water is absorbed) versus the square root of wetting time. Equation 1 is frequently used to describe the water absorption (total volume of fluid absorbed) and the sorptivity (related to the rate of absorption) [17].

$$i = S\tau^{1/2} \qquad \text{Eq. 1}$$

where i [mm^3/mm^2] is the cumulative water absorption, S [mm/s$^{1/2}$] is the sorptivity, and τ [s] is the elapsed time. It should be noted that additional equation have been proposed to account for time dependent properties [18].

Hall [9] proposed that the diffusion would scale proportionately with the ratio of surface tension (γ) and viscosity (η) of the fluid. Hall further related this to sorptivity since sorptivity is related to the square root of diffusion. Kelham [19] derived an expression for fluid absorption (Equation 2) that shows the relationship between depth of penetration and the square root of the ratio of surface tension and viscosity.

$$x(\tau) = \sqrt{\frac{4k\gamma\cos(\theta)\tau}{p\eta r}} \qquad \text{Eq. 2}$$

where $x(\tau)$ [mm] is the penetration depth, γ [N/mm] is the surface tension, θ [rad] is the liquid-solid contact angle, p [Dimensionless] dis the porosity of the medium, r [mm] is the pore radius, k [mm^2] is the intrinsic permeability of the material, and η [Pa.s] is the viscosity of fluid. An expression similar to equation 2 was derived by Scherer and Wheeler [20] for stone consolidates.

Previous research using organic fluids has shown an absorption rate that scales proportionally with the square root of the ratio of surface tension and viscosity of the fluid ($(\gamma/\eta)^{1/2}$). This work will use this approach to attempt to interpret results from absorption tests that used aqueous solutions containing deicing salts.

3. Properties of Deicing Salt Solutions

Physical properties of pure solutions were gathered from literature and compared with measured values for the industrially available deicing solutions tested in this research, and they are provided here for convenience in one location. The properties of the deicing solutions will be used in interpreting the wetting and drying results, discussed later in this paper. This section is divided into four sections. The first three sections describe the influence of the deicing solutions in terms of surface tension, viscosity, and equilibrium relative humidity over the aqueous solution. The fourth section describes the specific gravity of the solution as a function of concentration as this is used to determine the volume of solution absorbed during the absorption test.

3.1 Surface Tension of Deicing Salt Solutions

Figure 1 (a) shows surface tension measurements at different concentrations for the three solutions used in this research: NaCl, $CaCl_2$, $MgCl_2$. The surface tension for NaCl was obtained from [10], $CaCl_2$ from [21] and $MgCl_2$ from [22]. A Du Noüy Ring Tensiometer KRÜSS was used with a resolution of 0.1 mN/m for the industrial deicers tested in this study. The tensiometer was cleaned between measurements following ASTM D971-04 [24]. The tensiometer was first calibrated using de-ionized water, which provided a value of 71.0×10^{-6} N/mm. A series of three measurements were performed for each solution, with the average reported.

The closed points in Figure 1 (a) are the values measured for the industrially available solutions. The lines represent values taken from literature for pure salt solutions at different mass concentrations. While the general trends are consistent, differences between the solutions containing industrial deicing salts and literature values may be due to impurities or other additves however further work is needed to examine this in greater detail.

3.2 Viscosity of Deicing Salt Solutions

Figure 1 (b) shows a comparison of the viscosities for the solutions used in this research between pure solutions taken from literature and measurements of the deicing solutions. Viscosity measurements for the industrial deicers were performed on the salt solutions using an Anton-Parr rheometer, model Physica MCR 301. The rheometer kept the solution being tested at 23.0 ± 0.02 ºC and from the torque applied to the fluid that causes a shear from which the viscosity can be found. Calibration of the device was performed using a reference standard.

The dashed lines presented are viscosities at different concentrations and are taken from literature [10, 21-23], while the points represent measured viscosities of the industrially available solutions. Again, differences between literature values and those of the solutions measured can be explained by differences in possible additions or chemistries of the industrial deicers.

3.3 Relative Humidity of Deicing Salt Solutions

Relative humidity measurements were performed on the salt solutions using Rotronic HygrClip2S sensors (± 0.8 % RH at 23 ± 0.1 °C). The relative humidity probes were mounted in a 75 mm x 68 mm stainless steel cylinder that was placed over a water jacketed sample cup holder. The water jacket was connected with a water bath at a constant temperature of 23.0 ± 0.1 ºC.

Figure 1 (c) shows the relative humidity measured over salt solutions for a wide range of solution concentrations. As the concentration increased the relative humidity over the solution decreased. The measured relative humidities of these unsaturated salt solutions are higher than that of the saturated solution of these salts which are 75.4 % RH for NaCl [25], 33.0 % RH for $MgCl_2$ [25] and 22 % for $CaCl_2$ [21].

3.4 Specific Gravity of Deicing Salt Solutions

Figure 1 (d) shows the specific gravity of different deicing solutions as a function of concentration. The specific gravity of the solution increases with concentration. The $CaCl_2$ and $MgCl_2$ increase at very similar rates with an increase in concentration, while the NaCl increases slightly less than the $CaCl_2$ and $MgCl_2$ (i.e., 25 % less increase with concentration). This may be attributed to the colligative properties of solutions.

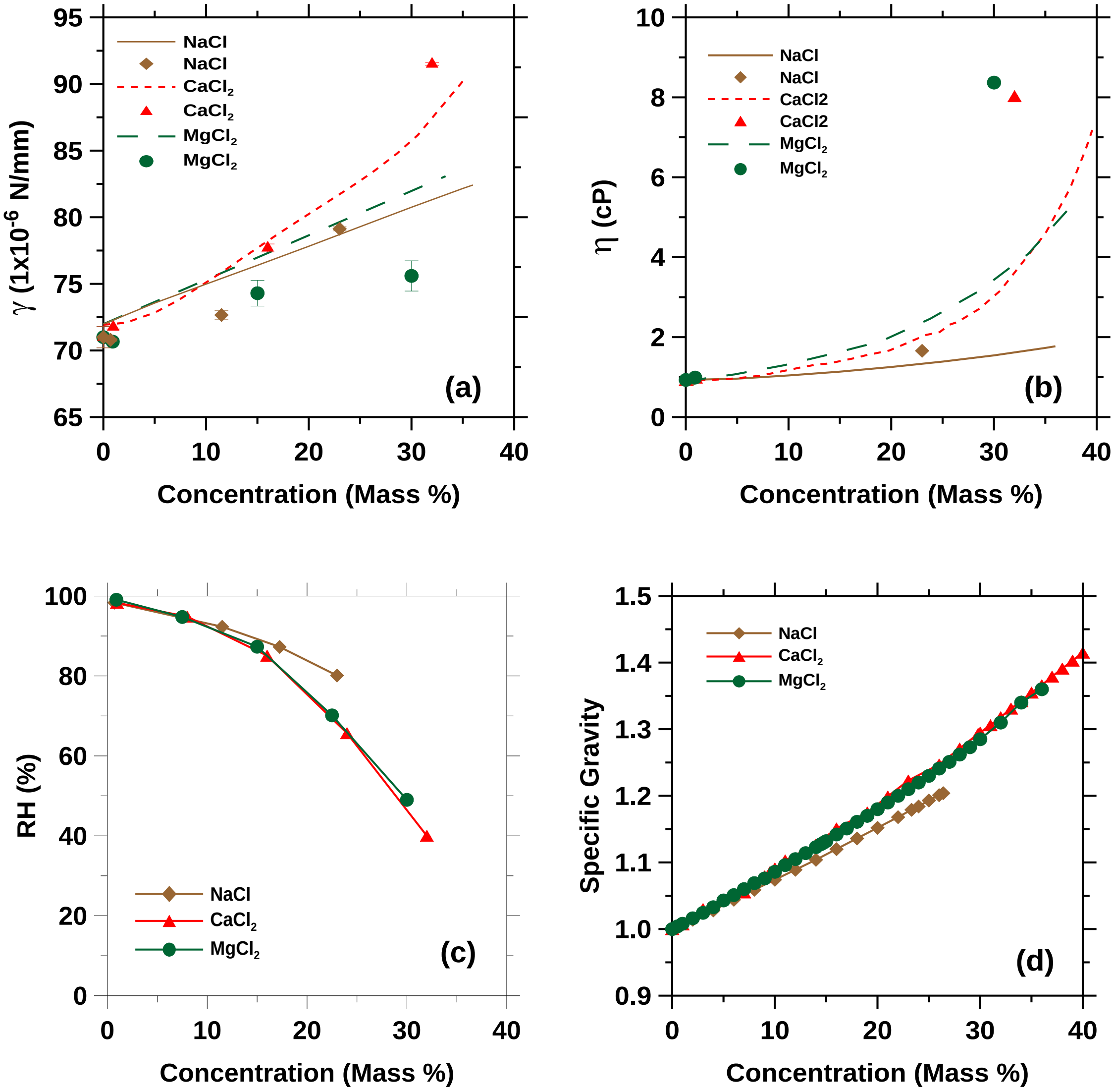

Fig .1. Properties of Deicing Salts at 23-25 ºC: (a) Surface Tension (b) Viscosity (c) Relative Humidty (d) Specific Gravity (Rosenburgh 2010, unpublished data)

4. Wetting and Drying for Concrete with Deicing Solutions

4.1 Experimental Program of Wetting and Drying of Concrete with Deicing Solutions

The concrete mixture that was used for these tests was a typical INDOT class C bridge deck concrete. The mixture proportions of this concrete are shown in Table 1. The fresh air content was 5.7 %, which was measured according to ASTM C231-09 [26]. The hardened air content of the concrete was 4.4 % as assessed using an automated optical scanning approach [18] based on the method proposed by Peterson et al. [28].

Table 1. Mixture Proportions of Concrete Assuming Saturated Surface Dry (SSD) Conditions

Material	Mass
Cement (kg/m^3)	316
Class C Fly Ash (kg/m^3)	60
Water (kg/m^3)	150
Fine Aggregate (kg/m^3)	736
Coarse Aggregate (kg/m^3)	1049
Air Entraining Admix. (ml/100 kg of cem. materials)	20
High Range Water Reducer Admix. (ml/100 kg of cem. materials)	456
Retarder Admixture (ml/100 kg of cem. materials)	98

The concrete was produced in a central mix plant and discharged from a ready mix concrete truck. A series of 100 mm × 200 mm cylinders were cast. After one day of curing, the cylinders were demolded and sealed in double plastic bags at 23 ± 0.5 °C until the samples reached an age of 28 d. After 28 days of curing the cylinders were removed from bags and three 50 mm ± 2 mm thick samples were cut from the central portion of each cylinder using a wet saw.

Two different sets of samples were used in this study. The first set of samples were used to evaluate the effect of sample conditioning on water absorption. In each condition, three samples were used. A total of five conditions were considered: ASTM C1585-04, oven-dry, 50 % RH, 65 % RH and 80 % RH. To ensure that these samples that were conditioned at 50 %, 65 %, and 80 % RH, reached equilibrium, a 12-month conditioning was period was considered. The second set of samples that were used for aqueous salt solution absorption, drying, and de-ionized water re-absorption were conditioned at 50 ± 2 % RH, 23 ± 0.5 °C for 36 months and two samples were tested for each salt solution.

To prepare the specimens for fluid absorption testing, the sides of the samples were sealed with epoxy. After the epoxy had hardened, the top surface was covered with plastic to avoid evaporation from the sample during testing.

The absorption test involves recording incremental mass change measurements during the first six hours after the sample comes in contact with the fluid and subsequently taking one measurement every day for the next eight days. The amount of absorbed fluid is normalized by the cross-section area of the specimen exposed to the fluid using Equation 3.

$$i = \frac{m_t}{(a \cdot \rho)} \qquad \text{Eq. 3}$$

where: i (mm^3/mm^2) is the normalized absorbed fluid, m_t (g) is the change in specimen mass at time t; a (mm^2) is the area of the specimen exposed to the fluid (i.e., that of the bottom face), and ρ (g/mm^3) is the density of the absorbed fluid (this is provided in greater detail in 3.1). These absorption measurements are then plotted as a function of the square root of time, as provided by Equation 1. The sorptivity is the slope of this graph.

The second series of samples were tested using seven different fluids. Their composition was primarily based on one of three different industrially available deicing products, either NaCl, $MgCl_2$ or $CaCl_2$. A low concentration was used for each salt solution as well as a higher concentration that was selected to be near the eutectic composition for each salt. De-ionized water was also used as a reference fluid.

4.2 Experimental Results from Wetting with Water for Different Conditioning Methods

Figure 2 shows the results from water absorption tests performed on the first series of samples that were conditioned with different environmental conditions as mentioned earlier (ASTM C1585-04 accelerated conditioning, 80 % RH, 65 % RH, 50 % RH and oven drying). It should be remembered that these samples were conditioned for 12 months while the remainder of the samples discussed in this paper were conditioned at 50 % RH for a much longer time. Sample preparation has an enormous impact on the water absorption results as more severe drying enables a greater volume of water to be absorbed during the test.

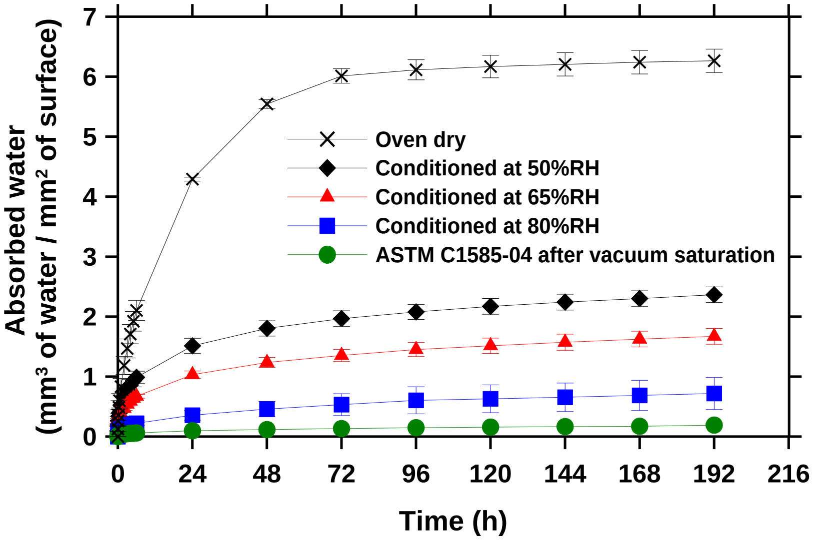

Fig. 2. Water absorption on samples subjected to different conditioning procedures.

4.3 Experimental Results from Wetting and Drying with Deicing Solutions

Figure 3 illustrates the results of the fluid absorption test as a function of time (for concrete at 50 % RH for a longer conditioning time than the samples in Figure 2). It can be seen that even though the concrete that is used for all the tests in Figure 3 has the same conditioning and exposure conditions, the volume of solution absorbed by each material is dependent on the deicing salt solution and the concentration of the deicing salt solution that was absorbed. The sample with the low concentration of NaCl showed a slight increase in the rate of absorption (as compared with water) as well as the amount of fluid absorbed. This is consistent with the data reported by

MacInnis and Nathawad [14]. The absorption of all the other fluids was reduced when compared with water. As a result, it can be concluded that in general as the salt concentration increased the rate of absorption reduced and and the total absorption was reduced. Further work is needed to examine lower concentrations for NaCl to ascertain why a slight increase is typically reported.

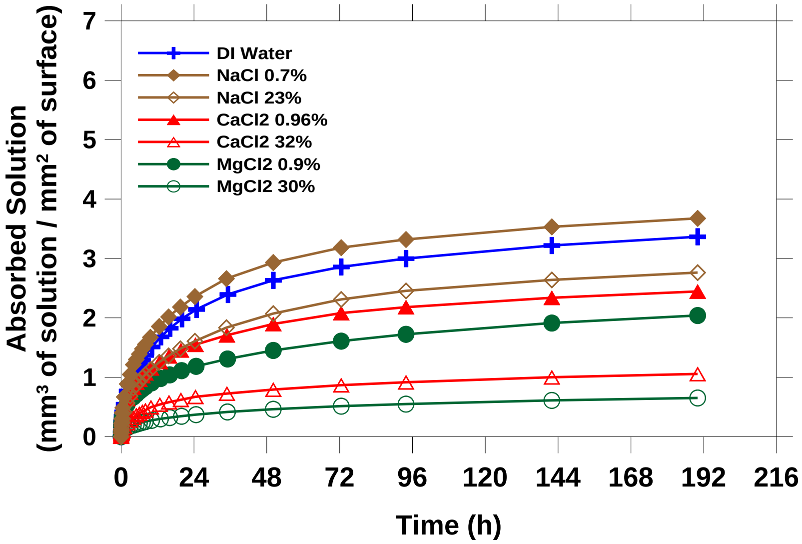

Fig. 3. Volume of deicing solutions absorbed by concrete as a function of time (typical standard deviation less than 0.1 mm^3/mm^2).

After the fluid absorption test was performed for 8 days the samples were dried at 50 ± 2 % RH, 23 ± 0.5 °C for seven days. The samples were kept in the same one-faced exposed condition for the drying test; however, the exposed surface that was facing down in the absorption testing was placed facing up to simulate drying from the top. During the drying test the mass of the samples was recorded at regular intervals.

Figure 4 shows the volume of water loss during the drying period. It is important to note that the drying test will result in only the water portion of the solution being evaporated from the system leaving the salt to become more concentrated in the solution before it eventually precipitates out. It can be noticed that as the concentration of deicing solution was increased the mass loss during drying decreased. This was particularly evident in the high concentration solutions, which showed nearly no mass loss or even a slight gain during drying.

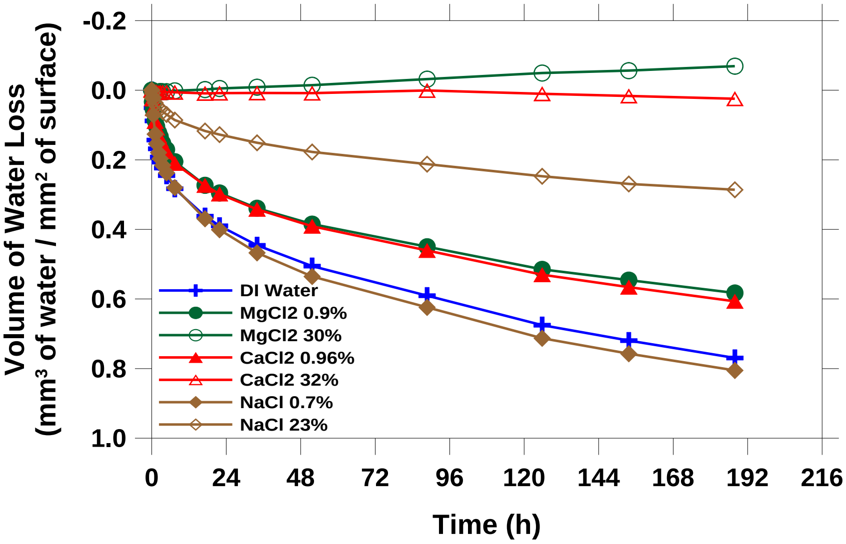

Fig. 4. Drying of concrete prewetted with different salt solutions as a function of time (typical standard deviation less than 0.03 mm^3 water/mm^2).

4.4 Experimental Results from Wetting Previously Exposed to Deicing Solutions

The same set of samples that were previously tested for absorption and drying were oven dried to be tested for second absorption test using de-ionized water. This was done to investigate the effects of previously absorbed salts on re-absorption of de-ionized water. However, in the case of the oven-dried samples, higher water absorption is expected. This can be due to the empty capillary pores and possibly to microcracking generated during oven drying [29-33].

To prepare the samples for the de-ionized water re-absorption test, the samples were placed in an oven at 105 ± 2 °C until they reached to equilibrium. The equilibrium condition was defined as a difference less than 0.5 % between two successive mass measurements (24 hours apart). It is important to note that this drying process will evaporate only the water portion of the solution pre-absorbed, leaving salt in the pores. Since these samples were oven dried, their absorption rates and absorbed water are not comparable with any previous tests.

Figure 5 shows the results for this second absorption test. It can be seen by comparing the results to the results in Figure 3 that the behavior of the samples was dependent on the deicing solutions and the concentrations of deicing solutions used in the first wetting test. These results are a clear indication that the history of the samples affects the results of fluid absorption. This suggests when sorption testing is preformed on field concretes, some understanding of the admixtures or salts that remain in the pore system is needed to fully interpret the results.

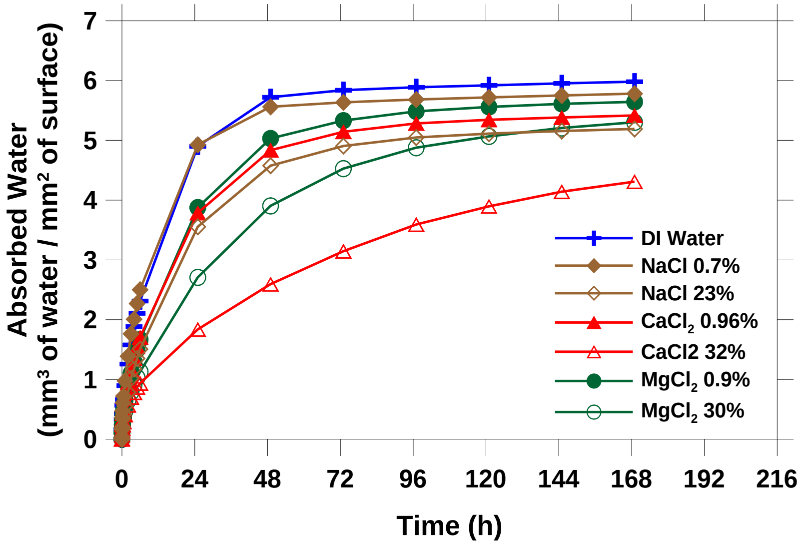

Fig 5. Volume of de-ionized water absorbed by concrete as a function of time in the second fluid absorption test (Fluid from the original test is shown in the caption).

4.5 Drying of Mortars Saturated with Different Deicing Salts

Moisture desorption is an established technique for evaluating the effect of moisture loss at a given humidity for a material. A TA Q5000 SA moisture sorption analyzer was used to carefully control temperature and humidity. Mortar samples were prepared (*w/c* = 0.42 and 55 % aggregate by volume) and cast in a cylindrical mold with a 34 mm diameter and 50 mm height. At an age of 28 days the specimens were demolded and 34 mm diameter 0.8 ± 0.05 mm thick slices were taken from the middle of the samples. The samples were dried under controlled conditions (at 23 ± 0.1 °C and 50 ± 1 % RH) in a CO_2 free chamber until they reach mass equilibrium. Then, samples were submerged for a minimum of 5 days in aqueous solutions with 23 % NaCl, 32 % $CaCl_2$, and 30 % $MgCl_2$ by mass.

For the samples submerged in NaCl, $CaCl_2$, and $MgCl_2$ solutions a 50 mg to 70 mg piece of sample was placed in a tared quartz pan after a minimum of 5 days of submersion. The pan containing the sample was then suspended from the balance (± 0.001 mg accuracy) and placed in the relative humidity chamber to equilibrate at 23.0 ± 0.1 °C and 97.5 ± 0.1 % RH for up to 96 h or until the sample had achieved a stable mass (less than an 0.001 % mass change/15 minutes). Then, the relative humidity was reduced to reach 95 %. After the sample mass equilibrated, the relative humidity in the chamber was changed in 10 % RH steps to 55 % RH, allowing the sample to attempt to equilibrate (12 h or 0.01% change in mass over 15 minutes) at each new humidity. After equilibrating at 55 % RH the samples were dried to 0 % RH. For the sample submerged in de-ionized water the procedure was similar, but the relative humidity was reduced in 5 % steps from 97.5 % to 2.5 %, and then reduced to 0 % RH.

Figure 6 shows the plot of mass change as a function of time for the mortar saturated in de-ionized water. The sample soaked in water can be seen to lose mass with the decrease of RH. For this system, when the environment is below 100 % RH, water will move from the pores to outside of the sample and classical drying behavior is observed. The maximum mass of the sample is 8.5 % higher than the mass of the oven dry sample.

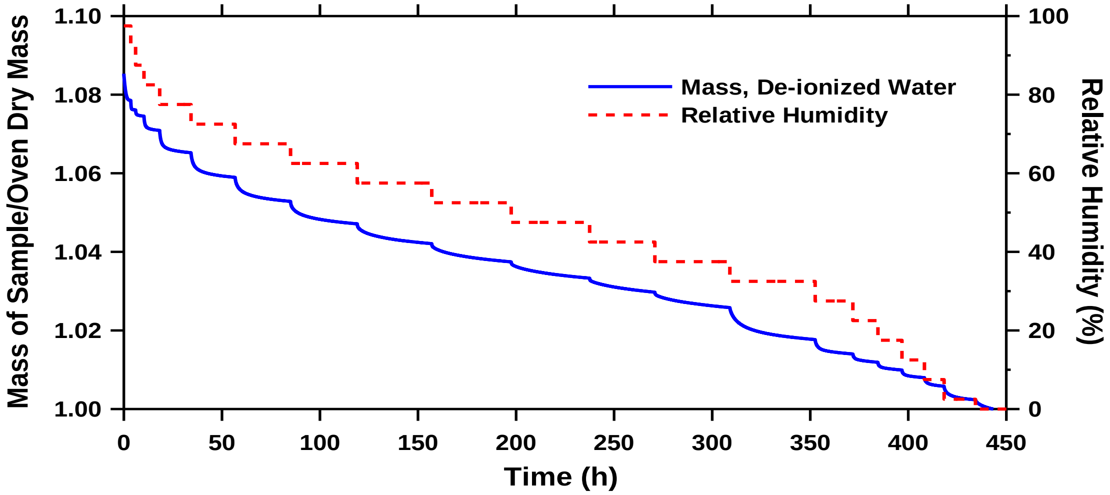

Fig. 6. Mass change at decreasing RH for samples containing de-ionized water

Figure 7 shows a plot of mass change for the mortar samples submerged in aqueous solutions of 23 % NaCl, 32 % $CaCl_2$, and 30 % $MgCl_2$. It can be observed that initially upon placement in the testing chamber at 97.5 % relative humidity the mass of the sample increases for the first 96 h until the relative humidity of the chamber is changed. The samples absorb water during this time of preconditioning, with values much higher than the 8.5 % increase in mass of the sample with de-ionized water as compared with the oven dry sample.

The sample loses weight as the relative humidity is decreased however it should be noted that the sample mass does not decrease to below the initial mass obtained from soaking the sample in the deicing solution until relative humidity was decreased below 85 %, 55 % and 55 % for NaCl, $CaCl_2$ and $MgCl_2$ respectively. This will be compared with the equilibrium relative humidity of the salt solution later in the paper.

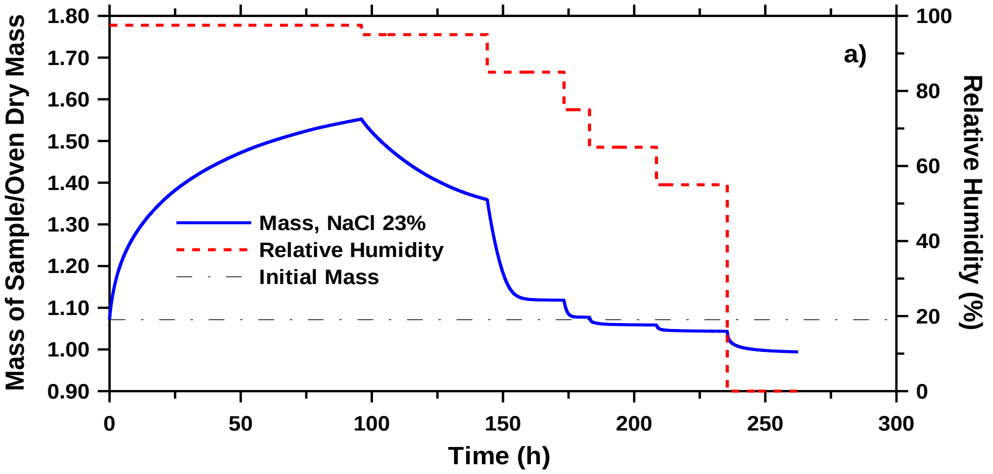
a)
Mass of Sample/Oven Dry Mass
1.80
1.70
1.60
1.50
1.40
1.30
1.20
1.10
1.00
0.90
Relative Humidity (%)
100
80
60
40
20
0
0
50
100
150
200
250
300
Time (h)
Mass, NaCl 23%
Relative Humidity
Initial Mass

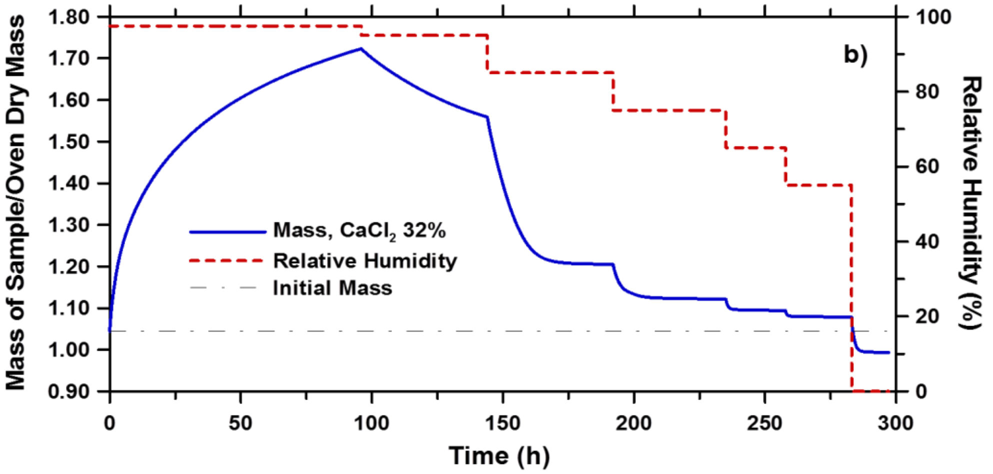
b)
Mass of Sample/Oven Dry Mass
1.80
1.70
1.60
1.50
1.40
1.30
1.20
1.10
1.00
0.90
Relative Humidity (%)
100
80
60
40
20
0
0
50
100
150
200
250
300
Time (h)
Mass, $CaCl_2$ 32%
Relative Humidity
Initial Mass

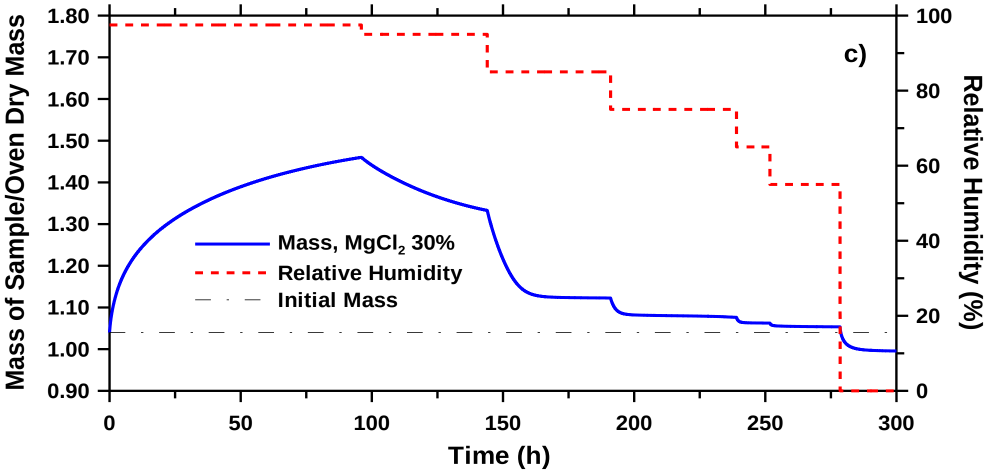
c)
Mass of Sample/Oven Dry Mass
1.80
1.70
1.60
1.50
1.40
1.30
1.20
1.10
1.00
0.90
Relative Humidity (%)
100
80
60
40
20
0
0
50
100
150
200
250
300
Time (h)
Mass, $MgCl_2$ 30%
Relative Humidity
Initial Mass

Fig. 7. Mass change for samples submerged in aqueous solutions containing deicing salts: (a) NaCl 23% (b) $CaCl_2$ 32 % and (c) $MgCl_2$ 30%.

5. Discussion of Results

5.1 Aqueous Solution Absorption Behavior as a Function of Surface Tension and Viscosity

Equation 3 showed that the rate of absorption was related to the square root of surface tension and viscosity. Figure 8 plots the square root of the ratio of surface tension and viscosity versus mass concentration of salt. Pure salt solutions are shown as lines while industrial deicing solutions are presented as solid points, and the open points represent the measured sorption response of concrete (i.e., salt sorptivity/water sorptivity) from Figure 3. Figure 8 confirms that as the solution concentration increases, the rate of fluid absorption (i.e., sorptivity) decreases. Further, while the properties of pure solutions may not exactly represent the response of industrially available deicing solutions they do provide a comparable trend. Reasonable agreement is seen between the measured sorption and square root of the ratio of surface tension and viscosity the measured properties. Additional work is currently being performed to extend these results to a wide range of temperatures.

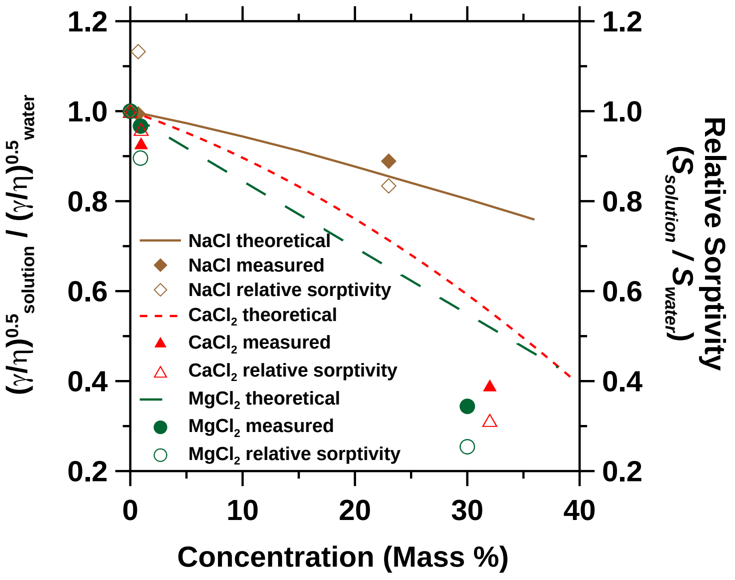

Fig 8. Relative sorptivity for deicing solutions.

5.2 Drying Time Versus Wetting Time

Comparing Figures 3 and 4 indicates that wetting happens much faster than drying. When de-ionized water was used as the absorbed fluid, the amount of fluid that was evaporated from the sample after eight days was 0.8 mm^3/mm^2. In contrast, it took just two hours for samples to absorb the same amount of fluid. These differences are even larger when salt solutions were used as the absorbed fluid. When $MgCl_2$ solution was used as the absorbed fluid, the amount of fluid that was evaporated from the sample after eight days was 0.07 mm^3/mm^2, but it took just ten minutes for the samples to absorb the same amount of fluid.

This is important as it suggests that field concrete may be more susceptible to increasing its level of saturation over time rather than drying out. Further, it shows that laboratory tests that use equal times for drying and wetting increase the saturation level of the concrete over time. Researchers [34] observed an increase in sample mass during wetting and drying cycling with deicers which was attributed to microcracking; however an increase in mass would be consistent with the wetting and behavior observed in this paper.

5.3 Reduced Drying with Salt Solutions – The Role of Solution Equilibrium Humidity

The relative humidity of different salt solutions presented in Figure 1 (b) help to understand the results from the drying tests. The equilibrium relative humidity for the 23% NaCl, 32% $CaCl_2$ and 30% $MgCl_2$ solutions are 80 %, 40 % and 50 % respectively. When the samples are placed in an environment with a relative humidity that is greater than or equivalent to the approximate equilibrium relative humidity over the aqueous solution in the pores water will not be lost to then environment. (Figure 4) and the sample can actually gain mass (Figure 4 and 7), most likely due to the water absorption on the surface of the sample. This can be seen by the thinner (dashed lines in Figure 7), which show the initial mass of the sample after it has been submerged in a aqueous solution for over 5 days. At relative humidity higher than the equilibrium of the aqueous salt solution the samples will increase in mass. At relative humidities where the environment is less than the equilibrium humidity over the salt solution, the samples will be expected to decrease in mass. The drying behavior of systems containing concentrated aqueous solutions of deicing salts is complex and requires additional research.

5.4 Effect of Solution on Rewetting

When samples of concrete that were previously exposed to deicing solutions were rewet with water they had an absorption and rate of absorption that depended on the history of the specimens (Figure 5). The absorption of water can be 30 % to 50 % less in specimens that were exposed to deicing solutions at some point in their lives. This is an important, yet subtle, factor to understand. This is important since absorption tests of field concrete may be mistakenly interpreted by relating the reduction in sorption to pore filling or delayed sorption. Both of these observations (lower sorptivity and delayed sorption) are consistent with data here for samples that did not have reduced porosity or differences in sample damage.

6. Summary and Conclusions

This paper has reported experimental results of fluid absorption measurements and drying of concrete in the presence of deicing solutions. The following observations can be made. First, the absorption of fluid in concrete depends on the drying environment used to condition the samples. Samples stored at a lower RH absorbed a greater volume of fluid. Second, it was observed that the deicing solutions reduce the rate of fluid absorption. This reduction can be related to the square root of the ratio of surface tension and viscosity [10]. Third, the time scale between drying and wetting is different and concrete is more likely to become preferentially increasingly wet over time. Fourth, the drying of concrete containing aqueous solutions with deicers differs from that of water. The equilibrium relative humidity of the aqueous solution plays an important role on limiting drying. Finally, the presence of deicing salts in field samples impacts the absorption when field samples are tested in the lab using water. This suggests that care must be taken in analyzing field concrete exposed to deicing salt solutions.

7. Acknowledgments

The experiments reported in this paper were conducted in the Pankow Materials Laboratories at Purdue University. This work was supported in part by the Joint Transportation Research Program administered by the Indiana Department of Transportation and Purdue University (SPR 3093 and 3200). The contents of this paper reflect the views of the authors, who are responsible for the facts and the accuracy of the data presented herein, and do not necessarily reflect the official views or policies of the Indiana Department of Transportation, nor do the contents constitute a standard, specification, or regulation.

8. References

1. Weiss J, Nantung T. INDOT Proposal on the Permeability of Concrete Pavement Performance Relative to Permeability, 2006.
2. Shi X, Fay L, Peterson MM, Yang Z. Freeze-Thaw damage and chemical change of a Portland cement concrete in the presence of diluted deicers. Mater Struct, 2010; 43(7): 933-946.
3. Hong K, Hooton RD. Effect of cyclic chloride exposure on penetration of concrete cover. Cement Concrete Res 1999, 29(9): 1379-1386.
4. Pour-Ghaz M, Rajabipour F, Couch J, Weiss J. Numerical and experimental assessment of unsaturated fluid transport in saw-cut (notched) concrete elements. SP-266 American Concrete Institute: Modeling as a solution to concrete problems, 2009.
5. Coates K, Mohtar S, Tao B, Weiss J. Can soy methyl esters reduce fluid transport and improve the durability of concrete? Transport Res Rec, 2009; 2113:.22-30.
6. ASTM International, ASTM C1585. Standard test method for measurement of rate of absorption of water by hydraulic cement concretes; 2004.

7. British Standard Institution, BS 1881. Methods of testing concrete part 5: Methods of testing hardened concrete for other than strength; 1990.
8. ASTM International, ASTM D6489. Standard test method for determining the water absorption of hardened concreted treated with a water repellent coating; 2006.
9. Hall C, Marchand J, Gerard G, Sosoro M. Chapter 2: Transport of fluids in homogenous isotropic cementitous composites. In: Reinhardt HW, editor. Penetration and permeability of concrete, RILEM report 16, 1997; pp. 5-79.
10. Hall C, Hoff WD. Water-transport in brick, stone and concrete. London: Spon Press, 2002.
11. Weiss WJ. Prediction of early-age shrinkage cracking in concrete. Ph.D. thesis. Evanston, IL Northwestern University, 1999.
12. Bentz DP, Peltz MA, Snyder KA, Davis JM. VERDiCT: Viscosity enhancers reducing diffusion in concrete technology. Concrete International, 2009; 31(1): 31-36.
13. Sant G, Eberhardt A, Bentz DP, Weiss J. Influence of shrinkage-reducing admixtures on moisture absorption in cementitious materials at early ages. J Mater Civil Eng, 2010; 22(3): 277-286.
14. MacInnis C, Nathawad YR. The effects of a deicing agent on the absorption and permeability of various concretes. In: Litvan GG, Sereda PJ, editors. Proceedings of the first international conference on durabaility of building materials and components, ASTM Special Technical Publication STP-691, 1980. pp 485-496.
15. Sutter L, Peterson K, Julio-Betancourt G, Hooton D, Van Dam T, Smith K. The deleterious chemical effects of concentrated deicing solutions on Portland cement concrete. South Dakota Department of Transportation, Final Report, 2008.
16. Janusz A. Investigation of Deicing Chemicals and Their Interactions with Concrete Materials. Master Thesis. West Lafayette, IN Purdue University, 2010.
17. Martys, NS. (1995). Survey of concrete transport properties and their measurments. NISTIR 5592, U.S. Departament of Commerce
18. Martys N, Ferraris CF. Capillary transport in mortar and concrete. Cement Concrete Res 1997; 27(5): 747-760
19. Kelham M. A Water absorption test for concrete. Mag Concrete Res, 1988; 40(143): 106-110.

20. Scherer G, Wheeler GS. Silicate consolidants for stone. Key Engineering Materials, 2009; 391: 1-25.
21. Conde M. Aqueous solutions of lithium and calcium chlorides: Property formulations for use in air conditioning equipment design. International Journal of Material Sciences, 2004; 43(4): 367-382.
22. Phang S, Stokes RH. Density, Viscosity, Conductance and transference numbers of concentrated aqueous magnesium chloride at 25C. J Solution Chem, 1980; 9(7): 497-505.
23. Afzai M, Saleem M, Mahmood MT. Temperature and concentration dependence of viscosity of aqueous electrolytes from 20 to 50C. Chlorides of Na+, K+, MG2+, Ca2+, Ba2+, SR2+ Co2+, Ni2+, Cu2+, and Cr3+. Journal of Chemical Engineering Data, 1989; 34(3): 339-346.
24. ASTM International, ASTM D971. Standard test method for interfacial of oil against water by the ring method; 2004.
25. Greenspan L. Humidity fixed points of binary saturated aqueous solutions. Journal of Research of the National Bureau of Standards – A, Physics and Chemistry, 1977; 81A(1): 89-96.
26. ASTM International, ASTM C231. Standard test method for air content of freshly mixed concrete by the pressure method; 2009.
27. Castro J, Kompare P, Poursaee A, Nantung T, Weiss J. JTRP Report SPR-3093, Portland cement concrete pavement performance relative to permeability. Indiana Department of Transportation, 2010.
28. Peterson KW, Swartz RA, Sutter LL, Van Dam TJ. Hardened concrete air void analysis with a flatbed scanner. Transport Res Rec 2001; 1775: 36-43.
29. Hwang C, Young J. Drying shrinkage of portland cement pastes. microcracking during drying. Cement Concrete Res 1984; 14(4): 585-594.
30. Chatterji S. (1976). Drying shrinkage of cement paste and concrete: a reappraisal of the measurement technique and its significance. Cement Concrete Res 1976; 6(1): 145-148.
31. Bisschop J, Van Mier J. How to study drying shrinkage microcracking in cement-based materials using optical and scanning electron microscopy? Cement Concrete Res 2002; 32(2): 279-287.
32. Samaha H, Hover K. Influence of microcracking on the mass transport properties of concrete. ACI Mater J 1992; 89(4): 416-424.

33. Yang Z, Weiss J, Olek J. Water transport on concrete damaged by tensile loading and freeze-thaw cycling. J Mater Civil Eng 2006; 18(3): 424-434.

34. Wang K, Nelsen D, Nixon W. Damaging effects of deicing chemicals on concrete materials. Cement and Concrete Composite, 2006; 28(2): 173-188.

Advances in Civil Engineering Materials, Vol. 1, No. 1
Paper ID ACEM104596
www.astm.org

R. P. Spragg,[1] *J. Castro,*[2] *T. Nantung,*[3] *M. Paredes,*[4] *and J. Weiss*[5]

Variability Analysis of the Bulk Resistivity Measured Using Concrete Cylinders

---

REFERENCE: Spragg, R. P., Castro, J., Nantung, T., Paredes, M., and Weiss, J., "Variability Analysis of the Bulk Resistivity Measured Using Concrete Cylinders," *Advances in Civil Engineering Materials*, Vol. 1, Issue 1, 2012, pp. 1–17, doi:10.1520/ACEM104596. ISSN 2165-3984.

ABSTRACT: Many agencies are interested in using a rapid test method for measuring the electrical properties of concrete (i.e., the resistivity or conductivity) because the electrical properties can be related to fluid transport (e.g., ion diffusion). The advantage of electrical testing is that it is relatively easy to perform, and the test method is relatively fast (it takes less than a minute). Over the past century, many studies have investigated different approaches for measuring electrical properties. This paper describes the variability associated with measuring the bulk resistivity along the longitudinal axis of a cylinder after placing electrodes on either end. A multi-laboratory evaluation was performed at ten laboratories. Data from this evaluation provided variability data for 12 concrete mixtures at testing ages of 28, 56, and 91 days. Information on the variability is important in the development of precision and bias statements for standard test methods. In addition, this work discusses how the resistivity results obtained from this test can be correlated with surface resistivity measurements made using a Wenner probe. Linear agreement was noticed between the Wenner test and the measurement through the cylinder, but with a factor confirmed by previous research by Morris et al. ("Practical Evaluation of Resistivity of Concrete in Test Cylinders Using a Wenner Array Probe," *Cem. Concr. Res.*, Vol. 26, 1996, pp. 1779–1787). Additionally, the effect of electrode resistance is discussed, and for high resistivity concrete such as that used in much transportation infrastructure, this effect appears to be negligible; however, it can be accounted for easily.

KEYWORDS: concrete, resistivity, surface resistivity, bulk resistivity, RCPT, electrical properties, electrode resistance, variability, precision statements, standard development, inter-laboratory test, round-robin test

Introduction

Over the past century, tests have been proposed for measuring the electrical properties of concrete [1–7]. These methods have the advantage of being relatively fast, and the principle behind these tests is relatively straightforward. Concrete is a composite consisting of a vapor phase (vapor filled porosity or "air"), a solid phase (aggregate and cementitious solids), and a fluid phase (the pore solution), and the resistivity of each of these individual phases is very different. The resistivities of the solid and vapor phases are extremely low, approximated as 10^9 and 10^{15} Ohm-meter, respectively, whereas the resistivity of the liquid phase is several orders of magnitude lower, ranging from 1×10^{-2} to 5×10^{-2} Ohm-meter [8,9]. As such, it can be assumed that the majority of conduction occurs through the pore fluid. A number of composite models have been developed in which this

---

Manuscript received December 2, 2011; accepted for publication April 3, 2012; published online July 2012.

[1] Graduate Research Assistant, Purdue Univ., School of Civil Engineering, 550 Stadium Mall Dr., West Lafayette, IN 47907, e-mail: rspragg@purdue.edu

[2] Assistant Professor, Pontificia Universidad Catolica de Chile, School of Civil Engineering, Casilla 306, Correo 22, Santiago, Chile 6904411, e-mail: jecastro@ing.puc.cl

[3] Manager for Pavement Materials and Construction Research, Indiana Dept. of Transportation, Division of Research and Development, P.O. Box 2279, West Lafayette, IN 47906, e-mail: tnantung@indot.in.gov

[4] State Corrosion Engineer, Florida Dept. of Transportation State Materials Office, Corrosion Research and Durability Laboratory, 6007 NE 39th Ave., Gainesville, FL 32609, e-mail: mario.paredes@dot.state.fl.us

[5] Professor of Civil Engineering, Director of Pankow Materials Laboratory, Purdue Univ., School of Civil Engineering, 550 Stadium Mall Dr., West Lafayette, IN 47907, e-mail: wjweiss@purdue.edu

concept is used [10–13]. Two of the more popular equations that are used in the cement and concrete literature are Archie's expression and the modified parallel expression [11,14]. Several documents have reviewed these methods previously; the goal of this section is to describe how the overall resistivity is dependent on three factors (the resistivity of the fluid in the pores, the degree of saturation of the concrete, and the volume and connectivity of the pore network), as illustrated in Eq 1.

$$\rho = \rho_0 \cdot F \cdot \frac{1}{f(S)} \tag{1}$$

where:

$\rho =$ bulk resistivity,

$\rho_0 =$ resistivity of the fluid phase,

$F =$ formation factor that is the product of the pore volume and a tortuosity coefficient, and

$f(s) =$ function that describes the degree of saturation, which is taken as 1 for a saturated system.

This implies that the resistivity decreases with a higher water content (i.e., pore volume) and a more open pore network (i.e., a lower tortuosity coefficient). This expression can also be written in terms of electrical conductivity, as it is simply the inverse of the electrical resistivity.

One of the more popular test methods that is currently performed based on electrical concepts is the rapid chloride permeability (RCP) test [15,16]. This test method involves placing a saturated concrete specimen, typically 102 mm in diameter and 51 mm thick, between electrodes in different solutions and integrating the charge that is passed over a 6 h testing period [15]. Although this test has come into wide use, a few drawbacks have been highlighted out [17–19]. First, this test is performed using high voltages and a direct current, which limits each sample to providing a single measurement at a single age. Second, saturating the specimen can require a relatively long preparation time. Third, there is potential for heating effects due to the large voltage and possible modification of the microstructure [20,21]. Research has been conducted regarding temperature correction for the RCP test [22,23], and many changes to this test have been proposed, including extrapolating the charge passed after a test duration of 30 min to the 6 h value [24], increasing the size of the reservoirs to reduce the heating effects [25], reducing the large voltages in the test [26], and using a single resistance reading measured at an early age, often 1 min or 5 min [18,19].

Alternative testing methods have been proposed that require little to no sample preparation and which allow the sample to be tested at different ages. One rapid test for the electrical resistivity of concrete is the Wenner probe. As with any test, there are certain considerations that can impact the results. For example, the probe spacing, the geometry of the sample, the aggregate size, and surface moisture conditions can all influence the measured electrical response [27]. Because the moisture conditions at the surface of the test specimen are quite important, care should be taken to protect against drying or using surface treated concretes [28–30]. Additionally, some work has suggested the need for an additional non-linear geometry factor for this method that occurs from the constricted geometry, such as that of a standard test cylinder [27]. Further, when this method is used on real structures, the location and proximity of the rebar need to be considered [31,32].

Several of these concerns can be addressed if a standard testing protocol is adopted. A draft test method has been developed that uses a four-probe Wenner configuration on a 102 mm × 204 mm standard test cylinder with a probe tip spacing of 38 mm. Temperature monitoring can be difficult and is frequently not done [33]. This surface resistivity (SR) test method places the probes directly on the surface of the test specimen. This test method has recently been accepted for use by the Louisiana Department of Transportation and the Florida Department of Transportation on select projects, and preliminary work has been done to expand its use for quality control [28,34]. Work has also been done to correlate RCP testing and diffusion testing with SR [28,35,36]. This method has a distinct advantage in that it can be performed rapidly and is easy to perform on the surface of a cylinder.

The resistance of a concrete cylinder can alternatively be evaluated by using plate electrodes that can be placed on the end of the sample [32,37]. The resistance value obtained can be normalized by means of specimen geometry—simply, the ratio of the sample cross-sectional area to the length—in order to obtain the sample resistivity, termed the bulk resistivity (BR). For this test, good electrical contact must be ensured between the plate electrodes and the test specimen [27,37]. This can be assisted through the use of a conductive medium, but the surface finish of the cylinder ends should be flat. Some work has previously been performed with regard to evaluating the contact pressure between the plate and the specimen [37]. Like other electrical tests, this method is subject to the influence of the specimen's moisture content and temperature. This test, however, has the distinct advantages of rapid testing and a simple geometry factor. To the best of the authors' knowledge, a multi-laboratory evaluation of variability has not been performed on this geometry, though some studies have reported exchanges of samples between two laboratories [37].

Three major factors that should be considered in any electrical resistivity testing are (1) the influence of geometry, (2) the influence of temperature, and (3) the influence of moisture. First, whereas the normalized BR of concrete can be considered a material property, the tests that are performed provide a measure of electrical resistance. The resistance measurements need to be corrected for the geometry of the test. Geometry factors can be determined experimentally [8,38] or numerically [27] and are largely dependent on the current flow through the material. A uniform current flow through the bulk of the geometry provides an easy geometry factor, the ratio of the cross-sectional area to the length. Other tests do not have this uniform current path, so the geometry factor is different. Temperature is another important factor in the testing of concrete resistivity. As the primary conduction path is through the ionic pore solution, an increase in the temperature increases the mobility of the ions, decreasing the resistivity. There has been work that has investigated the possibility of a temperature correction for resistivity tests [6,39–43]. In this work, the samples are all tested in laboratory conditions; as such, the sample temperature should be $23^\circ\text{C} \pm 2^\circ\text{C}$. Lastly, the degree of saturation is a major component in resistvity testing of concrete. As a result, knowledge of the moisture history and moisture content at testing are important considerations in the evaluation of resistivity data [44].

The main objectives of this evaluation are fourfold. First, it provides some background on electrical property measurements for concrete and provides some of the physical principles behind these tests. Second, it presents the results of an inter-laboratory evaluation of the variation in the electrical BR of concrete. This information can be used in the development of precision and bias statements. Third, it demonstrates the relationship between surface resistance test methods (e.g., Wenner) and measurements performed on a bulk cylindrical geometry. Fourth, it highlights important considerations in the development of testing standards and policies for the use of electrical methods as quality control/quality assurance tests.

Experimental Details

Materials

A round-robin testing program was proposed in 2009 for the evaluation of the repeatability of Wenner and bulk resistance tests on concrete cylinders. A series of 12 concrete mixtures were prepared at the laboratories that participated in this evaluation (Table 1). The mixtures are structural/bridge deck concretes used by state departments of transportation from around the United States. A final report detailing a parallel series of Wenner and BR tests conducted by the American Association of State Highway and Transportation Officials Technology Implementation Group is available [45]. It should be noted that a wide range of cements, supplementary materials, and aggregates were used in this investigation.

Sample Conditioning

The samples were demolded at an age of 48 h and placed into a saturated lime-water bath that was kept at a constant room temperature until the age of testing (23°C ± 2°C). At an age of 14 days, the respective laboratories removed the samples and wrapped them in paper towels soaked in saturated lime-water. The samples were then double-bagged and prepared for two-day shipping to the other participating laboratories. The goal was to ensure that the samples remained wet during testing.

After the samples were received by the other testing laboratories, they were removed from the bag and placed into saturated lime-water baths kept at room temperature (23°C ± 2°C). At ages of 28, 56, and 91 days, the samples were removed from the saturated lime bath, the surface was wiped dry, and the samples were tested for SR and BR. After this testing, the samples were placed back in the saturated lime-water.

Testing Procedure

It should be noted that the test described herein (with the plates placed on the end of the cylinder) was a part of a larger evaluation of variation conducted by the AASTHO TIG [45,46]. Not all of the laboratories chose to participate in this portion of the evaluation, and the nonparticipating

TABLE 1—*Summary of mixture proportions used in this evaluation (for Saturated Surface Dry conditions).*

Mixture Number	w/cm	Water, kg/m^3	Cement, kg/m^3	Fly Ash, kg/m^3	Micron Fly Ash, kg/m^3	Slag, kg/m^3	Silica Fume, kg/m^3	Meta-kaolin, kg/m^3	Coarse Aggregate 1, kg/m^3	Coarse Aggregate 2, kg/m^3	Fine Aggregate, kg/m^3
1	0.34	163	237	119	…	119	…	…	1059	…	717
2	0.40	144	285	71	…	…	…	…	282	854	824
3	0.39	199	392	119	…	…	…	…	785	…	724
4	0.35	158	279	178	…	…	…	…	940	…	793
5	0.40	164	308	103	…	…	…	…	909	…	879
6	0.37	145	390	…	…	…	…	…	1068	…	712
7	0.40	160	297	80	…	…	24	…	532	528	686
8	0.39	131	251	84	…	…	…	…	555	…	1295
9	0.41	151	291	65	…	…	15	…	1032	…	697
10	0.30	151	297	153	44	…	…	…	1009	…	638
11	0.30	157	430	95	…	…	…	…	1033	…	577
12	0.35	156	402	…	…	…	…	44	1009	…	624

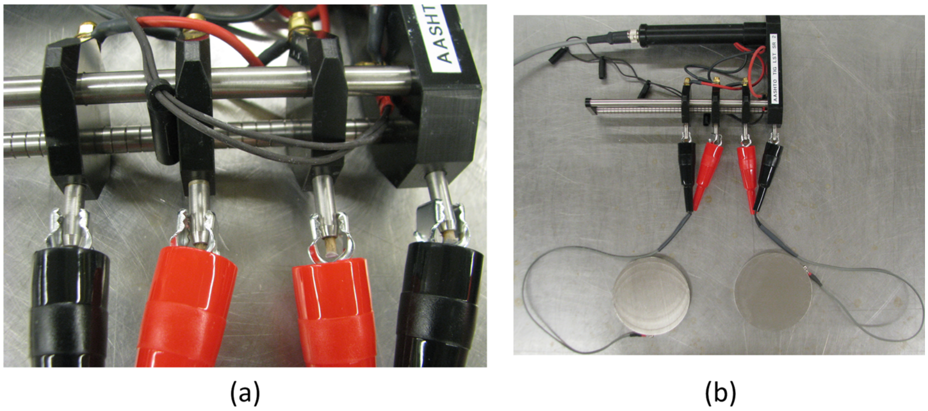

FIG. 1—*Attachment of the alligator clips to the Wenner probe tips: (a) close-up; (b) at a distance. The steel plates have a diameter of 102 mm, and the probe tip spacing is 38 mm.*

laboratories have been excluded from the following data; however, in order to avoid confusion, the original laboratory numbers were retained.

Equipment

The equipment involved in this test consisted of a CNS Farnell Mk II U95 SR meter using an alternating current at a frequency of 13 Hz, a set of 102 mm diameter stainless steel plate electrodes, and 16 AWG two-conductor wire used to connect the probe tips of the SR meter to the plate electrodes.

The cable was outfitted with alligator clips on one end to allow easy access to the probe tips of the resistivity meter. The other end of the cable was outfitted with a ring terminal to connect to the plate electrode. The plate electrode was drilled and tapped to allow easy and consistent attachment.

It is important to ensure proper electrical contact between the cylinder and the plate electrodes [27,37]. For this evaluation, this was done using thin lime-water-saturated sponges.

Testing Procedure

The plate electrodes should be connected to the pins of the SR meter. The first two pins that generate the current and measure the potential were connected to one of the steel plate electrodes, and likewise for the second set of pins, as shown in Fig. 1.

The resistances of the top and bottom sponges were then measured, as shown in Fig. 2. The resistance of each individual sponge is largely dependent on its moisture content. The moisture content of the sponge is dependent on the weight placed on top of it (e.g., large weights push more water from the sponge). In order to ensure that the moisture contents remain the same, the weight it carries during the test was used. For the top sponge, only the top plate was used as a weight. For the bottom cylinder, the top plate and the cylinder were used to provide the weight, but the cylinder was placed above the top plate, so its resistance was not measured. The goal of this was to provide a correction for sponge resistance, as discussed below. The concrete cylinder was then placed between the plate electrodes, with sponges being placed between the plates and the concrete cylinder, as shown in Fig. 3.

Calculations

The resistances of the top and bottom sponge are termed $R_{\text{top sponge}}$ and $R_{\text{bottom sponge}}$, respectively. The measured resistance of the system (two sponges and a specimen), as depicted in Fig. 3, is

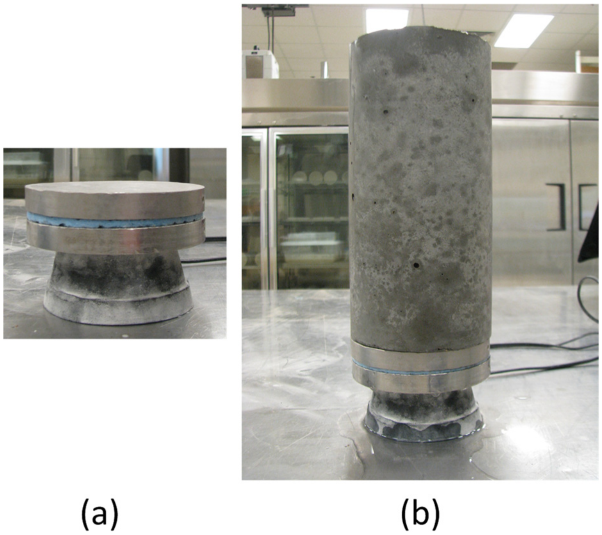

FIG. 2—*Measuring the sponge resistance for (a) the top and (b) the bottom sponges. The steel plates have a diameter of 102 mm, and the test cylinder is a standard 102 mm × 204 mm.*

termed R_{measured}. The measured resistance was corrected for the resistance of the sponges by treating the system as resistors in series, as shown in Fig. 2 [37]. It was noticed for the sponges used in this evaluation that the resistance values in each lab tended to remain relatively constant. Thus, for sponges that show this constant resistance, it is proposed that they be measured only periodically, and their resistances can be assumed to remain unchanged between measurements.

$$R_{\text{cylinder}} = R_{\text{measured}} - R_{\text{top sponge}} - R_{\text{bottom sponge}} \tag{2}$$

The BR, denoted as ρ, can be determined using Equation 3. The geometry factor K for the current flow through the bulk material is given by Equation 4. This can be extended to other sample geometries through experimental testing [8].

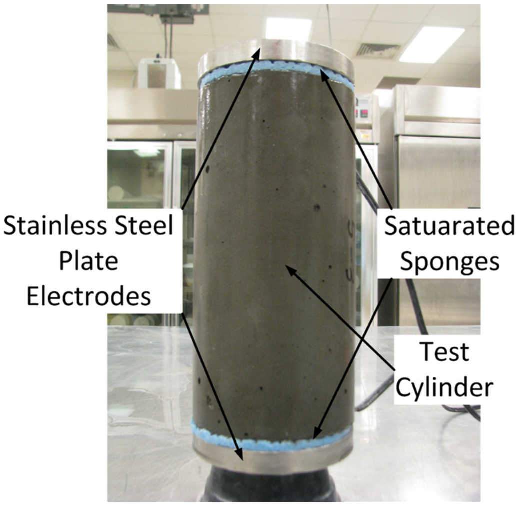

FIG. 3—*Measuring the resistance of the system. The test cylinder is a standard 102 mm × 204 mm.*

$$\rho = \mathrm{K}R_{\text{cylinder}} \tag{3}$$

$$\mathrm{K} = \frac{A}{L} \tag{4}$$

where:

R_{cylinder} = calculated resistance of the concrete test cylinder from Eq 1,
A = cross-sectional area, and
L = length of the test specimen.

Results and Discussion

Bulk Resistivity Data

The samples were tested at three ages: 28, 56, and 91 days. The average BR (Avg.) and variance (Var.) of three test cylinders measured at each testing age for each mixture by each testing laboratory are presented in Tables 2–4. Cells marked with "n/a" signify that no data were reported. The last row in each table represents the pooled statistics, calculated according to ASTM C802 [47].

Data measured at an age of 28 days are presented in Table 2. Mixtures 1 through 5 were not tested for 28 day BR, as the equipment was being distributed. Data measured at an age of 56 days are presented in Table 3. Mixture 1 was not tested for 56 day BR because the equipment had still not been received. Data measured at an age of 91 days are presented in Table 4.

TABLE 2—*Average BR and variance obtained at a testing age of 28 days, kohm-cm.*

		Mixture											
Laboratory		1	2	3	4	5	6	7	8	9	10	11	12
1	Avg.	n/a	n/a	n/a	n/a	n/a	5.29	13.41	14.97	8.84	12.67	6.46	14.89
	Var.	n/a	n/a	n/a	n/a	n/a	0.03	0.15	1.28	0.16	0.06	0.03	0.82
2	Avg.	n/a	n/a	n/a	n/a	n/a	5.27	14.12	16.98	8.36	13.49	6.73	18.84
	Var.	n/a	n/a	n/a	n/a	n/a	0.01	0.21	0.18	0.02	0.30	0.64	0.61
3	Avg.	n/a	n/a	n/a	n/a	n/a	5.19	13.54	14.03	7.69	11.53	5.43	16.04
	Var.	n/a	n/a	n/a	n/a	n/a	0.03	0.12	0.24	0.14	0.17	0.05	1.71
5	Avg.	n/a	n/a	n/a	n/a	n/a	5.65	15.19	16.73	8.31	16.93	7.36	n/a
	Var.	n/a	n/a	n/a	n/a	n/a	0.05	0.10	0.47	0.13	0.16	0.10	n/a
6	Avg.	n/a	n/a	n/a	n/a	n/a	5.55	15.24	15.69	9.60	13.72	6.68	20.24
	Var.	n/a	n/a	n/a	n/a	n/a	0.10	0.17	0.09	0.08	0.43	0.05	0.01
7	Avg.	n/a	n/a	n/a	n/a	n/a	5.03	13.59	15.01	8.91	12.87	6.88	16.90
	Var.	n/a	n/a	n/a	n/a	n/a	0.04	0.12	0.16	0.01	0.14	0.07	0.07
8	Avg.	n/a	n/a	n/a	n/a	n/a	5.84	14.36	16.58	8.63	14.59	6.81	18.21
	Var.	n/a	n/a	n/a	n/a	n/a	0.03	0.36	0.14	0.10	0.45	0.13	0.15
9	Avg.	n/a	n/a	n/a	n/a	n/a	5.31	14.39	16.37	8.91	13.15	7.00	16.48
	Var.	n/a	n/a	n/a	n/a	n/a	0.00	0.01	0.11	0.05	0.40	0.04	0.84
10	Avg.	n/a	n/a	n/a	n/a	n/a	5.12	14.20	15.60	8.62	14.22	6.77	18.55
	Var.	n/a	n/a	n/a	n/a	n/a	0.00	0.05	0.02	0.39	0.13	0.01	0.12
12	Avg.	n/a	n/a	n/a	n/a	n/a	5.68	14.02	15.11	8.30	12.30	6.40	16.76
	Var.	n/a	n/a	n/a	n/a	n/a	0.01	0.20	0.04	0.21	0.26	0.13	0.11
All labs	Mean	n/a	n/a	n/a	n/a	n/a	5.39	14.21	15.71	8.62	13.55	6.65	17.43
	Pooled variance	n/a	n/a	n/a	n/a	n/a	0.03	0.15	0.27	0.13	0.25	0.13	0.49
	Variance	n/a	n/a	n/a	n/a	n/a	0.07	0.40	0.90	0.26	2.22	0.26	2.72

TABLE 3—*Average BR and variance obtained at a testing age of 56 days, kohm-cm.*

		Mixture											
Laboratory		1	2	3	4	5	6	7	8	9	10	11	12
1	Avg.	n/a	6.73	8.76	12.63	8.07	6.56	24.34	29.99	14.78	22.20	11.98	18.14
	Var.	n/a	0.07	0.08	0.18	0.01	0.03	0.04	0.05	0.15	0.34	0.09	0.03
2	Avg.	n/a	8.64	9.10	12.05	10.83	7.22	24.52	27.25	13.14	22.53	12.69	20.12
	Var.	n/a	0.38	0.05	0.10	0.65	0.09	1.28	0.11	0.05	0.79	0.64	0.42
3	Avg.	n/a	6.18	7.81	12.26	7.71	5.81	23.13	21.61	12.17	17.26	n/a	17.71
	Var.	n/a	0.23	0.05	0.01	0.00	0.00	0.73	0.39	0.11	0.19	n/a	1.48
5	Avg.	n/a	7.98	9.26	11.41	7.26	7.08	24.10	29.12	14.92	22.48	10.91	n/a
	Var.	n/a	0.00	0.48	0.03	0.12	0.02	0.39	0.24	1.12	0.14	0.01	n/a
6	Avg.	n/a	7.70	9.16	12.89	9.99	6.70	n/a	25.02	n/a	19.62	10.09	21.49
	Var.	n/a	0.06	0.46	0.02	0.01	0.21	n/a	0.87	n/a	0.78	0.08	0.12
7	Avg.	n/a	8.38	8.55	12.34	8.33	6.57	24.20	27.18	16.50	21.37	12.16	19.88
	Var.	n/a	0.64	0.09	0.08	0.05	0.04	0.27	1.46	0.06	0.02	1.03	0.62
8	Avg.	n/a	7.18	9.27	13.64	9.31	6.72	25.89	31.29	14.38	24.98	12.55	20.85
	Var.	n/a	0.18	0.12	0.06	0.08	0.03	1.73	0.68	0.25	0.36	0.10	0.46
9	Avg.	n/a	n/a	9.20	13.50	8.59	6.52	26.09	30.28	15.13	23.23	13.43	20.27
	Var.	n/a	n/a	0.11	0.72	0.01	0.05	0.07	0.81	0.10	0.93	0.22	0.25
10	Avg.	n/a	7.98	8.92	14.85	7.94	6.26	26.58	26.03	14.20	22.24	11.22	21.46
	Var.	n/a	0.00	0.23	0.61	0.13	0.01	0.34	0.08	0.81	0.17	0.03	0.25
12	Avg.	n/a	6.10	8.34	11.94	7.90	6.52	22.21	23.65	13.06	18.67	9.95	15.99
	Var.	n/a	0.03	0.01	0.03	0.16	0.03	1.76	0.68	0.53	0.73	0.05	0.86
All labs	Mean	n/a	7.43	8.84	12.75	8.59	6.59	24.56	27.14	14.25	21.46	11.66	19.55
	Pooled variance	n/a	0.18	0.17	0.18	0.12	0.05	0.73	0.54	0.35	0.44	0.25	0.50
	Variance	n/a	0.86	0.23	1.02	1.25	0.15	2.02	9.74	1.70	5.29	1.44	3.52

The data presented in Tables 2 through 4 were analyzed according to ASTM C802 in order to determine the corresponding components of variance for the variability from within-laboratory and multi-laboratory data. The within-laboratory variability is typically attributed to variability stemming from the operator, as well as variability inherent in the test equipment and in the samples being tested. It should be noted that when using the approach taken for this round-robin testing, variations between samples arising from sample preparation issues could contribute to this component of variability. This is discussed later in this paper.

The data were also analyzed to evaluate the relationship between the variability of each of the mixtures and the properties of that mixture. Specifically, the w/c and the mass fraction of cementitious materials were evaluated. No significant correlation was seen between the variability and these mixture characteristics.

Within-laboratory Variability

The operator variability, the variability of specimens, and the inherent variability in the mixture are all grouped together into the within-laboratory variability. This value is computed using the average within-laboratory coefficient of variation (COV), presented in Table 5 [47]. Previous work evaluating the development of an automated resistivity testing system has reported a similar within-laboratory COV of around 3 % to 4 % for samples older than 24 h [48]. It should be noted that the variation increases over time. It is believed that this might be due to slight variations in

TABLE 4—*Average BR and variance obtained at a testing age of 91 days, kohm-cm.*

		Mixture											
Laboratory		1	2	3	4	5	6	7	8	9	10	11	12
1	Avg.	10.24	8.07	12.14	18.71	11.36	7.58	38.05	42.08	19.44	34.98	17.90	18.80
	Var.	0.19	0.05	0.23	0.39	0.02	0.06	0.01	7.14	0.37	1.22	0.20	0.79
2	Avg.	12.16	10.43	15.12	18.83	16.81	8.31	32.40	39.19	17.58	29.78	16.17	24.58
	Var.	0.48	0.12	0.94	0.77	0.62	0.04	2.72	0.25	0.04	1.25	0.89	1.08
3	Avg.	10.43	7.85	10.61	16.58	9.46	6.65	28.87	31.78	14.63	22.71	13.10	17.18
	Var.	0.16	0.43	0.68	0.07	0.19	0.26	2.12	2.63	0.32	0.21	0.79	0.36
5	Avg.	11.01	8.36	12.12	16.21	10.20	8.48	33.45	37.14	20.19	28.66	15.45	n/a
	Var.	0.20	0.02	0.47	0.05	0.16	0.02	0.50	1.07	2.72	0.27	0.29	n/a
6	Avg.	13.91	10.11	14.34	23.58	n/a	7.65	30.97	30.81	15.60	29.92	15.80	20.96
	Var.	0.00	0.03	1.04	0.09	n/a	0.40	0.98	0.05	0.35	0.89	0.06	0.01
7	Avg.	10.67	10.05	14.11	19.27	12.58	7.94	35.83	40.06	20.81	29.55	17.18	21.03
	Var.	0.15	0.44	0.83	0.04	0.08	0.03	0.70	2.41	0.05	0.10	0.03	0.48
8	Avg.	12.22	8.92	13.25	20.47	13.29	7.67	38.06	45.59	19.19	35.36	18.49	20.29
	Var.	0.02	0.23	0.18	0.23	0.11	0.05	4.03	1.94	0.43	1.04	0.18	0.51
9	Avg.	11.16	10.09	14.35	19.54	12.06	8.60	37.74	43.37	n/a	34.48	22.41	19.55
	Var.	0.00	0.59	0.05	2.77	0.10	0.42	0.02	9.91	n/a	3.77	4.91	0.79
10	Avg.	12.39	9.75	13.71	22.44	12.65	6.74	37.54	38.41	18.26	30.51	16.50	21.15
	Var.	0.07	0.80	0.34	2.00	1.42	0.00	0.24	0.08	1.21	0.46	0.14	0.23
12	Avg.	10.07	7.82	11.12	15.96	10.40	7.26	31.21	33.11	14.93	22.67	12.69	18.01
	Var.	0.23	0.02	0.00	0.04	0.15	0.04	3.08	1.92	0.52	0.78	0.01	0.02
All labs	Mean	11.43	9.15	13.09	19.16	12.09	7.69	34.41	38.15	17.85	29.86	16.57	20.17
	Pooled variance	0.15	0.27	0.47	0.65	0.32	0.13	1.44	2.74	0.67	1.00	0.75	0.47
	Variance	1.48	1.10	2.29	6.45	4.77	0.45	11.91	24.83	5.35	20.28	7.67	4.70

curing conditions that might have occurred at each lab, which could have amplified differences over time.

Multi-laboratory Variability

The multi-laboratory variability can be described by the average COV computed from the multi-laboratory component of variance [47]. The average values of the multi-laboratory COV are shown in Table 6. It should be noted that the variation increases over time. Again, slight variations in curing conditions that might have occurred at each lab could have amplified differences over time.

Precision Statements

Precision estimates were calculated [49]. For this experiment, the fundamental statistic was determined to be the COV, represented as 1s% in ASTM C670. Therefore, the calculated precision

TABLE 5—*Average within-laboratory coefficient of variation.*

Testing Age, days	Within-laboratory Coefficient of Variation, %
28	3.34
56	3.87
91	4.36

TABLE 6—*Average multi-laboratory coefficient of variation.*

Testing Age, days	Multi-laboratory Coefficient of Variation, %
28	7.75
56	9.83
91	13.22

indices correspond to d2s% as described in ASTM C670, determined by multiplying the average COV by the factor $2\sqrt{2}$ [49]. This index represents the maximum difference between two individual test results, expressed as a percentage of their average. The precision indices for different testing ages are shown in Table 7. The maximum precision index for within-laboratory and multi-laboratory variability is used to form the precision statements, which correspond to a testing age of 91 days.

The maximum pooled single-operator COV was found to be 4.36 %. Therefore, the results of two tests properly conducted by the same operator on the same concrete material at the same age are not expected to differ by more than 12.34 % of their average. The maximum pooled multi-laboratory COV was found to be 13.22 %. Therefore, the results of two tests properly conducted by different laboratories on the same concrete material at the same age are not expected to differ by more than 37.38 % of their average.

The precision statements for BR presented in this paper can be compared with the precision statements for other electrical test methods, namely, the RCP test and a corresponding SR test The variability of the RCP test was obtained from the corresponding ASTM standard [15], and SR data were obtained from a report detailing the resistivity round robin [45]. For consistency, the SR data from Ref 45 were analyzed according to the same procedure described in this paper. Two tests done by the same operator on material from the same concrete mixture should not differ from their average by more than 42 % for the RCP test, 13.28 % for the SR test (with each test consisting of eight average measurements), and 12.34 % for the BR test (with each test consisting of one measurement). For tests conducted in separate laboratories, results should not differ from their average by more than 51 % for the RCP test, 34.55 % for the SR test, and 37.38 % for the BR test. It should be noted that because the SR test is sensitive to the specific location in which measurements is taken, an average of eight measurements is taken for each sample, which contributes to smaller variability in the pooled statistics. However, this means that more time is needed in order to perform the test. Conversely, the bulk measurement described herein is a single measurement.

Correlation with Other Electrical Test Methods

SR measurements were conducted as a part of this evaluation [45]. Figure 4 compares the measured SR and the calculated BR.

TABLE 7—*Precision indices for bulk resistivity.*

Testing Age, days	Within-laboratory	Multi-laboratory
28	9.44	21.93
56	10.94	27.82
91	12.34	37.38

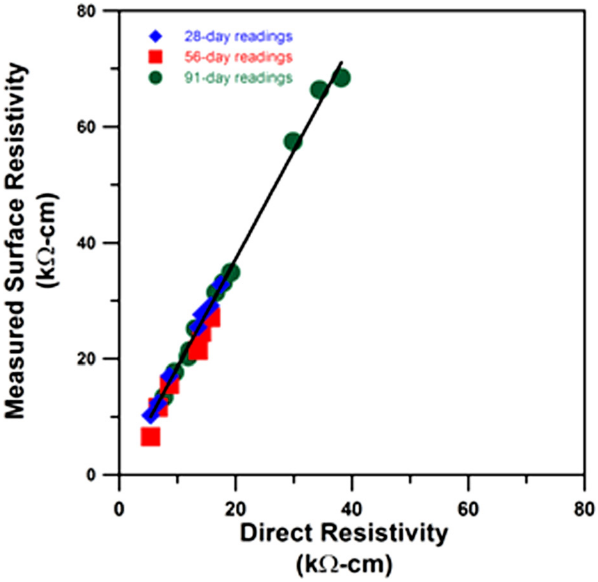

FIG. 4—*Correlation of measured SR and BR of samples of differing ages; each data point represents the average of three samples.*

A linear correlation was noticed, with $R^2 = 0.9986$, and with SR measurements tending to be 1.86 times higher than the BR. The large data in the experimental results support previous work using finite element methods that showed that additional geometry factors must be used in order to account for aspects of the test geometry, such as probe spacing, cylinder length, and cylinder diameter [27]. The factor of 1.86 is in good agreement with the geometric correction proposed by Morris et al. [27] for a cylinder with a length of 205 mm, a diameter of 102 mm, a probe spacing of 38.1 mm, and a maximum aggregate size of 19 mm, which was approximately 1.9.

As the RCP test is a widely used test for mixture characterization, Table 8 has been prepared to relate concrete resistivity to values obtained from RCP and SR testing. Previous empirical studies have also shown that RCP values can be related to concrete resistivity, termed the Berke empirical, and to the apparent SR, termed the Paredes empirical [28,36]. The total charge passed during the RCP test is used with Ohm's law, an assumed testing period of 6 h, and a voltage of 60 V to

TABLE 8—*Relationships between values obtained via different electrical test methods.*

ASTM C1202 Classification[a]	Charge Passed, Coulombs[a]	Direct Resistivity, kohm-cm[b]	Berke Empirical, kohm-cm	Paredes Empirical, kohm-cm[c]	Apparent Surface Resistivity (102 mm × 205 mm), kohm-cm[d]
High	>4000	<5.2	<4.9	<6.5	<9.7
Moderate	2000–4000	5.2–10.4	4.9–8.76	6.5–11.3	9.7–19.3
Low	1000–2000	10.4–20.8	8.8–15.6	11.3–19.9	19.3–38.6
Very low	100–1000	20.8–207	15.6–105.9	19.9–136.6	38.6–386
Negligible	<100	>207	>105.9	>136.6	>386

[a] From ASTM C1202 [15].
[b] Calculated using Ohm's law and geometry.
[c] Corrected for geometry from Kessler et al. [28].
[d] Bulk resistivity multiplied by geometry factor.

determine the resistance. The standard test specimen (i.e., a 102 mm × 51 mm disc) can be normalized by the geometry using the factor described in Eq 4 to determine the BR [15]. This is a direct computation that does not consider the temperature effects or possible damage previously discussed. The values for the BR or apparent SR can then be ranked as classified by the RCP test method [15].

Effects of Electrode Resistance

Previous work has shown that electrode resistance (and other factors involved in ensuring connectivity between the electrode and sample) can influence the results as shown in Equation 2.

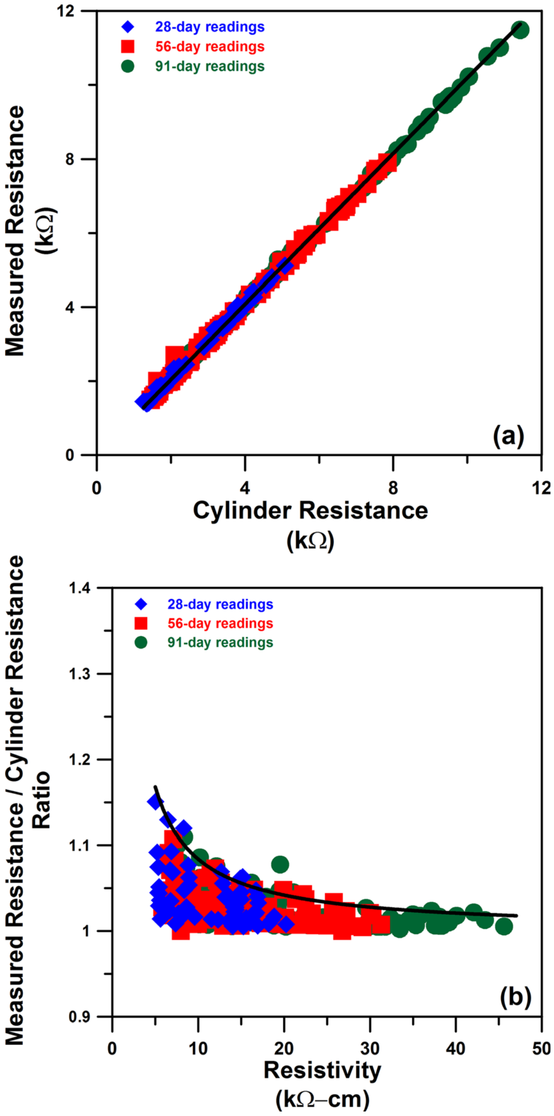

FIG. 5—*Influence of electrode resistance on (a) the measured resistance (sample and electrodes) as a function of the cylinder (sample) resistance and (b) the ratio of measured resistance (sample and electrodes) to cylinder (sample) resistance as a function of concrete resistivity.*

The major contributor to electrode resistance is poor contact between the plate electrode and the surface of the test cylinder. Some work has suggested the possibility of using flexible electrodes [27]. An alternative solution is to use an aid that allows for good electrical contact. In the laboratory, this can be accomplished through the use of an electrically conductive gel [50,51]. The alternative is to use another soft, conductive medium. Popular solutions have included the use of saturated sponges, chamois cloth, and paper towels [21,37].

An important issue becomes the associated resistance of the sponges. Previously, this associated resistance has been treated as a series of resistors in parallel with the test cylinder, which produces the correction shown and described by Equation 2.

The sponge resistance is largely dependent on the moisture content of the sponges and the conductivity of the solution in which they are saturated. For this evaluation, the solution was saturated lime-water, which was also used as the storage solution for the test cylinders. Furthermore, in order to ensure the proper moisture content, the contact pressure for the sponge was kept constant between the sponge resistivity test and the cylinder test, as shown in Figs. 2 and 3.

Although this correction provides the truest value of the BR, the results of this evaluation show that this correction might not always be very large. For the sponges used in this evaluation, the resistances of the two sponges were much less than the resistance of the cylinder. Figure 5(*a*) shows the measured resistance (i.e., sample, sponges, and electrodes) as a function of the cylinder resistance (i.e., the sample alone), as defined in Equation 2. The best fit line, given by Eq 5*a* with an R^2 of 0.9997, shows an average difference of less than 2 % between the measured resistance and the cylinder resistance.

Additionally, the ratio of the measured resistance to the actual cylinder resistance, as defined in the preceding paragraph, can be shown against the concrete resistivity, depicted in Fig. 5(*b*). This ratio represents the correction from the cylinder resistance. Figure 5(*b*) shows an upper bound of this ratio, given by Eq 5*b*. We can see that for lower concrete resistivities, the ratio can be significant. However, for better concrete (i.e., higher resistivity concrete), this ratio approaches 1.

$$\text{Measured Resistance} = 1.019 \times \text{Cylinder Resistance} \tag{5a}$$

$$\frac{\text{Measured Resistance}}{\text{Cylinder Resistance}} = 1.0 + 0.84 \times \frac{1}{\text{Concrete Resistivity}} \tag{5b}$$

Summary and Conclusions

This paper reports results from a multi-laboratory investigation of the variability associated with testing the electrical BR of concrete cylinders by placing plate electrodes on the ends of the cylinder. An analysis of the data is presented. It should be noted that the samples used in this evaluation were conditioned by storing the samples in lime-saturated water between test measurements. The following observations can be made regarding the variability of the resistivity test method: First, resistivity testing is a rapid test that drastically reduces the amount of time a technician needs to spend conditioning the sample and conducting the test. Therefore, this test is well suited for quality control testing. Second, resistivity testing can be considered a non-destructive test. This means that for each mixture being evaluated using resistivity, only a small number of samples need be prepared, and these samples can be measured at several different ages. This can be contrasted with other destructive electrical tests that require a larger series of samples for proper mixture evaluation. In fact, this testing can be performed on cylindrical samples before they are tested for compressive or splitting tensile strength. Third, the operator and multi-laboratory precision of this test method have been quantified using data from the average COV obtained from an interlaboratory evaluation consisting of ten laboratories and twelve different mixtures. For the BR test method, the within-laboratory COV is 4.36 %, and the multi-laboratory COV is 13.22 %. Fourth, the specimen geometry can greatly influence the results of an electrical test, and the use of a geometry correction factor is often required. For the BR test, this geometry factor is simply the ratio of the sample cross-sectional area to the sample length. Finally, the effects of electrode resistance were addressed using a series model. Whereas previous work described corrections for end plate resistance, the variability data from this investigation show that for the materials used in this evaluation, the correction that is needed is quite small. It is suggested that a standard resistivity test be developed that could allow samples to be tested using a variety of sample geometries, including (1) the Wenner probe geometry, (2) the bulk resistance described herein, and (3) alternative geometries, provided the geometry factor can be quantified. This could enable the use of all the different methods to obtain the material property known as BR.

Acknowledgments

The experiments reported in this paper were conducted as part of a larger evaluation sponsored by the Pooled Fund Program and the American Association of American Highway and Transportation Official's Technology Implementation Group and organized by the Florida Department of Transportation. The contents of this report reflect the views of the authors, who are responsible for the facts and the accuracy of the data presented herein. The contents do not necessarily reflect the official views or policies of the Indiana Department of Transportation or the Federal Highway Administration at the time of publication. This report does not constitute a standard, specification, or regulation. The writers would like to thank the participating laboratories and testing personnel for their time and efforts in collecting data. This includes, but is not limited to: Rob Reis, Cipriano Manansala, and Joe Shanabrook, California Department of Transportation; Jagan Gudimettla, FHWA Mobile Concrete Laboratory; Celik Ozyildirim and Bill Ordel, Virginia Department of Transportation; Wilfredo Malpica and Javier Molinari, Grupo-Carmelo; Ed McGaffin and Dan Dennis, New York State Department of Transportation; Lieska Halsey, Jeremy Weigel, and Tim Krason, Nebraska Department of Transportation; Eric Prieve and Azis Khan, Colorado Department of Transportation; John Kern and Wayne DeMarco, CEMEX; Thomas Frank and Ronald Simmons, Florida Department of Transportation; and Jeremiah Hersey and Professor Mike Jackson, University of North Florida. The writers also appreciate useful discussions with Ken Snyder and Dale Bentz of the National Institute of Standards and Technology and Kyle Bemis and Professor Bruce Craig of the Statistics Consulting Service at Purdue University

References

[1] Hammond, E. and Robson, T. D., "Comparison of Electrical Properties of Various Cements and Concretes. I-II," *The Engineer*, Vol. 199, 1955, pp. 78–80.

[2] Shimizu, Y., "An Electrical Method for Measuring the Setting Time of Portland Cement," *Concrete*, Vol. 32, 1928, pp. 111–113.

[3] Calleja, J., "Effect of Current Frequency on Measurement of Electrical Resistance of Cement Pastes," *J. Am. Concr. Inst.*, Vol. 24, 1952, pp. 329–332.

[4] Weiss, W. J., Shane, J. D., Mieses, A., Mason, T. O., and Shah, S. P., "Aspects of Monitoring Moisture Changes Using Electrical Impedance Spectroscopy," *Second Symposium on the Importance of Self Desiccation in Concrete Technology*, June 18, 1999 Lund, Sweden: Lund Institute of Technology, Division of Building Materials.

[5] Monfore, G. E., *The Electrical Resistivity of Concrete*, Portland Cement Association, Research and Development Laboratories, Skokie, IL, 1968.

[6] Whittington, H. W., McCarter, J., and Forde, M. C., "The Conduction of Electricity through Concrete," *Mag. Concrete Res.*, Vol. 33, 1981, pp. 48–60.

[7] Christensen, B. J., Coverdale, R. T., Olson, R. A., Ford, S. J., Garboczi, E. J., Jennings, H. M., and Mason, T. O., "Impedance Spectroscopy of Hydrating Cement-based Materials: Measurement, Interpretation, and Application," *J. Am. Ceram. Soc.*, Vol. 77, 1994, pp. 2789–2804.

[8] Rajabipour, F., 2006, "In Situ Electrical Sensing and Material Health Monitoring in Concrete Structures," Ph.D. dissertation, Purdue University, West Lafayette, IN.

[9] Rajabipour, F. and Weiss, J., "Linking Health Monitoring in Concrete Structures with Durability Performance Simulations," *ASCE Structures Congress*, B. Cross and J. Finke, Eds., ASCE, St. Loius, MO, 2006.

[10] Torquato, S., *Random Heterogeneous Materials: Microstructure and Macroscopic Properties*, Springer, New York, 2002.

[11] Archie, G. E., "The Electrical Resistivity Log as an Aid in Determining Some Reservoir Characteristics," *Society of Petroleum Engineers* Reprint Series, 2003, pp. 9–16.

[12] Aplin, K. L., "Aspirated Capacitor Measurements of Air Conductivity and Ion Mobility Spectra," *Rev. Sci. Instrum.*, Vol. 76, 2005, 104501.

[13] McLachlan, D. S., Blaszkiewicz, M., and Newnham, R. E., "Electrical Resistivity of Composites," *J. Am. Ceram. Soc.*, Vol. 73, 1990, pp. 2187–2203.

[14] Garboczi, E. J., "Permeability, Diffusivity, and Microstructural Parameters: A Critical Review," *Cem. Concr. Res.*, Vol. 20, 1990, pp. 591–601.

[15] ASTM C1202, 2010, "Standard Test Method for Electrical Indication of Concrete's Ability to Resist Chloride Ion Penetration," ASTM International, West Conshohocken, PA.

[16] AASHTO T277, 2007, "Standard Method of Test for Electrical Indication of Concrete's Ability to Resist Chloride Ion Penetration," American Association of State Highway and Transportation Officials, Washington, D.C.

[17] Shane, J. D., Aldea, C. D., Bouxsein, N. F., Mason, T. O., Jennings, H. M., and Shah, S. P., "Microstrucutral and Pore Solution Changes Induced by the Rapid Chloride Permeability Test Measured by Impedance Spectroscopy," *Concr. Sci. Eng.*, Vol. 1, 1999, pp. 110–119.

[18] Riding, K. A., Poole, J. L., Schindler, A. K., Juenger, M. C. G., and Folliard, K. J., "Simplified Concrete Resistivity and Rapid Chloride Permeability Test Method," *ACI Mater. J.*, Vol. 105, 2008, pp. 390–394.

[19] Snyder, K. A., Ferraris, C., Martys, N. S., and Garboczi, E. J., "Using Impedance Spectroscopy to Assess the Viability of the Rapid Chloride Test for Determining Concrete Conductivity," *J. Res. Natl. Inst. Stand. Technol.*, Vol. 105, 2000, pp. 497–509.

[20] Sohn, D. and Mason, T. O., "Electrically Induced Microstructural Changes in Portland Cement Pastes," *Adv. Cem. Based Mater.*, Vol. 7, 1998, pp. 81–88.

[21] Shane, J. D., 2000, "Electrical Conductivity and Transport Properties of Cement-based Materials Measured by Impedance Spectroscopy," Ph.D. dissertation, Northwestern University, Evanston, IL.

[22] Julio-Betancourt, G. A. and Hooton, R. D., "Study of the Joule Effect on Rapid Chloride Permeability Values and Evaluation of Related Electrical Properties of Concretes," *Cem. Concr. Res.*, Vol. 34, 2004, pp. 1007–1015.

[23] Bentz, D. P., "A Virtual Rapid Chloride Permeability Test," *Cem. Concr. Compos.*, Vol. 29, 2007, pp. 723–731.

[24] McGrath, P. F. and Hooton, R. D., "Re-evaluation of the AASHTO T259 90-day Salt Ponding Test," *Cem. Concr. Res.*, Vol. 29, 1999, pp. 1239–1248.

[25] Yang, C. C., Cho, S. W., and Huang, R., "The Relationship between Charge Passed and the Chloride-ion Concentration in Concrete Using Steady-state Chloride Migration Test," *Cem. Concr. Res.*, Vol. 32, 2002, pp. 217–222.

[26] Nokken, M. R. and Hooton, R. D., "Electrical Conductivity Testing," *Concr. Int.*, Vol. 28, 2006 pp. 58–63.

[27] Morris, W., Moreno, E. I., and Sagues, A. A., "Practical Evaluation of Resistivity of Concrete in Test Cylinders Using a Wenner Array Probe," *Cem. Concr. Res.*, Vol. 26, 1996, pp. 1779–1787.

[28] Kessler, R. J., Powers, R. G., and Paredes, M. A., "Resistivity Measurements of Water Saturated Concrete as an Indicator of Permeability," *Corrosion*, NACE International, Houston, TX, 2005.

[29] Millard, S. G., "Reinforced Concrete Resistivity Measurement Techniques," *Proc. Inst. Civ. Eng., Part 2. Res. Theory*, Vol. 91, 1991, pp. 71–88.

[30] Rajabipour, F., Weiss, J., Shane, J. D., Mason, T. O., and Shah, S. P., "Procedure to Interpret Electrical Conductivity Measurements in Cover Concrete during Rewetting," *J. Mater. Civ. Eng.*, Vol. 17, 2005, pp. 586–594.

[31] Presuel-Moreno, F., Liu, Y., and Paredes, M., "Concrete Resistivity on the Apparent Surface Resistivity Measured via the Four-point Wenner Method," *Corrosion*, NACE International, Atlanta, GA, 2009.

[32] Polder, R. B., "Test Methods for On Site Measurement of Resistivity of Concrete—A RILEM TC-154 Technical Recommendation," *Constr. Build. Mater.*, Vol. 15, 2001, pp. 125–131.

[33] FM 5-578, 2004, "Florida Method of Test for Concrete Resistivity as an Electrical Indicator of Its Permeability," Florida Department of Transportation, Tallahassee, FL.

[34] Rupnow, T. D. and Icenogle, P., *Evaluation of Surface Resistivity Measurements as an Alternative to the Rapid Chloride Permeability Test for Quality Assurance and Acceptance*, Louisiana Department of Transportation, Baton Rouge, LA, 2011, p. 68.

[35] Vivas, E., Hamilton, H. R. I., and Boyd, A. J., *Permeability of Concrete—Comparison of Conductivity and Diffusion Methods*, Department of Civil and Coastal Engineering, University of Florida, Gainsville, FL, 2007, p. 238.

[37] Berke, N. S. and Hicks, M. C., "Estimating the Life Cycle of Reinforced Concrete Decks and Marine Piles Using Laboratory Diffusion and Corrosion Data," *Corrosion Forms and Control for Infrastructure*, ASTM STP 1137, V. Chaker, Ed., ASTM International, West Conshohocken, PA, 1992, pp. 207–231.

[37] Newlands, M. D., Jones, M. R., Kandasami, S., and Harrison, T. A., "Sensitivity of Electrode Contact Solutions and Contact Pressure in Assessing Electrical Resistivity of Concrete," *Mater. Struct.*, Vol. 41, 2008, pp. 621–632.

[38] Castro, J., Spragg, R., Kompare, P., and Weiss, W. J., "Portland Cement Concrete Pavement Permeability Performance," Joint Transportation Research Program, Indiana Department of Transportation and Purdue University, West Lafayette, IN, 2010.

[39] Nokken, M., Boddy, A., Wu, X., and Hooton, R. D., "Effects of Temperature, Chemical, and Mineral Admixtures on the Electrical Conductivity of Concrete," *J. ASTM Int.*, Vol. 5:5, 2008.

[40] Castellote, M., Andrade, C., and Alonso, C., "Temperature Correction, from 3 to 25C of the Electrical Resistivity of Mortars and Concretes," *Industria Italiana del Cemento*, Vol. 71, 2001, pp. 850–851, 916–923.

[41] Sant, G., Rajabipour, F., and Weiss, J., "The Influence of Temperature on Electrical Conductivity Measurements and Maturity Predictions in Cementitious Materials during Hydration," *Indian Concr. J.*, Vol. 82, 2008, pp. 7–16.

[42] Villagran Zaccardi, Y. A., Fullea Garcia, J., Huelamo, P., and Di Maio, A. A., "Influence of Temperature and Humidity on Portland Cement Mortar Resistivity Monitored with Inner Sensors," *Mater. Corros.*, Vol. 60, 2009, pp. 294–299.

[43] McCarter, W. J., Forde, M. C., and Whittington, H. W., "Resistivity Characteristics of Concrete," *Proc. Inst. Civ. Eng. (UK)*, Vol. 71, 1981, pp. 107–117.

[44] Castro, J., Spragg, R., and Weiss, J., "Water Absorption and Electrical Conductivity for Internally Cured Mortars with a w/c between 0.30 and 0.45," *J. Mater. Civ. Engr.*, Vol 24:2, 2012, pp. 223–231.

[45] Jackson, N. M., *Results of Round-robin Testing for the Development of Precision Statements for the Surface Resistivity of Water Saturated Concrete*, Report Number: FL/DOT/SMO/11-549, Jackson Research Engineers, Ponte Vedra Beach, FL, 2011.

[46] AASHTO TP95, 2011, "Draft Standard Method of Test for Surface Resistivity Indication of Concrete's Ability to Resist Chloride Ion Penetration," American Association of State Highway and Transportation Officials, Washington, D.C.

[47] ASTM C802, 2009, "Standard Practice for Conducting an Interlaboratory Test Program to Determine the Precision of Test Methods for Construction Materials," ASTM International, West Conshohocken, PA.

[48] Poursaee, A. and Weiss, W. J., "An Automated Electrical Monitoring System (AEMS) to Assess Property Development in Concrete," *Autom. Constr.*, Vol. 19, 2010, pp. 485–490.

[49] ASTM C670, 2010, "Standard Practice for Preparing Precision and Bias Statements for Test Methods for Construction Materials," ASTM International, West Conshohocken, PA.

[50] Henkensiefken, R., Castro, J., Bentz, D. P., Nantung, T., and Weiss, J., "Water Absorption in Internally Cured Mortar Made with Water-filled Lightweight Aggregate," *Cem. Concr. Res.*, Vol. 39, 2009, pp. 883–892.

[51] Thomas, M. D. A., "The Use of Conductive Gel," personal communication, W. J. Weiss, 2008.

Journal of Materials in Civil Engineering. Submitted April 25, 2012; accepted July 13, 2012;
posted ahead of print August 29, 2012. doi:10.1061/(ASCE)MT.1943-5533.0000549

Using a Saturation Function to Interpret the Electrical Properties of Partially Saturated Concrete

Jason Weiss,[1] Ken Snyder,[2] Jeff Bullard,[2] and Dale Bentz[2]

1 Purdue University, West Lafayette, IN

2 National Institute of Standards and Technology, Gaithersburg, MD

Abstract

Electrical properties are frequently measured in the concrete construction industry as a part of mixture qualification and quality control testing. While there are several factors that influence the electrical response of concrete, one of the most important factors is its degree of saturation. Although current standard tests rely on the concrete being saturated, this can be difficult to accomplish, is time consuming, and can artificially increase the degree of hydration of the test sample in comparison to that of concrete in field structures (when the test samples are stored in water). While some studies have measured the electrical response of concrete for samples with different moisture content (i.e., stored at different relative humidities), a single expression has not been proposed that predicts how drying changes the electrical response. This paper suggests that a saturation function should be considered as a possible method to account for, and to correct for, less than complete saturation in concrete. This function would provide one term that accounts for changes in pore fluid volume, pore solution concentration, and pore fluid connectivity. While preliminary, this approach has several potential benefits: 1) it could enable testing of partially saturated concrete, thus saving time; 2) it could be used to predict properties under different exposure conditions; 3) it may facilitate more comprehensive service life models; and 4) it may enable a wider use of embedded sensor technology.

Background

Journal of Materials in Civil Engineering. Submitted April 25, 2012; accepted July 13, 2012;
posted ahead of print August 29, 2012. doi:10.1061/(ASCE)MT.1943-5533.0000549

Several test methods exist in the construction industry that use measures of the electrical properties of concrete as an indicator of potential durability performance. The so-called rapid chloride permeability (RCP) test (e.g., AASHTO T277/ASTM C1202) is one example of an electrical test for concrete. For nearly three decades, the concrete profession has qualified concrete mixtures using the RCP testing procedure. While rapid in comparison to long-term ponding tests, the RCP test procedure applies an electrical potential to the test sample for 6 h and requires that the sample be vacuum saturated prior to testing. Several researchers have suggested that the testing time could be dramatically shortened without compromising the quality of the data. Snyder et al. (2000) illustrated that there was no need for the 6 h measurement because values after 1 min or 5 min provide an equally valid indication of the electrical resistivity of the concrete. Other researchers have confirmed that the test can be performed with shorter test times (Shane et al. 1999, Riding et al. 2008). In fact, shortening the test would improve the quality of the results, as it reduces the potential for Joule heating, which artificially increases the measured response of charge passed over time (Julio-Betancourt and Hooton 2004). Since the time of the preparation of this paper, ASTM committee C09 has accepted a new test method to implement this more rapid measurement protocol (ASTM C1760). But, even if the measurement time is reduced, the sample preparation time is still inconveniently long. RCP testing (or ASTM C1760) requires saturation of the sample, a task which is time consuming, labor intensive, and difficult to accomplish in many cases. The cost of testing (in terms of time and money) could be significantly reduced if reliable measurements could be made on partially saturated specimens. Such a measurement also has value in that it can provide information on the transport properties under partially saturated conditions.

Similarly, time might be saved by using test geometries and methods other than the rapid chloride permeability test. Surface measurements of electrical properties are popular (FM-5-578 2004), and AASHTO has recently developed a provisional standard (TP95-11) based on the Wenner four probe

Journal of Materials in Civil Engineering. Submitted April 25, 2012; accepted July 13, 2012;
posted ahead of print August 29, 2012. doi:10.1061/(ASCE)MT.1943-5533.0000549

surface resistance test (Morris et al. 1996, Berke and Hicks 1992, Kessler et al. 2005, UNE 2008a, Jackson 2011, Rupnow and Icenogle 2011). Although this test procedure can be performed in less than 2 min, it frequently requires the storage of samples in lime-saturated water. While storage in water is intended to ensure that the samples are saturated, low-permeability concretes may not maintain saturation even after long immersion times, due to self-desiccation (internal drying). Likewise, samples stored in air, even humid air, are not fully saturated. Furthermore, storage in water may provide additional curing and/or leaching that are not representative of what may be happening in actual field structures.

Other test procedures have also been proposed for rapid electrical testing. Specifically, a test procedure has been proposed that measures a bulk resistivity through cylinders (Whittington et al. 1981, Newlands et al. 2008, UNE 2008b, Spragg et al. 2011). Tests could be conducted on samples of other geometries or even between embedded electrodes (Monfore 1968, McCarter et al. 1981, Hansson and Hansson 1983, Christensen et al. 1994, Tumidajski et al. 1996 , Gu et al. 1992, Raupach and Scheissl 1997, Scheissl et al. 1999, Sellevold et al. 1997, Shane et al. 1999, Weiss et al. 1999, Rajabipour et al. 2007, Poursaee et al. 2009, Castro et al. 2010). Each of these methods uses a different electrode configuration and sample size, thereby requiring a separate geometric correction factor; however, the fundamental principles of the tests are similar. Details on many of the geometric correction factors are available in the literature (e.g., Rajabipour 2006).

It is interesting to note that, when the appropriate geometric corrections are made and the samples are uniform (i.e., relatively homogenous) and properly conditioned, an intrinsic material property (conductivity or resistivity) is obtained that is independent of sample geometry. Therefore, all of these methods have great promise for moving the field towards qualification and quality control test methods that are simple and related to durability performance, but it should be noted that their results can be dramatically influenced by the degree of saturation of the concrete (Monfore 1968, Scheissl et al.

Journal of Materials in Civil Engineering. Submitted April 25, 2012; accepted July 13, 2012;
posted ahead of print August 29, 2012. doi:10.1061/(ASCE)MT.1943-5533.0000549

1999, Andrade et al. 2011). This paper will focus on understanding how the moisture content (i.e., degree of saturation) influences the overall measured electrical response. Specifically, this paper suggests that a universal expression could be used to interpret measurements for partially saturated concrete.

Electrical Conductivity Expression for Saturated Concrete

The electrical conductivity (inverse of resistivity) of concrete depends on five factors: the conductivity of the solution in the pores, the volume of saturated pores (porosity), their connectivity within the microstructure (tortuosity), temperature, and the degree of saturation. Although there are several expressions that could be used to estimate the electrical response of a composite like concrete (Torquato 2002), the two most commonly used are a modified parallel law (i.e., a model of straight non intersecting tubes which is modified to account for tortuosity and connectivity with the term β, Garboczi 1990) and Archie's equation (originally developed in 1942 and reprinted in 2003). Of the two, Archie's equation for the electrical conductivity of a rock soaked (saturated) in brine provides a useful starting point:

$$\frac{\sigma_r}{\sigma_b} = a\phi^m \qquad [1]$$

where a is a parameter that depends upon the rock type, σ_r is the rock conductivity, σ_b is the brine conductivity, and ϕ is the pore volume fraction (porosity). The exponent m is a fitting parameter that is referred to as the cementation factor. It should be noted that the cementation factor refers to how the microstructure is formed, and is not related to the actual cementitious content of the material. Archies law can be related to the modified parallel law as shown by Garboczi (1990).

Electrical Conductivity Expression for Partially Saturated Concrete

Journal of Materials in Civil Engineering. Submitted April 25, 2012; accepted July 13, 2012;
posted ahead of print August 29, 2012. doi:10.1061/(ASCE)MT.1943-5533.0000549

Several researchers have developed expressions similar to equation 1 for partially saturated concrete. These modifications consist of reinterpreting the pore volume as only the volume of the pore fluid (Weiss 1999, Andrade et al. 2011). While that simple correction may be expedient, it leads to some confusion between pore volume and fluid-filled pore volume. Further, additional complications arise since several factors in Eq. 1, including the pore solution conductivity and solution connectivity, change as the degree of saturation changes. As such, previous work has accounted for each factor individually (Rajabipour et al. 2007); however this can be very time consuming and does not lend itself to easy use for quality control testing during construction.

An alternative approach is to start with the expression that characterizes the pore structure of the concrete called the formation factor (a uniquely defined parameter for a material with a given composition and degree of hydration) and to incorporate an empirical expression for the effects of partial saturation. For a fully saturated concrete, the ratio of the pore solution conductivity at saturation $\sigma_p{}^o$ to the concrete conductivity at saturation $\sigma_c{}^o$ is the formation factor *F* (Snyder, 2001):

$$\frac{\sigma_p^o}{\sigma_c^o} = F \qquad [2]$$

For a partially saturated concrete, the concrete conductivity σ_c decreases as the saturation level of the concrete decreases (assuming the pore solution composition remains constant). This is due, in part, to the reduction in the pore fluid volume but also due to changes in the connectivity of the connected pathways and changes in the pore solution in the system (Rajabipour et al. 2007). For a concrete, the relationship between the concrete conductivity and the saturation could be accounted for using an expression that will be referred to as the saturation factor, *f(S)*:

$$\frac{\sigma_c}{\sigma_p} = \frac{1}{F} f\ \ S \qquad [3]$$

Journal of Materials in Civil Engineering. Submitted April 25, 2012; accepted July 13, 2012;
posted ahead of print August 29, 2012. doi:10.1061/(ASCE)MT.1943-5533.0000549

The function *f*(*S*) has the property that *f*(*S*=1) =1 and *f*(*S*<1) < 1. Furthermore, if one assumes that the pore solution at saturation (σ_p^o) is known, the pore solution conductivity at values other than saturation (e.g., due to drying) can be, as a first approximation, related to the degree of saturation:

$$\sigma_p = \frac{\sigma_p^o}{S} \qquad [4]$$

This is an assumption that is not accurate for concentrated solutions, so an additional correction is discussed later in the paper. Combining equations 3 and 4 results in equation 5:

$$\sigma_c = \frac{\sigma_p^o}{S} \quad \frac{1}{F} \quad f \; S \qquad [5]$$

It should be remembered that this is not a rigorous algebraic derivation but the development of a trial form for the equation based on fundamental engineering assumptions.

While the left hand side of the equation is the conductivity of the concrete as a function of saturation, the right side of the equation has three terms. The first term accounts for the pore solution conductivity (due to the mixture design and subsequent concentration due to water loss), the second term accounts for the total pore space and the third term accounts for the connectivity of the fluid in the pore space. Each term is independent of the others, and all of the parameters are related to well defined properties of the matrix and the solution filling its pores. It should be noted that it is assumed that the sample/solution does not carbonate or precipitate salts in this simplified analysis.

The saturation function is used in other transport problems and could be formulated in a number of ways (Millington and Quirk 1961, Martys 1999, Samson and Marchand 2008, Schlumberger (2011)). Within the constraint is that at saturation (S=1), the function's value is unity (f(S=1)=1), there is flexibility in how the saturation function is approximated. One viable function that has been used to describe the influence of saturation is a power-law relationship:

Journal of Materials in Civil Engineering. Submitted April 25, 2012; accepted July 13, 2012;
posted ahead of print August 29, 2012. doi:10.1061/(ASCE)MT.1943-5533.0000549

$$f\ S\ = S^n \qquad [6]$$

where n is a fitting parameter called the saturation coefficient. As described later in this paper, n is typically of the order of 1.5 to 3 for porous rocks, while it may be slightly higher for cement and concrete (i.e., in the range of 3.5 to 5 for the paste and mortar samples or for the computer simulations discussed in this paper).

It should also be mentioned that the degree of saturation (*S*) is frequently determined using the difference in mass before and after drying at 100°C normalized by the equivalent difference in mass for a saturated system. This mass-based form of the degree of saturation is used since it is easy to determine experimentally in the laboratory. But, the mass-based determination is equal to the saturation in terms of fluid volume only if the filling liquid is water. For concentrated electrolytes such as concrete pore solutions, there may be merit in interpreting *S* as a volumetric degree of saturation (volume of the fluid as compared with the overall volume of fluid that can be held by the pore system of the sample at saturation). For this paper the mass based definition was used.

Figure 1 shows a plot of the saturation function S^n along with estimates based on experimental data from Rajabipour et al. (2007), calculated from Eq. 3 using known values for the pore solution conductivity at each step. In figure 1, the degree of saturation was determined on a mass basis. As may be expected, the cement system behaves slightly differently than the siltstone that has larger pores, few if any 'ink bottle pores', and a more open pore network. The saturation coefficient for the siltstone is approximately 2 (which is a value consistent with that reported in the geological literature (Schlumberger Oilfield Glossary 2011)). However, for the cement-based system with a ratio of water mass to cement mass (*w/c*) of 0.50, the value of the saturation coefficient is approximately 3.5, and the saturation coefficient approaches 5 for the system containing silica fume (*w/c* = 0.35 + 5 % silica fume). The saturation function shown as the dashed line in Figure 1, using equation 6, assumes *n* = 4. It should

Journal of Materials in Civil Engineering. Submitted April 25, 2012; accepted July 13, 2012;
posted ahead of print August 29, 2012. doi:10.1061/(ASCE)MT.1943-5533.0000549

be noted that the saturation function shown in Figure 1 is equivalent to the normalized conductivity ratio (the ratio of the conductivity of the concrete to the conductivity of the pore solution, normalized by the value of this ratio at saturation). As such, data like those in Figure 1 are currently quite rare in the concrete literature, as the changes in the pore solution with saturation must be included when developing such data.

Saturation Functions from Simulation (Considering pore fluid volume and connectivity)

The Virtual Cement and Concrete Testing Laboratory software (VCCTL), used to predict degree of hydration, microstructure development, and physical properties of cement paste, mortar, or concrete (Bullard et al., 2008), was adapted in this study to estimate the form of a saturation function. One advantage of the numerical simulations is that they automatically account for the pore solution conductivity, a property which may be difficult to measure experimentally in many partially saturated cementitious samples for three reasons. First, it becomes difficult to extract the pore solution using the pressurized approach like the one proposed by Barneyback and Diamond (1981) in partially saturated conditions, due to the very low volume of available pore fluid. Second, the loss of water by drying can also increase the ionic concentration of the solution, which concurrently increases the pore solution conductivity (Rajabipour et al. 2007). Finally, pore solutions can be susceptible to rapid carbonation, which will also significantly alter their conductivity (Rajabipour 2006).

Using the VCCTL, 3D virtual microstructures of cement paste were generated that were chemically and physically representative of the real systems considered in this paper. Hydration and microstructure development, under either saturated or sealed moisture conditions, were simulated out to ages of 1 d, 2 d, 3 d, 7 d, 28 d, 90 d, and 365 d. The 3D microstructures at each age were input into a finite difference model that calculated the net charge flux across the microstructure in response to a fixed applied electric field (Garboczi 1998). The relative conductivity of the microstructure was

Journal of Materials in Civil Engineering. Submitted April 25, 2012; accepted July 13, 2012;
posted ahead of print August 29, 2012. doi:10.1061/(ASCE)MT.1943-5533.0000549

computed by dividing the charge flux by the electric field (Ohm's law). In addition, the formation factor, F, was calculated by saturating the capillary pore volume (for the sealed curing condition specimens) and repeating the calculation of effective conductivity. Effective conductivities calculated in this way are reproducible to within ±5 % for different realizations of a representative volume element of the paste microstructure.

Figure 2 shows the simulated cement paste microstructures for a sealed mortar with a *w/c* of 0.42 and an aggregate volume fraction of 55 % at 3 d (Figure 2a) and at 365 d (Figure 2b). Over time, the capillary porosity of the system decreases due to hydration. In addition, since the system is sealed, the vapor-filled space increases due to chemical shrinkage and self-desiccation. To estimate the saturation function, the conductivity of the sealed mortar was compared with the sealed mortar that was 'resaturated' by altering the conductivity of the vapor-filled space to be equivalent to that of the pore solution.

It should be noted that two types of porosity are generally considered to exist in a hydrated cement paste system. The capillary pores are larger pores (shown in black in Figure 2) which remain from the original space occupied by mix water that has not filled in during hydration. The gel pores are smaller pores that are created within hydration products. In the VCCTL model, microstructure is represented as a 3D digital image where each voxel, a 1 μm cube, is assigned a particular cement phase. Therefore, capillary pores are computed directly from the voxels that represent pores in the simulation, but the gel pores are assumed to occupy 38 % of the volume of any C-S-H voxel. This compares favorably and is consistent with the calculations from a Powers' model type approach (Powers and Brownyard 1942). An advantage of the VCCTL model as compared with the Powers' calculations is that it provides a 3D spatial distribution of the porosity, including its tortuosity, which can be used in conductivity computations. A disadvantage is that the capillary pores have a lower size limit of 1 μm because of the

Journal of Materials in Civil Engineering. Submitted April 25, 2012; accepted July 13, 2012;
posted ahead of print August 29, 2012. doi:10.1061/(ASCE)MT.1943-5533.0000549

finite voxel size. This lower limit is relatively coarse compared with the smaller capillary pores in a typical hydrated portland cement, although comparisons of capillary porosity correlation functions determined on model and real microstructures for a *w/c*=0.47 cement paste are quite favorable (Bentz 2006).

Figure 3a shows results from the VCCTL simulation of a paste with a *w/c* of 0.50 and a degree of hydration of 65 % yielding a similar formation factor (24.2) as that from the experimental data shown in Figure 1. The formation factor was selected to match the formation factor that was measured experimentally. A series of simulations were subsequently performed where fluid was systematically removed from the capillary pores to simulate the influence of a change in the degree of saturation caused by drying (after Bentz 1998) . To do so, the pore size surrounding each pore voxel was estimated as the number of pore voxels within a 7 x 7 x 7 box centered on the given voxel, thereby quantifying pore size as an integer between 1 (smallest) and 343 (largest). The pore voxels were ranked in descending order of this size estimate, and water removal was simulated by switching the state of the largest pore voxels from “saturated” to “empty”. While the general trend between the experiment and the simulation is similar, it can be noticed that the simulation shows a more dramatic influence of drying on the saturation function than is observed experimentally (n = 5 for the simulations, while n = 3.5 for the experiment shown in Figure 1).

Figure 3b plots the simulated saturation function for a series of sealed specimens with different *w/c* ratios. The saturation function was determined by using the conductivity of a sealed mortar and the conductivity of that sealed mortar after being ‘resaturated’, (i.e., by altering the conductivity of the vapor-filled space to be equivalent to that of the pore solution). The results in Figure 3b represent mortars with a wide range of *w/c* (0.30 to 0.45) and ages of 3 d to 365 d, along with the 0.50 paste that was dried after reaching 65 % hydration (as shown in Figure 3a). The results of these simulations appear to collapse reasonably close to the same line (*n*=5).

Journal of Materials in Civil Engineering. Submitted April 25, 2012; accepted July 13, 2012;
posted ahead of print August 29, 2012. doi:10.1061/(ASCE)MT.1943-5533.0000549

While these results indicate the potential that a single function may work for cementitious systems (with *n* equals approximately 4 from the limited experimental data), it should be noted that an exhaustive examination of all cement compositions, particle size distributions and degrees of hydration were not considered, as small changes in *n* may be observed. It is recommended that experiments be performed over a wide range of concrete mixture compositions to determine the best choice for this saturation coefficient.

Correction for High Pore Solution Concentration on Drying

The parameter S appearing in Eq. 4 approximates the influence of the water loss from the pore solution which increases concentration and conductivity (one example is due to drying). It was mentioned that equation 4 is a good first approximation for the pore solution conductivity; however, it does not account for the nonlinear relationship between conductivity and concentration that arises from ionic interactions. A more thorough expression can be developed based on the work of Snyder (2001). While the full derivation that is provided in Snyder (2001) was used in the analysis here, a simplified version is presented that produces nearly identical results where the conductivity of the solution is assumed to be proportional to the ionic strength I_M (for species with valence z and molar concentration *c*):

$$I_M = \frac{1}{2} \sum_{i=1}^{N} z_i^2 \, c_i \qquad [7]$$

The expression developed by Snyder (2001) for approximating the conductivity of a concentrated solution required a correction parameter for each species. Here, the assumption is that the composition of different concrete pore solutions are somewhat similar, so the expression in Snyder (2001) is modified by using a single parameter for the solution:

$$\sigma \propto \frac{I_M}{1+G\sqrt{I_M}} \qquad [8]$$

where G is the conductivity parameter (assumed to be approximately 0.4 $(\text{mol/L})^{-1/2}$ for a typical pore solution). Starting at saturation, as the specimen dries, the ionic strength is inversely proportional to the saturation (this is the same as increasing the concentration). The ratio of the pore solution conductivity to the initial pore solution conductivity is given in equation 9. The expression in equation 8 can be approximated by a power-law relationship where the degree of saturation is raised to a correction exponent, δ-1 where the value of δ is a function of the pore solution ionic strength as shown in Figure 4.

$$\frac{\sigma_p}{\sigma_p^o} \cong \frac{1}{S} \quad \frac{1+G \quad \overline{I_M}}{1+G \quad \overline{\frac{1}{S}} \quad \overline{I_M}} \quad = S^{\delta-1} \qquad [9]$$

The parameter δ represents the degree to which the pore solution conductivity is not inversely proportional to the water content. It could be determined by experiment or calculation: extract the pore solution, measure the conductivity, add water, re-measure the conductivity, and fit data to $S^{\delta-1}$; or determine the ionic strength I_M of the pore solution and use the right two terms in Eq. 9. Combining equations 2, 3, and 9 yields a result for the ratio of the conductivity of drying concrete to saturated concrete accounting for the saturation coefficient and the concentration of the pore solution due to drying, where δ is based on the ionic strength:

$$\frac{\sigma_c}{\sigma_c^o} = S^{n-1+\delta} \qquad [10]$$

Therefore, once the value of δ has been determined by either direct measurement of the pore fluid ionic strength (by elemental analysis) or by estimation based on the mixture design using the alkali content (i.e., the ionic strength), and assuming that *n* is known for a material or there exists a universal value of *n* for concrete, one can use equation 8 to estimate the change in a concrete conductivity due to changes in its degree of saturation.

Example Application 1 - Comparing Sealed and Saturated Curing Conditions

Journal of Materials in Civil Engineering. Submitted April 25, 2012; accepted July 13, 2012;
posted ahead of print August 29, 2012. doi:10.1061/(ASCE)MT.1943-5533.0000549

To illustrate the need for a method that enables electrical conductivity measurements to be corrected based upon the degree of saturation in the concrete, the variation in conductivity was measured from a series of concrete cylinders that were cast along with a bridge deck, made with an ordinary portland cement concrete having a *w/c* of 0.39. These cylinders were demolded at 24 h and were stored for a year (DiBella et al. 2011). The concrete cylinders were conditioned in one of three ways after demolding. First, some samples were stored in limewater after demolding to simulate water curing. Second, other samples were sealed in a double layer of thermally sealed plastic bags. The samples that were sealed in bags were removed from the bags and tested in the sealed state. The degree of saturation for the concrete sealed in a bag after 1 year was measured to be 0.56, which corresponds to a relative humidity of approximately 85 % to 90 % (Li et al. 2012). Third, after initial testing, the sealed concrete samples were then cut to size for RCP testing and water saturated under vacuum in accordance with the ASTM C1202 procedures. Before conducting the 6 h measurement in ASTM C1202, the resistivity was measured using plates on either side of the concrete disk (52 mm tall by 102 mm in diameter). At an age of 365 d, the measured conductivity of the concrete stored in limewater was 0.0143 S/m. In contrast, the sealed concrete conductivity was 0.0037 S/m, and after being resaturated, its conductivity was 0.0296 S/m, which is eight times greater than before resaturation. These values are shown in Figure 5. Therefore, the measured conductivity strongly depends on how the sample was cured and conditioned prior to testing.

This sensitive dependence of conductivity on sample storage and preparation implies that there are at least two potential pitfalls when interpreting these kinds of measurements, both of which can cause an underestimation of the conductivity. First, if a conductivity measurement were made on a partially saturated sample, one could mistakenly believe that the material has a conductivity (diffusivity) that is nearly an order of magnitude lower than it actually is when saturated. The second pitfall is to neglect the effect of storage conditions. The concrete stored in lime water has approximately half the

Journal of Materials in Civil Engineering. Submitted April 25, 2012; accepted July 13, 2012;
posted ahead of print August 29, 2012. doi:10.1061/(ASCE)MT.1943-5533.0000549

conductivity of the concrete that was sealed during curing and saturated at the time of testing. Therefore, a sample stored in lime water in the laboratory would appear to have a lower conductivity than the same concrete that was sealed and saturated at the time of testing due to additional hydration that occurs in the sample stored in water (i.e., a sample in the field can be expected to behave like it is sealed if the curing/sealing compounds were working perfectly and this may different from the sample tested in the lab due to how the material has been cured)..

A mortar similar to that used in the experiments shown in Figure 5 was modeled using the VCCTL (w/c = 0.39 and an aggregate volume of 55 %). To do so, the effective conductivity both of the cement paste and of the interfacial transition zone (ITZ) region were first calculated as described earlier. Next, the paste conductivity was used as input to a differential effective medium theory calculation (Garboczi and Berryman (2000)), along with the aggregate volume fraction, grading, and mean ITZ thickness, to calculate the effective conductivity of the mortar. This approach yields effective mortar conductivities that are usually within 10 % of the value predicted by more accurate random walk simulations on the same structure (Garboczi and Berryman (2000)). However, the simulation should not be compared directly to the field concrete since it was performed on mortar and did not include entrained air. The simulation is still helpful, however, since it can provide some useful insights regarding trends and for interpreting the results as a function of their curing conditions and the saturation function. The simulated normalized conductivity obtained using the VCCTL is 0.00047 for the lime water saturated specimen, 0.000266 for the sealed specimen, and 0.00134 for the sealed sample that was resaturated. The conductivity of the pore solution was estimated using an equivalent sodium content of 0.67 (http://concrete.nist.gov/poresolncalc.html; Bentz (2007)) with a resulting pore solution conductivity between 12.4 S/m and 14.9 S/m. These estimated mortar conductivities are also shown in Figure 5.

Journal of Materials in Civil Engineering. Submitted April 25, 2012; accepted July 13, 2012;
posted ahead of print August 29, 2012. doi:10.1061/(ASCE)MT.1943-5533.0000549

In comparing the sample that was continuously stored in lime water with the sample that was sealed and saturated at each age, the overall conductivity of the continually saturated sample is lower, presumably due to the differences in the extent of hydration. The experiments also likely show the influence of leaching OH, K and Na ions. Figure 6a shows the simulated degree of hydration as a function of time as obtained from the VCCTL simulations. As one may expect, the system that is saturated has a higher degree of hydration (87 % at one year) than a system that is simply sealed cured (75 % at one year) (Bentz and Stutzman 2006). In this particular experiment, the lime-water cured sample will have a lower porosity (albeit a relatively small decrease from 38 % of the paste volume fraction to 36 % of the paste volume fraction). It should be noted, however, that this small reduction in porosity is actually a relatively large reduction in the fraction of the capillary porosity. For the mixtures being discussed, nearly 65 % of this porosity at this degree of hydration is gel porosity. Figure 6b illustrates the degree of saturation in the simulated mortars. While the saturated sample from the simulation remains at 100 % saturation, the sealed sample has a degree of saturation that progressively decreases to approximately 81% at an age of 1 year. It should be noted that the VCCTL simulation did not include entrained air which would comprise approximately 20 % of the *paste volume* for this mixture. If the degree of saturation for the concrete sample is adjusted to account for entrained air (i.e., the air is added to the VCCTL simulation as additional porosity of the system), the degree of saturation of the concrete cylinder is more similar to that of the simulation (approx. 0.76 vs. 0.81).

The normalized conductivity for the simulated mortar is plotted as a function of time in Figure 7a. This is similar to results previously shown by Bentz (1998). It can be noticed that the samples have a similar conductivity at early ages as one may expect; however over time substantial differences in conductivity begin to develop. To better illustrate the influence of the degree of hydration on the resulting pore structure, the normalized conductivity is plotted in terms of total pore volume in Figure 7b. Figure 7b shows that a single curve begins to appear that describes the specimens with water

Journal of Materials in Civil Engineering. Submitted April 25, 2012; accepted July 13, 2012;
posted ahead of print August 29, 2012. doi:10.1061/(ASCE)MT.1943-5533.0000549

(saturated) curing and the samples with sealed curing when they are tested in a saturated state. This again confirms that the 'formation factor' (a normalized conductivity/pore solution conductivity) is a material property that varies with degree of hydration (or pore volume) for the saturated system. The primary difference between the samples cured under lime water and the samples that were sealed and resaturated is that the samples that are cured under lime water exhibit more hydration, thereby achieving a lower porosity and a lower normalized conductivity than the sealed/resaturated sample at the same age (Figure 7b). Again, this is consistent with the experimental observations.

The results from Example Application 1 show that while the electrical conductivity may be a simple property to measure, it can be significantly influenced by curing conditions (sealed versus lime water saturated) and sample preparation (testing the sealed sample versus testing the sealed sample that was resaturated).

Example Application 2 - Measurements Made on Samples Exposed to Drying

In addition to using electrical property measurements on quality control samples, several researchers have measured electrical properties in concrete systems exposed to drying or wetting (Schieβl 1999, Weiss et al 1999, 1999b, Sellevold 2000, Andrade et al. 2011). While the drying process takes place over a long time period and may set up moisture gradients inside of the concrete (Weiss et al. 1999 and Rajabipour et al. 2005), moisture gradients are not considered here. The saturation approach may be useful in estimating the response of a concrete equilibrated to different levels of drying.

Figure 8 illustrates equation 8 plotted as a function of relative humidity (RH) for a series of concretes with a *w/c* of 0.4 that were allowed to dry for nearly a year (Weiss et al. 1999). The equation with a saturation coefficient of n = 4 provides a reasonable shape response at higher humidities, but this relationship begins to break down for RH less than approximately 60 %. At these lower relative

Journal of Materials in Civil Engineering. Submitted April 25, 2012; accepted July 13, 2012;
posted ahead of print August 29, 2012. doi:10.1061/(ASCE)MT.1943-5533.0000549

humidities, the saturation function is low (approximately 0.1) and the capillary pore water is likely lost, suggesting that the main conduction pathway likely changes from the large capillary pore network to the gel pores or along the walls of the capillary pores. If this is true, the breakdown of the relation valid at higher RH is not surprising.

The data for samples with a *w/c* of 0.4 and having no chemical admixtures (Schiessl et al. 1999) were compared with equation 8 and a saturation coefficient of 3.9 was obtained for concrete with a *w/c* of 0.4 for data at relative humidities greater than 60 %. A similar assessment of the data reported by Andrade et al. (2011) would be consistent with saturation coefficients that are approximately 3.5. These coefficients are similar to those observed from the numerical simulations reported in Figures 3 and 4 and from the plain pastes in Figure 1. This suggests that this approach may be applicable to drying samples. Figure 8b illustrates the desorption isotherm to relate relative humidity and the degree of saturation. It also illustrates the saturation function (assuming two different values for the saturation coefficient (i.e., n = 4 and n = 5)). This illustrates that once the relative humidity drops below 65 % to 70 % RH, the saturation function is very low.

As such, it appears that it may be quite reasonable to design an experiment where the saturation coefficient is determined for a concrete mixture by measuring the conductivity of a sample with two different degrees of saturation (provided they are relatively high). Equation 5 could then be fitted to determine the exponent for the particular mixture design used. For example, this could consist of measuring the conductivity of a sealed sample and then measuring the conductivity of the same sample after vacuum saturation. Assuming the mass of the sample is measured along with the electrical properties, the degree of saturation could be obtained by oven drying the sample after testing and measuring its oven-dried mass. This could then provide an estimate of *n* for each mixture.

Journal of Materials in Civil Engineering. Submitted April 25, 2012; accepted July 13, 2012;
posted ahead of print August 29, 2012. doi:10.1061/(ASCE)MT.1943-5533.0000549

A further illustration of this approach can be seen in Figure 9 where the surface resistivity was measured on mortar specimens exposed to drying at 50 +/- 2% relative humidity (1 in. (25 mm) square cross section and a 10.6 inch length (262.5 mm) (Bentz et al. 2012)). It can be noticed that despite the samples not being in equilibrium during the test (i.e., the samples were drying and likely continuing to hydrate slightly) a similar trend emerges for the saturation function. The mixture with a lower w/c would be expected to have a more uniform moisture content and follow the expected function a little more closely than the samples with a higher w/c that likely show some influence of the moisture gradients.

Summary

Tests that measure the electrical conductivity of concrete are sensitive to the degree of saturation of the concrete. This paper explores the potential for testing partially saturated concrete and correcting this data based on its measured degree of saturation to obtain the formation factor, which is a material property. This could have substantial impact when rapid field tests or embedded sensors are used to provide measures of properties related to durability performance. Similarly, this approach could be used to solve the equally important problem of converting measured transport coefficients for saturated concrete to values that would correspond to field conditions with a lower degree of saturation.

This paper suggests that the general form of Archie's Law can be written in a way that describes the electrical conductivity of partially saturated concrete, using a stand-alone saturation function. It appears that the saturation function can be written as the degree of saturation raised to an exponent called the saturation coefficient (*n*). A suggestion for the form of this equation is shown in equation 8 which accounts for both drying effects and changes in the pore solution concentration and conductivity during drying. While the saturation coefficient varies from approximately 1.5 to 2.5 for many rocks

Journal of Materials in Civil Engineering. Submitted April 25, 2012; accepted July 13, 2012;
posted ahead of print August 29, 2012. doi:10.1061/(ASCE)MT.1943-5533.0000549

(shown in this paper for siltstone as 2), it is slightly higher for cement-based materials, ranging from approximately 3.5 to 5.5 for the limited data from experiments. Simulations made using the VCCTL show a coefficient of approximately 5; however these simulations also showed that the saturation coefficient exhibited little variation with changes in the degree of hydration or the water to cement ratio, over the ranges investigated. The use of a saturation value of 4 provided reasonable correlation with the limited experimental data for the plain portland cement-based systems described in this paper.

The saturation function in equation 8 accounts for changes in pore solution, pore fluid volume and pore connectivity. The saturation function was used in two examples where the electrical properties were measured, the first being concrete exposed to sealed curing and the second being concretes and mortars exposed to drying. Future studies should be conducted to better understand the response of partially saturated concrete and to obtain experimental values for *n* for a wider range of concrete mixture compositions. When this work is performed, it would be helpful to describe the pore solution conductivity (or to report the sodium and potassium alkali contents of the cement), so that the role of pore solution concentration can be estimated. It would also be helpful to provide the degree of saturation of the concretes in addition to their measured internal relative humidity.

Acknowledgments

This first author is grateful for support from the Joint Transportation Research Program administered by the Indiana Department of Transportation and Purdue University. The contents of this paper reflect the views of the authors, who are responsible for the facts and the accuracy of the data presented herein, and do not necessarily reflect the official views or policies of the Indiana Department of Transportation, nor do the contents constitute a standard, specification, or regulation.

Disclaimer

Journal of Materials in Civil Engineering. Submitted April 25, 2012; accepted July 13, 2012;
posted ahead of print August 29, 2012. doi:10.1061/(ASCE)MT.1943-5533.0000549

Certain commercial products are identified in this paper to specify the materials used and procedures employed. In no case does such identification imply endorsement or recommendation by the National Institute of Standards and Technology or Purdue, nor does it indicate that the products are necessarily the best available for the purpose.

References

Andrade, M. C., Bolzoni, F. and Fullea, J. (2011). “Analysis of the relation between water and resistivity isotherms in concrete”, Materials and Corrosion, Vol. 62(2), 130-138.

Archie, G. E. (2003). “The electrical resistivity log as an aid in determining some reservoir characteristics”, SPE Reprint Series, (9-16.

ASTM C1202 (2010). Standard test method for electrical indication of concrete's ability to resist chloride ion penetration, ASTM International, West Conshohocken, PA.

AASTHTO T277 (2007)., Standard method of test for electrical indication of concrete’s ability to resist chloride ion penetration, American Association of State Highway and Transportation Officials, Washington, D.C.

Barneyback, S. and Diamond, S.(1981). “Expression and analysis of pore fluids from hardened cement pastes and mortars “, Cem Concr Res 11, 279.

Bentz, D.P. (1998) "Modelling Cement Microstructure: Pixels, Particles, and Property Prediction," Materials and Structures, 32, 187-195

Bentz, D.P. and Stutzman, P.E., "Curing, Hydration, and Microstructure of Cement Paste," *ACI Materials Journal*, **103**(5), 348-356, 2006

Bentz, D. P. (2007). “A virtual rapid chloride permeability test”, Cem Concr Compos, 29, 723-731.

Journal of Materials in Civil Engineering. Submitted April 25, 2012; accepted July 13, 2012;
posted ahead of print August 29, 2012. doi:10.1061/(ASCE)MT.1943-5533.0000549

Bentz, D.P., "Quantitative Comparison of Real and CEMHYD3D Model Microstructures Using Correlation Functions," Cement and Concrete Research, 36 (2), 259-263, 2006.

Bentz, D. P., Stutzman, P., Sakulich, A., and Weiss, W. J., (2012), "Study of Early-Age Bridge Deck Cracking in Nevada and Wyoming", NISTIR 7841, January 2012.

Berke, N. S. and Hicks, M. C. (1992). "Estimating the Life Cycle of Reinforced Concrete Decks and Marine Piles Using Laboratory Diffusion and Corrosion Data", in,.

Bullard, J. W. , Ferraris, C. F., Garboczi, E. J., Martys, N., Stutzman, P. E. and Terrill, J. E. (2008). "Virtual Cement and Concrete." Chapter 10 in Innovations in Portland Cement Manufacturing. Edited by J.I. Bhatty, F.M. Miller, and S.H. Kosmatka. Portland Cement Association, Skokie, IL.

Christensen, B. J., Coverdale, R. T., Olson, R. A., Ford, S. J., Garboczi, E. J., Jennings, H. M. and Mason, T. O. (1994). "Impedance spectroscopy of hydrating cement-based materials: measurement, interpretation, and application", J Am Ceram Soc, 77 , 2789-2804.

Castro, J., Spragg,, R., Kompare, P. and Weiss, W. J. (2010). "Portland Cement Concrete Pavement Permeability Performance", Joint Transportation Research Program, Indiana Department of Transportation and Purdue University, West Lafayette, Indiana.

Dibella, Carmello (in progress). "Transport and Shrinkage Properties in Plain and Internally Cured "., MSThesis, Purdue University.

FM 5-578 (2004). "Florida method of test for concrete resistivity as an electrical indicator of its permeability", Flordia Department of Transportation, Tallahassee, FL.

Garboczi, E. J. (1990). "Permeability, diffusivity, and microstructural parameters: A critical review", Cem Concr Res, 20 , 591-601.

Journal of Materials in Civil Engineering. Submitted April 25, 2012; accepted July 13, 2012;
posted ahead of print August 29, 2012. doi:10.1061/(ASCE)MT.1943-5533.0000549

Garboczi, E. J. (1998) Finite Element and Finite Difference Programs for Computing the Linear Electric and Elastic Properties of Digital Images of Random Materials. NISTIR 6269; 211 p. December 1998.

Garboczi, E. J. and Berryman, J.G. (2000). “New effective medium theory for the diffusivity or conductivity of a multi-scale concrete microstructure model”, Concr Sci Eng, 2, 88-96.

Gu, P., Xie, P., Beaudoin, J. J. and Brousseau, R. (1992). « A.C. Impedance Spectroscopy 1 : A New Equivalent Circuit Model for Hydrated Portland Cement Paste », Cement and Concrete Research 22, 833-840.

Julio-Betancourt, G. A. and Hooton, R. D. (2004). “Study of the Joule effect on rapid chloride permeability values and evaluation of related electrical properties of concretes”, Cem Concr Res, 34, 1007-1015.

Hansson, I.L.H. and Hansson, C. M. (1983). « Electrical resistivity measurements of Portland cement based materials », Cement and Concrete Research, Vol. 13(5), 675-683.

Jackson,, N. M. (2011). “Results of round-robin testing for the development of precision statements for the surface resistivity of water saturated concrete”, Ponte Vedra Beach, Florida.

Kessler, R. J., Powers, R. G. and Paredes, M. A. (2005). “ Resistivity Measurements of Water Saturated Concrete as an Indicator of Permeability”, in: Corrosion 2005, NACE International, Houston, TX.

Li, W., Pour-Ghaz, M., Castro, J., and Weiss, W. J., (2012) “Water Absorption and the Critical Degree of Saturation as it relates to Freeze-Thaw Damage in Concrete Pavement Joints,” ASCE Journal of Civil Engineering Materials

Martys, N.S., "Diffusion in Partially-Saturated Porous Materials," Materials and Structures, 32, pp 555-562 (1999).

Journal of Materials in Civil Engineering. Submitted April 25, 2012; accepted July 13, 2012;
posted ahead of print August 29, 2012. doi:10.1061/(ASCE)MT.1943-5533.0000549

Millington, R. J., and Quirk, J. P., (1961) ‘Permeability of Porous Solids,’ Transactions of the Faraday Society, 57, pp. 1200-1207

McCarter, W. J., Forde, M. C. and Whittington, H. W. (1981). “Resistivity characteristics of concrete”, Proceedings of the Institution of Civil Engineers (London) Part 1 - Design & Construction, 71, 107-117.

Monfore, G. E. (1968). “The electrical resistivity of concrete”, Portland Cement Association, Research and Development Laboratories, Skokie, IL,.

Morris, W., Moreno, E. I. and Sagues, A. A. (1996). “Practical evaluation of resistivity of concrete in test cylinders using a Wenner array probe”, Cem Concr Res, 26, 1779-1787.

Newlands, M. D., Jones, M. R., Kandasami, S. and Harrison, T. A. (2008). ,” Sensitivity of electrode contact solutions and contact pressure in assessing electrical resistivity of concrete”, Mater Struct, 41, 621-621-632.

Powers, T. C., and Brownyard, T.L., (1942) ‘Studies of the Physical Properties of Hardened Portland Cement Paste’, Bulletin 22 Research and Development Laboratories of the Portland Cement Association, Chicago, Illinois (1948)

Poursaee, A. and Weiss, W. J.(2009). « An automated electrical monitoring system (AEMS) to assess property development in concrete », Automation in Construction, Vol. 19(4), 485-490.

Rajabipour, F., Weiss,, J. and Shane, J. D., Mason, T. O. and Shah, S. P. (2005) Procedure to interpret electrical

Rajabipour, F. and Weiss, J. (2007). « Electrical conductivity of drying cement paste », Materials and Structures, Vol. 40(10), 1143-1160.

Journal of Materials in Civil Engineering. Submitted April 25, 2012; accepted July 13, 2012;
posted ahead of print August 29, 2012. doi:10.1061/(ASCE)MT.1943-5533.0000549

Rajabipour, F. (2006). “Insitu electrical sensing and material health monitoring in concrete structures”, Ph.D. Dissertation, Purdue University, West Lafayette, Indiana.

Raupach, M. and Schiessl, P. (1997). « Monitoring system for the penetration of chlorides, carbonation and the corrosion risk for the reinforcement », Construction and Building Materials, Vol. 11(4), 207-214.

Riding, K. A., Poole, J. L., Schindler, A. K., Juenger, M.C.G. and Folliard, K. J. (2008). “ Simplified concrete resistivity and rapid chloride permeability test method”, ACI Mater J, 105, 390-394.

Rupnow,. T. D., and Icenogle, P. (2011). “Evaluation of surface resistivity measurements as an alternative to the rapid chloride permeability test for quality assurance and acceptance”, Louisiana Department of Transportation, Baton Rouge, LA, pp. 68.

Samson, E., and Marchand, J., (2007) ‘Modeling the Transport of Ions in Unsaturated Cement-Based Materials,’ Computers and Structures, 85, pp. 1740-1756

Schissl, A., Weiss, W. J., Shane, J. D., Berke, N. S., Mason, T.O., and Shah, S. P., (2000) "Assessing the Moisture Profile of Drying Concrete Using Impedance Spectroscopy," Concrete Science and Engineering, Vol. 2, pp. 106-116

Sellevold, E. J., Larsen, C. K. and Blankvoll, A. A. (1997). « Moisture State of Concrete in a Coastal Ridge », Special Publication, SP170-42, Vol. 170, 823-834.

Schlumberger (2011), Oilfield Glossary

Shane, J. D., Aldea, C. D., Bouxsein,, N. F. Mason, T. O., Jennings, H. M. and Shah, S. P. (1999). “Microstrucutral and pore solution changes induced by the rapid chloride permeability test measured by impedance spectroscopy”, Concr Sc Eng, 1 , 110-119.

Journal of Materials in Civil Engineering. Submitted April 25, 2012; accepted July 13, 2012;
posted ahead of print August 29, 2012. doi:10.1061/(ASCE)MT.1943-5533.0000549

Shane, J. D. (2000). “Electrical conductivity and transport properties of cement-based materials measured by impedance spectroscopy”, Ph.D. Dissertation, Northwestern University, Evanston, IL.

Snyder, K.A., (2001) "The relationship between the formation factor and the diffusion coefficient of porous materials saturated with concentrated electrolytes: Theoretical and experimental considerations," Concrete Science and Engineering, 3 (12), 216-224, (2001).

Snyder, K. A., Ferraris, C., Martys, N. S. and Garboczi, E. J. (2000). “Using impedance spectroscopy to assess the viability of the rapid chloride test for determining concrete conductivity”, J NIST, 105, 497-509.

Spragg, R, Castro, J., Nantung, T., Parades, M, and Weiss, W. J., (2011) “Variability Analysis of the Bulk Resistivity Measured Using Concrete Cylinders,” JTRP Report SPR-3509, FHWA/IN/JTRP-2011/21 DOI: 10.5703/1288284314646

Torquato, S. (2002). “Random heterogeneous materials: microstructure and macroscopic properties”, Springer, New York, NY.

TP95-11 (2011) Draft standard method of test for surface resistivity indication of concrete’s ability to resist chloride ion penetration, American Association of State Highway and Transportation Officials, Washington, D.C.

Tumidajski, P. J., Schumacher, A. S., Perron, S., Gu. P. and Beaudoin, J. J. (1996). « On the relationship between porosity and electrical resistivity in cementitious systems », Cement and Concrete Research, Vol. 26(4), 539-544.

UNE (2008a), “Concrete durability. Test methods. Determination of the electrical resistivity. Part 1: Direct test (reference method), UNE 83988-1, AENOR, February, 9 pp.

Journal of Materials in Civil Engineering. Submitted April 25, 2012; accepted July 13, 2012; posted ahead of print August 29, 2012. doi:10.1061/(ASCE)MT.1943-5533.0000549

UNE (2008b), "Concrete durability. Test methods. Determination of the electrical resistivity. Part 2: Four points or Wenner method, UNE 83988-2, AENOR, February, 8pp.

Weiss, W. J., Shane, J. D., Mieses, A., Mason, T. O. and Shah, S. P. (1999). "Aspects of monitoring moisture changes using electrical impedance spectroscopy", Second symposium on the importance of self desiccation in concrete technology, Lund, Sweden.

Whittington, H. W., McCarter, J., and Forde, M. C. (1981). "The conduction of electricity through concrete", Mag Concr Res, 33 , 48-60.

Journal of Materials in Civil Engineering. Submitted April 25, 2012; accepted July 13, 2012;
posted ahead of print August 29, 2012. doi:10.1061/(ASCE)MT.1943-5533.0000549

Figure 1: Experimentally measured saturation coefficients for siltsone and cementitious materials. (Containing data from Rajabipour 2006)

Figure 2: Microstructural images developed using the VCCTL model for a mortar with a *w/c* of 0.42 and an aggregate volume of 55 % at a) 3 d and b) 365 d hydrated under saturated conditions. The phases are color-coded as follows: black = capillary porosity, brown = alite, light blue = belite, white = ferrite, beige = C-S-H gel, dark blue = CH, and green = ettringite and monosulfoaluminate combined.

Figure 3: a) A Saturation Function Interpreted for VCCTL computer simulations b) Calculated saturation functions obtained from a series of simulated microstructures. The dashed curve corresponds to a saturation coefficient n=4 and the dotted and dashed line corresponds to a saturation coefficient n=5.

Figure 4: A correction term (δ) to account for the ionic interactions in a pore solution, having an ionic strength I_M when the sample is saturated, as it becomes more concentrated due to drying

Figure 5: Measured electrical conductivity from RCP tests using a field concrete and simulated mortar with a w/c of 0.39 under different curing and sample conditioning (A maximum coefficient of variation of 3.2% was observed for the experiments)

Figure 6: Mortar with a w/c of 0.39: a) Degree of hydration and b) Degree of saturation
Figure 7: Normalized conductivity of mortar with a w/c of 0.39: a) as a function of time and b) as a function of the pore volume in the paste as computed using Powers' model

Figure 8: a) Normalized conductivity as a function of drying and b) rhe relationship between relative humidity and saturation for the data

Figure 9: The application of the saturation function to mortar prisms during drying (the dashed line and dot-dash line denote a $n-1+\delta$ value of 3 and 4, respectively).

Figure 1

Journal of Materials in Civil Engineering. Submitted April 25, 2012; accepted July 13, 2012;
posted ahead of print August 29, 2012. doi:10.1061/(ASCE)MT.1943-5533.0000549

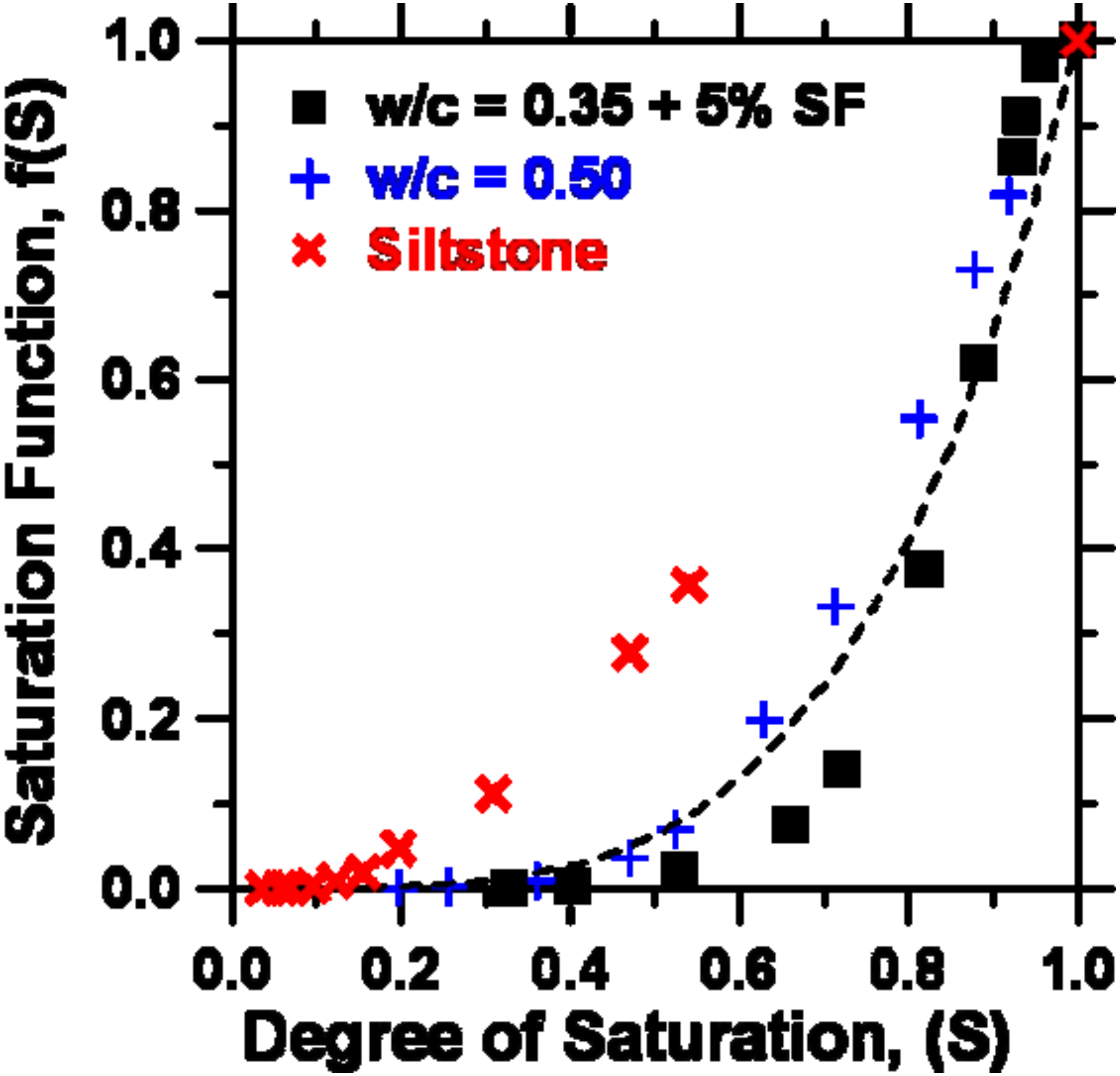

Figure 2

Journal of Materials in Civil Engineering. Submitted April 25, 2012; accepted July 13, 2012; posted ahead of print August 29, 2012. doi:10.1061/(ASCE)MT.1943-5533.0000549

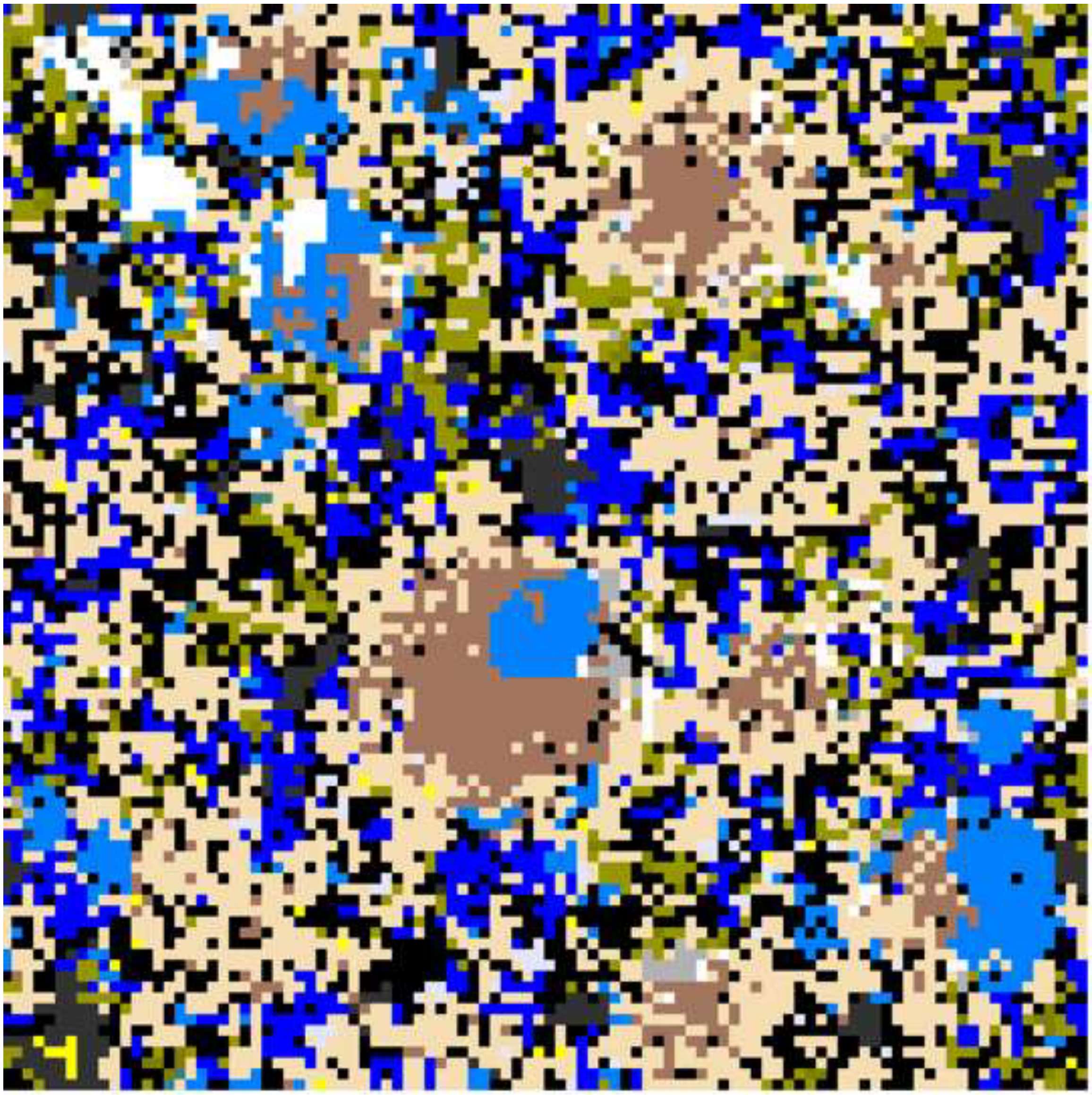

Figure 2b

Journal of Materials in Civil Engineering. Submitted April 25, 2012; accepted July 13, 2012;
posted ahead of print August 29, 2012. doi:10.1061/(ASCE)MT.1943-5533.0000549

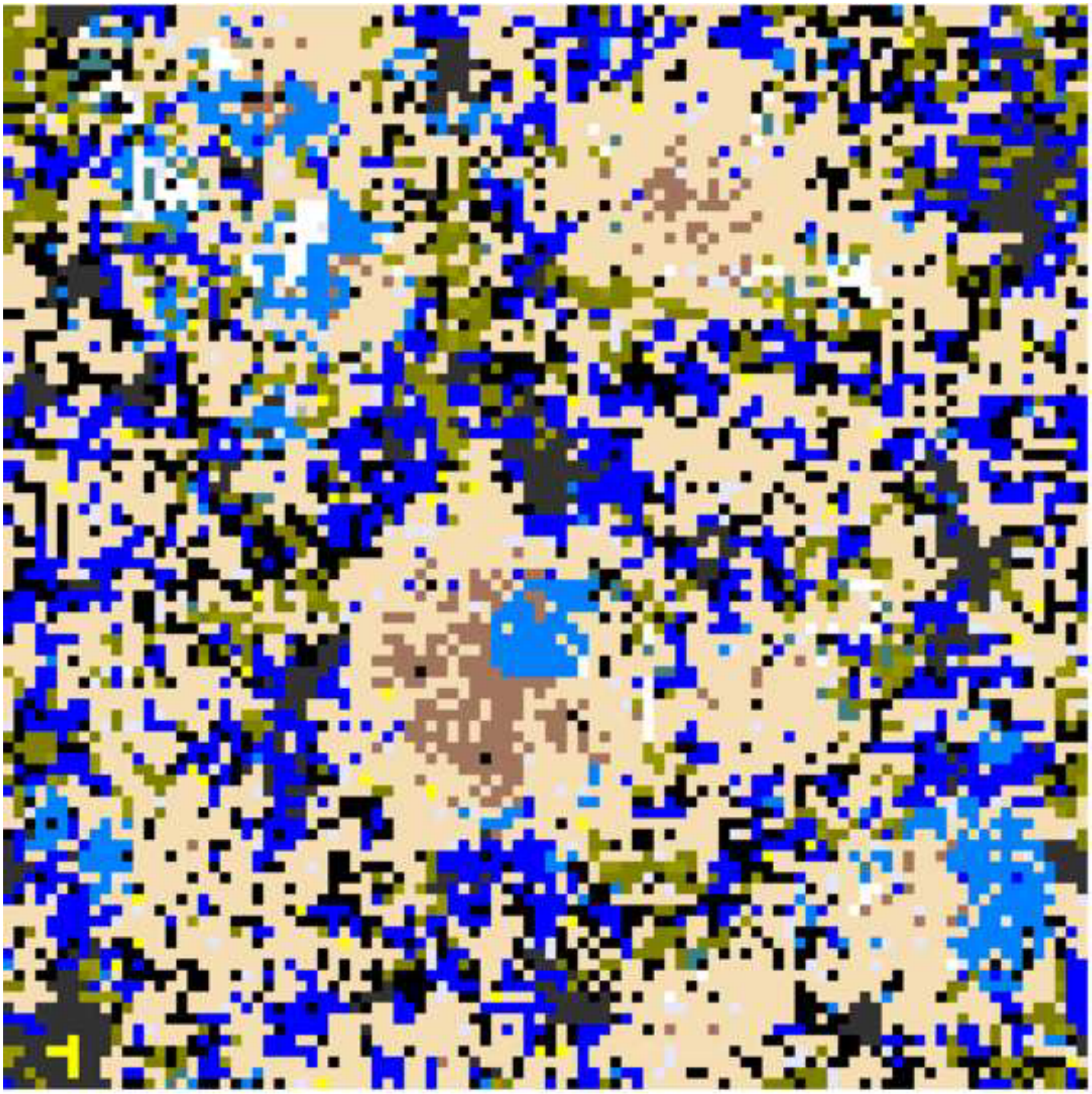

Figure 3

Journal of Materials in Civil Engineering. Submitted April 25, 2012; accepted July 13, 2012;
posted ahead of print August 29, 2012. doi:10.1061/(ASCE)MT.1943-5533.0000549

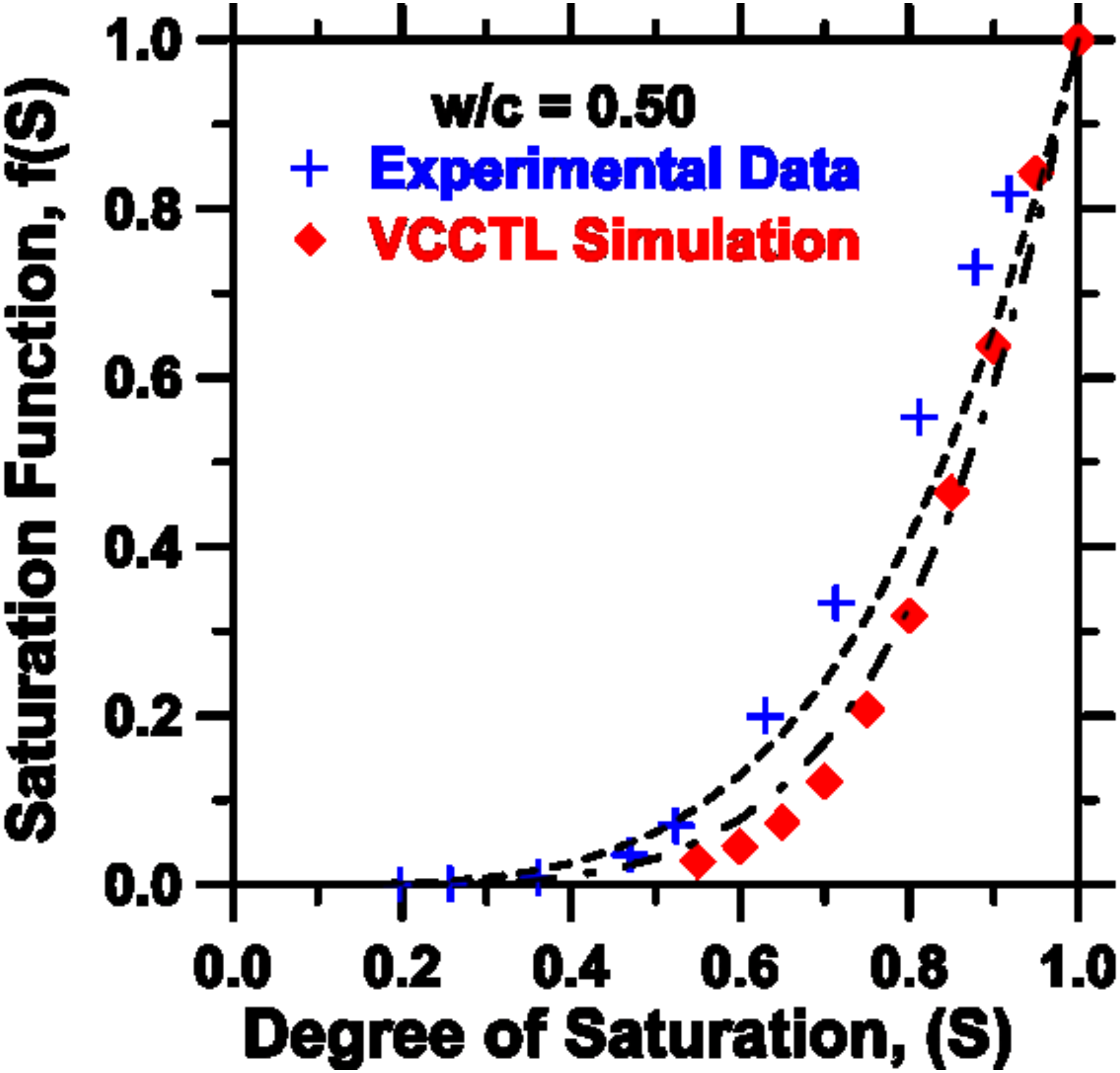

Figure 3b

Journal of Materials in Civil Engineering. Submitted April 25, 2012; accepted July 13, 2012;
posted ahead of print August 29, 2012. doi:10.1061/(ASCE)MT.1943-5533.0000549

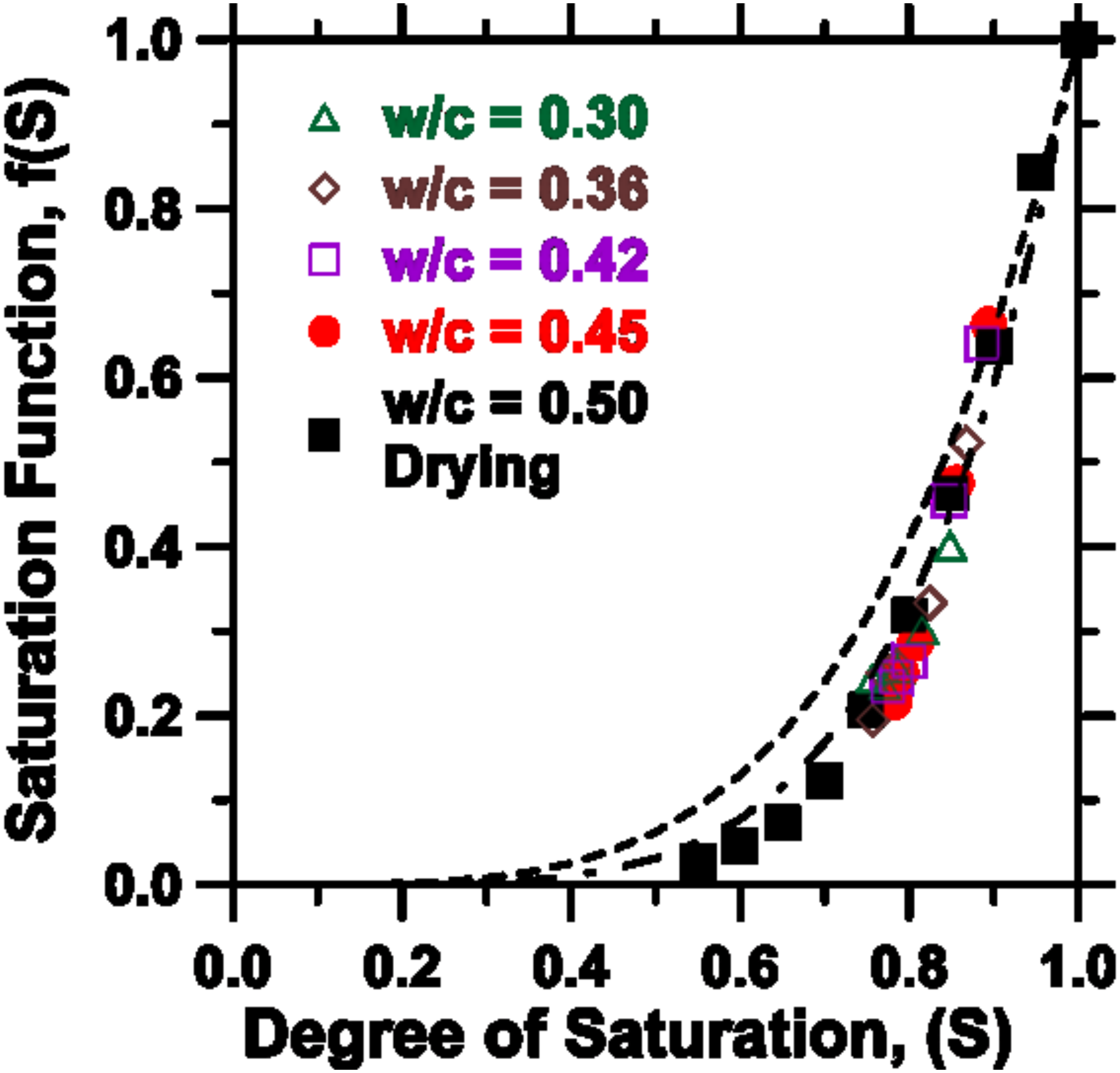

Figure 4

Journal of Materials in Civil Engineering. Submitted April 25, 2012; accepted July 13, 2012;
posted ahead of print August 29, 2012. doi:10.1061/(ASCE)MT.1943-5533.0000549

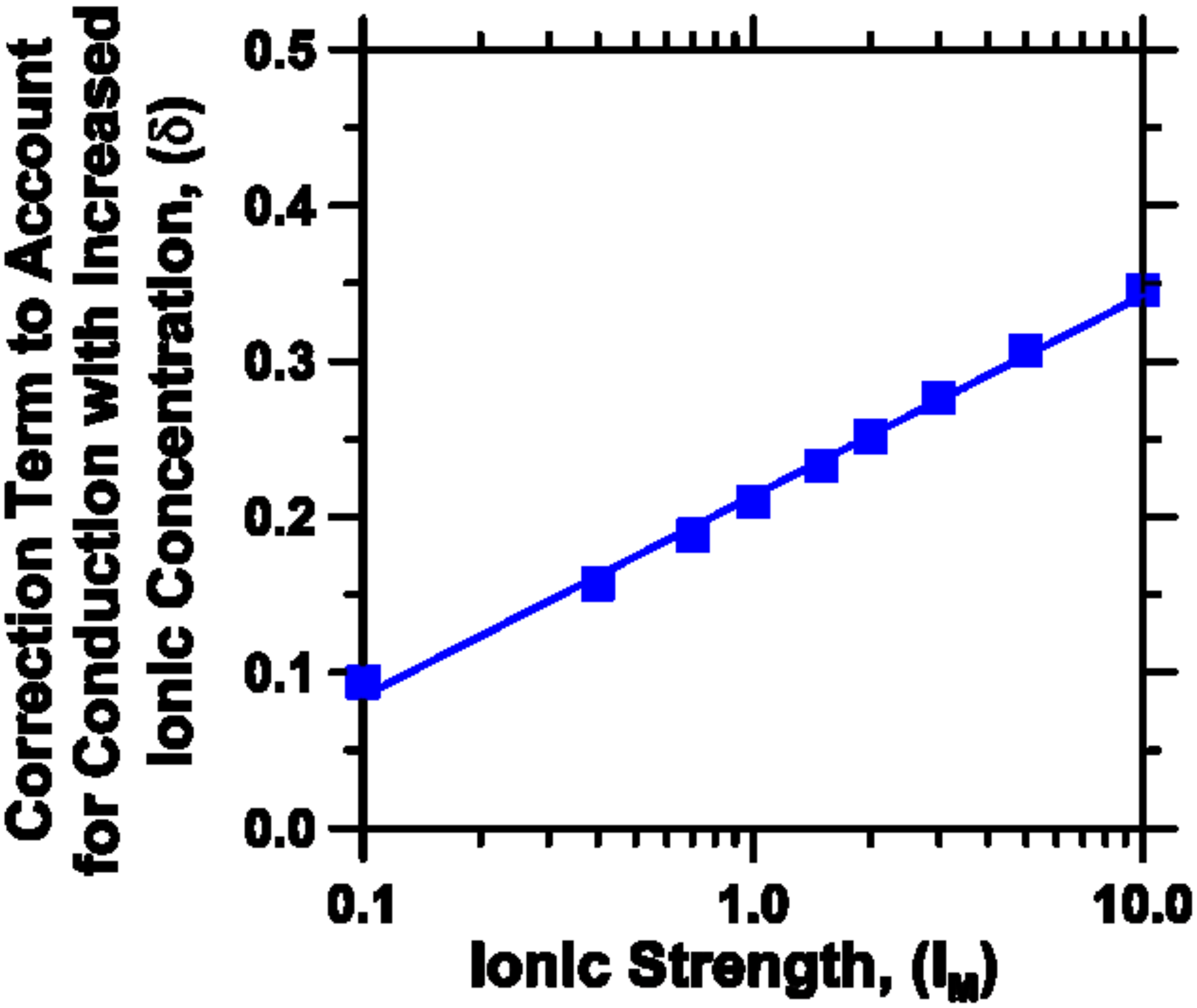

Figure 5

Journal of Materials in Civil Engineering. Submitted April 25, 2012; accepted July 13, 2012;
posted ahead of print August 29, 2012. doi:10.1061/(ASCE)MT.1943-5533.0000549

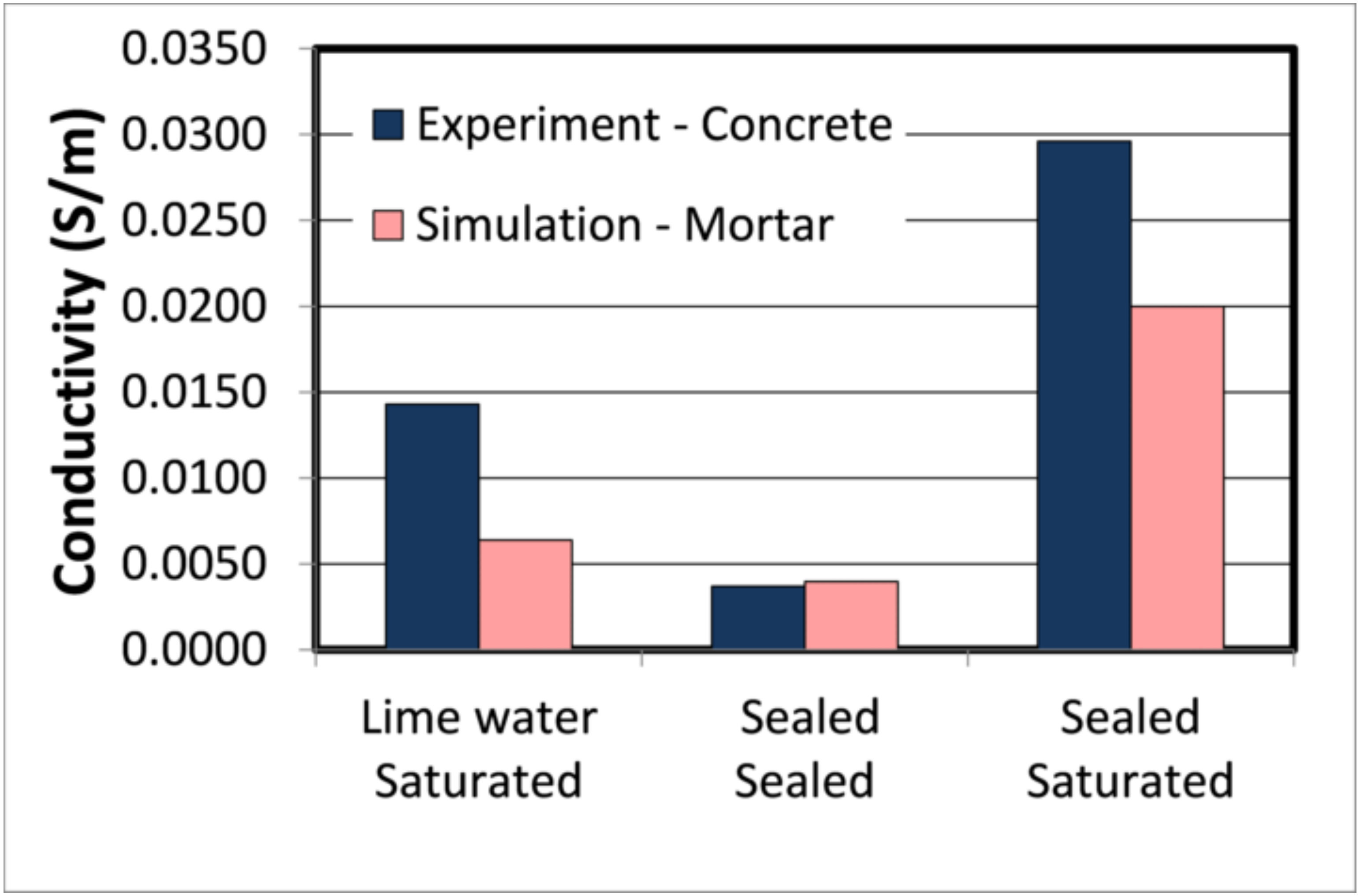

Figure 6a

Journal of Materials in Civil Engineering. Submitted April 25, 2012; accepted July 13, 2012; posted ahead of print August 29, 2012. doi:10.1061/(ASCE)MT.1943-5533.0000549

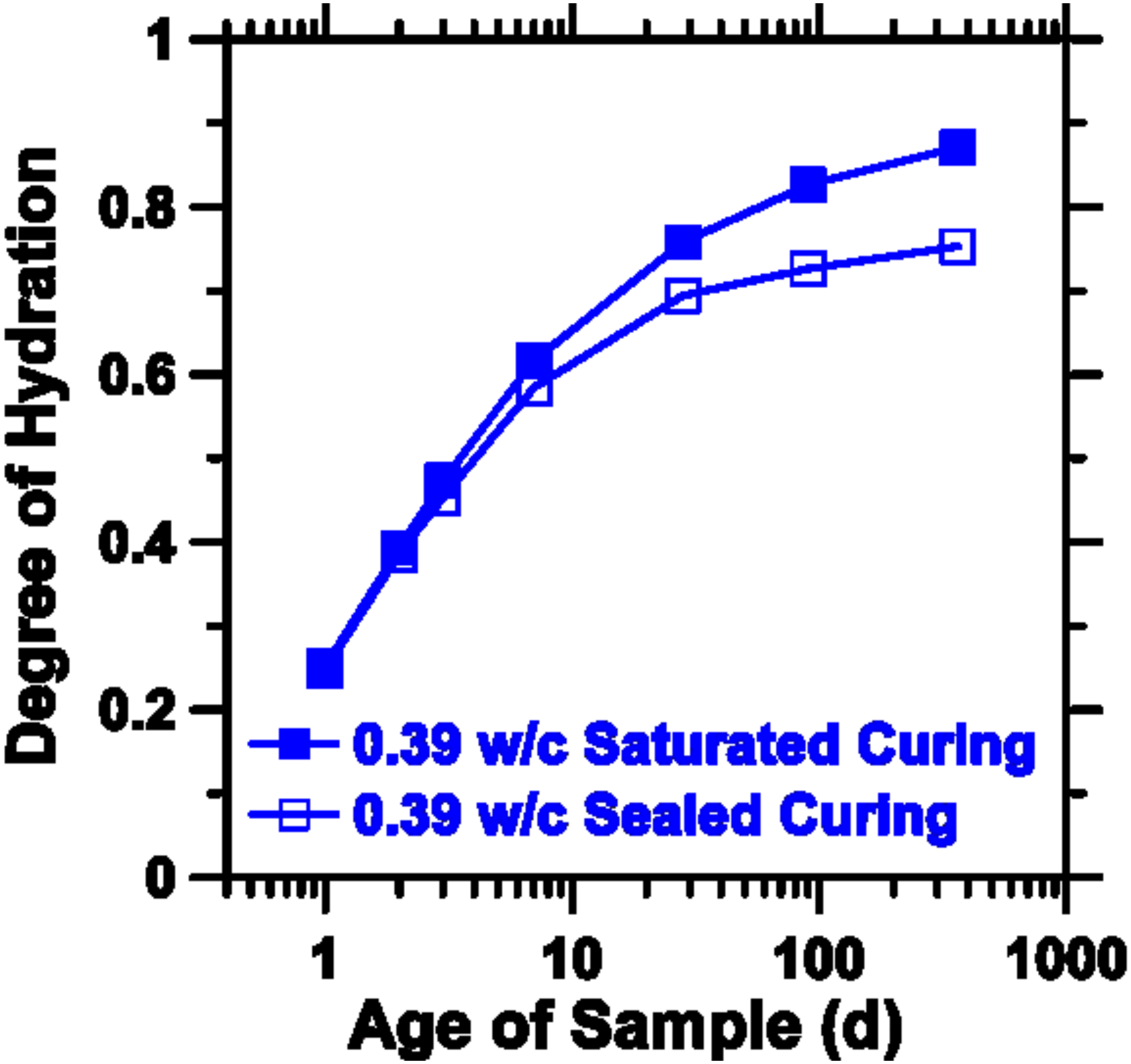

Figure 6b

Journal of Materials in Civil Engineering. Submitted April 25, 2012; accepted July 13, 2012;
posted ahead of print August 29, 2012. doi:10.1061/(ASCE)MT.1943-5533.0000549

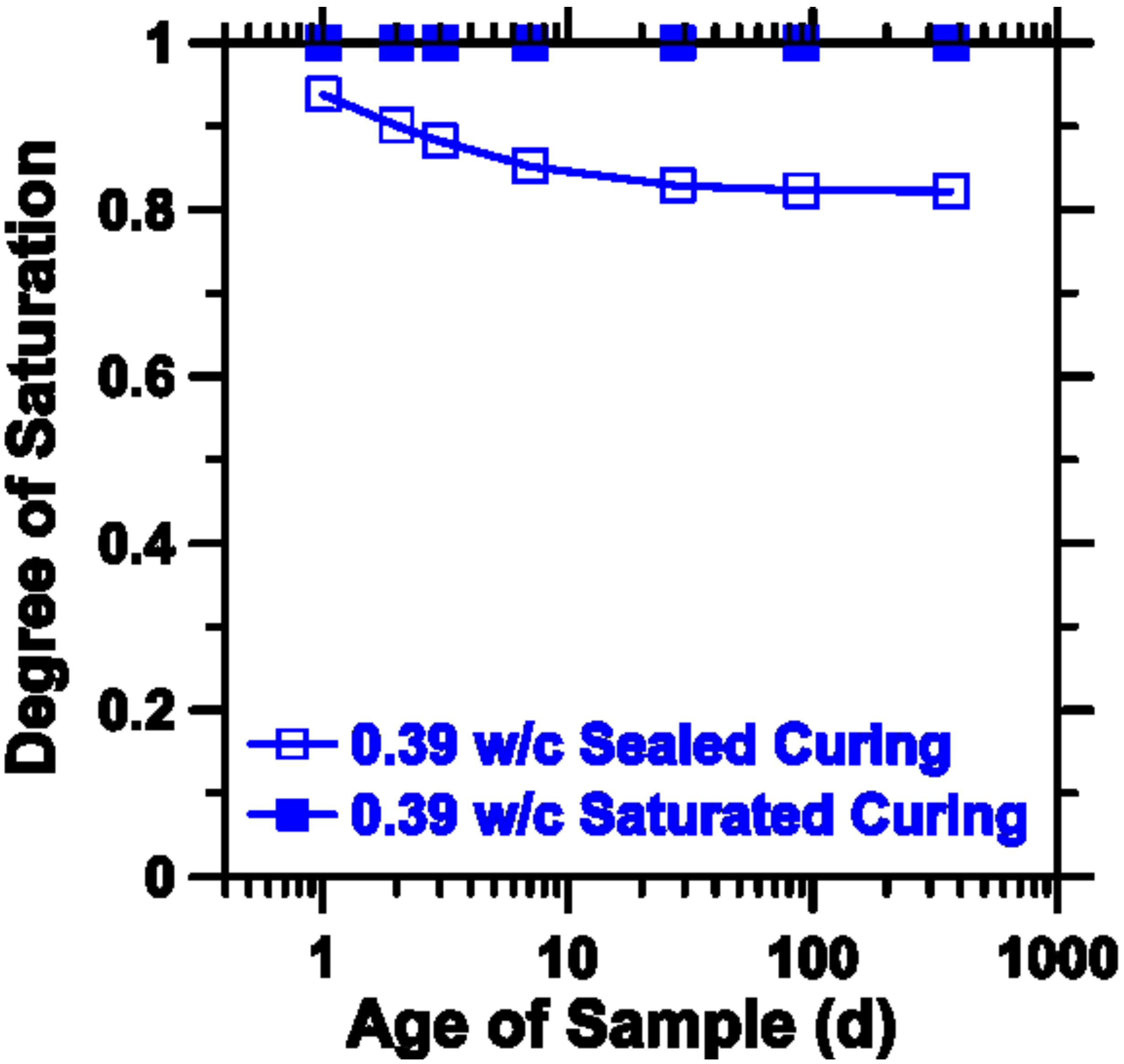

Figure 7a

Journal of Materials in Civil Engineering. Submitted April 25, 2012; accepted July 13, 2012;
posted ahead of print August 29, 2012. doi:10.1061/(ASCE)MT.1943-5533.0000549

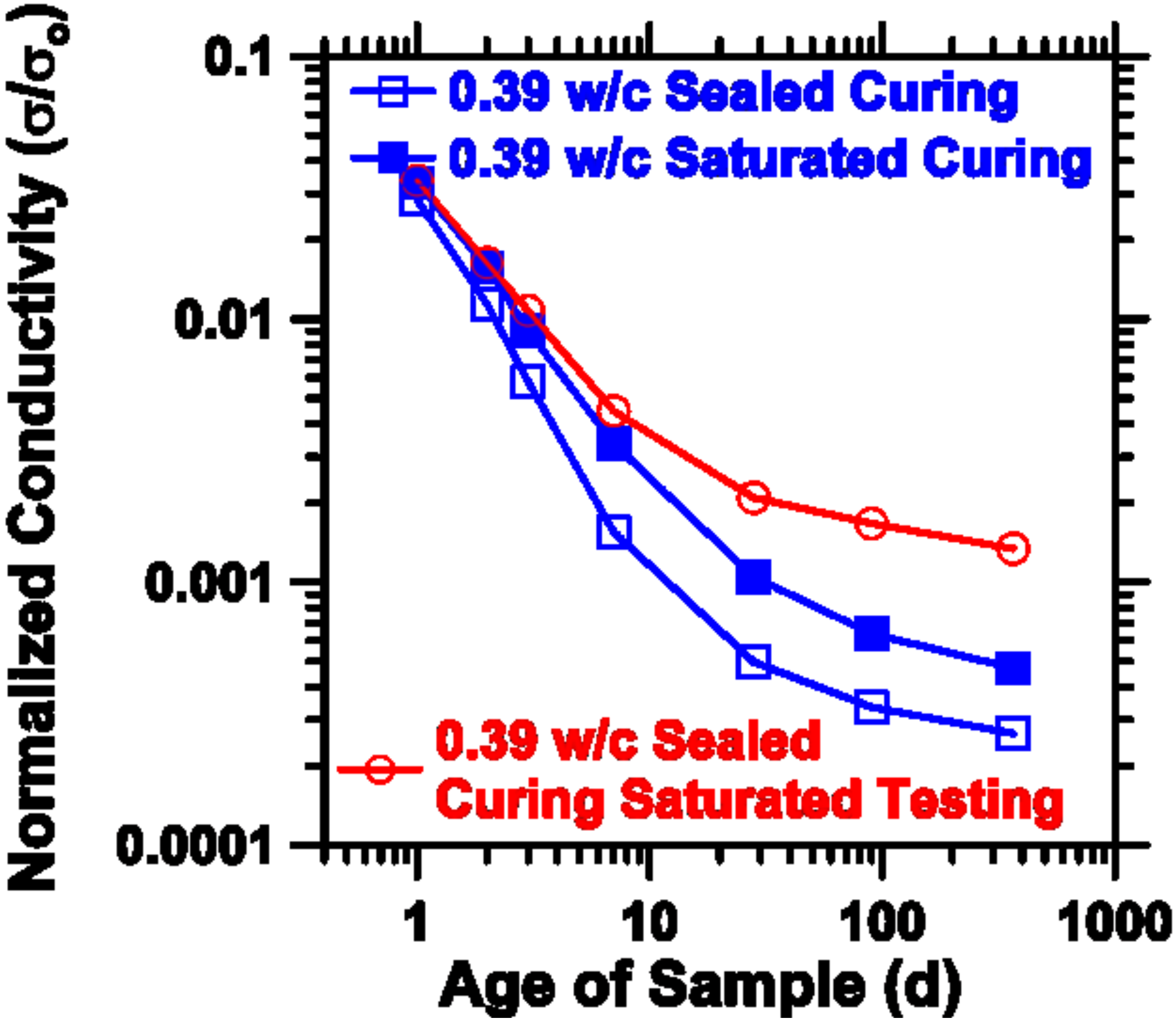

Figure 7b

Journal of Materials in Civil Engineering. Submitted April 25, 2012; accepted July 13, 2012;
posted ahead of print August 29, 2012. doi:10.1061/(ASCE)MT.1943-5533.0000549

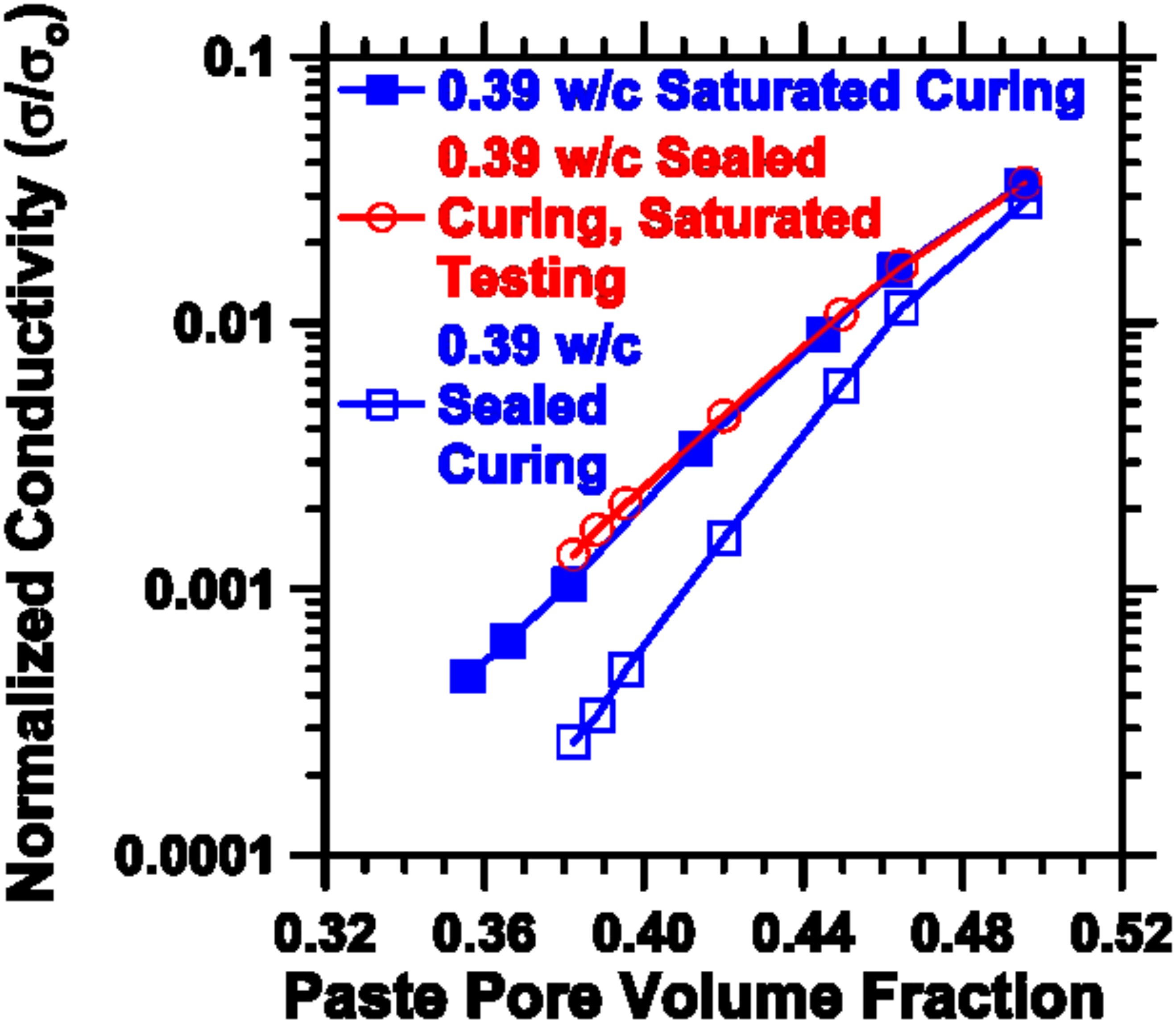

Figure 8a

Journal of Materials in Civil Engineering. Submitted April 25, 2012; accepted July 13, 2012;
posted ahead of print August 29, 2012. doi:10.1061/(ASCE)MT.1943-5533.0000549

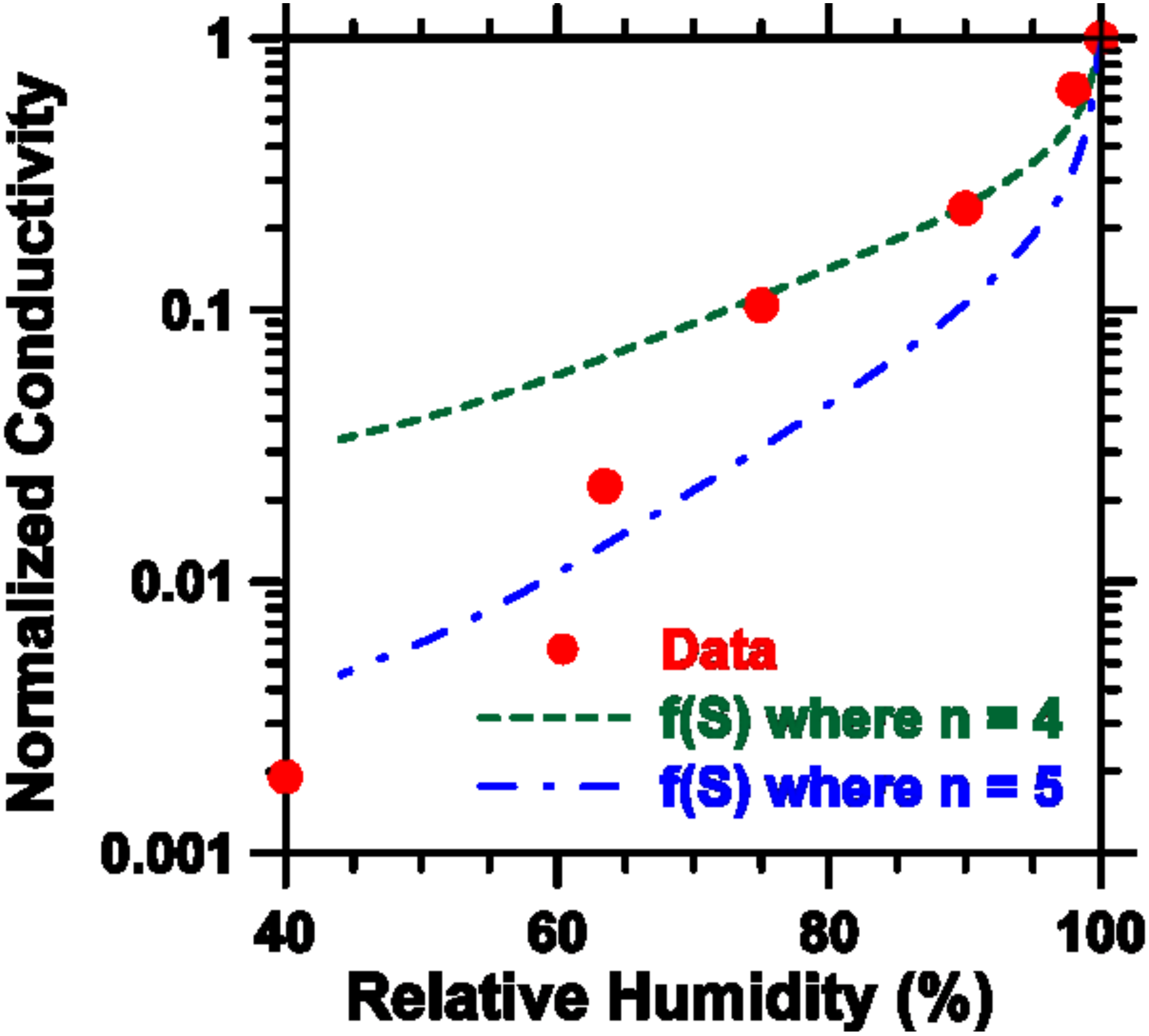

Figure 8b

Journal of Materials in Civil Engineering. Submitted April 25, 2012; accepted July 13, 2012;
posted ahead of print August 29, 2012. doi:10.1061/(ASCE)MT.1943-5533.0000549

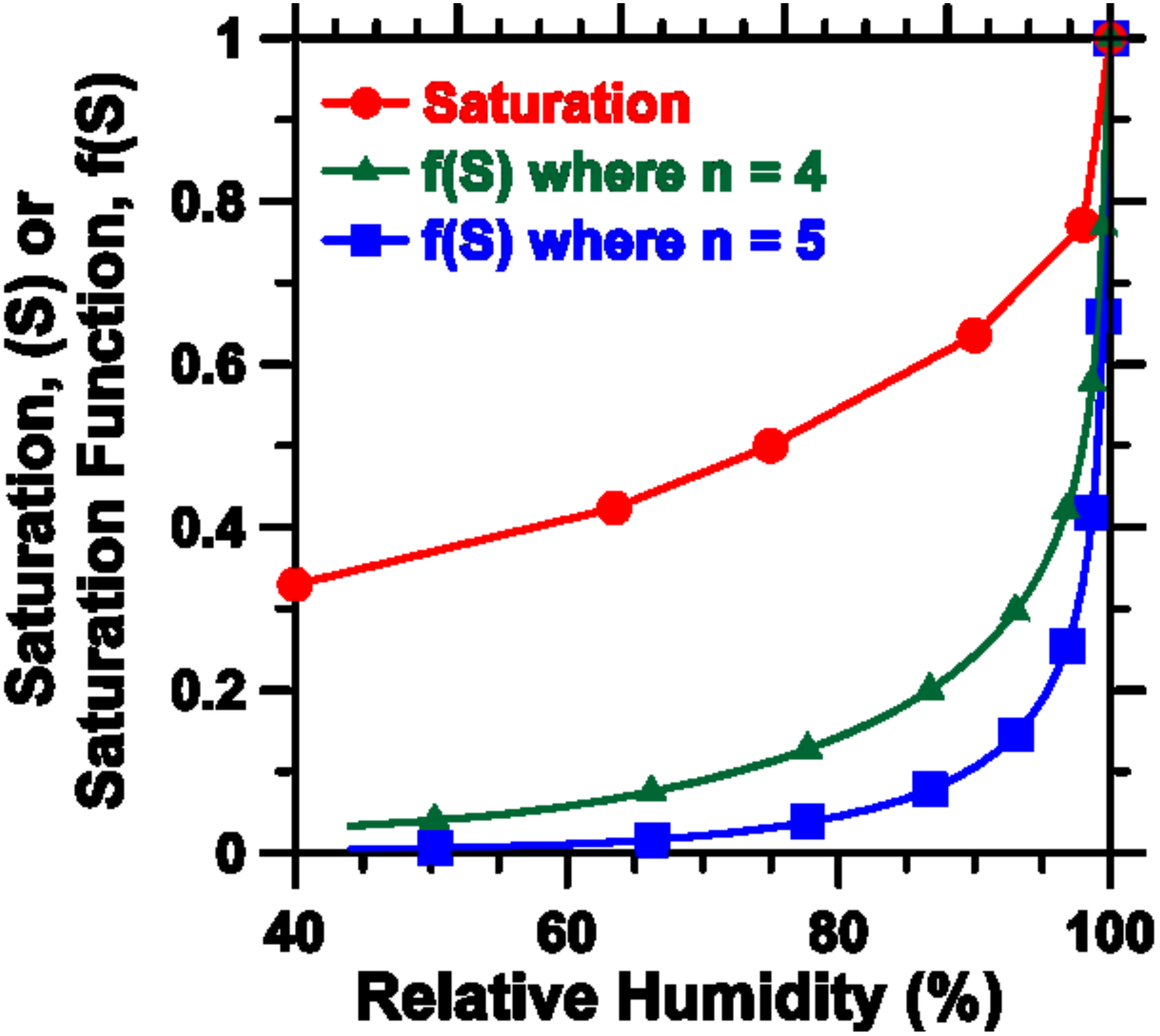

Figure 9

Journal of Materials in Civil Engineering. Submitted April 25, 2012; accepted July 13, 2012;
posted ahead of print August 29, 2012. doi:10.1061/(ASCE)MT.1943-5533.0000549

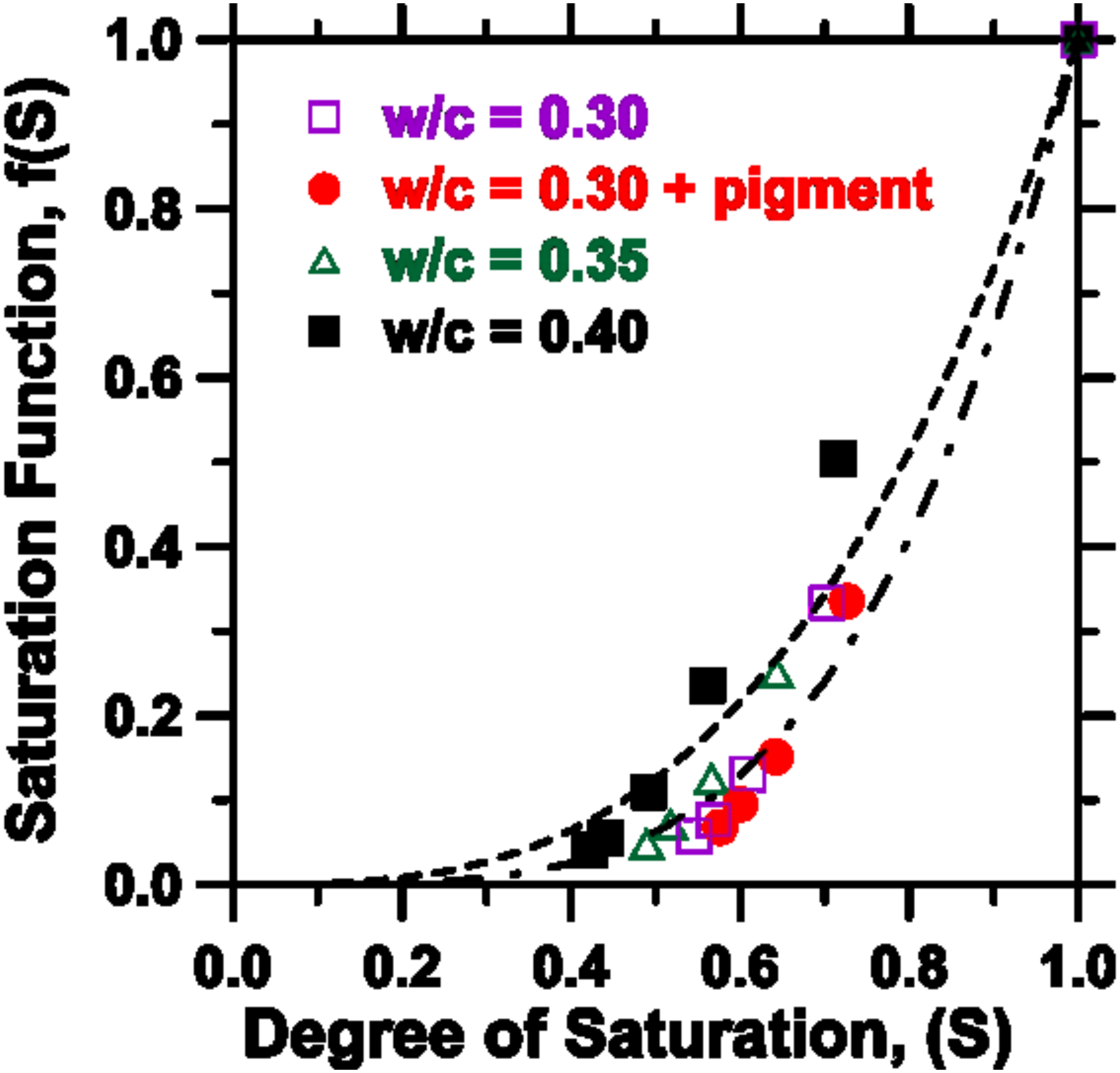

THE ROLE OF DEICING SALTS ON THE NON-LINEAR MOISTURE DIFFUSION COEFFCIENT OF CEMENTITIOUS MATERIALS DURING DRYING

C. VILLANI [a] (cvillani@purdue.edu), R. SPRAGG [a] (rspragg@purdue.edu), M. POUR-GHAZ [b] (mpourghaz@ncsu.edu) and W. J. WEISS [a] (wjweiss@purdue.edu)

[a] Purdue University, School of Civil Engineering, 550 Stadium Mall Drive, West Lafayette, IN 47906, USA

[b] North Carolina State University, Department of Civil, Construction, and Environmental Engineering, Campus Box 7908, Raleigh, NC 27695-7908, USA

ABSTRACT

The drying of cementitious materials is of interest in volume change (i.e., shrinkage) research. However, the movement of water due to drying and wetting also plays a significant role in many durability related problems (e.g., corrosion, alkali silica reactivity, freezing and thawing). Many factors can influence the drying and wetting process in concrete including: pore structure, environmental conditions, and liquid properties. This paper describes the influence of the liquid properties on the drying process. Specifically, this work examines the non-linear moisture diffusion coefficient that is used in a differential equation that describes drying. This paper describes how the non-linear moisture diffusion coefficient is influenced by the presence of deicing salts solutions. The relationship between the equilibrium relative humidity and the solution properties is also discussed in this paper. A higher degree of saturation was observed for the samples containing deicing salt solutions, as compared to the plain samples at any given humidity. The presence of deicing salt causes a shift of the non-linear moisture diffusion coefficient as a function of relative humidity. The non-linear moisture diffusion coefficient curves have near zero rates of drying at low relative humidity with a rapid increase in drying rate as the relative humidity is increased (especially near the equilibrium relative humidity) followed by diffusion coefficient of 0 between RHeq and 100% RH.

Keywords

Diffusion process, drying process, salt, degree of saturation

INTRODUCTION

Understanding how water enters and leaves cementitious materials is of immense interest to the concrete community. Moisture diffusion is known to be related to the moisture content and pore size [4]. In addition, internal moisture profiles influence the rate of hydration, electrical properties, fluid transport, and many aspects of durability [3, 14, 21].

Numerous concrete pavements in the US have shown premature deterioration at joints. While several causes have been suggested to be responsible for the distress that develops, it is clear that the movement of moisture is an important aspect for several of these distress mechanisms including those associated with freeze/thaw and/or physical salt attack. For example, Li et al and others [10, 11] showed that freeze-thaw damage is related to the degree of saturation. As such the wetting and drying of concrete may be of great importance in understanding joint durability, especially in the presence of deicing salts. Salts can also reduce the rate of fluid absorption when compared with water [18] as also altering the drying process resulting in a mass gain in some samples when they are placed in a drying environment.

Although few have studied the influence of deicing salts on drying, deicing salts have been the subject of research over the years, with special attention to their influence on concrete degradation [19], on absorption [18], on hysteresis during drying and wetting [9,18], on freeze/thaw and salt solutions damage [5,20] or crystallization pressure [16]. The influence of salts on evaporation processes has been studied for rocks [6,7], and it has been shown that the presence of salts modifies the desorption behavior of lightweight aggregate [8].

The response of the liquid in the pores can be visualized in Figure 1 as one moves from high relative humidity (on the right hand side of the image) to lower relatively humidity (on the left hand side of the image) for water (case “a” shown on top) and a salt solution (case “b” as shown in the center). The drying process is generally considered to be a two stage process. The first stage (the constant rate period) consists in the evaporation of surface water (not shown), while the second stage (the falling rate period) consists of water leaving the pores [6,12,15]. It can be noticed that at saturation both the water and the salt solution contain completely filled the pore space. Water does not leave the pores if the RH of the environment the sample is placed in remains above the equilibrium relative humidity (RH_{eq}) (i.e., $RH > RH_{eq}$) of the solution in the pores [6,18]. The RH_{eq} of the salt solutions is lower than that of water which implies that the specimens containing salt solutions will remain saturated at lower relative humidities than the plain system [18]. As the liquid is drawn out of the pores a meniscus forms. The meniscus is curved at the liquid-vapor interface as a result of the tension generated at the liquid-vapor interface [15]. The radius of the meniscus changes depending on both the external RH and the properties of the solution (Figure 1). It can be noticed that as the RH decreases (i.e., $RH < RH_{eq}$) fluid leaves the pores. After the water is lost only the solid salt will remain in the pores.

The desorption spectra (water loss versus relative humidity) depends on the pore structure (in terms of size distribution, degree of connectivity or total volume of porosity) and the properties of the liquid. The properties of the liquid, usually identified through surface tension, density, viscosity and water activity (or equilibrium relative humidity) [7].

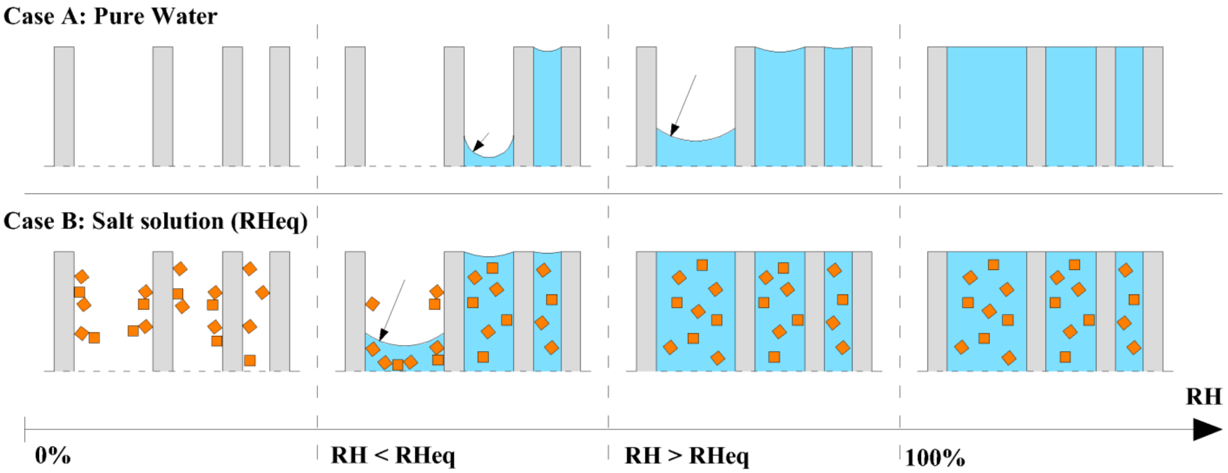

Figure 1: Schematic of the drying process in a fictitious case of drying in a system containing pure water (Case a) and salt solution (Case b), assuming cylindrical meniscus and possible issue when crystals tap pores avoid the complete evaporation of the solution

While the previous paragraphs provide a conceptual illustration of how different fluids will leave an idealized system with pores of different sizes during drying it is also important to consider how these effects can be considered numerically on the macro scale. Toward this end this paper uses a differential equation that is formulated in terms of relative humidity (to avoid complications due to hydration that can exist if this is formulated in terms of water content) with a non-linear diffusion coefficient as developed by Bazant and Najjar [4]

$$\frac{\partial RH}{\partial t} = \frac{\partial}{\partial x}\left[D_h(RH)\frac{\partial RH}{\partial x}\right] \tag{1}$$

where RH is the relative humidity (~), x is position from the surface (m), t is drying time (s) and D_h(RH) is the non-linear moisture diffusion coefficient. It should be noted that this formulation does not consider the influence of self-desiccation which can occur in system with a low water to binder ratio however a term can be added to consider self-desiccation with a term on the right hand side of the equation that is typically related to the degree of hydration. Bazant and Najjar [4] developed a formulation for non-linear water diffusion coefficient (D_h(RH)) and this expression was extended by Xi et al. [22]. While the non-linear water diffusion coefficient is widely used, these expressions have been developed nearly exclusively for systems with conventional pore solution chemistries like those experienced in the majority of typical concretes. The non-linear water diffusion coefficient is discussed in more detail later in this paper. The objective of this paper is to experimentally measure the influence of deicing salt solutions on drying of cementitious materials, specifically as it relates to the non-linear moisture diffusion coefficient.

EXPERIMENTAL DETAILS

Mixture Proportions and Samples Preparation

The mixture proportions of the mortar are presented in Table 1. This mortar represents the mortar fraction of a typical concrete pavement in the state of Indiana.

Table 1: Mortar mixture proportions assuming saturated surface dry (SSD) conditions

Material	Mass
Cement [kg/m^3]	609
Water [kg/m^3]	256
Fine aggregates [kg/m^3]	1418
w/c	0.42

The mixing process began by placing the fine aggregate in a Hobart mixer. Water was then added to the mixture followed by cement. After all materials were placed in the mixer, they were mixed for 3 minutes, followed by a 3 minutes rest and a 2 minutes final mixing in accordance with [2].

For desorption analysis, mortar was cast in cylindrical molds (34 mm of diameter and 50 mm tall). The samples were sealed until they were demolded at 28 days. Thin slices of mortar (0.80 ± 0.05 mm) were cut using a water cooled diamond tipped wafer cut saw and stored at 23° C ± 0.1° C and 50% ± 2% RH, in a CO_2 free chamber. Prior to testing, samples were submerged for 24 hours in aqueous solutions (water, 32% $CaCl_2$, 30% $MgCl_2$ and 23% NaCl) before they were tested.

Experimental setup

The non-linear moisture diffusion coefficient was calculated using a sorption isotherm measured using an automated sorption-desorption analyzer (TGA Q5000) where the samples have subjected to a constant temperature while the relative humidity was varied and the mass recorded as a function of time. The instrument is shown in Figure 2a. A flow of dry nitrogen is separated into two gas streams metered with two mass flow controllers in an insulated aluminum block. One of the gas streams is saturated with water vapor with a humidifier and is then mixed with the dry stream in different proportions so then an RH between 0% and 98% can be generated. The instrument is depicted in Figure 2b.

From the slices submerged in the aqueous solutions, a 50 to 70 mg piece of sample was taken and placed in a tared quartz pan. The balance has an accuracy of ±0.1% over a dynamic range of 100 mg. The relative humidity was then reduced in 10% RH or 5% RH steps to reach 8% RH. The sample was allowed to equilibrate for 12 hours or 0.001% (of initial mass of the sample) change in mass over 15 min at each humidity. The sample was finally dried to 0% RH (pure dry nitrogen purge) to obtain the oven dry condition.

Two different initial conditions were used (series I or II). Series I began by placing the sample in a relative humidity chamber at 23.0 ± 0.01°C and 97.5 ± 1% RH for either 96 hours or until the sample had achieved a stable mass (less than an 0.001% mass change/15 min). Series II began by placing the sample in a relative humidity chamber at 23.0 ± 0.01°C and at the equilibrium relative humidity for either 96 hours or until the sample had achieved a stable mass (less than an 0.001% mass change/15 min). The equilibrium RH was the water activity of the salt solution in which the samples were stored for 24 hours.

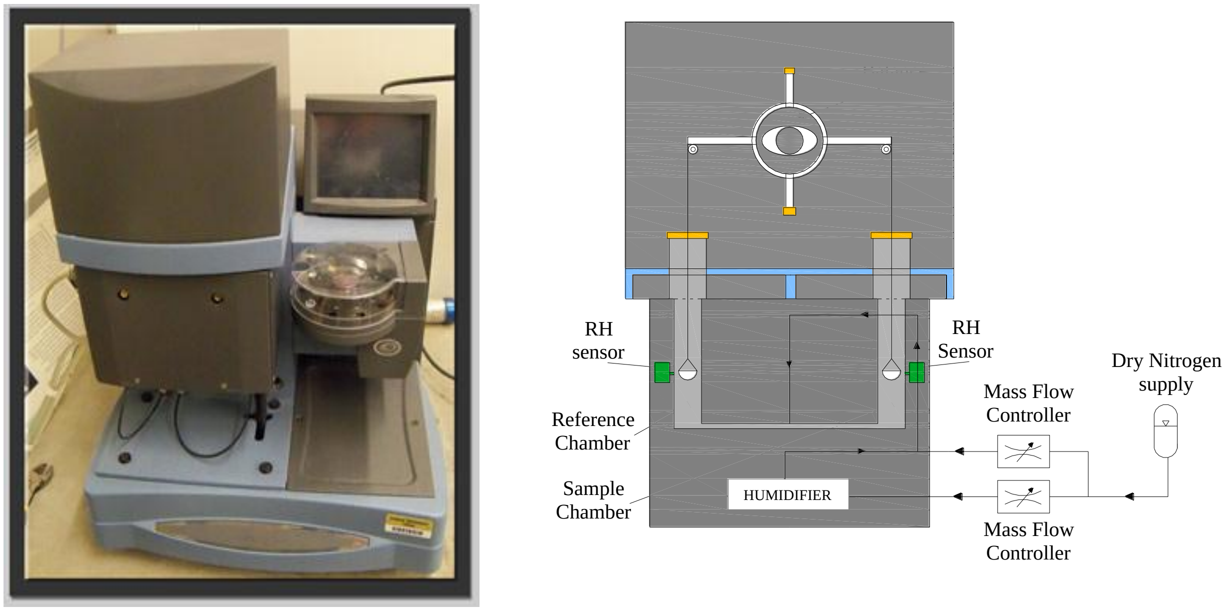

(a) (b)

Figure 2: (a) Automatic sorption/desorption analyzer used in this study, (b) Schematic of the instrument

EXPERIMENTAL RESULTS

Influence of salts on equilibrium relative humidity

Salt solutions can alter transport in cementitious materials. A thermodynamic model has been proposed [6] to describe the influence of the properties of the solution and of the pore structure on the drying process. Benavente et al. [6] defines the Gibbs free energy ΔG for the condensation-evaporation reaction as in Equation (2):

$$\Delta G = RT\ ln\left(\frac{a_w}{RH_{env}}\right) - \frac{2\sigma v_i^0}{r} cos\Phi \qquad (2)$$

where R is the universal gas constant (8.314 N·m/K·mol), T is the temperature (K), a_w is the water activity of the solution (-), RH_{env} is the environmental relative humidity (-), σ is the surface tension (N/m), v_i^0 is the molar volume of the liquid (m^3/mol), r is the pore radius (m) and Φ is the contact angle (deg) which is assumed to be zero [17]. The first term is a measure of the energy of the liquid in a specific environment. The second term involves the properties of the porous media. Equation (2) is derived from the Kelvin-Laplace equation and represents the variation of the saturated vapor pressure with pores size. Imposing the equilibrium of the system (ΔG = 0), a critical relative humidity can be obtained for a salt solution with a given pore size. The boundary between evaporation and condensation (or absorption) can be obtained by rearranging Equation (2) into Equation (3):

$$RH_{eq}(r) = a_w \cdot e^{-\frac{2\sigma v_i^0}{RTr} cos\Phi} \qquad (3)$$

If the environmental relative humidity is lower than RH_{eq} evaporation occurs and the pore will empty, meanwhile if the environmental relative humidity is higher than the critical value of pore size it will remain full (Figure 1).

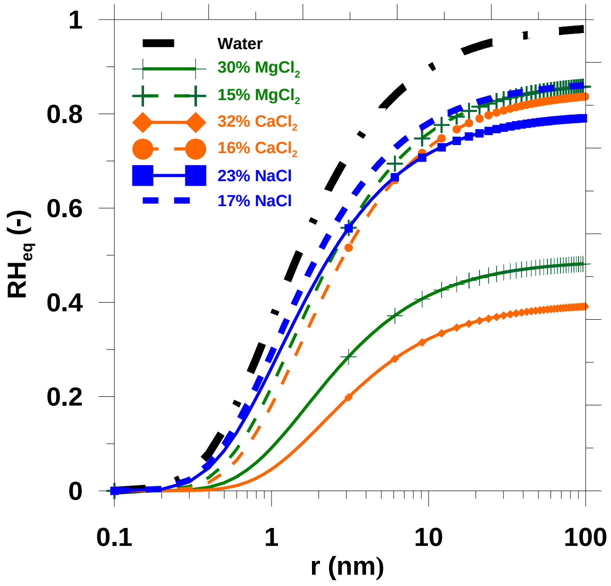

Figure 3: Equilibrium relative humidity as function of the pore radius for different aqueous solutions

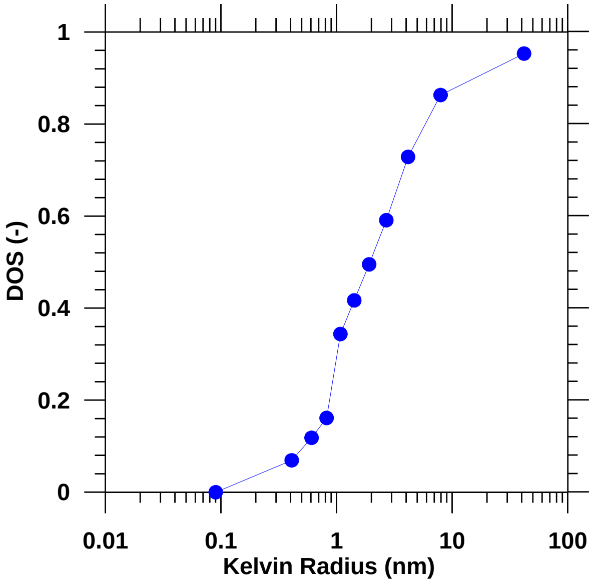

Figure 4: Pore size distribution for 0.42 w/c mortar sample using water vapor desorption

The equilibrium relative humidity (RH_{eq}) was determined using the experimentally measured surface tension [18]. Solution properties are shown in Table 2. The solution properties (i.e., water activities) were determined from experiments assuming a very large pore size. The results are presented in Figure 3 where the equilibrium relative humidity is presented as function of the pore radius (performed using equation 3). All calculation has been done considering the temperature at 23 °C and contact angle equal to 0°. It is interesting to note for example pores with a 100 nm meniscus are full at 52% relative humidity for 30% $MgCl_2$ while at the same humidity the larges pore that is full with only water has a radius that is between 1 and 2 nm. In Figure 4 is also presented the pore size distribution of the mortar used in this study and evaluated through a desorption analysis of a sample saturated in deionized water. Figure 4 illustrates that nearly 70% of the pore volume consists of pores with a radius between 1 and 100 nm. As a result, it is clear that the salt concentration can dramatically alter the degree of saturation.

Table 2: Properties of different salt solutions evaluated experimentally

	Surface Tension (N/m)	Molar Volume (m^3/mol)	Experimental Water Activity (-)
16% $CaCl_2$	0.076	2.51E-05	0.85
32% $CaCl_2$	0.083	3.22E-05	0.40
15% $MgCl_2$	0.074	2.28E-05	0.87
30% $MgCl_2$	0.075	2.77E-05	0.49
17% NaCl	0.076	1.78E-05	0.87
23% NaCl	0.078	1.77E-05	0.80
Water	0.073	1.71E-05	0.99

Influence of salts on desorption response

Figure 5 shows a plot of mass change for mortar samples that were submerged in salt solution and then placed in the desorption testing device. Two different behaviors were observed depending on how the sample was tested (i.e., series I or series II). For series I, the desorption response is evaluated by initially holding the sample at a relative humidity of 98% (which is higher than the RHeq of the salt solution) before drying was initiated. A typical sample from series I can be seen in Figure 5a. An initial gain is observed for the sample in series I due to the hygroscopic effect of salt. This increase in mass can be quite dramatic (over a 70% increase in mass as shown in Figure 5a). Obviously the change in mass cannot be due to water absorption in the sample due to its magnitude. This mass increase appears to be related to water absorption on the sample. It is also interesting to note that the sample appears to ‘break into smaller pieces’ creating more surface area. Once the relative humidity is decreased the mass decreases. The samples in series II are conditioned differently. Instead of starting at a high humidity (e.g., 98%), the samples in series II were equilibrated at a relative humidity that was intended to be equal to the equilibrium relative humidity (RHeq) of the salt solution the sample used to condition the samples. It can be noted that when this was done the mass of the sample did not increase and only small fluctuation in terms of mass can be expected before the drying process starts. The behavior expected is presented in Figure 5b. Unlike the samples from Series I that broke apart during testing the samples in Series II remained intact throughout the test. As a result, series II appeared more appropriate and was used for the testing reported later in this paper.

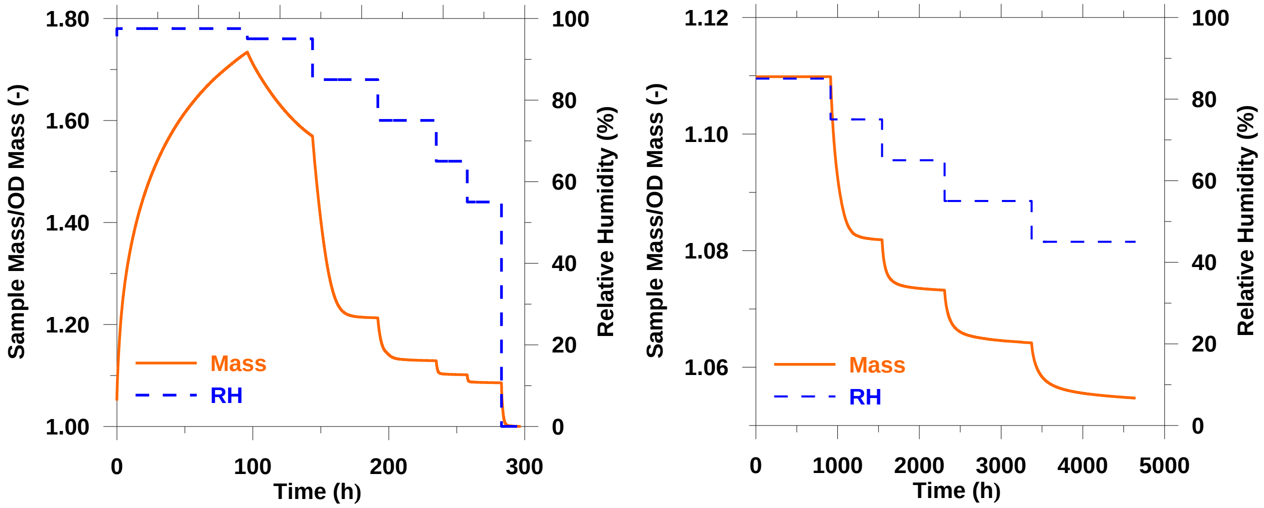

(a) (b)

Figure 5: Desorption response of mortar samples containing salt solution: (a) Series I where the sample (32% $CaCl_2$) was initially equilibrated at 98% RH; (b) Series II where the sample (16% $CaCl_2$) was equilibrated at 85% RH which was equation to RH_{eq} (i.e., 85%)

Figure 6 illustrates the influence of salt presence on the desorption responses. Figure 6a is a conceptual illustration of the pore volume that is occupied by water at a given relative humidity. Two systems are shown: a plain system that contains water in the pores and a system containing a salt solution. While the system with plain water illustrates a behavior that follows the typical desorption response, the sample with salt solution shows that the pores will be saturated at high RH values. Once the RH decreases to RH_{eq} water starts to leave the pore system. This continues until the RH reaches a value of zero which also differs from the plain system in that a volume of salt is left in the pores. Figure 6b shows the mass loss for a system containing water and a system containing different salt solutions. It can be noticed that for low salt solutions the behavior does not vary significantly; however, for higher salt concentrations less water is lost during the evaporation process when salt is present in the system. Figure 5b illustrates that the water does not begin to evaporate until the RH decreases below the RH_{eq}.

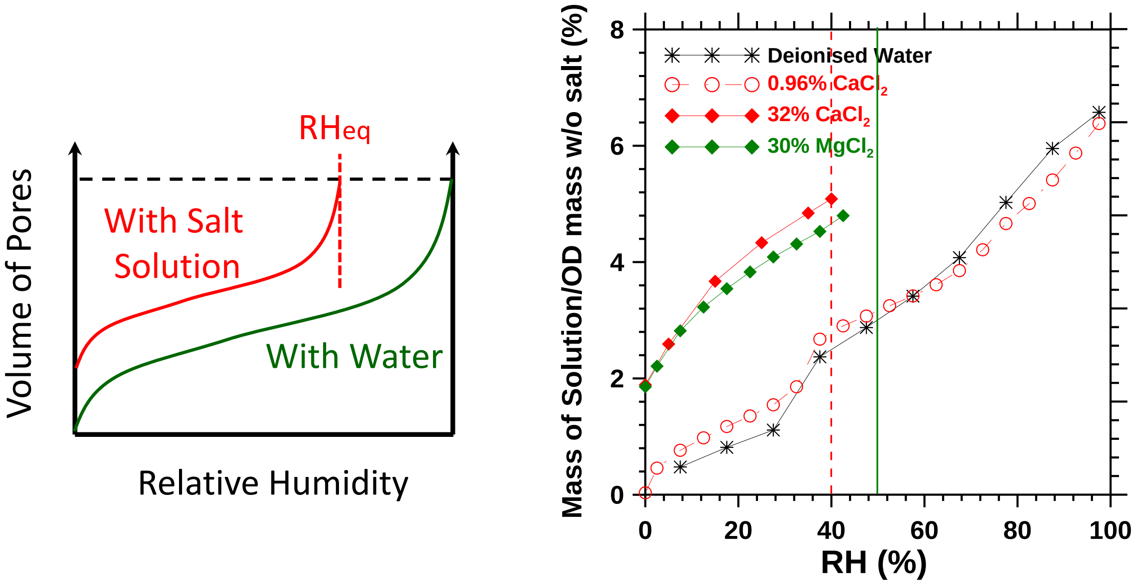

(a) (b)

Figure 6: Desorption Response of calcium chloride, magnesium chloride and pure water. Vertical lines represent the water activity of 32% $CaCl_2$ (dotted line) and 30% $MgCl_2$ (continuous line)

Influence of salts on diffusivity

The desorption data can be used to determine the diffusion coefficient as a function of relative humidity (actually each range of relative humidities tested) by assuming the mortar samples are slab samples drying from the two flat faces [1,13]. The calculation has been done using Equation (4) that enables a diffusion coefficient D_w (m^2/s) to be determined for a given relative humidity range:

$$D_w = \frac{L^2\pi}{16}\left[\frac{\partial}{\partial\sqrt{t}}\left(\frac{\Delta m}{\Delta m_\infty}\right)\right]^2 \qquad (4)$$

where L is the sample's thickness (m), Δm is the mass change (g) at time t (s), Δm_∞ the mass change at equilibrium (g) and $\partial/\partial(\sqrt{t}\,)$ represents the variation with respect to the square root of time. In the diffusivity calculation the mass change was evaluated considering the linear range 10% to 30% of the total mass change in each RH step [1].

The calculated diffusion coefficients shown in Equation 4 were determined with respect to the mass of water or moisture content. Therefore the diffusion coefficient from equation 4 was multiplied by the slope of the sorption isotherm (moisture capacity) to obtain the diffusion coefficient with respect to relative humidity [22]. The diffusion coefficients were plotted as a function of relative humidity and compared with a proposed formulation by Xi et al. [22]. This formulation considers the diffusion process to be a combination of molecular, Knudsen, and surface diffusion. The formula for the non-linear moisture diffusion coefficient D_h(RH) (non-linear with relative humidity) can be written as Equation (5):

$$D_h(RH) = \alpha_h + \beta_h\left[1 - 2^{10^{\gamma_h(RH-1)}}\right] \tag{5}$$

where α_h, β_h, and γ_h are coefficients. In particular: α_h represents asymptotic diffusion coefficient at low humidity level, $\beta_h/2$ is difference in the diffusion coefficient between low and high relative humidities. The γ_h factor is related to the shape of the diffusion coefficient (Figure 7).

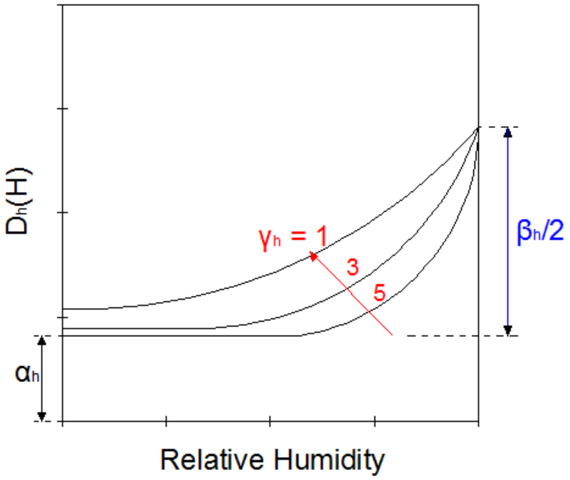

Figure 7: Graphical representation of Equation (5) after Xi et al. [22]

This model was applied to the experimental results and the parameters for each sample were evaluated. In Figure 8 the diffusion coefficients are shown for each range of relative humidity. It is apparent that in presence of salt there is a substantial shift of the diffusion coefficient-RH curve towards lower values of humidity that increases with salts concentration. The vertical straight lines represent the equilibrium relative humidities (or water activities) evaluated experimentally.

Equation (6) was modified as shown to account for the change in RH_{eq} that occurs for each salt.

$$\begin{aligned} &RH > RH_{eq} && D_h(RH) = 0 \\ &RH \leq RH_{eq} && D_h(RH) = \alpha_h + \beta_h\left[1 - 2^{10^{\gamma_h(RH-RHeq)}}\right] \end{aligned} \tag{6}$$

The curve was fit using a least-squares method to determine the fitting parameters. The best fit-parameters from Equation (6) are presented in Table 3.

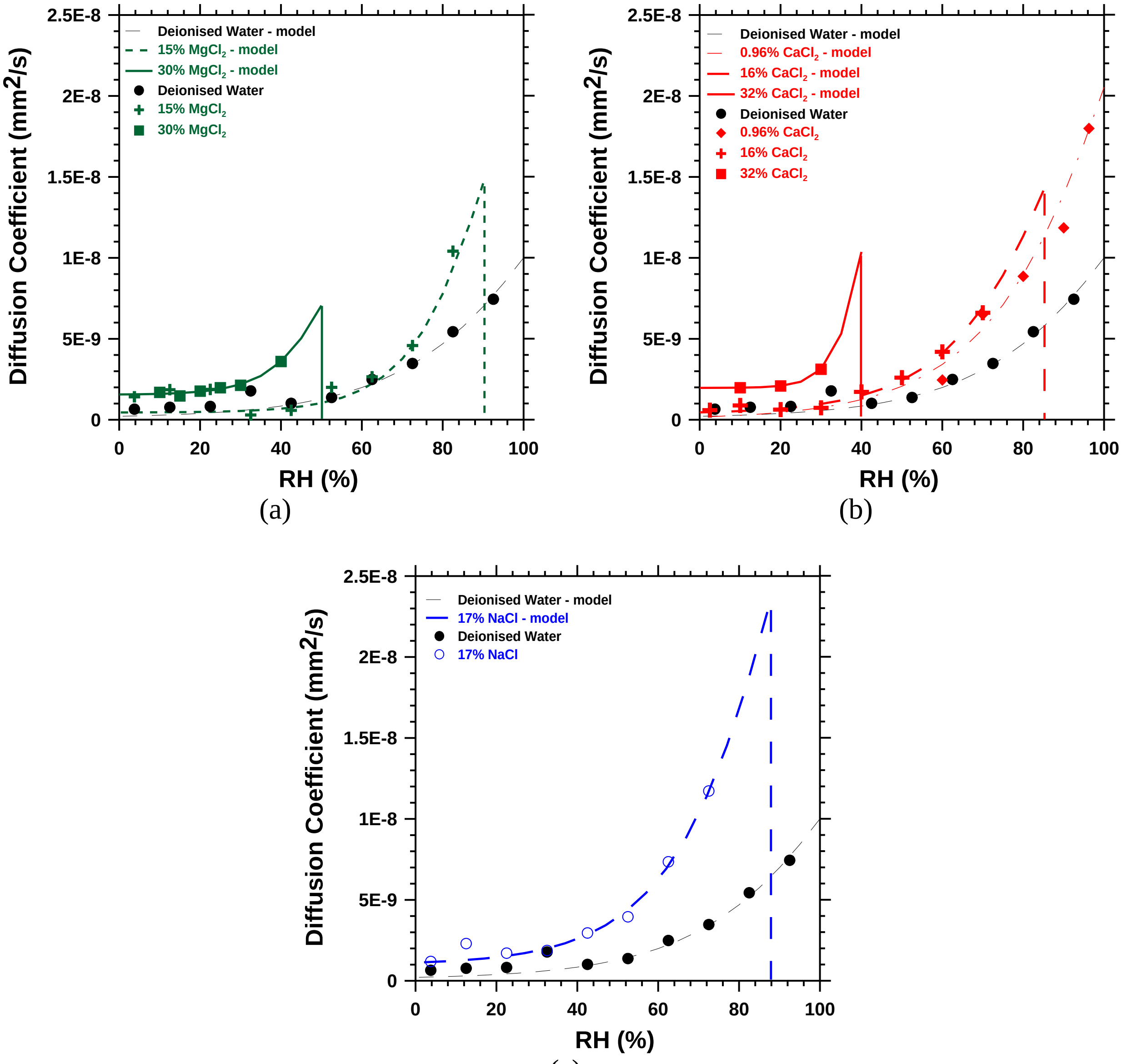

(a) (b)

(c)

Figure 8: Diffusion coefficient versus relative humidity for (a) Magnesium Chloride solutions, (b) Calcium Chloride solutions and (c) Sodium Chloride solutions

A few trends can be observed when a reference is submerged in tap water as well as salt solutions of varying concentration. The diffusion coefficient at low relative humidity (α_h) tends to increase as the concentration of salt increases. This may be due to the salt competing with absorption on the pore walls for the low relative humidity levels. Conversely, the diffusion coefficient at the high relative humidities (β_h) decreases with increasing salt concentration. Finally, the shape of the effective diffusivity curve becomes steeper when the salt concentration increases; accordingly the γ_h coefficient increases.

Table 3: Fit-parameters for diffusion coefficients for samples containing different salt solutions

		α_h (m^2/s)	β_h (m^2/s)	γ_h (-)	R_2
Salts solutions in pores	Tap water	0.0108	1.9814	2.1003	0.9956
	$MgCl_2$ - 15%	0.0444	2.3737	3.9007	0.9869
	$MgCl_2$ - 30%	0.1545	1.0131	5.4038	0.9829
	$CaCl_2$ - 0.96%	0.0018	3.9595	2.2765	0.9637
	$CaCl_2$ - 16%	0.0359	2.7580	2.7060	0.9971
	$CaCl_2$ - 32%	0.1968	1.6797	9.8892	1
	NaCl - 17%	0.0992	4.3585	2.7011	0.9987

CONCLUSIONS

This study investigated the influence of absorbed deicing salt solutions on the drying of cementitious materials. The main findings of this experimental investigation are:

- The presence of deicing salts changes the properties of the solution in the pores. Most notably the equilibrium relative humidity, viscosity (mentioned in [18]), and surface tension change when deicing salt is absorbed into the concrete. A thermodynamic model was used to relate the properties of the fluid to the equilibrium relative humidity and pore structure. The equilibrium relative humidity decreased with salt concentration.
- Desorption analysis confirms the increase in the degree of saturation of the material in presence of salts. This effect was shown to be function of the salt composition and of the concentration of the solution.
- The non-linear moisture diffusion coefficient ($D_h(H)$) was evaluated. The experimental data was able to be fitted using the model proposed by Xi et al. [22]. The diffusivity versus relative humidity curves tend to shift to lower RH values and to cover a narrower range of humidities starting from the equilibrium relative humidity.
- The results are in agreement with observations in [18] that illustrate that samples with high concentrations of salt do not show a reduction in sample mass until the RH decreases below RH_{eq}. In fact, samples may gain mass at high RH due to the hygroscopic nature of the salt. As a result, samples containing deicing salt solutions are likely to have a higher degree of saturation than samples without deicing salt solutions in practice.

In conclusion, the results of this study show the importance of considering the properties of solutions when describing drying (i.e., in presence of salts or other chemical species).

ACKNOWLEDGEMENTS

The authors gratefully acknowledge support from the Indiana Department of Transportation through the Joint Transportation Research Program and through the national concrete consortium as a part of DTFH61-06-H-00011 (Work Plan 26). Any opinions, findings, and conclusions or recommendations expressed in this material are those of the author(s) and do not necessarily reflect the views of a sponsoring agency.

REFERENCES

1. A. Anderberg and L. Wadsö, Method for simultaneous determination of sorption isotherms and diffusivity of cement-based materials, *Cement and Concrete Research*, Vol. 38 (2008), pp. 89-94

2. ASTM International, ASTM C192. Standard Practice for Making and Curing Concrete Test Specimens in the Laboratory; 2007

3. Z. P. Bazant and L. J. Najjar, Drying of concrete as a nonlinear problem, *Cement and Concrete Research*, Vol. 1 (1971), pp. 461-473

4. Z. P. Bazant and L. J. Najjar, Nonlinear water diffusion in nonsaturated concrete, *Matériaux et Constructions*, Vol. 5 (1972), pp. 3-20

5. D. Benavente, M.A. García del Cura, A. Bernabéu, and S. Ordonez Quantification of salt weathering in porous stones using an experimental continuous partial immersion method, Engineering Geology, Vol. 59 (2001), pp. 313-325

6. D. Benavente, M.A. García del Cura and S. Ordonez, Salt Influence on evaporation from porous building rocks, *Construction and Building Materials,* Vol. 17 (2003), pp. 113-122

7. D. Camuffo, Condensation-Evaporation cycles in pore and capillary systems according to the Kelvin model, *Water, Air and Soil Pollution*, Vol. 21 (1982), pp. 151-159

8. J. Castro, P. Lura, F. Rajabipour, R. Henkensiefken and J. Weiss, Internal curing: discussion of the role of pore solution on relative humidity measurements and desorption of lightweight aggregate, ACI SP-270 Advances in the Material Science of Concrete (2010), pp. 89-100.

9. S. Jacobsen, J. Marchand, L. Boisvert, M. Pigeon and E. Sellevoid, Frost deicer salt scaling testing of concrete: Effect of drying and natural weathering, *Cement, Concrete and Aggregates*, Vol. 19 (1997), pp. 8-16

10. W. Li, M. Pour-Ghaz, J. Castro and W.J. Weiss, Water absorption and critical degree of saturation as it relates to freeze-thaw damage in concrete pavement joints, *Journal of Materials in Civil Engineering*, Vol. 24 (2011), pp. 299–307.

11. G.G. Litvan and P.J. Sereda, Freeze-thaw durability of porous building materials, Durability of Building Materials and Components, ASTM STP 691, ASTM International, West Conshohocken, PA, (1980) pp. 455–463.

12. P. Lura, B.J. Pease, G. Mazzotta, F. Rajabipour, W.J. Weiss. Influence of shrinkage reducing-admixtures on the development of plastic shrinkage cracks. *ACI Materials Journal*, Vol. 104 (2007), pp. 187-194.

13. M. Pour-Ghaz, R. Spragg and J. Weiss, Moisture profiles and diffusion coefficient in mortars containing shrinkage reducing admixtures, *International RILEM Conference on Use of Superabsorbent Polymers and Other New Additives in Concrete*, 15-18 August 2010, Technical University of Denmark, Lyngby, Denmark

14. E. Samson and J. Marchand, Modeling the effect of temperature on ionic transport in cementitious materials, *Cement and Concrete Research*, Vol. 37 (2007), pp. 455-468.

15. G. W. Scherer, The drying process, Journal of the American Ceramic Society, Vol. 73 (1990), pp. 3-14

16. G. W. Scherer, Crystallization in pores, *Cement and Concrete Research*, Vol. 29 (1999) pp. 1347–1358

17. A. Selander, Hydrophobic impregnation of concrete structures. Effect on concrete properties, Ph.D. Thesis, Royal Institute of Technology, Stockholm, Sweden

18. R. Spragg, J. Castro, W. Li, M. Pour-Ghaz, P.T. Huang and J. Weiss, Wetting and drying of concrete using aqueous solutions containing deicing salts, Cement and Concrete Composites, Vol. 33 (2011), pp. 535-542

19. L. Sutter, K. Peterson, G. Julio-Betancourt, D. Hooton, T. Van Dam and K. Smith, The deleterious chemical effects of concentrated deicing solutions on Portland cement concrete, *South Dakota Department of Transportation. Final report*. (2008)

20. K. Wang, D. Nelsen and W. Nixon, Damaging effects of deicing chemicals on concrete materials, *Cement and Concrete Composites*, Vol. 28 (2006), pp. 88-173.

21. W. J. Weiss, K. A. Snyder, J. W. Bullard and D. P. Bentz, Using a Saturation Function to Interpret the Electrical Properties of Partially Saturated Concrete, *Journal of Materials in Civil Engineering* (2012), accepted

22. Y. Xi, Z. P. Bazant, L. Molina and H. M. Jennings, Moisture diffusion in cementitious materials. Moisture capacity and diffusivity, *Advanced Cement Based Materials,* Vol. 1 (1994) pp. 258-266

The Influence of Deicing Salt Exposure on the Gas Transport in Cementitious Materials

C.Villani[1], T.Nantung[2] and W.J. Weiss[1*]

[1]Purdue University, USA
[2]Indiana Department of Transportation, USA
[*] Purdue University, School of Civil Engineering, 550 Stadium Mall Drive,
West Lafayette, IN 47906, USA

cvillani@purdue.edu, tnantung@indot.IN.gov, wjweiss@purdue.edu

ABSTRACT

The gas transport properties of concrete can provide information that can be used in the prediction of the service life of concrete facilities. However, to interpret the transport properties properly, some corrections may be needed since the gas transport properties are known to be strongly related to the moisture content and the distribution of moisture in the concrete. This paper investigates the influence of deicing salts on the gas permeability and gas diffusivity of mortar. Specifically, oxygen permeability and oxygen diffusion were examined for mortar samples that were initially saturated with different deicing salt solutions and then exposed to drying. The deicing salt solutions were found to influence the degree of saturation and as such they influenced the gas transport properties. Mortar containing deicing salts had lower permeability and diffusivity due to higher degree of saturation, compared to samples saturated with pure water. These findings were further confirmed through the evaluation of the desorption spectra of samples saturated in aqueous solution containing salts. This study suggests that care must be taken when performing investigations using concrete that may have been previously exposed to deicing salts either in situ or when this concrete is taken back to the laboratory.

Keywords. Deicing salts, gas transport, degree of saturation, desorption

INTRODUCTION

A considerable portion of building materials research focuses on the study of the durability. In concrete research, a large portion of research has focused on developing transport tests that can be used for service life prediction. Specifically, gas permeability and gas diffusivity measurements have attracted the interest of the concrete community due to their quasi-non-destructive nature, the short testing time that is required to perform the test (Kropp & Hilsdor, 1995), and the high reproducibility of the results (Abbas et al., 1999). Moreover, several methods have been developed to measure in-situ the gas permeability of concrete (RILEM TC 189, 2007) (Figg, 1973) (Hong & Parrott, 1989) (Basheer et al., 2001) (Torrent, 1992).

The description of gas transport is complex and three distinct mechanisms are considered to occur simultaneously or independently. These mechanisms include 1) free-molecule or Knudsen diffusion, 2) molecular or ordinary diffusion and 3) surface diffusion (Sercombe et al., 2007). Each mechanism is not completely understood but there is some evidence that it is greatly affected by total pressure, temperature, type of gas considered and properties of pore structure available to gas, in terms of pores size and pores connectivity (Sercombe et al., 2007), (Houst & Wittmann, 1994).

In the literature many studies have focused on the analysis of the parameters that influence gas transport and gas transport testing. It has been shown that porosity and tortuosity can greatly influence the gas permeability and diffusivity measurements (Wong et al., 2006), (Wong et al., 2009). From the idealized gas theory, gas permeability varies with pore diameter squared (Dullien, 1992) while gas diffusivity in large pores is independent of the pore size (Mason & Malinauskas, 1983) (Garboczi, 1990). It is important to note however that this depends on both the total porosity and the vapor filled porosity. This points to the fact that the gas transport properties are strongly dependent on the amount of moisture and on its distribution inside the concrete element (Abbas et al., 1999) (Houst & Wittmann, 1994). For specimens with a higher moisture content, the thickness of the layer of moisture that covers the pores walls increases (Hagymassy et al., 1969) (Badmann et al., 1981) causing the decrease of the mean free path of gas molecules (Xi et al., 1994) and the reduction of gas transport (Abbas et al., 1999). It has been shown that a reduction in gas transport is considerable when the degree of saturation is greater than 60% since the pores relevant for transport process are increasingly filled as the degree of saturation increases (Parrott, 1994) (Ollivier et al., 1995).

Many concrete structures are exposed to salts due to either a marine environment or the application of deicing salts to pavements (Spragg et al., 2011), bridge decks (Wallbank, 1989), or parking lots. The presence of deicing salt is known to influence the durability performance of concrete structures. Evidence of salt deterioration has been reported in masonry structures (Lubelli et al., 2004), building stones (Birginie et al., 2000), coastal structures (Berke & Hicks, 1991) and concrete elements (Sutter et al., 2006).

Several mechanisms may be associated with deicing salt damage including pressure that develops due to osmosis, crystallization, intermediate compounds, or the increase of the risk of frost damage due to the increase in the degree of saturation (Litvan, 1976), (Li et al., 2012) (Scherer, 1999) (Scherer December 2011, Personal Communication). Salts are also responsible of chemical interaction within the concrete, resulting in leaching and decomposition of the hydrated cement products, accelerated concrete carbonation, or alkali-silica reaction (Wang et al., 2006) (Rangaraju et al., 2005). This paper will focus on the potential influence of deicing salts on the gas transport properties.

The effect of salts on gas transport properties has been studied for rocks (Peysson et al., 2011) (Birginie et al., 2000) (Giorgis et al., 2007). However, very few studies can be found that investigate the influence of salt on gas transport for concrete. One study was found where salt saturated concretes were preferentially used to help the concrete for use in transuranic waste repository (Pfeifle & Hansen, 1995) (Davies, 1991).

The presence of deicing salts alters gas transport due to two primary reasons. First, the salts can change the moisture content (degree of saturation) and moisture distribution in the pore structure of the cementitious system. It is known that deicing salts change the density, viscosity, surface tension, and water activity of the solution (Spragg et al., 2011). Salts change the drying process (Villani et al., 2012) and alter the equilibrium relative humidity of the pore solutions (Benavente et al., 2003) (Villani et al., 2012). Consequently, samples containing deicing salt are likely to have a higher degree of saturation when compared with a sample containing water at the same relative humidity (Villani et al., 2012) (Castro et al., 2011) (Litvan, 1976). Since the degree of saturation is higher in systems containing salts, a lower gas permeability/diffusivity can be expected (Abbas et al., 1999). Second, the salt can precipitate in the pores (Scherer, 1999). In cementitious systems that initially contain salt solutions, it is known that when the water evaporates the solution becomes more concentrated. The concentration gradient generated causes the salt to begin to diffuse in the concrete, tending to homogenize the salt profile (Scherer, 2003). If however the convective flow is much higher compared to the diffusive flow (Peysson et al., 2011), the system will results in non-homogeneous salts distribution. Non-linear slat distributions can also develop if the sample has a moisture gradient before the deicing salt is introduced.

This paper investigates the influence of deicing salts on gas permeability and gas diffusivity measurements on mortar samples. The effect of moisture content (degree of saturation) and salt precipitation on gas permeability and diffusivity will be investigated.

MATERIALS AND SAMPLES PREPARATION

Gas permeability, gas diffusivity and desorption tests were performed using mortar. The mortar had a water-to-cement ratio of 0.42 with 55% aggregate by volume. The mixing procedure was in accordance with ASTM C 192.

For gas permeability and gas diffusivity, cylindrical samples (diameter of 102 mm (4 in.) and length of 204 mm (8 in.)) were prepared. The samples were demolded at an age of 24-hours and then sealed in double plastic bags for approximately 12 months. The cylinders were then cored using a 68 ± 2 mm diameter bit. The samples were then cut using a wet saw to obtain samples with a height of 25 ± 2 mm (1 in.) for oxygen permeability measurements. For oxygen diffusivity measurements larger samples were used. The oxygen diffusion samples were obtained from 102 by 204 mm cylinders (4x8 in.) using a wet saw to obtain samples with 102 mm (4 in.) of diameter and 50 mm (2 in.) length.

A total of 16 samples were prepared for oxygen permeability and 8 samples were prepared for oxygen diffusivity. Specimens were initially oven dried at 50° ± 0.5° C and 30% ± 1% RH until constant mass and subsequently submerged in four different aqueous solutions: deionized water, 16% calcium chloride ($CaCl_2$), 15% magnesium chloride ($MgCl_2$) and 17.5% sodium chloride (NaCl). In each solution, four oxygen permeability samples and two oxygen diffusivity samples were placed and kept submerged until their mass reached the equilibrium ($\Delta m < 0.2\%$ within 7 days). The specimens were then conditioned in a temperature and humidity controlled chamber at 65%°±1% RH and at 23° ± 0.5° C until equilibrium ($\Delta m < 0.1\%$).

For desorption analysis, smaller cylinders (34 mm of diameter and 50 mm tall) were prepared. The samples were sealed after casting and remained sealed until demolding (at 28 days). Thin slices of mortar (0.80 ± 0.05 mm) were cut from the cylinder using a water cooled diamond tipped wafer cut saw. The slices of material were stored at 23° C ± 0.1° C and 50% ± 2% RH, in a CO_2 free chamber. Prior to testing, samples were submerged for 24 hours in aqueous solutions (water, 16.0% calcium chloride $CaCl_2$, 15.0% magnesium chloride $MgCl_2$, and 17.5% sodium chloride NaCl) before they were tested.

TESTING METHODS AND ANALYSIS

Oxygen Permeability

The oxygen permeability has been measured using a falling head permeameter (Ballim, 1991) (Alexander et al., 1999), commonly known as the South African permeability apparatus. A picture of the South African test apparatus is shown in Figure 1. The South African test involves the measurement of a unidirectional flow of gas through the specimen due to the presence of a pressure gradient between the upper and the lower side of the sample. The bottom surface of the sample is in contact with the oxygen contained in the vessel at a known pressure, while the top surface is at the atmospheric pressure. The sides of the sample are sealed using a compressed rubber collar to insure unidirectional flow. The gas flow is quantified by monitoring the pressure drop with time, with the pressure of the initial time of 100 kPa. The pressure is monitored for a 6 hours period (or until the pressure has decreased to a pressure of 50 kPa (Alexander et al., 1999)).

The oxygen permeability (k) can be evaluated by combining D'Arcy's law for the case of flow of compressible gas with the ideal gas law as shown in Equation (1) (Ballim, 1991):

$$k = \frac{\omega \cdot V \cdot g \cdot d}{R \cdot A \cdot T} \cdot \frac{1}{t} \cdot ln\left(\frac{P_0}{P}\right) \qquad (1)$$

where ω is the molecular mass of oxygen (0.032 kg/mol), V is the volume of oxygen under pressure, which is precisely known from the instrument manufacturer (m^3), g is the acceleration due to gravity (9.81 m^2/s), R is the universal gas constant (8.314 N·m/K·mol), A is the cross sectional area of the sample (m^2), d is the sample thickness (m) and T is the absolute temperature, 296.15° K (23±1° C). The term *[(1/t)·ln(Po/P)]* has been evaluated according to Alexander et al. (1999) considering a linear regression curve that is forced to pass through the origin of the *ln(Po/P)* versus t plot.

Figure 1: Oxygen permeability – South African instrument

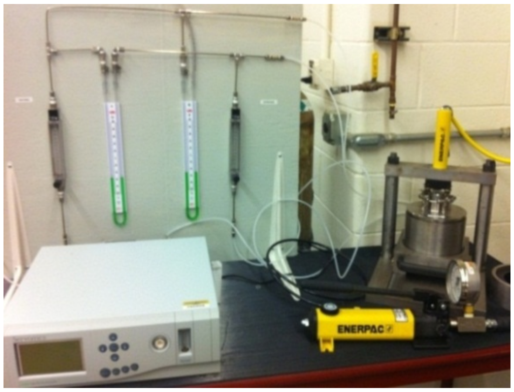

Figure 2: Oxygen diffusivity test device

Oxygen Diffusivity Tests

The oxygen diffusivity was measured using an instrument originally developed by Lawrence et al. (1984).

The samples used for oxygen diffusivity testing are fitted in a silicon rubber ring that is compressed to provide a condition that insures unidirectional flow. The test is performed by exposing one surface of the disc to a stream of pure oxygen and the opposite face to a stream of pure nitrogen at the same pressure. The oxygen and nitrogen gasses counter diffuse through the sample and the oxygen concentration in the outlet cell is measured with a zirconia analyzer (Servomex 4100) at 0, 10, 20, 60 and 90 minutes as shown in Figure 2.

To compute the oxygen diffusivity from the test it is assumed that oxygen is transported in concrete by ordinary and Knudsen diffusion (Schwiete et al., 1969). Equation (2) has been developed based on Fick's law which enables an average diffusion coefficient (D_N) as shown (Lawrence, 1984):

$$D_N = \frac{RT}{P}\frac{Q_{mol/s} \cdot L}{A \cdot \Delta C} = \frac{Q_{m^3/s} \cdot L}{A \cdot \Delta C} \qquad (2)$$

where $Q_{mol/s}$ *or* $Q_{m3/s}$ is the rate of oxygen diffusion at atmospheric pressure, either (mol/s) or (m^3/s) respectively, L the thickness of the sample (m), A the cross section area of the sample (m^2) and ΔC is change in concentration through the specimen (%). The change in concentration ΔC is evaluated considering the flow rate of oxygen and the flow rate of nitrogen, the pressure of the gas stream, and the initial and final concentration of oxygen.

Desorption

Desorption isotherms have been measured using an automated sorption/desorption analyzer (TA Q5000) where the samples have been subjected to drying at a constant temperature over a range of relative humidity. The relative humidity between 0% and 98.5% are generated by mixing dry and wet nitrogen streams. The schematic of the instrument is shown in Figure 3.

The 50 to 70 mg samples were submerged in an aqueous solution before being placed in a tared quartz pan. The pan was then suspended in a relative humidity chamber to equilibrate at 23.0 ± 0.1°C and at the equilibrium relative humidity for up to 96 hours or until the sample had achieved a stable mass (less than an 0.001% mass change/15 min). The equilibrium RH is the water activity of the deicing salt solution in which the samples were stored for 24 hours (85.0% for 16.0% calcium chloride solution ($CaCl_2$), 87% for 15.0% magnesium chloride ($MgCl_2$) solution and 87% for 17.5% sodium chloride solution (NaCl) (Spragg et al., 2011). The relative humidity was then reduced in 10% RH steps until 5% RH, allowing the sample to equilibrate (12 hours or 0.001% change in mass over 15 min) at each humidity. After that the sample was dried to 0% RH.

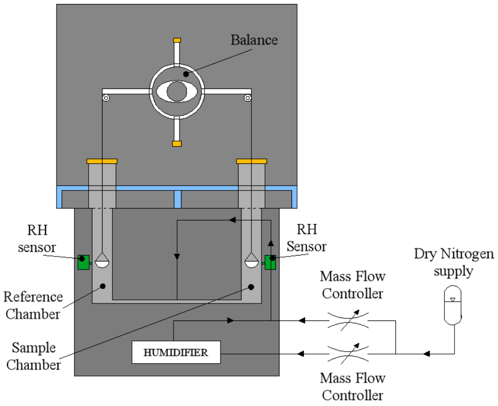

Figure 3: Schematic of automatic sorption/desorption analyzer

RESULTS AND DISCUSSION

Oxygen Permeability and Oxygen Diffusivity Results

Oxygen permeability results are presented in Figure 4 while oxygen diffusivity results are shown in Figure 5. The error bars shown in Figure 4 and Figure 5 indicate the variability (in terms of standard deviation) between four samples for oxygen permeability and between two samples for oxygen diffusivity. The results shown in Figure 4 and in Figure 5 are presented as function of the degree of saturation in Figure 6 and in Figure 7.

The degree of saturation (DOS) has been calculated by dividing the mass of solution (water or salt solution) present in the sample at the moment of the test, over the mass of solution at saturation. As a result, when a sample that contains a salt solution is completely dried (i.e., 0% RH) the degree of saturation is not zero and this could be expected since salt will remain in the system and the difference is relate to the mass of the salt crystals.

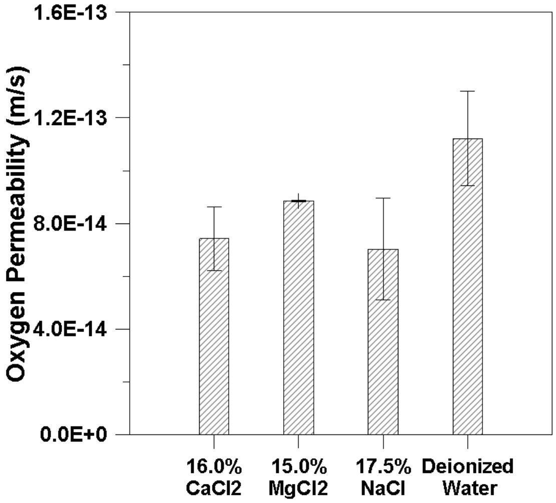

Figure 4: Oxygen permeability results

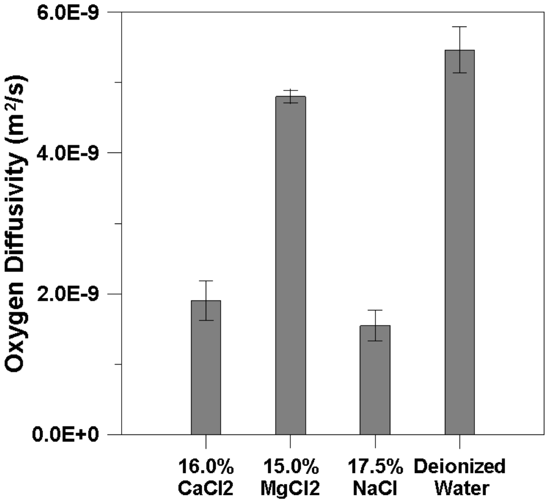

Figure 5: Oxygen diffusivity results

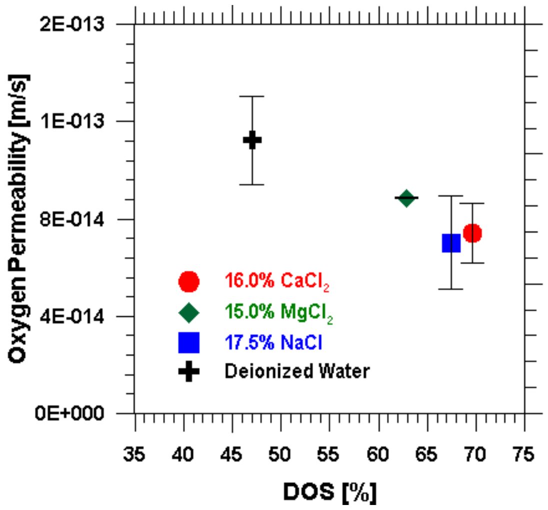

Figure 6: Oxygen permeability versus degree of saturation (DOS)

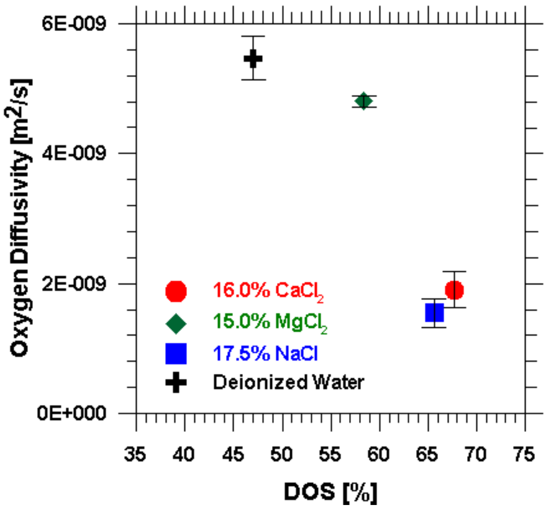

Figure 7: Oxygen diffusivity versus degree of saturation (DOS)

Table 1: Oxygen permeability and oxygen diffusivity values and test parameters

	Oxygen Permeability	Oxygen Diffusivity		
	k (m/s)	D_N (m/s)	Pressure (bar)	Oxygen Flow rate (ml/min)
16.0% $CaCl_2$	7.42E-14	1.90E-09	1.0005	55
15.0% $MgCl_2$	8.85E-14	4.80E-09	1.0006	55
17.5% NaCl	7.03E-14	1.55E-09	1.0005	55
Water	1.12E-13	5.47E-09	1.0006	55

It is apparent from Figures 4 to 7 that the presence of deicing salts increases the degree of saturation. As the degree of saturation increases a reduction is observed for the oxygen permeability and diffusivity. A sudden decrease in the case of oxygen diffusivity (Figure 7), can be seen when the DOS is higher than 60% since the main pores involved in gas transport are becoming filled and disconnected. This is in accordance to previous research results that related the degree of saturation with transport properties (Abbas et al., 1999).

The difference in the magnitude of the decrease in the oxygen permeability compared to oxygen diffusivity is likely related to the different sensitivity that occurs between the two instruments. Since it has been shown (Villani et al. - In preparation) that the oxygen diffusivity apparatus is more effective in capturing even small differences among materials, showing also higher repeatability. Moreover, the higher influence of pore size for oxygen permeability compared to oxygen diffusivity in large pores might have also affected the results.

The difference in DOS seen in the case of magnesium chloride may also be due to an alteration of the cement paste structure. Magnesium (Mg^{2+}) and chloride (Cl^-) ions tend to deplete calcium hydroxide ($Ca(OH)_2$) forming magnesium hydroxide $Mg(OH)_2$ and calcium chloride. (Sutter et al., 2006). Further the magnesium may substitute for the calcium in calcium silicate hydrate. It is however believed that for the samples tested in this study that this would have little impact.

Influence of Deicing Salts on the Desorption of Samples

The higher degree of saturation seen in Figure 6 and Figure 7 can be explained by the drying of mortar containing deicing salts. The drying behavior was examined using desorption tests conducted on mortar samples.

The results presented in Figure 8 show the mass of solution (i.e., the mass of the salt and water) in the sample as function of relative humidity. It should be noted that the tests were initiated by equilibrating the sample at the equilibrium relative humidity of the solution to ensure that drying occurs at the beginning of the test (Villani et al., 2012).

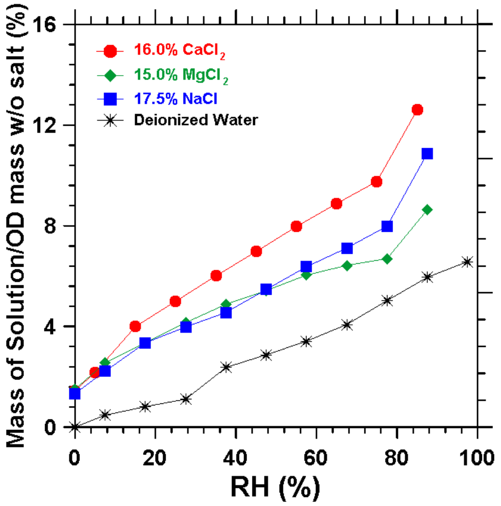

Figure 8: Desorption curves for mortar samples submerged in salt water solutions

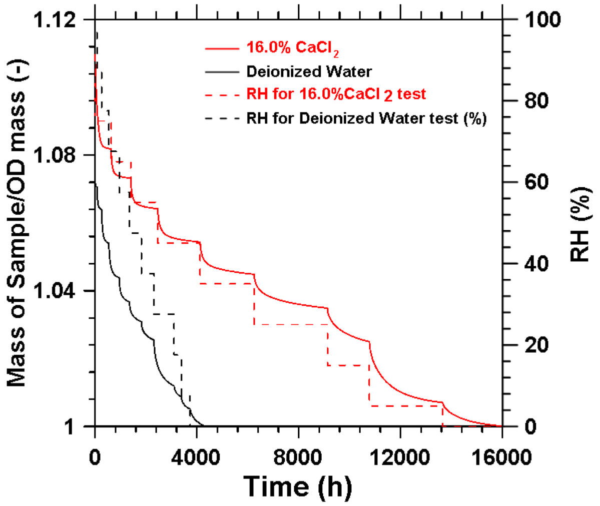

Figure 9: Mass change during each RH step for samples submerged in 16% calcium chloride and deionized water. Solid lines show the change in mass, while dashed lines show the RH steps.

It can be seen that for a given relative humidity (RH) the amount of solution in the samples that contain salt is higher than it is for samples containing only water. During drying, water evaporates from the solution while salts remain in the samples. Consequently, an increase in salt solution concentration occurs during drying as shown in Figure 10. The total amount of salt, with respect to the oven dry mass of the sample, corresponds to the point at 0% RH of the relative curve in Figure 8.

A slower drying process occurred when salts are present due primarily to the ionic interaction between solute (salts) and solvent (water) (Benavente et al., 2003). The ionic interaction reduces the water loss in a given time period, when compared to drying of samples containing only water. This behavior was noticed during the desorption analysis as samples containing salts showed an average equilibrium time (for each RH step) 2 to 5 times longer than the sample with only water (Figure 9). This change has been shown in the diffusion coefficient for a wider range of deicing salts and salt solutions (Villani et al., 2012).

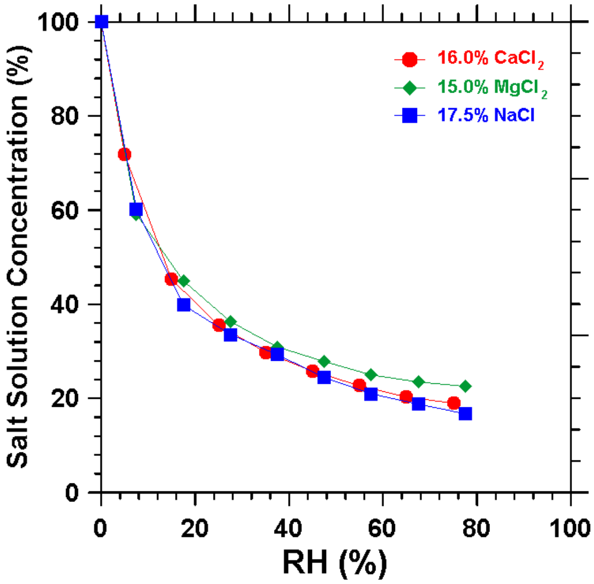

Figure 10: Salt solution concentration as a function of drying

The slower rate of drying that occurs when salts are present is also related to the change in the equilibrium relative humidity of the solutions (Benavente et al., 2003) (Villani et al., 2012). The reduction of the equilibrium relative humidity is a consequence of the change in the liquid properties in terms of surface tension, molecular volume and activity for solution containing salts compared to pure water. For a system initially saturated, the decrease in equilibrium relative humidity causes a delay in the initiation of drying (as RH is decreased) since the drying will start only when the external relative humidity is lower than the equilibrium relative humidity of the solution in which the sample was saturated. This is true assuming the same pore structure for the samples tested. If the relative humidity is higher than the equilibrium relative humidity the sample may gain mass due to hygroscopic nature of salts (Koelhler et al., 2006) (Spragg et al., 2011) (Villani et al., 2012).

Salt distribution analysis

As mentioned in the introduction, the decrease of gas permeability and diffusivity in presence of deicing salts might be due also to the salts precipitation in the pores during drying. To investigate this, chloride profiles were determined from samples previously used for oxygen diffusivity measurements. The samples were ground with a milling machine using diamond tipped drill bit and the powders was collected every 2 mm depth. The chloride content was then measured using an automated titration procedure, which is a modification of AASHTO T260 (Di Bella et al., 2012). The results and the distribution of salts inside the sample are pictured in Figure 11.

It should be mentioned that although the samples were totally submerged and all surfaces were exposed to solution, the analysis of chloride distribution has been done only in the direction of gas flow (along the height of the cylinder). The influence of lateral absorption is assumed constant for all depths.

A similar trend in the chloride profile can be observed for the three salts. A higher salt concentration occurs in the first 15 mm and the inner core (20 mm) shows a uniform salt distribution. Since the samples have reached equilibrium while submerged in solution, we expect the solution have saturated the all sample and consequently the non-uniform distribution has been generated during drying (wicking action). A more uniform salt distribution could be expected if the samples, after drying, were sealed for months allowing moisture and salts redistribution. The conditioning process used in this study is however more representative of what happens in real concrete structures.

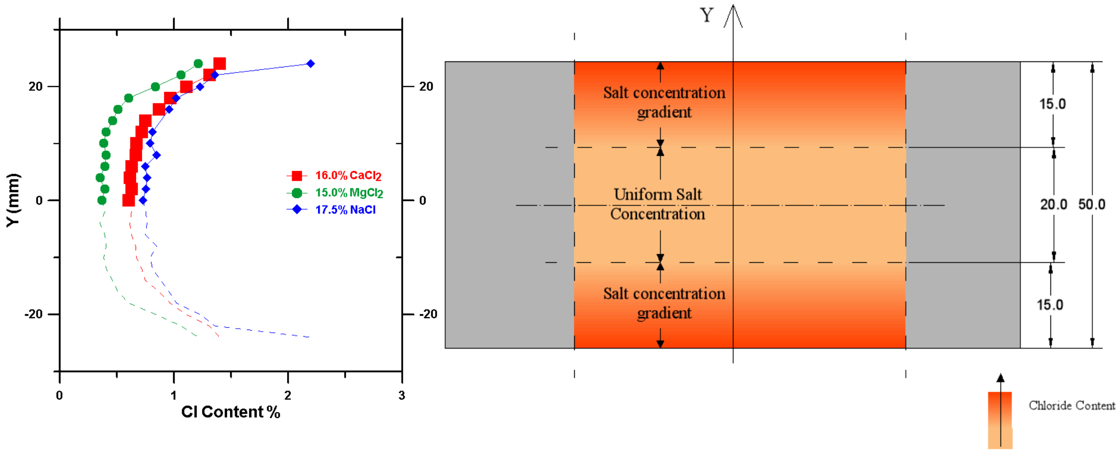

Figure 11: Chloride Profiles in Oxygen Diffusivity Sample

The reduction of porosity due to possible salts precipitation has been calculated. The following assumptions have been made. First, during drying, only water is lost. We assume that the relative amount of salt (referred to the original concentration) precipitated. Second, salt precipitation occurred primarily in the external layer (15 mm thick) where the chloride profiles show a gradient (Figure 11).

The amount of salt precipitated m_{salt} has been calculated using the following equation:

$$m_{salt} = \left(\frac{C}{1 - C}\right) \cdot m_{water} \tag{3}$$

where C is the initial concentration of the salts solutions where the samples have been submerged (-) and m_{water} is the amount of water evaporated during drying (g).

The results are presented in Table 2. The total porosity has been evaluated according to ASTM C642, substituting the boiling procedure suggested with vacuum saturation. The reduction in porosity $\Delta\Phi$ has been evaluated dividing the volume occupied by salts ($m_{salt}/2\cdot/\rho_s$) over the total porosity on the 15 mm thick cylinder ($\Phi_0\cdot V_{cyl-15}$). The densities used for the evaluation of the salts are referred to the solid state of salts.

Table 2: Porosity Reduction due to Salt Precipitation

	m_{salt} (g)	Density solid salt ρ_s (g/mm^3)	Total Porosity Φ_0 (%)	Reduction in Porosity $\Delta\Phi$ (%)
15.0% $MgCl_2$	5.98	2.32E-03	20.3	4.2
16.0% $CaCl_2$	6.00	2.15E-03	20.3	5.8
17.5% NaCl	3.36	2.16E-03	20.3	2.5

It can be seen that the reduction in porosity (5% of the total porosity), even having assumed the worst conditions, is much smaller compared to the actual reduction in oxygen diffusivity seen (12% to 70% in presence of salts, with respect to water submerged samples). Some obstruction may occur at pore necks which could have a greater impact.

It should be mentioned that magnesium chloride ($MgCl_2$) showed a lower chloride content in the sample. This may be related to the slightly lower concentration of magnesium chloride solution (15.0%) when compared to the calcium chloride $CaCl_2$ (16.0%) and sodium chloride NaCl (17.5%).

CONCLUSIONS

The influence of deicing salts on gas transport properties has been examined experimentally in the lab using mortar samples. Two factors have been observed to influence the gas transport properties in samples containing deicing salts. The first factor is that deicing salts in solution may precipitate in the pores due to drying and therefore reduce the gas transport (i.e., occlude). The second factor is that deicing salts in solution can increase the degree of saturation of the sample.

The first factor has been demonstrated to be relatively small in our study (assuming a generally homogenous distribution of salt). As a result, it is assumed to have a small influence on the oxygen diffusivity. The decrease in the total porosity due to salt precipitation was found to be between 2% and 4%, which is small in comparison to the reduction of up to 70% in oxygen diffusivity. It may be possible that the salt precipitates at the pores neck; however this has not been explored in depth.

The second factor that is believed to be a primary cause for the reduction in gas permeability and diffusivity in the mortar samples is the higher degree of saturation in samples containing deicing solutions. The desorption isotherm of concrete containing deicing salt solution showed a considerable increase in the degree of saturation (DOS) when compared to system that contains pure water. The results from the mortar samples indicated that deicing salts influence the gas permeability and diffusivity of concrete. The practical implications are that testing of field samples needs to carefully consider the conditioning history of the samples.

References

Abbas, A., Carcasses, M. & Ollivier, J.-P., 1999. Gas permeability of concrete in relation to its degree of saturation. *Materials and Strcutures*, 32, pp.3-8.

Alexander, M.G., Ballim, Y. & Mackechnie, J.M., 1999. *Concrete durability index testing manual*. Research Monograph no. 4. University of Cape Town and University of the Witwatersrand.

Anderberg, A. & Wadso, L., 2008. Method for simultaneous determination of sorption isotherm and diffusivity of cmeent-based materials. *Cement and Concrete Research*, 38, pp.89-94.

Arya, C., Buenfeld, N.R. & Newman, J.B., 1990. Factors influencing chloride-binding in concrete. *Cement and Concrete Research*, 20, pp.291-300.

Badmann, R., Stockhausen, N. & Setzer, M.J., 1981. The statistical thickness and the chemical potential of adsorbed water films. *Journal of Colloid and Interface Science*, 82, pp.534-542.

Ballim, Y., 1991. A low cost, falling head permeameter for measuring concrete gas permeability. *Concrete Beton*, 61, pp.13-18.

Basheer, P.M.A., Nolan, E. & Long, A.E., 2001. Near surface moisture gradients and in-situ permeation tests. *Construction and Building Materials*, 15, pp.105-14.

Bazant, Z.P. & Najjar, L.J., 1971. Drying of concrete as a nonlinear problem. *Cement and Concrete Research*, 1, pp.461-73.

Benavente, D., Garcia del Cura, M.A. & Ordonez, S., 2003. Salt Influence on evaporation from porous building rocks. *Construction and Building Materials*, 17, pp.113-22.

Berke, N.S. & Hicks, M.C., 1991. Estimating the life cycle of reinforced concrete decks and marine piles using laboratory diffusion and corrosion data. In *Corrosion forms and control for infrastructures symposium.* San Diego (CA), 1991.

Birginie, J.-M., Auger, F. & Brea, T.R., 2000. Changes in the permeability to gas of calcareous stone core samples exposed to salt spray. *Materials and Structures*, 33, pp.331-37.

Castro, J., Bentz, D. & Weiss, J., 2011. Effect of sample conditioning on the water absorption of concrete. *Cement and Concrete Composites*, pp.805-13.

Davies, P.B., 1991. *Evaluation of the role of threshold pressure in controlling flow of waste-generated gas into bedded salt at the Waste Isolation Pilot Plant*. Sandia National Laboratories.

Di Bella, C., Villani, C., Hausheer, E. & Weiss, J., 2012. Chloride transport measurements for a plain and internally cured concrete mixture. *ACI Special Publication* , 290.

Dullien, F.A., 1992. *Porous Media: Fluid Transport and Pore Structure*. 2nd ed. San DIego.

Figg, J.W., 1973. Methods of measuring the air and water permeability of concrete. *Magazine and Concrete Research*, 25, pp.213-19.

Garboczi, E.J., 1990. Permeability, diffusivity, and microstructural parameters: a critical review. *Cement and Concrete Research*, 20(4), pp.591-601.

Giorgis, T., Carpita, M. & Battistelli, A., 2007. 2D modeling of salt precipitation during the injection of dry CO2 in a depleted gas reservoir. *Energy Conversion & Management*, 48, pp.1816-26.

Hagymassy, J., Brunauer, S. & Mikhail, R.S., 1969. Pores structure analysis by water vapor adsorption: I. T-curves for water vapor. *Journal Of Colloid and Interface Science*, 29, pp.485-91.

Hong, C.Z. & Parrott, L.J., 1989. *Air permeability of cover concrete and the effect of curing*. British Cement Association.

Houst, Y.F. & Wittmann, F.H., 1994. Influence of porosite and water content on the diffusivity of CO2 and O2 through hydrated cement paste. *Cement and Concrete Research*, 24(6), pp.1165-76.

Koelhler, K.A. et al., 2006. Water activity and activation diameters from hygroscopicity data - Part II: Application to organic species. *Atmosferic Chemistry Physics*, 6, p.795–809.

Kropp, J. & Alexander, M.A., 2007. Transport Mechanisms and Reference Tests. *Cover-State-of-the-Art Report of RILEM Technical Committee*, pp.13-34.

Kropp, J. & Hilsdor, H.K., 1995. *Performance Criteria for Concrete Durability*. RILEM Technical Committee TC 116-PCD.

Lawrence, C.D., 1984. Transport of oxygen through concrete. In Glasser, D.P., ed. *The chemistry and Chemical-related Properties of Cement*., 1984. British Ceramic Society Proceedings.

Li, W., Pour-Ghaz, M., Castro, J. & Weiss, J.W., 2012. Water Absorption and Critical Degree of Saturation Relating to Freeze-Thaw Damage in Concrete Pavement Joints. *Journal of Materials in Civil Engineering*, pp.299-307.

Litvan, G.G., 1976. Frost action in cement in the presence of de-icers. *Cement and Concrete Research*, pp.351-56.

Lubelli, B., Van Hees, R.P.J. & Groot, C.J.W.P., 2004. The role of sea salts in the occurrence of different damage mechanisms and decay patterns on brick masonry. *Construction and Building Materials*, p.119–124.

Macinnis, C. & Nathawad, Y.R., 1980. The effect of deicing agent on the absorption and permeability of various concretes. *ASTM special technical publication*, pp.485-96.

Mason, E.A. & Malinauskas, A.P., 1983. *Gas Transport in Porous Media: The Dusty-Gas Model*. Amsterdam.

Mussato, B.T., Gepraegs, O.K. & Farnden, G., 2004. Relative effects of sodium chloride and magnesium chloride on reinforced concrete. *Journal of the Transportation Research Board*, 1866(59-66).

Ollivier, J.P., Massat, M. & Parrott, L., 1995. Parameters influencing transport characteristics. In E.&. FN, ed. *Performance Criteria for Concrete Durability, RILEM Report*. 12th ed. London. pp.33-92.

Parrott, L.J., 1994. Moisture conditioning and transport properties of concrete test specimens. *Materials and Structures*, 27, pp.460-68.

Peysson, Y. et al., 2011. Permeability alteration due to salt precipitation driven by drying in the context of CO2 injection. *Energy Procedia*, 4, pp.4387-94.

Pfeifle, T.W. & Hansen, F.D., 1995. Salt-Saturated concrete strenght and permeability. In *4th Materials Engineering Conference*. Washington, 1995.

Pour-Ghaz, M., Spragg, R. & Weiss, J.W., 2010. Moisture profiles and diffusion coefficient in mortars containing shrinkage reducing admixtures. In Denmark, T.U.o., ed. *International RILEM Conference on Use of Superabsorbent Polymers and Other New Additives in Concrete*. Lyngby, Denmark, 2010.

Rangaraju, P., Rao, P., Sompura, K.R. & Olek, J., 2005. Potential for development of alkali-silica reaction in concrete in the presence of airfield deicing chemicals. In *8th International Conference on Concrete Pavements*. Colorado Springs, USA, 2005.

Scherer, G.W., 1999. Crystallization in pores. *Cement and Concrete Research*, p.1347–1358.

Scherer, G.W., 2003. Stress from crystallization of salt. *Cement and Concrete Research*, 34, pp.1613-24.

Schonlin, K. & Hilsdorf, H.K., 1988. Permeability as a measure of potential durability of concrete - development of a suitable test apparatus. In Whiting, D. & Walitt, A., eds. *ACI SP-108*. Detroit, 1988.

Schwiete, H.E., Bohme, H.J. & Ludwig, U., 1969. Measuring gas diffusion for the valuation of open porosity on mortars and concrete. *Materiaux et Constructions*, 2, pp.43-48.

Sercombe, J., Vidal, R., Gallé, C. & Adenot, F., 2007. Experimental study of gas diffusion in cement paste. *Cement and Concrete Research*, pp.579-88.

Spragg, R. et al., 2011. Wetting and drying of concrete using aqueous solutions containing deicing salts. *Cement and Concrete Composites*, pp.535-42.

Staples, B.R. & Nuttall, R.L., 1977. *The activity and osmotic coefficient of aqueous calcium chloride at 298.15 K.* American Chemical Society and American Institute of Physics for the National Bureau of Standards.

Sutter, L., Van Dam, T., Peterson, K.R. & Johnston, D.P., 2006. Long-term effects of magnesium chloride and other concentrated salt solutions on pavement and structural Portland cement concrete: Phase I results. *Transportation Research Record: Journal of the Transportation Research Board 1979*, 1, pp.60-68.

Sutter, L., Van Dam, T., Peterson, K.R. & Johnston, D.P., 2006. Long-term effects of magnesium chloride and other concentrated salt solutions on pavement and structural portland cement concrete: Phase I results. *Transport Research Record: Journal of the Transportation Research Board*, 1979(1), pp.60-68.

Torrent, R.J., 1992. A two-chamber vacuum cell for measuring the coefficient of permeability to air of the concrete cover on site. *Materials and Structures*, pp.358-65.

Villani, C., Spragg, R., Pour-Ghaz, M. & Weiss, J.W., 2012. The role of deicing salts on the non-linear moisture diffusion coefficient of cementitious materials during drying. In Brandt, A.M., Olek, J., Glinicki, M.A. & Leung, C.K.Y., eds. *10th Tenth International Symposium on Brittle Matrix Composites*. Warsaw, 2012. Institute of Fundamental Technological Research PAS.

Wallbank, E.J., 1989. *The Performance of Concrete in Bridges. A survey of 200 Highway Bridges.*

Wang, K., Nelsen, D.E. & Nixon, W.A., 2006. Damaging effects of deicing chemicals on concrete materials. *Cement & Concrete Composites*, pp.173-88.

Wong, H.S., Buenfeld, N.R.,. & Head, M.K., 2006. Estimating transport properties of mortars using image analysis on backscattered electron images. *Cement and Concrete Research*, 36, pp.1556-66.

Wong, H.S., Zobel, M., Buenfeld, N.R. & Zimmerman, R.W., 2009. nfluence of the interfacial transition zone and microcracking on the diffusivity, permeability and sorptivity of cement-based materials after drying. *Magazine of Concrete Research*, 61, pp.571-89.

Xi, Y., Bazant, Z.P., Molina, L. & Jennings, H.M., 1994. Moisture Diffusion in Cementitious Materials. *Advanced Cement Based Materials*, 1, pp.258-66.

Xi, Y., Bazant, P., Molina, L. & Jennings, H.M., 1994. Moisture diffusion in cementitious materials. Moisture capacity and diffusivity. *Advanced cement based materials*, 1, pp.258-66.